Paleogene Chronostratigraphy of the SE Margin of the Ebro Basin: Biochronological and Tectonosedimentary Evolution Implications

(Cronostratigrafia del paleogen del marge SE de la conca de l'Ebre: Implicacions biocronològiques i evolució tectonosedimentaria)

Elisenda Costa Gisbert

Departament d'Estratigrafia, Paleontologia i Geociències Marines
Grup de Recerca Consolidat de Geodinàmica i Anàlisi de Conques
Institut Geomodels
Universitat de Barcelona

PALEOGENE CHRONOSTRATIGRAPHY OF THE SE MARGIN OF THE EBRO BASIN: BIOCHRONOLOGICAL AND TECTONOSEDIMENTARY EVOLUTION IMPLICATIONS

(CRONOSTRATIGRAFIA DEL PALEOGEN DEL MARGE SE DE LA CONCA DE L'EBRE: IMPLICACIONS BIOCRONOLÒGIQUES I EVOLUCIÓ TECTONOSEDIMENTARIA)

Memòria de Tesi Doctoral presentada per **Elisenda Costa Gisbert** per optar al grau de Doctora en Ciències Geològiques per la Universitat de Barcelona. Aquesta memòria ha estat realitzada dins el Programa de Doctorat Exploració, Anàlisi i Modelització de Conques i Sistemes Orogènics (Bienni 2005-2007) i sota la direcció del **Dr. Miguel Garcés Crespo** i del **Dr. Miguel López Blanco**.

Elisenda Costa Gisbert

Barcelona, Juny 2011

Dr. Miguel Garcés Crespo

Dr. Miguel López Blanco

This PhD-Thesis has been carried out in the *Departament d'Estratigrafia, Paleontologia i Geociències Marines*, the *Geodinàmica i Anàlisi de Conques* research group (sponsored by la Comissió d'Universitats i Recerca; reference 2009GGR 1198), and the *Institut Geomodels*. Financial support was provided by a grant from the *Ministerio de Ciencia e Innovación* (reference BES-2005-7860). Additional support was obtained from the *Ministerio de Ciencia e Innovación* (projects CENOCRON CGL2004-00780, REMOSS 3D-4D CGL2007-66431-C02-02/BTE, and INTERBIOSTRAT CGL2008-0809/BTE). Short stays in Utrecht (The Netherlands) and La Jolla (San Diego, United States of America) were funded by travel grants of the *Ministerio de Ciencia e Innovación* (references EST20060527081 and EST200706110937).

A la Fundació Costa-Gisbert,
per la millor herència rebuda:
l'estima i l'educació.

TOT TORNA A COMENÇAR

Quan d'un cel blau del nord somriguin
núvols blancs i bufi el vent,
i els teus pulmons s'inflin com veles,
i el sol t'escupi raigs al front.

Quan els pit-rojos i les caderneres,
els gaigs, les garces i els mussols
refilin a l'uníson una melodia
que tens al cor, potser comencis
a sospitar.

I tothom sap que la sospita és la primera forma de la fe.

Quan recuperis tots els fragments
d'aquest naufragi que és la memòria,
d'aquests parracs ja no en direm corbates,
d'aquesta espelma ja no en direm llum.

Quan de la fosca nit salvatge
l'udol dels llops, convocant la lluna,
recorri calfreds els petits cossos
dels vostres fills, és que tot
torna a començar.

O potser tu mai has tingut un amic imaginari.
O potser tu mai has demanat res al teu àngel de la guarda.
O potser tu mai t'has sentit fill d'un pare desconegut.

Mishima (David Carabén)

AGRAÏMENTS / ACKNOWLEDGEMENTS

De vegades, i quan menys t'ho esperes, arriba el moment. Tot comença i tot s'acaba i ara, després d'uns anys, poso punt i final a "la tesi". Però m'ha fet falta l'ajuda de molta gent per posar aquest punt i final.

En primer lloc vull agrair als Miguels el repte de dirigir aquesta tesi. Gràcies Miguel (Garcés) per aquesta darrera setmana desenfrenada tot tancant capítols. Però també per tenir sempre una total disponibilitat, per ser el *llevat royal* que fa esponjar els meus articles, per recollir-me del terra quan caic (en tots els sentits) i per tot el que m'has ensenyat, molt i d'una manera que sembla que ho hagi fet gairebé jo tota sola quan no ha estat així. Gràcies Miguel (López) per la precisió i exactitud que has posat en tota la feina feta, per les presses d'última hora i també, per escoltar-me en els moments de dubte. A tots dos moltes gràcies per respectar el meu *tempus*, però sobretot per la confiança.

Aquesta tesi ha estat realitzada com a compendi de publicacions, per tant molta gent s'hi ha vist involucrada. Gràcies a tots els coautors per l'ajuda, els suggeriments i discussions: Miguel Garcés, Miguel López Blanco, Bet Beamud, Lluís Cabrera (sovint fent funcions de tercer director), Miriam Gómez-Paccard, Juan Cruz Larrasoaña, Alberto Sáez (*amigo y compañero*), Josep Serra Kiel (amb els *macros balladors*), Gilen Bernaola (amb els nannos). Thank you to the reviewers for fruitful comments, suggestions, and discussions which have greatly improved the papers: anonymous reviewers, Dave Barbeau, Jaume Dinarès-Turell, Guillaume Dupont-Nivet, Jerry Hooker, Brian Horton, Timothy Lawton, Andrew Meigs, and Simonetta Monechi.

Thank you to Cor Langereis, Wout Krijgsman, and all the people in the Foort Hoofddijk to open the doors of this wonderful lab in Utrecht. Specially, to Iuliana Vasiliev for teaching me how to use the Micromag, to Silja Hüsing for being the best office mate there, and to Ángel Carrancho, por escucharme y ser una gran compañía en ese frío y lluvioso otoño del 2006, "vivan las noches del martes pizza!!!". Anne Ku, Robert Bekkers, and Carolina Castaldi were my family there. Thanks for the music, the house-concerts and for all the shared cooking-dinner's with Carolina. Dank jullie vel, Hemmo en Lies, voor het pannekoeken in de bos een voor jou rondleidingen aan Barcelona.

Thank you to Lisa Tauxe at Scripps. Your lab was completely open and available for me. My California experience was *awesome*, including getting stuck in the desert, the wildfires and the visit to the ER in Saint Francis Memorial. Marcel Croon, Mitra, and Isa were grate mates there, but I'm really grateful to Carmen Luna and Isidro. You open the doors of your house and became my family there!

De vegades els mariners (337) arriben a les platges (336), als companys de Departament. No us mereixo, quina emoció em fa donar-vos les gràcies!!! Per començar, a la 336, hi trobem en Rubén, sempre disposat a donar un cop de mà en tot. En Xavi s'ha convertit en un molt bon alumne de CorelDraw i a ell li dec la figura 2.4. En Yaniel hi posa el toc "caribenyo" i l'Enric, discret i treballador, sempre atent a com anava avançant la cosa. La Mireya i la Patri enfeinades amb els seus microfossils. La Mayte, ànims que ja queda poc... i si vols la taula del racó és tota teva. En Lluís, per ser un gran i atent company en el nostre estiu italià i pels divendres ploraners. L'Aitor, la darrera incorporació a la sala, sempre amb gran disposició per tot. A la 337, en David, en Jaume, la Olaia, les Ruts, la Pilar, en Sergi, la Catalina, en Xavi, l'Uri i l'Aaron han estat ben pendents de com anava tot. També vull donar les gràcies a la gent que durant aquest temps ha anat passant per la 336 i ara ja no hi son (l'Elias, la Marina, l'Ona, la Silvana, en Miki i la Xènia).

Als habitants d'aquest món tant estrany que és el laboratori. A l'Anna Gómez, la Ylènia Almar, en Rubén Calvo, la Mireia Butillé i l'Anna Quintà per mesurar part de les mostres d'aquesta tesi. A la Bet, per fer que tot funcioni. A en Juan, la Miriam, la Rut Soto per fer que els cafès/tes fossin genials. Al compressor per distorsionar la banda sonora del vell transistor de ràdio (on RAC 1 i iCatFm formen la banda sonora més habitual), als forns i al 2G per portar-se com campions.

Al meu iPod i la meva llibreta negra (gràcies, pares, per aquests regals). L'iPod m'ha salvat de l'avorriment que un experimenta davant del magnetòmetre i la llibreta negra ha estat allà on s'han dipositat totes les idees d'aquesta tesi. A les tasses de tè i a les til·les!

A les paleomagnetonenes (Bet, Ylènia, Míriam) i les nostres nits magnètiques. Allá que vamos perforando el mundo sin cesar!!! A la Bet, per tantes i tantes coses, però d'entre elles els tuppers, la piscina, fer pdf's, el resum extens en català i ser una molt bona amiga i companya. A la Ylènia, per ser tan bona amiga i tenir tant bona sort ;-), per ser l'altra "alegria de la autovía". A la Míriam, por los conglomerados que bailan, los chiribitos, los buenos

consejos, los ánimos y los cien ojos en las revisiones. Al final vamos a tener que subir a ver a La Moreneta...

A la Patricia Cabello, l'Oriol Falivene per amoïnar-vos de com m'anaven les coses. A la Sara Lafuerza, perquè cada dia et superes més i jo no seria aquí sense aquell correu teu que em deia "ei, que al departament hi ha un tal Miguel Garcés que busca becari". A la Desi, l'Esteban, la Cinta, la Laura, en Ricard, en Dani, en Victor, l'Álvaro, la Carme, i demés colla pessigolla de la facultat.

A en Pol i l'Anna, per tot. Fins i tot per no fer massa cas als convidats a sopar durant la final de la Champions... A en Nacho, per ser tant després i bon veí, que és capaç d'entrar a la cuina i fer el sopar entre d'altres coses. A en Daniel i l'Helena, per Budapest, Sardegna, Llagostera, cines frustrats i tantes i tantes aventures (incloent-hi els cinc errors que pot cometre tot bon turista). A l'Anna Cuixart, per acollir-nos sempre a Santa Coloma i perquè quan ens ajuntem fem un gran trio calavera!

A la família tota. Pròpia i trobada pel camí: Joan, Clara, Alba, Jofre, Dolors, Albert, Pere, Xaro, Maria i Ivan... i la resta que li penja. Perquè sempre hi sou, estimant-me i ensenyant-me, en definitiva fent-me créixer cada dia.

I a tu Arnau, per tantes i tantes coses, com la portada (tan xula), però sobretot per l' "*aguanta bonica que això ja ho tens*" d'aquest matí.

Barcelona, Maig i Juny de 2011.

INDEX

FIGURES AND TABLES INDEX

CHAPTER 1: INTRODUCTION

CHAPTER 2: METHODOLOGY

Chapter 3.2: Chronology of the Marine-Continental Transition in the Igualada Area (Paper2)

an open to a closed basin, while no changes are observed in the eastern regions.

Appendix of Chapter 3.2: Supporting Electronic Information

Chapter 3.3: Chronology of the Continental and Transitional Units in the Montserrat Area (Paper3)

Appendix of Chapter 3.3: Supporting Electronic Information

Chapter 3.4: Chronology of the Continental Units of the Vic-Manresa Area (Paper4)

SIGNIFICANT ABBREVIATIONS, ACRONYMS AND SYMBOLS

Abbreviations and Acronyms

Geoscientific Concepts

AF	alternating field
C	chron
CCR	Catalan Coastal Ranges
ChRM	characteristic remanent magnetization
CRM	chemical remanent magnetization
Dec	declination
EOT-1	Eocene-Oligocene Transition event 1
EOT-2	Eocene-Oligocene Transition event 2
Fm	formation
FO	first occurence
GPTS	geomagnetic polarity time scale
Gr	group
GSSP	global stratotype and section point
GTS	geologic time scale
I.	*Isthmolithus*/*Istmolithus*
Inc	inclination
IRM	isothermal remanent magnetization
LO	last occurrence
Mb	member
MFS	maximum flooding surface
MP	Mammal Paleogene reference level
N.	*Nummulites*
N1, N2,…	normal magnetozones in local magnetostratigraphies
NP	calcareous nannofossil Biozones
NRM	natural remanent magnetization
Oi-1	Oligocene isotope event 1
Oi-1a	Oligocene isotope event 1a
R	regressive
R1, R2,…	reverse magnetozones in local magnetostratigraphies
SB	sequence boundary
SBZ	larger (benthic) foraminifers Bioznes
T	transgressive
T-R	transgressive to regressive
TRM	thermoremament magnetization
VGP	virtual geomagnetic pole

Magnetostratigraphic Sections

BM / MM	Miralles
CB	Collbató
CM	Carretera Montserrat
EL	Eix Llobregat
LT	La Tossa

MN	Maians
MO	Moià
RB	Rubió
SJ	Sant Jaume
SP	Santpedor

Fossil Sites

BeM1	Bembridge Marls 1
CA	Calaf
CA l.	Lower Calaf
CA u.	Upper Calaf
CI	Ciutadilla
FO	Forés
Ham 1-3	Hampstead Member 1, 2, and 3
Ham 4-6	Hampstead Member 4, 5, and 6
HL	Hartherwood Lignite Bed
LBL	Limestone of the Bembridge Limestone Formation
LF	Lacey's Farm Member
PQ	Porquerisses
RO	Roquefort de Queralt
SCG	Sant Cugat de Gavadons
SP	Santpedor
TA	Tàrrega
TR	Tarrés
VI	Vimbodí
VN	Vinaixa
WB2	Whitecliff Bay 2

Montserrat Conglomeratic Units

Br1	Les Bruixes 1
Br2	Les Bruixes 2
Fe	Feixades
Mu	Mullapans
Pb	Pas de la Barra
Va	La Valentina

Montserrat Composite Sequences

B	Bogunyà
CP	Cal Padró
M	Manresa
Mo	Monistrol
SS	Sant Salvador
SV	Sant Vicenç
V	Vilomara

Other Abbreviations and Acronyms

aff.	(*affinis*) related

ca.	(*circa*) arround, about, approximately
e.g.	(*exempli gratia*) for example
et al.	(*et alii*) and coworkers
etc.	(*et cetera*) and other things
i.e.	(*id est*) that is
vs.	versus

Symbols

a	annum
°C	degree Celcius
cm	centimeters (=10^{-2} m)
K	magnetic susceptibility
ka	kilo annum
kyr	kilo year (=10^{3}yr)
m	meters
Ma	Million annum
mT	mili Tesla (=10^{-3} T)
Myr	mega year (=10^{6} yr)
yr	year

ABSTRACT

This PhD-Thesis presents a new chronostratigraphy of the Paleogene sedimentary record of the SE margin of the Eastern Ebro Basin. It is based on a number of magnetostratigraphic sections and its integration with marine and continental biochronological data. A robust correlation with the geomagnetic polarity time scale is obtained and provides the record with absolute ages, ranging from chron C20n to chron C12r (Lutetian to Rupelian stages, *ca.* 43.0-31.0 Ma). The new chronology provides with the tools for the quantification and further comprehension of the tectonosedimentary evolution of the adjacent margins of the Ebro Basin. In addition, the manetostratigraphy-based chronology contributes to the calibration of calcareous nannofossil, larger foraminifers (Shallow Benthic Zones), and calibration of the European vertebrate Mammal Paleogene (MP).

Main differences with respect to the current chronostratigraphic scheme of the Eastern Ebro Basin include the age of the uppermost marine units in the Eastern Ebro Basin. While earlier schemes attributed a Bartonian age to these units regarding its biostratigraphical contents, results of this PhD-Thesis supports a Lower Priabonian age, yielding an interpolated age of *ca.* 36.0 Ma (within chron C16n.2n) for the continentalization process. This age is in concordance with a reinterpretation of earlier magnetostratigraphic data from the Western South Pyrenean Foreland Basin, and indicates that continentalization of the basin occurred as a rapid and isochronous event. The analysis of the observed sedimentation trends in opposite sectors of the basin are used to evaluate the character of this continentalization process. Thus, contrasting sedimentation trends between the Western and Eastern sectors of the South Pyrenean foreland are proposed to indicate that basin closing preferentially affected those areas subjected to sediment bypass towards the ocean domain. As a result, sediment ponding after basin closure is responsible for a two-fold increase of sedimentation rates in the Western sector, while changes of sedimentation rates are undetected in the more restricted scenario of the Eastern Ebro Basin.

In the same way, results of this PhD-Thesis provide improved temporal constraints for the sediments of the Eocene Montserrat alluvial fan and fan-delta complex. Thus a Lutetian age is ascribed to the whole La Salut Formation and the age of the Montserrat Conglomerates spans from C19r to C16n (*i.e.*, Upper Lutetian to Lower Priabonian). The new chronological framework is used to unravel the forcing controls on the sequential arrangement of the

Montserrat alluvial fan and fan-delta complex at different temporal scales, and also to revise the tectonosedimentary history of this sector of the SE margin of the Eastern Ebro Basin. Results of this PhD-Thesis shows a correlation between (tectonic) subsidence and forelimb rotation measured on basin-margin deformed strata of Montserrat. Furthermore, integration of subsidence curves from different sectors of the Eastern Ebro Basin allows estimating the variable contribution of tectonic loads from the two active basin margins: the Catalan Coastal Ranges and the Pyrenees. The results support the presence of a double flexure from Late Lutetian to Late Bartonian, associated to the two tectonically active margins. From Late Bartonian to Early Priabonian the homogenization of subsidence values is interpreted as the result of the coupling of the two sources of tectonic load.

Finally, the magnetostratigraphy-based chronology derived from this PhD-Thesis contributes to the calibration of several biostratigraphic zonations to the geomagnetic polarity time scale. In the marine realm, the base of calcareous nannofossil Zone NP19-20 is pinned down to an older age than its currently accepted attribution, whereas the time span assigned to Zone NP18 is significantly reduced. A revised calibration of larger foraminifers indicates that Zone SBZ18, formerly assigned exclusively to Late Bartonian, extends its range to the earlymost Priabonian, being the Bartonian stage almost entirely represented by Zone SBZ17. A division of Zone SBZ18 into two subzones is also proposed. In the continental realm, the magnetostratigraphic record of the Eastern Ebro Basin yields accurate ages for the immediately pre- and post-Grand Coupure mammal fossil assemblages found in this basin. Thus, the Grande Coupure, a major terrestrial faunal turnover recorded in Eurasia associated with the overall climate shift at the Eocene-Oligocene transition, is found to occur with a maximum allowable lag of 0.5 Myr with respect to this boundary. Furthermore, the new results from this PhD-Thesis allow revisiting correlations for the controversial Eocene-Oligocene record of the Hampshire Basin (Isle of Wight, UK), and their implications for the calibration of the Mammal Paleogene reference levels MP18 to MP21.

RESUM EXTENS EN CATALÀ

Motivació i Objectius

En el camp de les Ciències de la Terra un cop es disposa d'un bon control temporal, es possible conèixer l'evolució dels sistemes geològics com per exemple el conjunt que formen les conques d'avantpaís i els seus cinturons orogènics adjacents i, per tant, es poden deduir i establir les relacions causa-efecte d'aquests sistemes. De la mateixa, es poden establir correlacions amb el registre global. En aquest sentit, doncs, el registre sedimentari d'una conca d'avantpaís esdevé un arxiu de l'evolució dels seus marges, així com del sistema Terra mitjançant el registre dels processos tectònics i/o climàtics.

Al NE de la Península Ibèrica, el registre estratigràfic de la Conca de l'Ebre constitueix un cas extraordinari entre les conques d'avantpaís alpines de la regió circummediterrània. En ell s'hi enregistra l'evolució cenozoica del NE de la placa Ibèrica que, durant l'Eocè superior, es caracteritzà pel pas d'unes condicions de connexió amb l'Oceà Atlàntic a l'aïllament, esdevenint una conca restringida (Riba *et al.*, 1983; Vergés *et al.*, 2002). Després del tancament de la conca, es dipositù una successió excepcionalment potent de fins a 5000 m de sediments al·luvials, fluvials i lacustres durant un període de 25 Myr. L'alt nivell de colmatació, juntament amb l'erosió parcial del rebliment sedimentari arran de l'obertura del drenatge cap al Mar Mediterrani ha facilitat l'observació de les relacions estratigràfiques, així com de l'estudi de les relacions tectònica-sedimentació, fent que actualment es disposi d'un gran nombre d'estudis versant sobre aquest tema. D'altra banda, i per tal d'interpretar el registre en termes d'evolució tectonosedimentària i paleoclimàtica es fa necessari disposar d'un marc temporal precís de les unitats sedimentàries a escala de conca, així com de la correlació del registre d'aquestes unitats amb el registre global. Els primers intents d'obtenció de cronologies d'aquest registre a partir de dades biomagnetostratigràfies es centraren, principalment, o bé en el registre fòssil marí (Burbank *et al.*, 1992; Taberner *et al.*, 1999; López-Blanco *et al.*, 2000a; Cascella & Dinarès-Turell, 2009), o bé en el registre fòssil continental (Barberà *et al.*, 2001). Malgrat tot, i a data d'avui, encara no s'ha assolit una integració completa de totes les eines cronostratigràfiques (biostratigrafia i magnetostratigrafia de les unitats marines i continentals) disponibles.

El principal objectiu de la present Tesi Doctoral és l'obtenció d'una biomagnetocronologia integrada de les unitats sedimentàries paleògenes de la Conca de l'Ebre. Mitjançant la

construcció d'un marc cronostratigràfic robust, aquesta Tesi contribueix a la comprensió dels factors que han influenciat en l'evolució de la Conca de l'Ebre i els seus marges adjacents, així com les implicacions biocronològiques derivades de la correlació amb l'Escala de Temps de Polaritat Geomagnètica (ETPG). Per tot això, els objectius específics de la present Tesi Doctoral són:

i. obtenir una cronologia independent basada en magnetostratigrafia per a les unitats marines i continentals de l'Eocè mitjà-Oligocè inferior del sector oriental de la Conca de l'Ebre
ii. calibrar les biozonacions de macroforaminífers i de nanofòssil calcari bartonians i priabonians amb l'escala de temps de polaritat geomagnètica
iii. calibrar la biocronologia europea de mamífers de l'Eocè superior-Oligocè (nivells de referència MP) acotant, posteriorment, l'edat de la *Grande Coupure*, un important canvi de les faunes de mamífers terrestres enregistrat a Euràsia i associat al canvi de clima en el límit Eocè-Oligocè.
iv. mitjançant la construcció d'un marc cronostratigràfic precís, contribuir a la comprensió dels factors que han determinat la evolució sedimentària de la conca.

Estructura

Aquesta Tesi Doctoral, confeccionada sota la modalitat de compilació d'articles publicats i/o enviats a revistes pertanyents al *Journal Citation Report* de l'*Institute for Scientific Information*, consta de 5 capítols. Com a introducció, al Capítol 1, s'hi presenta el context geològic de la Conca d'Avantpaís Sudpirinenca i els seus marges, incloent una visió general dels treballs previs duts a terme en aquesta regió. Al Capítol 2, es descriu la metodologia utilitzada en aquesta Tesi Doctoral en més detall que en els articles presentats en el Capítol 3.

El Capítol 3 conté el gruix dels resultats d'aquesta Tesi Doctoral i inclou 4 articles; dos d'ells ja publicats, un altre acceptat per publicació i un quart article que, en aquests moments, es troba en procés de revisió. El Capítol 3.1 constitueix el primer article científic d'aquesta Tesi Doctoral: *Costa, E., Garcés, M., López-Blanco, M., Serra-Kiel, J., Bernaola, G., Cabrera, L., Beamud, E., (accepted). The Bartonian-Priabonian marine record of the Eastern South Pyrenean Foreland Basin (NE Spain): A new calibration of the larger foraminifers and calcareous nannofossil biozonation. Geologica Acta.* En aquest capítol es presenta la nova cronologia per les unitats marines de l'àrea d'Igualada sorgida de la integració biostratigràfica (nanofòssil

calcari i macroforaminífers) i magnetostratigràfica de les unitats marines de l'Eocè superior d'aquest sector de la Conca de l'Ebre. Aquesta nova cronologia modifica les interpretacions cronostratigràfiques existents i proporciona una nova calibració de les biozonacions de nanofòssil calcari i de macroforaminífers.

El Capítol 3.2 conforma el segon article científic d'aquesta Tesi Doctoral: *Costa, E., Garcés, M., López-Blanco, M., Beamud, E., Gómez-Paccard, M., Larrasoaña, J.C., (2010). Closing and continentalization of the South Pyrenean foreland basin (NE Spain): magnetochronological constraints. Basin Research, 22, 904-917.* En aquest capítol s'integra una cronologia independent, obtinguda de manera exclusiva a partir de dades magnetostratigràfiques, amb la reinterpretació d'altres registres magnetostratigràfics de la Conca d'Avantpaís Sudpirinenca. D'aquesta manera, en resulta una cronologia d'alta resolució del procés de continentalització de la Conca de l'Ebre que ajuda a constrènyer el seu context i factors de control.

La Doctoranda es coautora del Capítol 3.3: *Gómez-Paccard, M., López-Blanco, M., Costa, E., Garcés, M., Beamud, E., Larrasoaña, J.C., (submitted). Tectonic and climatic controls on the sequential arrangement of an alluvial fan/fan-delta complex (Montserrat, Eocene, Ebro basin, NE Spain). Basin Research.* En aquest capítol s'estableix un marc cronològic precís pels sediments eocens que conformen el complex de ventall al·luvial i de ventall costaner de Montserrat. El nou marc cronològic permet avaluar la subsidència i l'evolució tectonosedimentària del sector central del marge SE de la Conca de l'Ebre. A més a més, la cronologia de Montserrat s'utilitza per desxifrar la interacció entre els factors que controlen la sedimentació a diferents escales temporals, incloent-hi també el control orbital (Milankovitch).

El Capítol 3.4 constitueix el tercer i darrer article científic d'aquesta Tesi Doctoral: *Costa, E., Garcés, M., Sáez, A., Cabrera, L., López-Blanco, M., (2011). The age of the "Grande Coupure" mammal turnover: New constraints from the Eocene-Oligocene record of the Eastern Ebro Basin (NE Spain). Palaeogeography, Palaeoclimatology, Palaeoecology, 301, 97-107.* Aquest capítol presenta una cronologia basada en la magnetostratigrafia de les unitats continentals de l'Eocè superior-Oligocè inferior del sector oriental de la Conca de l'Ebre. La nova cronologia aporta edats precises per a les associacions de mamífers fòssils immediatament anteriors i posteriors a la *Grand Coupure*, i la seva posició respecte el límit Eocè-Oligocè i els esdeveniments isotòpics relacionats amb aquesta transició. Aquests resultats, juntament amb altres registres rellevants de l'Eocè-Oligocè d'Europa es fan servir per calibrar els nivells de referència de Mamífers Paleògens MP18 a MP21.

El Capítol 4 s'ha concebut com una discussió integradora dels resultats obtinguts i presentats en el Capítol 3. Finalment, al Capítol 5 s'hi presenten les principals conclusions obtingudes en aquesta Tesi Doctoral.

Les Seccions Magnetostratigràfiques Mostrejades

En aquesta Tesi Doctoral s'han distingit tres sectors al llarg del marge SE de la Conca de l'Ebre en base a criteris geològics i geogràfics. De SW a NE, aquests sectors són: l'àrea d'Igualada, l'àrea de Montserrat i la de Vic-Manresa. A cadascun d'aquests sectors, s'han mostrejat un conjunt de seccions correlacionables i amb diversos graus de solapament amb l'objectiu principal d'obtenir una magnetostratigrafia local llarga i contínua. En aquest sentit, aconseguir un registre magnetostratigràfic prou llarg és rellevant per tal d'obtenir un patró d'inversions de polaritat únic i característic. Aquesta singularitat del registre magnetostratigràfic ha estat clau per tal d'establir una correlació independent amb l'ETPG de Gradstein *et al.* (2004) i, posteriorment, poder constrènyer la calibració de les biostratigrafies marina i continental.

A l'àrea d'Igualada, s'han obtingut dues sèries magnetostratigràfiques compostes: la sèrie de Miralles-La Tossa (Capítol 3.1) i la sèrie de Maians-Rubió (Capítol 3.2). Ambdues seccions comprenen les unitats marines més altes de la Conca d'Avantpaís Sudpirinenca amb edats que van del Lutecià al Bartonià/Priabonià (Ferrer, 1971; Puigdefàbregas & Souquet, 1986; Riba *et al.*, 1983; Serra-Kiel *et al.*, 2003). La sèrie de Miralles-La Tossa inclou els materials continentals del Grup Pontils i els materials marins del Grup Santa Maria i el "Complex Terminal", materials que constitueixen l'anomenada transgressió "Bartoniana" (Serra-Kiel & Travé, 1995). La sèrie de Maians-Rubió comprèn exclusivament els materials continentals de la Formació Artés d'edat Priaboniana-Rupeliana. No obstant, les correlacions litostratigràfiques de detall portades a terme indiquen que els 50 m superiors de la secció de Maians-Rubió passen cap a conca als sediments marins més alts del Grup Santa Maria, el "Complex Terminal" i la Formació Guixos d'Òdena (cinturó de fàcies sulfatades associades a les sals de la Formació Cardona; Fig. 2 del Capítol 3.2).

A l'àrea de Montserrat, la potent seqüència de conglomerats que hi aflora representa el desenvolupament de complexes de ventall al·luvial i de ventall costaner com a resultat del creixement tectònic de les Serralades Costaneres Catalanes durant el Paleogen (Guimerà,

1984; Anadón *et al.*, 1985; López-Blanco *et al.*, 2000b; López-Blanco, 2002, 2006). En aquest sector proximal, els sediments continentals (Conglomerats de Montserrat i Conglomerats de Sant Llorenç del Munt) alternen amb sediments marins (Grup Santa Maria) de la Conca d'Avantpaís Sudpirinenca (Fig. 2 dels Capítols 3.1 i 3.3). En aquesta àrea, s'ha obtingut una nova sèrie magnetostratigràfica, que cobreix la Formació La Salut i els Conglomerats de Montserrat (incloent-hi també els equivalents laterals del Grup Santa Maria), amb l'objectiu de precisar la cronologia d'aquestes unitats en comparació a estudis anteriors duts a terme en aquesta mateixa àrea (López-Blanco *et al.*, 2000a).

A l'àrea de Vic, es disposava d'un gran nombre de dades magnetostratigràfiques prèvies per les unitats marines de l'Eocè Mitjà i Superior (Burbank *et al.*, 1992; Taberner *et al.*, 1999). Per aquest motiu, l'esforç principal s'ha dedicat a l'obtenció de dades magnetostratigràfiques per les unitats continentals que recobreixen els sediments marins de la Formació La Tossa del Grup Santa Maria (Capítol 3.4). Les sèries de Moià i Santpedor enregistren la Formació Artés i han estat correlacionades de manera robusta mitjançant el nivell guia del Membre Moià de la Formació Castelltallat, d'origen lacustre, que es troba interestratificat amb els materials al·luvials distals i fluvials de la Formació Artés (Figs. 1 i 4 del Capítol 3.4).

Correlació de les Seccions Magnetostratigràfiques Estudiades amb l'Escala de Temps de Polaritat Geomagnètica

La integració de les sèries magnetostratigràfiques locals amb tot el conjunt de les dades biostratigràfiques disponibles permet una aproximació a l'interval d'edat representat en el registre sedimentari estudiat. No obstant, en aquesta Tesi Doctoral, les calibracions existents de *datums* biostratigràfics específics no es tenen en compte com a punts d'ancoratge per la correlació de les diferents seccions magnetostratigràfiques amb l'ETPG. La correlació amb l'escala de temps es guia pel patró d'inversions característic de les magnetostratigrafies locals i el seu millor encaix amb l'ETPG. Això és possible perquè les inversions del camp geomagnètic no tenen lloc de manera periòdica. Per tant, si es disposa d'un registre suficientment llarg, hom s'assegura l'obtenció d'un patró de polaritat prou característic per establir una correlació amb l'ETPG. Per exemple, en aquesta Tesi Doctoral la magnetostratigrafia local més curta (sèrie composta de Moià-Santpedor; Capítol 3.4) té prop de 500 metres i està integrada en un conjunt d'altres sèries magnetostratigràfiques correlacionables i/o solapades amb ella com són les sèries compostes de Maians-Rubió (Capítol 3.2) i la de Rocafort-Vinaixa de Barberà *et al.* (2001). Això resulta en un registre magnetostratigràfic llarg que permet una calibració

independent amb l'ETPG 2004 (Gradstein *et al.*, 2004), en el sentit que la biostratigrafia no s'usa per ancorar magnetozones específiques amb un cron en concret de l'escala de temps. La correlació resultant d'aquestes sèries amb l'ETPG (Gradstein *et al.*, 2004) es mostra a la Fig. 4.1 i, a continuació, es presenta una visió general del procediment de correlació.

A l'àrea d'Igualada es disposa de dues fonts de dades biocronològiques, els macroforaminífers i el nanofòssil calcari. A partir de l'estudi biostratigràfic dut a terme a la secció composta de Miralles-La Tossa (Fig. 3 del Capítol 3.1) es conclou que les unitats marines de l'àrea d'Igualada es mouen en el rang d'edat que va del Bartonià al Priabonià. A partir d'aquesta acotació temporal de primer ordre, s'obté un bon ajust de la magnetostratigrafia de Miralles-La Tossa amb l'ETPG (Gradstein *et al.*, 2004) correlacionant els tres llargs intervals de magnetització normal amb els conjunt de crons que van del C18n a C16n, cobrint tot el Bartonià i el Priabonià inferior.

Tot i no disposar de dades biostratigràfiques directes en el registre continental de l'àrea d'Igualada, la secció composta de Maians-Rubió es correlaciona litostratigràficament amb altres seccions que contenen associacions de vertebrats fòssils de l'Eocè superior i de l'Oligocè inferior (Agustí *et al.*, 1987; Anadón *et al.*, 1987, 1992; Sáez, 1987; Arbiol & Sáez, 1988; Barberà *et al.*, 2001), tal i com s'argumenta als Capítols 3.2 i 3.4. La sèrie composta de Maians-Rubió es correlaciona cap al sud-oest amb la secció magnetostratigràfica de Rocafort-Vinaixa de Barberà *et al.* (2001) tal i com es mostra a la Fig. 6 del Capítol 3.2, mentre cap al nord-est es correlaciona amb la sèrie de Moià-Sanpedor de l'àrea de Vic-Manresa (Fig. 5 del Capítol 3.4). La correlació de la sèrie composta de Maians-Rubió amb les sèries de Rocafort-Vinaixa i Moià-Santpedor s'estableix mitjançant la presència d'estrats conglomeràtics a sostre de la sèrie de Maians i a la base de la sèrie de Rubió. Aquests estrats conformen un horitzó competent i continu amb significança regional (unitat de gresos de Santpedor) que pot ser traçat durant desenes de quilòmetres al llarg del marge SE del sector oriental de la Conca Ebre (Figs, S4, 5 i 6 del Capítol 3.2; Fig. 5 del Capítol 3.4). Per tant, i en aquesta àrea de la Conca de l'Ebre, la millor correlació de la part mostrejada de la Formació Artés amb l'ETPG (Gradstein *et al.*, 2004) s'estableix amb els crons C16n a C12r, en base a la presència del parell característic de magnetozones predominantment inverses enregistrades a les magnetostratigrafies de Maians-Rubió i Moià-Santpedor, que contenen associacions de vertebrats fòssils d'edats compreses entre l'Eocè superior i l'Oligocè inferior. Finalment, tampoc es disposa de dades biostratigràfiques per a la secció de Montserrat (Capítol 3.3). No obstant, aquesta sèrie es pot

correlacionar litostratigràficament amb la sèrie composta de Maians-Rubió, tal i com s'exposa al Capítol 3.3 i es mostra a la seva Fig. 6.

Cronostratigrafia Paleògena del Marge SE del Sector Oriental de la Conca de l'Ebre

La cronologia basada en la bio-magnetostratigrafia derivada d'aquesta Tesi Doctoral (Fig. 4.1), juntament amb la integració de dades biomagnetostratigràfiques prèvies disponibles en aquest sector de la conca (Burbank *et al.*, 1992; Taberner *et al.*, 1999; Barberà *et al.*, 2001), ha permès l'establiment d'una cronostratigrafia robusta per a les unitats paleògenes del marge SE de la Conca de l'Ebre. La Figura 4.2 mostra aquest nou marc cronostratigràfic, que comprèn del cron 20n al cron 12r (43-31 Ma aproximadament), és a dir, del Lutecià al Rupelià. A continuació, s'exposa una síntesi de com aquesta nova cronologia modifica resultats anteriors.

Cronologia de les Unitats Marines de l'Eocè Mitjà-Superior i de la Transició Marí-Contiental de la Conca d'Avantpaís Sudpirinenca al Sector Oriental de la Conca de l'Ebre

A partir de la biomagnetostratigrafia de la sèrie composta de Miralles-La Tossa i de la magnetostratigrafia de Maians-Rubió s'esdevenen canvis importants en l'atribució cronològica de les unitats marines de l'àrea d'Igualada. Mentre que estudis anteriors atribuïen al Grup Santa Maria una edat bartoniana en funció del seu contingut fòssil (Serra-Kiel *et al.*, 2003; Fig. 1.4; Fig. 2 del Capítol 3.1), la nova magnetostratigrafia de les sèries de Miralles-La Tossa demostra que la Formació Igualada comprèn una gran part del Priabonià, en concordança amb l'estudi pioner de foraminífers planctònics de Ferrer (1971a,b). A més, les unitats marines més altes com ara la Formació Tossa, el "Complex Terminal" i la Formació Guixos d'Òdena es correlacionen amb el cron C16n (Priabonià). Aquesta correlació, recolzada pels resultats d'ambdues sèries compostes de Miralles-La Tossa i de Maians-Rubió (Fig. 4.1; Fig. 6 del Capítol 3.1; Figs. 2 i 6 del Capítol 3.2), indica que la darrera transició marí-continental a l'àrea d'Igualada es correlaciona amb el Priabonià, i té una edat interpolada de prop de 36 Ma (Capítol 3.2).

Els resultats obtinguts a l'àrea d'Igualada fan necessària la reinterpretació d'estudis magnetostratigràfics anteriors que comprenien les unitats marines de l'Eocè mitjà i superior del sector oriental de la Conca de l'Ebre a l'àrea de Vic (Burbank *et al.*, 1992; Taberner *et al.*, 1999). La correlació amb l'ETPG en aquests estudis estava fortament condicionada per la presumible edat "Bartoniana" de les unitats marines més altes a partir del seu contingut fòssil. En aquest sentit, al Capítol 3.2 es presenta una correlació alternativa convincent de la sèrie

magnetostratigràfica de Burbank *et al.* (1992) (Fig. S5 del Capítol 3.2) assumint l'edat obtinguda per a la transició marí-continental a l'àrea d'Igualada i integrant dades biomagnetostratigràfiques recents de la mateixa regió (Cascella & Dinarès-Turell, 2009). La nova calibració de la magnetostratigrafia de Vic proporciona un millor ajust amb l'ETPG (Gradstein *et al.*, 2004), suavitzant així les taxes de sedimentació i mostrant una major coincidència amb les tendències de llarg període observades en altres registres del sector oriental de la Conca de l'Ebre (Fig. 8 del Capítol 3.2). Al panell cronostratigràfic mostrat a la Fig. 4.2, el conjunt de les seccions magnetostratigràfiques de Taberner *et al.* (1999) també es correlacionen amb l'ETPG (Gradstein *et al.*, 2004) d'acord a la nova edat obtinguda per a la transició marí-continental a les àrees de Vic i Igualada. Per tant, les unitats marines més altes a l'àrea de Vic, tals com les Margues de Vespella i La Guixa, la part superior dels Gresos de Centelles, el complex deltaic de Sant Martí Xic i les evaporites de la Formació Cardona tenen una edat priaboniana, d'acord amb la revisió de la seva correlació amb l'ETPG, que va dels cron C17n al C16n. Cal remarcar que l'edat obtinguda per a la transició marí-continental és significativament més antiga que l'assignada a la Formació Cardona en base als valors de les relacions isotòpiques de $^{87}Sr/^{86}Sr$ en mostres d' anhidrita (Taberner *et al.*, 1999). Tal i com es discuteix al Capítol 3.2, l'ambient sedimentari durant la sedimentació de la Formació Cardona probablement correspondria a una massa d'aigua molt restringida, amb relacions isotòpiques molt influenciades per l'entrada d'aigües continentals (Ayora *et al.*, 1994; Cendón *et al.*, 2003). En aquest escenari se'n dedueix que, la significació cronostratigràfica dels índexs isotòpics de $^{87}Sr/^{86}Sr$ és molt precària i, d'aquesta manera, s'explica fàcilment la discrepància observada amb la cronologia obtinguda a partir de la magnetostratigrafia.

Finalment, dels resultats integrats de les àrees d'Igualada i Vic (Fig. 4.2) se'n desprèn com a conclusió que l'anomenat 2on cicle Bartonià de Serra-Kiel & Travé (1995) i Serra-Kiel *et al.* (2003) té en realitat una edat Priaboniana.

Cronologia de les Unitats Continentals de l'Eocè Mitjà-Superior del Marge SE al Sector Oriental de la Conca de l'Ebre

La nova secció magnetostratigràfica de Montserrat (Capítol 3.3) modifica les atribucions magnetocronològiques prèvies del complex de ventall al·luvial i ventall costaner de Montserrat (López-Blanco *et al.,* 2000a). Aquests autors basaven la seva correlació en l'edat "Bartoniana" que s'assumia per a les unitats marines del Grup Santa Maria (Serra-Kiel *et al.*, 2003). D'acord a les Figs. 4.1, 4.2 i la Fig. 6 del Capítol 3.3, es pot assignar una edat luteciana a la totalitat de la Formació La Salut i, l'edat dels Conglomerats de Montserrat, s'acota entre els crons C19r i

C16n (és a dir, del Lutecià superior al Priabonià inferior). Els resultats d'aquesta Tesi Doctoral porten a la conclusió que els 330 m superiors de la secció de Montserrat, corresponents a la part alta de les seqüències compostes de Vilomara, Manresa i San Salvador de López-Blanco *et al.* (2000a), tenen una edat Priaboniana.

La correlació litostratigràfica del complex de ventall al·luvial i ventall costaner de Montserrat amb el sistema veí de Sant Llorenç del Munt (López-Blanco *et al.*, 2000b) mostra que els conglomerats més alts de Sant Llorenç del Munt també tenen una edat priaboniana inferior. Finalment, i tal com es deriva de les seccions compostes de Maians-Rubió (àrea d'Igualada; Capítol 3.2) i Moià-Santpedor (àrea de Vic-Manresa; Capítol 3.4), la Formació Artés té un rang temporal comprès entre el Priabonià i el Rupelià (Fig. 4.2).

Implicacions Biocronològiques

L'Escala de Temps Geològic (ETG) està intrínsecament unida amb les Ciències de la Terra, ja que constitueix tant l'eina de mesura com la clau per a la reconstrucció de la història de la Terra. La construcció de l'ETG deriva de la integració de les disciplines cronostratigràfiques relatives, tals com la biostratigrafia i la magnetostratigrafia amb tècniques de datació absoluta com la geocronometria radiomètrica i l'astrocronologia. A data d'avui i pel Paleogen, la integració de les diverses escales cronostratigràfiques no ha assolit un estadi d'estabilitat; en canvi es troba en constant evolució a mesura que es refinen les cronologies disponibles (Gradstein *et al.*, 2004; Hilgen, 2008). A partir de la cronologia resultant d'aquesta Tesi Doctoral, basada en la biomagnetostratigrafia, es pot anar més enllà en el refinament de l'ETG mitjançant la calibració dels biohoritzons enregistrats en les successions estudiades al llarg del sector central del marge SE de la Conca de l'Ebre. Pel que fa al registre marí, l'estudi biostratigràfic de la sèrie composta de Miralles-La Tossa (Capítol 3.1) contribueix a la intercalibració del nanofòssil calcari i les *Shallow Benthic Zones* de macroforaminífers bartonians-priabonians, així com la seva calibració amb l'escala de temps absolut. Finalment, respecte al registre continental, les associacions de fòssils presents a la Formació Artés contribueixen a la calibració dels nivells de referència de mamífers paleògens europeus (MP) de l'Eocè superior a l' Oligocè basal (Capítol 3.4).

El Domini Marí: Calibració de les Biozonacions de Nanofòssil Calcari i Macroforaminífers Bartonians-Priabonians

Els nanofòssils calcaris formen un grup heterogeni de partícules diminutes (1-30 μm) que constitueixen una fracció important dels sediments marins profunds. En general, s'accepta que el nanofòssil calcari són restes fòssils de les algues unicel·lulars Haptophyceae. La seva identificació en el registre sedimentari ha estat usada amb èxit com a eina de correlació biostratigràfica ja que mostren una distribució biogeogràfica àmplia i presenten ràpides tendències evolutives (Gradstein *et al.*, 2004; Fornaciari *et al.*, 2010). Els esquemes de zonació paleògens més utilitzats són dos, un per a latituds altes i l'altre per a latituds baixes. La zonació NP de Martini (1971) es basa principalment en estudis de seccions exposades en terra de zones temperades, mentre que la zonació CP (Bukry, 1973, 1975; Okada & Bukry, 1980) es va confeccionar a partir de seccions oceàniques de latituds baixes. Estudis d'alta resolució posteriors han redefinit i subdividit aquestes zonacions (Gradstein *et al.*, 2004; i referències contingudes) i, més recentment, Fornaciari *et al.* (2010) han proposat l'aplicació de biohoritzons addicionals per tal de millorar la precisió d'aquestes zonacions com a eina de correlació, ja que els marcadors adoptats en ambdós esquemes de zonació es basen en espècies índex restringides latitudinalment, dependents de les fàcies i/o pobrament definides.

Els macroforaminífers han estat durant molt de temps una eina estratigràfica important en ambients marins soms de les zones tropicals i temperades. Les biozonacions de macroforaminífers es basen idealment en successions de poblacions biomètriques dins de línies filogenètiques, considerant-se les espècies com a unitats morfomètriques (Gradstein *et al.*, 2004). La utilitat d'aquests fòssils com a eina biostratigràfica es feu pal·lesa entre els anys 60 i 80 del segle passat, quan es publicaren un important nombre de monografies sobre els macroforaminífers (Hottinger, 1960, 1977; Schaub, 1981; Less, 1987). Més endavant, Serra-Kiel *et al.* (1998) van publicar una zonació de macroforaminífers del Paleocè i Eocè de la regió del *Tethys*. Cal destacar que a l'ETG2004 (Gradstein *et al.*, 2004) no proporciona una correlació entre la biozonació de macroforaminífers paleògens amb l'ETPG, tot i que Serra-Kiel *et al.* (2003) van fer un intent de calibració magnetostratigràfica basada en les dades de la sèrie de Vic (Burbank *et al.,* 1992). A més, la intercalibració entre les zonacions de nanofòssil calcari i les de macroforaminífers és encara, en certa manera, fragmentària i discontínua, deixant un cert marge per a interpretacions subjectives (Luciani *et al.*, 2002; Gradstein *et al.*, 2004).

A partir de la cronostratigrafia del registre marí de l'Eocè Mitjà-Superior de l'àrea d'Igualada (Fig. 6 del Capítol 3.1 i Fig. 4.2), es fa una revisió de la calibració del nanofòssil

calcari i dels macroforaminífers amb l'ETPG (Gradstein *et al.*, 2004) (Capítol 3.1). La calibració magnetostratigràfica del nanofòssil calcari de la Conca de l'Ebre posa de manifest un desajust amb l'actual calibració de la Zona NP19-20 (Fig. 7 del Capítol 3.1), suggerint que la FO de l'*Isthmolithus recurvus* és un event diacrònic, i per tant, de poca confiança per a establir correlacions a llarga distància. Són particularment rellevants els resultats obtinguts pels macroforaminífers, ja que es canvia la tradicional divisió del Bartonià que constava de dues biozones de macroforaminífers, SBZ17 i SBZ18 (Fig. 7 del Capítol 3.1). Així, la Zona SBZ17 comprèn la major part del Bartonià, mentre que la Zona SBZ18 inclou del Bartonià superior al Priabonià inferior. A més, es proposa la nova Subzona (SBZ18b = Biozona *Nummulites variolarius/incrassatus*), reconeguda tant a la Conca de l'Ebre com a la seccions tipus italianes del Priabonià, mentre que la Subzona SBZ18a seria equivalent a l'anterior Zona SBZ18 de Serra-Kiel *et al.* (1998). Finalment, s'estableix una correlació de la Zona NP19-20 de nanofòssil calcari amb la Zona SBZ18 de macroforaminífers (Bartonià terminal-Priabonià inferior) (Fig. 7 del Capítol 3.1).

El Domini Continental: Calibració dels Nivells de Referència MP de l'Eocè Superior-Oligocè

Durant el Paleogen, les diverses masses continentals posseïen faunes de mamífers terrestres distintives. El fet que aquestes faunes mostren tendències evolutives ràpides, ha propiciat abastament el seu ús com a eina de correlació biostratigràfica en estrats no marins (Gradstein *et al.*, 2004). De tota manera, les correlacions de mamífers fòssils sempre han resultat "més problemàtiques" respecte altres biozonacions, a causa de: *i)* una menor presència de fòssils de mamífers comparats amb altres grups faunístics; *ii)* endemisme; *iii)* el caràcter intrínsecament discontinu dels estrats continentals, que pot fer que la presència de mamífers fòssils es doni en afloraments aïllats i amb relacions de superposició desconegudes. Malgrat tot, s'ha vist que quan existeixen marcs estratigràfics sòlids (sèries llargues i contínues que inclouen altres dades biostratigràfiques i/o ancoratges com els isòtops radiomètrics), les associacions de mamífers fòssils poden representar una eina biostratigràfica valuosa (Woodburne & Swisher, 1995).

Per al Paleogen, l'esquema de zonació utilitzat per a correlacionar les associacions de mamífers fòssils a través d'Europa és l'escala de Mamífers Paleògens (MP). Aquesta consisteix en una llista de nivells de referència (localitats) ordenats per un grau teòric d'evolució, sense límits reals definits entre els nivells de referència successius (Schmidt-Kittler, 1987). És a dir, aquestes unitats no estan definides per l'aparició o desaparició de cap taxó en concret. La primera llista de nivells de referència MP es va elaborar a l'*International Symposium on*

Mammal Stratigraphy of the European Tertiary celebrat a Munich el 1975 (Fahlbusch, 1976). Posteriorment, es van realitzar revisions i actualitzacions a l'*International Symposium on Mammalian Biostratigraphy and Paleoecology of the European Paleogene* celebrat a Mainz el 1987 i al congrés *BiochroM'97* celebrat a Montpellier el 1997 (Schmidt-Kittler, 1987; Aguilar *et al.*, 1997). Al congrés *BiochroM'97* es van reafirmar els acords del simposi de Mainz. Així, les localitats de mamífers fòssils d'Europa podien en principi assignar-se a un nivell de referència MP determinat en funció de les seves afinitats expressades per estadis evolutius.

La calibració de les associacions de mamífers fòssils amb l'ETPG s'ha aconseguit amb èxit en el registre sedimentari extraordinàriament continu de Nord Amèrica gràcies a mètodes radioisotòpics combinats amb magnetostratigrafia (Emry, 1992; Woodburne & Swisher, 1995). A Europa, no obstant, la calibració dels nivells de referència MP s'ha limitat a la Conca de Hampshire (Illa de Wight, Regne Unit), a través de la intercorrelació amb altres biozonacions del registre marí (Hooker, 1992, 2010; Hooker *et al.*, 2004, 2007, 2009; Gale *et al.*, 2006, 2007), o en magnetostratigrafies fragmentàries focalitzades a les localitats de mamífers fòssils de l'oest de França i Espanya (Lévêque, 1993). A la Conca de l'Ebre, estudis magnetostratigràfics previs han aportat un marc cronostratigràfic robust per a correlacionar les localitats de mamífers MP de la Península Ibèrica (Barberà *et al.*, 2001; Beamud *et al.*, 2003).

A partir de la cronostratigrafia del registre continental de l'Eocè superior-Oligocè inferior del marge SE de la Conca de l'Ebre a l'àrea de Vic-Manresa (Fig. 7 del Capítol 3.4 i Fig. 4.2), s'obté una cronologia per a les associacions de mamífers fòssils de l'Eocè superior a l'Oligocè inferior del sector oriental de la Conca de l'Ebre (Capítol 3.4). Les noves dades magnetostratigràfiques de la sèrie composta de Moià-Santpedor, juntament amb la sèrie composta de Rocafort-Vinaixa de Barberà *et al.* (2001), confirmen l'edat Oligocena basal (*ca.* 33.4 Ma) per a la localitat fòssil post-*Grand Coupure* de Sanpedor. Això, a la vegada, reforça l'estreta correlació entre el dràstic canvi de faunes continentals conegut com a *Grande Coupure* (Stehlin, 1910) i la transició Eocè-Oligocè, amb un retràs (màxim) de 0.5 Ma (Fig. 5 del Capítol 3.4). Igual que en altres registres eocens-oligocens d'Euràsia, al sector oriental de la Conca de l'Ebre, la *Grande Coupure* podria coincidir amb un canvi cap a condicions més àrides, tal i com es dedueix de les evidències sedimentològiques (unitats de gresos de Santpedor), que inclouen la incisió de dipòsits de canal de ventall fluvial com a conseqüència del descens del nivell de base a escala regional. A més, la precisa cronologia continental eocena-oligocena de la Conca de l'Ebre permet una interpretació alternativa del registre sedimentari de la Conca

de Hampshire (Illa de Wight, Regne Unit) que reconcilia tota la biostratigrafia marina i continental disponible per a la successió del Grup Solent (Fig.6 del Capítol 3.4). A partir de la integració dels registres de les conques de l'Ebre i de Hampshire, es produeix una calibració basada en magnetostratigrafia de la biocronologia de mamífers europeus de l'Eocè superior-Oligocè (Fig. 7 del Capítol 3.4).

Implicacions Tectonosedimentàries

A partir de la cronologia de les unitats sedimentàries marines i continentals del marge SE de la Conca de l'Ebre (Fig. 4.2), es pot acotar la cronologia dels events tectonosedimentaris que van modelar la Conca de l'Ebre i els cinturons orogènics circumdants. A l'àrea de Montserrat, els Conglomerats de Montserrat (Capítol 3.3) enregistren l'evolució tectònica de les Serralades Costaneres Catalanes. La magnetostratigrafia de Maians-Rubió a la zona d'Igualada (Capítol 3.2) aporta nova informació sobre la cronologia i el caràcter del procés de continentalització de la Conca d'Avantpaís Sudpirinenca. A continuació es presenta un petit resum de les implicacions de l'evolució tectonosedimentària derivades d'aquesta Tesi Doctoral.

Evolució Tectonosedimentària del Sector Central de les Serralades Costaneres Catalanes

A la zona proximal de Montserrat (Capítol 3.3), la nova secció magnetostratigràfica s'usa per realitzar una anàlisi geohistòrica que aporta noves idees sobre la història del desenvolupament de plecs i encavalcaments en aquesta àrea (López-Blanco *et al.*, 2002). Els resultats de l'anàlisi geohistòrica revelen una correlació directa entre la subsidència (tectònica) i els índex de rotació dels flancs d'encavalcament (*forelimbs*) mesurades als estrats deformats dels marges de la conca de l'àrea de Montserrat (Figs. 7 i 8 del Capítol 3.3). La durada de l'estadi de plegament sinsedimentari (López Blanco *et al.*, 2002) s'acota entre el Lutecià superior i el Bartonià mitjà (*ca.* 40.9 a 38.7 Ma) i l'inici de l'estadi d'encavalcaments de fora-seqüència es data com a Bartonià mitjà (*ca.* 38.7 Ma), ajustant la seva durada mínima al voltant de 2.2 Myr (Fig. 8 del Capítol 3.3). L'anàlisi de la subsidència i les corbes d'acumulació suggereixen que durant el plegament sinsedimentari i els estadis d'encavalcaments fora-seqüència la subsidència estaria controlada per la càrrega tectònica, mentre que la càrrega sedimentària hauria tingut una contribució major a la subsidència total durant el darrer estadi.

La integració de les corbes de subsidència de Montserrat amb les corbes de subsidència recalibrades per a altres sectors situats més al centre de conca del sector oriental de la Conca

de l'Ebre (sondatges de Castellfollit i Sanpedor de Vergés *et al.*, 1998), posa de manifest la contribució variable de les càrregues tectòniques de les Serralades Costaneres Catalanes i els Pirineus a l'àrea de Montserrat (Figs. 11 i 12 del Capítol 3.3). A partir d'aquesta integració, es suggereixen tres estadis evolutius durant l'Eocè mitjà i superior a l'àrea de Montserrat (Capítol 3.3). Durant el Lutecià (*ca.* 42 Ma) aquesta àrea formava un marge relativament passiu amb índex de subsidència baixos si es compara amb les àrees més septentrionals, on la subsidència estaria relacionada amb la càrrega dels Pirineus. A partir del Lutecià superior fins al Bartonià superior (*ca.* 40.9 a 38.7 Ma) l'àrea de Montserrat va esdevenir un marge molt actiu amb alts índex de subsidència, afavorint així el desenvolupament d'una flexió de doble vergència associada als dos marges tectònicament actius de la conca, els Pirineus al nord i les Serrades Costaneres Catalanes al sud. Finalment, del Bartonià superior al Priabonià inferior (*ca.* 38.7 a 36.5 Ma), l'homogeneïtzació dels valors de subsidència de l'àrea de Montserrat i de les posicions més properes a centre de conca, s'interpreta com el resultat de la combinació de les dues fonts de càrrega tectònica després de la migració de la flexió pirinenca.

Finalment, a la Fig. 4.3 s'hi representa una comparativa de les taxes d'acumulació dels sediments sense descompactar de l'àrea de Montserrat respecte altres successions al·luvials sinorogèniques d'edat priaboniana i oligocena en altres àrees marginals del SE de la Conca de l'Ebre. Cal destacar que els índex d'acumulació de sediment a Montserrat (de fins a 42 cm/kyr) són notablement més alts que el promig per altres sectors del marge SE de la conca (20 cm/kyr). Aquests patrons d'acumulació diferencials al llarg del sistema Serralades Costaneres Catalanes-Conca de l'Ebre es relacionen amb diferències de subsidència associades a l'estil estructural. Tal i com es discuteix al Capítol 3.3, la zona de Montserrat es caracteritzà per presentar un estil tectònic de caràcter *thick-skinned*, on la deformació s'acomodava en un cinturó estret amb falles profundes d'alt angle que crearen un apilament vertical de les unitats de basament en una zona molt estreta. Com a resultat, la subsidència es focalitzava en una posició pròxima al front muntanyenc. En altres regions de les Serralades Costaneres Catalanes, l'estil tectònic va ser de tipus *thin-skinned*, amb la migració cap a centre de conca del front de deformació. En aquests casos, la subsidència es va distribuir al llarg d'una regió més àmplia davant del front muntanyenc.

Cronologia i Caràcter de la Continentalització de la Conca d'Avantpaís Sudpirinenca

El marc magnetocronològic integrat del sector oriental de la Conca de l'Ebre permet acotar la cronologia del procés de continentalització en aquest sector de la conca en el cron C16n (Fig. 4.2). Al Capítol 3.2, es discuteix la cronologia de la transició marí-continental en la

Conca d'Avantpaís Sudpirinenca occidental en base a la reavaluació dels registres magnetostratigràfics d'Arguis i Salinas (Hogan & Burbank, 1996). Tal i com es mostra a la Fig. 7 del Capítol 3.2, la transició marí-continental a la Conca de Jaca-Pamplona presenta una millor correlació amb el cron C16n. Per tant, tota la informació cronostratigràfica disponible indica que la transició de la sedimentació marina a la continental va ser un esdeveniment ràpid i probablement isòcron a tota la conca, al voltant dels 36 Ma (Priabonià superior). Aquest resultat contrasta amb la natura transgressiva en el temps de les unitats litostratigràfiques en els sistemes d'avantpaís, però és coherent amb un escenari de continentalització de la conca com a resultat del tancament del corredor marí provocat per la càrrega tectònica en els seus marges. Coincidint amb la transició marí-continental, la Conca d'Avantpaís Sudpirinenca va experimentar un increment sobtat de les taxes de sedimentació, de 25 cm/kyr durant l'etapa de sedimentació marina a 63 cm/kyr durant el període de sedimentació continental (Fig. 4.3). Aquest canvi en les taxes de sedimentació s'interpreta com la conseqüència de la interrupció del *bypass* de sediments cap al domini oceànic després del tancament del corredor marí, ja que l'acceleració del creixement de la Zona Axial dels Pirineus Centrals postdata clarament aquest canvi, tal i com han posat de manifest els estudis recents combinant magnetostratigrafia i traces de fissió en apatits de Beamud *et al.* (2011). Durant aquest procés, el solc de Jaca-Pamplona va evolucionar de zona de transferència de sediment a zona de trampa de sediment per a tots els productes de la Zona Axial dels Pirineus Centrals. A més, tal i com es menciona en el Capítol 3.3, el rebliment progressiu de la Conca de l'Ebre podria haver forçat la migració de la deformació cap a l'interior de l'orogen, un escenari plausible i coherent amb la cronostratigrafia i la història de l'exhumació derivada de la termocronologia (Fitzgerald, *et al.*, 1999; Sinclair *et al.*, 2005; Beamud *et al.*, 2011). Per concloure, tal i com es mostra a la Fig. 4.3, al sector oriental de la Conca de l'Ebre, el canvi d'una conca amb drenatge obert a una de tancada no va tenir efectes significatius en les taxes de sedimentació a causa de la configuració paleogeogràfica restringida i a la seva connectivitat limitada amb l'oceà obert.

Referències

AGUILAR, J.P., LEGENDRE, S., MICHAUX, J., (1997). Actes du Congrès BiochroM'97. Mémoires et Travaux de l'Institut de Montpellier de l'École Pratique des Hautes Études, Montpellier. 818pp.

AGUSTÍ, J., ANADÓN, P., ARBIOL, S., CABRERA, L., COLOMBO, F., SÁEZ, A., (1987). Biostratigraphical characteristics of the Oligocene sequences of North-Eastern Spain (Ebro and Campins Basins). *Münchner Geowissenschaftliche Abhandlungen*, **10**, 35-42.

ANADÓN, P., CABRERA, L., CHOI, S.J., COLOMBO, F., FEIST, M., SÁEZ, A., (1992). Biozonación del Paleógeno continental de la zona oriental de la Cuenca del Ebro mediante carófitas;

implicaciones en la biozonación general de carófitas de Europa occidental. *Acta Geologica Hispanica*, **27**, 69-94.

ANADÓN, P., MARZO, M., PUIGDEFÀBREGAS, C., (1985). The Eocene fan-delta of Montserrat (Southeastern Ebro Basin, Spain). In: Milà, M.D., Rosell, J., (Eds.). *6th European Meeting Excursion Guidebook*, pp. 109-146. Institut d´Estudis Ilerdencs, Lleida.

ANADÓN, P., VIANEY-LIAUD, M., CABRERA, L., HARTENBERGER, J.L., (1987). Gisements à vertébrés du paléogène de la zone orientale du bassin de l'Ebre et leur apport à la stratigraphie. *Paleontologia i Evolució*, **21**, 117-131.

ARBIOL, S., SÁEZ, A., (1988). Sobre la edad oligocénica inferior del yacimiento de Santpedor (Cuenca del Ebro, provincia de Barcelona). *Acta Geologica Hispanica*, **23**, 47-50.

AYORA, C., GARCÍA-VEIGAS, J., PUEYO, J.J., (1994). The chemical and hydrological evolution of an ancient potash-forming evaporite basin as constrained by mineral sequence, fluid inclusion composition, and numerical simulation. *Geochemica et Cosmochimica Acta*, **58**, 3379-3394. doi:10.1016/0016-7037(94)90093-0

BARBERÀ, X., CABRERA, L., MARZO, M., PARÉS, J.M., AGUSTÍ, J., (2001). A complete terrestrial Oligocene magnetostratigraphy from the Ebro Basin, Spain. *Earth and Planetary Science Letters*, **187**, 1-16. doi: 10.1016/S0012-821(01)00270-9

BEAMUD, E., GARCÉS, M., CABRERA, L., MUÑOZ, J.A., ALMAR, Y., (2003). A new middle to late Eocene continental chronostratigraphy from NE Spain. *Earth and Planetary Science Letters*, **216**, 501-514. doi: 10.1016/S0012-821X(03)00539-9

BEAMUD, E., MUÑOZ, J.A., FITZGERALD, P.G., BALDWIN, S.L., GARCÉS, M., CABRERA, L., METCALF, J.R., (2011). Magnetostratigraphy and detrital apatite fission track thermochronology in syntectonic conglomerates: constraints on the exhumation of the South-Central Pyrenees. *Basin Research*, **23**, 309-331. doi: 10.1111/j.1365-2117.2010.00492.x

BUKRY, D., (1973). Low latitude coccolith biostratigraphic zonation. In: Edgar, N., Kaneps, A., Herring, J., (Eds.). *Initial Reports of the Deep Sea Drilling Project*, **15**, pp. 658-677. Washington DC. doi:10.2973/dsdp.proc.15.116.1973

BUKRY, D., (1975). Coccolith and silicoflagellate stratigraphy, northwestern Pacific Ocean. In: Gardner, J., (Ed.). *Initial Reports of the Deep Sea Drilling Project*, **32**, pp. 677-701. Washington DC. doi:10.2973/dsdp.proc.32.124.1975

BURBANK, D.W., PUIGDEFÀBREGAS, C., MUÑOZ, J.A., (1992). The chronology of the Eocene tectonic and stratigraphic development of the eastern Pyrenean foreland basin, northeast Spain. *Gelogical Society of America Bulletin*, **104**, 1101-1120. doi: 10.1130/0016-7606(1992)104<1101:TCOTET>2.3.CO;2

CASCELLA, A., DINARÈS-TURELL, J., (2009). Integrated calcareous nannofossil biostratigraphy and magnetostratigraphy from the uppermost marine Eocene deposits of the southeastern pyrenean foreland basin: evidences for marine Priabonian deposition. *Geological Acta*, **7**, 281-296. doi: 10.1344/105.000000282

CENDÓN, D.I., AYORA, C., PUEYO, J.J., TABERNER, C., (2003). The geochemical evolution of the Catalan potash subbasin, South Pyrenean foreland basin (Spain). *Chemical Geology*, **200**, 339-357. doi: 10.1016/S0009-2541(03)00195-5

COSTA, E., GARCÉS, M., LÓPEZ-BLANCO, M., BEAMUD, E., GÓMEZ-PACCARD, M., LARRASOAÑA, J.C., (2010). Closing and continentalization of the South Pyrenean foreland Basin (NE Spain): Magnetochronological constraints. *Basin Research*, **22**, 904-917. doi: 10.1111/j.1365-2117.2009.00452.x

COSTA, E., GARCÉS, M., LÓPEZ-BLANCO, M., SERRA-KIEL, J., BERNAOLA, G., CABRERA, L., BEAMUD, E., (*accepted*). The Bartonian-Priabonian marine record of the eastern South Pyrenean Foreland Basin (NE Spain): A new calibration of the larger foraminifers and calcareous nannofossil biozonation. *Geologica Acta*.

COSTA, E., GARCÉS, M., SÁEZ, A., CABRERA, L., LÓPEZ-BLANCO, M., (2011). The age of the "Grande Coupure" mammal turnover: New constraints from the Eocene-Oligocene record of the

Eastern Ebro Basin (NE Spain). *Palaeogeography, Palaeoclimatology, Palaeoecology*, **301**, 97-107. doi: 10.1016/j.palaeo.2011.01.005

EMRY, R.J., (1992). Mammalian range zones in the Chadronian White River Formation at Flagstaff Rim, Wyoming. In: Prothero, D.R., Berggren, W.A., (Eds.). *Eocene-Oligocene Climatic and Biotic Evolution*, pp. 106-115. Princeton University Press, Princeton.

FAHLBUSCH, V., (1976). Report on the International Symposium on Mammalian Stratigraphy of the European Tertiary. *Newsletters on Stratigraphy*, **5**, 160-167.

FERRER, J., (1971a). El Paleoceno y Eoceno del borde suroriental de la Depresión del Ebro (Cataluña). *Mémoires suisses de Paléontologie*, **90**, 1-70.

FERRER, J., (1971b). Presencia de macroforaminíferos priabonienses en el Eoceno de Igualada. *Acta Geologica Hispanica*, **6**, 4-7.

FITZGERALD, P.G., MUÑOZ, J.A., CONEY, P.J., BALDWIN, S.L., (1999). Asymmetric exhumation across the Pyrenean orogen: implications for the tectonic evolution of a collisional orogen. *Earth and Planetary Science Letters*, **173**, 157-170. doi: 10.1016/S0012-821X(99)00225-3

FORNACIARI, E., AGNINI, C., CATANZARITI, R., RIO, D., BOLLA, E.M., VALVASONI, E., (2010). Mid-Latitude calcareous nannofossil biostratigraphy and biochronology across the middle to late Eocene transition. *Stratigraphy*, **7**, 229-264.

GALE, A.S., HUGGETT, J.M., LAURIE, E., (2007). Discussion on the Eocene-Oligocene boundary in the UK. *Journal*, Vol. 163, pp. 401-415. *Journal of the Geological Society*, **164**, 685-688. doi: 10.1144/0016-76492006-098

GALE, A.S., HUGGETT, J.M., PÄLIKE, H., LAURIE, E., HAILWOOD, E.A., HARDENBOL, J., (2006). Correlation of Eocene-Oligocene marine and continental records: orbital, cyclicity, magnetostratigraphy and sequence stratigraphy of the Solent Group, Isle of Wight, UK. *Journal of the Geological Society*, **163**, 401-415. doi: 10.1144/0016-764903-175

GÓMEZ-PACCARD, M., LÓPEZ-BLANCO, M., COSTA, E., GARCÉS, M., BEAMUD, E., LARRASOAÑA, J.C., (*submitted*). Tectonic and climatic controls on the sequential arrangement of an alluvial fan/fan-delta complex (Montserrat, Eocene, Ebro basin, NE Spain). *Basin Research*.

GRADSTEIN, F.M., OGG, J.G., SMITH, A.G., (2004). *A Geologic Time Scale 2004*. Cambridge University Press, Cambridge. 589pp.

GUIMERÀ, J., (1984). Paleogene evolution of deformation in the northeastern Iberian Peninsula. *Geological Magazine*, **121**, 413-420. doi: 10.1017/S0016756800029940

HILGEN, F.J., (2008). Recent progress in the standardization and calibration of Cenozoic Time Scale. *Newsletters on Stratigraphy*, **43**, 15-22. doi: 10.1127/0078-0421/2008/0043-0015

HOGAN, P.J., BURBANK, D.W., (1996). Evolution of the Jaca piggyback basin and emergence of the External Sierra, southern Pyrenees. In: Friend, P.F., Dabrio, C.J., (Eds.). *Tertiary basins of Spain. The stratigraphic record of crustal kinematics*, pp. 153-160. Cambridge University Press, Cambridge.

HOOKER, J.J., (1992). British mammalian paleocommunities across the Eocene–Oligocene transition and their environmental implications. In: Prothero, D.R., Berggren, W.A., (Eds.). *Eocene-Oligocene Climatic and Biotic Evolution*, pp. 494-515. Princeton University Press, Princeton.

HOOKER, J.J., (2010). The "Grande Coupure" in the Hampshire Basin, UK: taxonomy and stratigraphy of the mammals on either side of this major Paleogene faunal turnover. In: Whittaker, J.E., Hart, M.B., (Eds.). *Micropalaeontology, Sedimentary Environments and Stratigraphy: A Tribute to Dennis Curry (1912–2001)*, pp. 147–215. The Micropalaeontological Society, Special Publications. doi: 10.1144/TMS004.8

HOOKER, J.J., COLLINSON, M.E., GRIMES, S., SILLE, N., MATTEY, D., (2007). Discussion on the Eocene-Oligocene boundary in the UK. *Journal*, Vol. 163, 2006, pp.401-415. *Journal of the Geological Society*, **164**, 685-688. doi: 10.1144/0016-7692006-098.

HOOKER, J.J., COLLINSON, M.E., SILLE, N., (2004). Eocene-Oligocene mammalian faunal turnover in the Hampshire Basin, UK: calibration to the global time scale and the major cooling event. *Journal of the Geological Society*, **161**, 161-172. doi: 10.1144/0016-764903-091

HOOKER, J.J., GRIMES, S.T., MATTEY, D.P., COLLINSON, M.E., SHELDON, N.D., (2009). Refined correlation of the UK Late Eocene-Early Oligocene Solent Group and timing of its climate history. In: Koeberl, C., Montanari, A., (Eds.). *The Late Eocene Earth-Hothouse, Icehouse and Impacts*, pp. 179-195. The Geological Society of America, Special Paper 452. doi: 10.1130/2009.2452(12)

HOTTINGER, L., (1960). Recherches sur les Alvéolines du Paléocène et de l'Éocène. *Mémoires suisses de Paléontologie*, **75/76**, 1-243.

HOTTINGER, L., (1977). Foraminifères operculiniformes. *Mémoires du Museum National d'Histoire Naturelle de Paris*, **C40**, 1-159.

LESS, G., (1987). The zonation of the Mediterranean Upper Paleocene and Eocene by Orthophragminae. *Slovenska Akademija Znanosti in Umetnosti, Razred za Naravoslovne Vede Dela*, **34**, 21-43.

LÉVÊQUE, F., (1993). Correlating the Eocene-Oligocene mammalian biochronological scale from SW Europe with the marine magnetic anomaly sequence. *Journal of Geological Society of London*, **150**, 661-664. doi: 10.1144/gsjgs.150.4.0661

LÓPEZ-BLANCO, M., (2002). Sedimentary response to thrusting and fold growing on the SE margin of the Ebro basin (Paleogene, NE Spain). *Sedimentary Geology*, **146**, 133-154. doi: 10.1016/S0037-0738(01)00170-1

LÓPEZ-BLANCO, M., (2006). Stratigraphic and tectonosedimentary development of the Eocene Sant Llorenç del Munt and Montserrat fan-delta complexes (Southeast Ebro basin margin, Northeast Spain). *Contributions to Science*, **3,** 125-148. doi: 10.2436/20.7010.01.1

LÓPEZ-BLANCO, M., MARZO, M., BURBANK, D.W., VERGÉS, J., ROCA, E., ANADÓN, P., PIÑA, J., (2000a). Tectonic and climatic controls on the development of foreland fan deltas: Montserrat and Sant Llorenç del Munt systems (Middle Eocene, Ebro Basin, NE Spain). *Sedimentary Geology*, **138**, 17-39. doi: 10.1016/S0037-0738(00)00142-1

LÓPEZ BLANCO, M., MARZO, M., PIÑA, J., (2000b). Transgressive-regressive sequence hierachy of foreland, fan-delta clastic wedges (Montserrat and Sant Lloarenç del Munt, Middle Eocene, Ebro Basin, NE Spain). *Sedimentary Geology*, **138**, 41-69. doi: 10.1016/S0037-0738(00)00143-3

LUCIANI, V., NEGRI, A., BASSI, D., (2002). The Bartonian-Priabonian transition in the Mossano section (Colli Berici, north-eastern Italy): a tentative correlation between calcareous plankton and shallow-water benthic zonations. *Geobios*, **35**, Supplement 1, 140-149. doi: 10.1016/S0016-6995(02)00055-4

MARTINI, E., (1971). Standard Tertiary and Quaternary calcareous nannoplankton zonation. In: Farinaci, A., (Ed.). *Proceedings of the II Planktonic Conference, Roma 1970, vol. 2*, pp. 739-785. Edizioni Tecnoscienza, Roma.

OKADA, H., BUKRY, D., (1980). Supplementary modification and introduction of code numbers to the low-latitude coccolith biostratigraphic zonation (Buckry, 1973; 1975). *Marine Micropaleontology*, **5**, 321-325. doi: 10.1016/0377-8398(80)90016-X

PUIGDEFÀBREGAS, C., SOUQUET, P., (1986). Tecto-sedimentary cycles and depositional sequences of the Mesozoic and Tertiary from the Pyrenees. *Tectonophysics*, **129**, 173-203. doi: 10.1016/0040-1951(86)90251-9

RIBA, O., REGUANT, S., VILLENA, J., (1983). Ensayo de síntesis estratigráfica y evolutiva de la cuenca terciaria del Ebro. In: Comba, J.A., (Ed.). *Geología de España. Libro Jubilar J.M. Ríos, Tomo II*, pp. 131-159. Instituto Geológico y Minero de España, Madrid.

SÁEZ, A., (1987). Estratigrafía y sedimentología de las formaciones lacustres del tránsito Eoceno-Oligoceno del noreste de la cuenca del Ebro. PhD-Thesis, Universitat de Barcelona. 353pp.

SCHAUB, H., (1981). Nummulites et Assilines de la Tethys Paléogène. Taxonomie, phylogénèse et biostratigraphie. *Mémoires suisses de Paléontologie*, **104/105/106**, 1-236.

SCHMIDT-KITTLER, N., (1987). European reference levels and correlation tables. *Münchener Geowissenschaftliche Abhandlungen*, **10**, 13–32.

SERRA-KIEL, J., HOTTINGER, L., CAUS, E., DROBNE, K., FERRÀNDEZ-CAÑADELL, C., JAUHRI, A.K., LESS, G., PAVLOVEC, R., PIGNATTI, J., SAMSÓ, J.M., SCHAUB, H., SIREL, E., STROUGO, A., TAMBAREAU, Y., TOSQUELLA, J., ZAKREVSKAYA, E., (1998). Larger Foraminiferal Biostratigraphy of the Tethyan Paleocene and Eocene. *Bulletin de la Societé géologique de France*, **169**, 281-299.

SERRA-KIEL, J., TRAVÉ, A., (1995). Lithostratigraphic and chronostratigraphic framework of the Bartonian sediments in the Vic and Igualada areas. In: Perejón, A., Busquets, P., (Eds.). *Field Trip C: Bioconstructions of the Eocene South Pyrenean Foreland Basin (Vic and Igualada Areas) and the Upper Cretaceous South Central Pyrenees (Tremp Area). VII International Symposium on Fossil Cnidaria and Porifera*, pp. 11-14., Madrid.

SERRA-KIEL, J., TRAVÉ, A., MATÓ, E., SAULA, E., FERRÀNDEZ-CAÑADELL, C., BUSQUETS, P., TOSQUELLA, J., VERGÉS, J., (2003). Marine and Transitional Middle/Upper Eocene Units of the Southeastern Pyrenean Foreland Basin (NE Spain). *Geologica Acta*, **1**, 177-200.

SINCLAIR, H.D., GIBSON, M., NAYLOR, M., MORRIS, R.G., (2005). Asymmetric growth of the Pyrenees revealed through measurement and modeling of orogenic fluxes. *American Journal of Science*, **305**, 369-406. doi: 10.2475/ajs.305.5.369

STEHLIN, H.G., (1910). Remarques sur les faunules de Mammifères des couches Éocènes et Oligocènes du Bassin de Paris. *Bulletin de la Société Géologique de France*, **9**, 488–520.

TABERNER, C., DINARÈS-TURELL, J., GIMÉNEZ, J., DOCHERTY, C., (1999). Basin infill architecture and evolution from magnetostratigraphic cross-basin correlations in the southeastern Pyrenean foreland basin. *Geological Society of America Bulletin*, **111**, 1155-1174. doi: 10.1130/0016-7606(1999)111<1155:BIAAEF>2.3.CO;2

VERGÉS, J., FERNÀNDEZ, M., MARTÍNEZ, A., (2002). The Pyrenean orogen: pre-, syn-, and post-collisional evolution. In: Rousenbaum, G., Lister, G.S., (Eds.). Reconstruction of the Evolution of the Alpine-Himalayan Orogen. *Journal of the Virtual Explorer*, **8**, 55-74.

VERGÉS, J., MARZO, M., SANTAEULÀRIA, T., SERRA-KIEL, J., BURBANK, D.W., MUÑOZ, J.A., GIMÉNEZ-MONTSANT, J., (1998). Quantified vertical motions and tectonic evolution of the SE Pyrenean foreland basin. In: Mascle, A., Puigdefàbregas, C., Luterbacher, M., (Eds.). *Cenozoic Foreland Basins of Western Europe*. Geological Society, Special Publication, **134**, 107-134.

WOODBURNE, M.O., SWISHER, C.C. III, (1995). Land mammal high-resolution geochronology, intercontinental overland dispersals, sea level, climate, and vicariance. In: Berggren, W.A., Kent, D.V., Aubry, M.P., Hardenbol, J., (Eds.). *Geochronology, Time Scales and Global Stratigraphic Correlation.* Society for Sedimentary Geology, SEPM Special Publication, **54**, 335-364.

MOTIVATION, OBJECTIVES AND STRUCTURE OF THE THESIS

TIME (noun) 1. A period or interval. 2. The period between two events or during which something exists, happens or acts; measured or measurable interval.
Concise Oxford English Dictionary

GEOLOGIC TIME. The period of time dealt with by historical geology, or the time extending from the end of the formative period of the Earth as a separate planetary body to the beginning of written or human history; the part of Earth's history that is represented by and recorded in the succession of rocks.
Glossary of Geology

Motivation and Objectives

In Earth science research, once a good age-control is achieved, rates of change in geodynamic systems such as foreland basins and their adjacent orogenic belts are feasible, and therefore unraveling cause-effect relationships can be established. In the same way, correlation with the global record can also be attained. The sedimentary record of a foreland basin constitutes thus an archive of the history of the evolution of its margins and also of the Earth-system by recording tectonic and/or climatic processes.

The stratigraphic record of the Ebro Basin, in NE Spain, is particular among circum-Mediterranean alpine foreland basins. It records the evolution of the NE Iberian plate during the Cenozoic, evolving from marine conditions into a land-locked closed basin since the Late Eocene (Riba *et al.*, 1983; Vergés *et al.*, 2002). After the closure of the basin, an exceptionally thick succession of up to 5000 m of alluvial, fluvial and lacustrine sediments was deposited for a period of 25 Myr. In order to interpret this record in terms of tectonosedimentary and paleoclimatic evolution a precise time frame of the sedimentary units at a basin scale and a correlation with the global record is needed. Earlier attempts to build biomagnetochronostratigraphy-based chronologies of this region were focused on either the marine (Burbank *et al.*, 1992; Taberner *et al.*, 1999; López-Blanco *et al.*, 2000; Cascella & Dinarès-Turell, 2009) or the continental fossil record (Barberà *et al.*, 2001), but full integration of all chronostratigraphic tools (marine and continental biostratigraphy and magnetostratigraphy) was to date not achieved.

The main objective of this PhD-Thesis is to obtain an integrated bio-magnetochronology of the Paleogene sedimentary units of the Ebro Basin. By building a robust chronostratigraphic framework this Thesis contributes to the comprehension of the factors that have influenced the evolution of the Ebro Basin and its adjacent margins, as well as biochronological

implications derived from the correlation with the geomagnetic polarity time scale. Thus, specific objectives of this PhD-Thesis are:

i. to obtain a robust and independent magnetostratigraphy-based chronology of the Middle Eocene-Lower Oligocene marine and continental units of the Eastern Ebro Basin

ii. to calibrate to the geomagnetic polarity time scale the Bartonian and Priabonian larger foraminifers and calcareous nannofossil biozonations

iii. to calibrate the Late Eocene-Oligocene European mammal biochronology (MP reference levels) further bracketing the age of the *Grande Coupure*, a major terrestrial faunal turnover recorded in Eurasia associated with the climate shift of the Eocene-Oligocene transition

iv. to constrain the timing and nature of the final marine-continental process of the Ebro Basin

Structure

This PhD-Thesis, prepared under the modality of a compilation of published and submitted papers indexed in the *Journal Citation Report* of the *Institute for Scientific Information*, is composed by 5 Chapters. A first introductory Chapter 1 presents the geological setting of the South Pyrenean Foreland Basin and its margins including an overview of the previous works carried out in this region. In Chapter 2 the methodology used in this PhD-Thesis is described with further detail than presented in papers of Chapter 3.

In Chapter 3 the results of this PhD-Thesis are presented. It includes 4 papers; two of them already published, one accepted for publication, and the fourth currently under the revision process. Chapter 3.1 constitutes the first scientific paper of this PhD-Thesis: *Costa, E., Garcés, M., López-Blanco, M., Serra-Kiel, J., Bernaola, G., Cabrera, L., Beamud, E., (accepted). The Bartonian-Priabonian marine record of the Eastern South Pyrenean Foreland Basin (NE Spain): A new calibration of the larger foraminifers and calcareous nannofossil biozonation. Geologica Acta.* In this chapter an integrated biostratigraphic (calcareous nannofossil, larger foraminifers) and magnetostratigraphic study of the Late Eocene marine units of the Igualada area (Eastern Ebro Basin) has resulted in a new chronology for the marine units of this area that challenges existing chronostratigraphic interpretations, and provides a new calibration of the calcareous nannofossil and larger foraminifers biozonations.

Chapter 3.2 constitutes the second scientific paper of this PhD-Thesis: *Costa, E., Garcés, M., López-Blanco, M., Beamud, E., Gómez-Paccard, M., Larrasoaña, J.C., (2010). Closing and continentalization of the South Pyrenean foreland basin (NE Spain): magnetochronological constraints. Basin Research, 22, 904-917.* In this chapter an independent magnetostratigraphy-based chronology has been integrated with existing, here re-interpreted, magnetostratigraphic records of the South Pyrenean Foreland Basin. This has resulted in a high-resolution chronology of the process of continentalization of the Ebro Basin that helps constraining its context and forcing factors.

The PhD candidate is coauthor of Chapter 3.3: *Gómez-Paccard, M., López-Blanco, M., Costa, E., Garcés, M., Beamud, E., Larrasoaña, J.C., (submitted). Tectonic and climatic controls on the sequential arrangement of an alluvial fan/fan-delta complex (Montserrat, Eocene, Ebro basin, NE Spain). Basin Research.* In this chapter a magnetostratigraphy-based chronological framework has been used to further constrain the timing of the architectural arrangement of the Eocene sediments from the Montserrat alluvial fan and fan-delta complex, and for assessing the subsidence and tectonosedimentary history of the central SE margin of the Ebro Basin. The Montserrat chronology has been used to investigate the interplay between factors controlling the deposition at different temporal scales, orbital (Milankovitch) forcing included.

Chapter 3.4 constitutes the third and final scientific paper of this PhD-Thesis: *Costa, E., Garcés, M., Sáez, A., Cabrera, L., López-Blanco, M., (2011). The age of the "Grande Coupure" mammal turnover: New constraints from the Eocene-Oligocene record of the Eastern Ebro Basin (NE Spain). Palaeogeography, Palaeoclimatology, Palaeoecology, 301, 97-107.* This chapter presents a magnetostratigraphy-based chronology of a continental succession along the Eocene-Oligocene record of the Eastern Ebro Basin which has yield accurate ages for the immediately pre- and post-*Grand Coupure* mammal fossil assemblages found in this sector of the basin. These results, together with other relevant European Eocene-Oligocene records have been used to calibrate the Mammal Paleogene reference levels MP18 to MP21.

Chapter 4 has been conceived as an integrative discussion of the obtained results presented in Chapter 3. Finally, concluding remarks of this PhD-Thesis are presented in Chapter 5.

References

BARBERÀ, X., CABRERA, L., MARZO, M., PARÉS, J.M., AGUSTÍ, J., (2001). A complete terrestrial Oligocene magnetostratigraphy from the Ebro Basin, Spain. *Earth and Planetary Science Letters*, **187**, 1-16. doi: 10.1016/S0012-821(01)00270-9

BATES, R.L., JACKSON, J.A., (1987). *Glossary of Geology, 3rd Edition*. American Institute of Geology, Alexandria (VI). 788pp.

BURBANK, D.W., PUIGDEFÀBREGAS, C., MUÑOZ, J.A., (1992). The chronology of the Eocene tectonic and stratigraphic development of the eastern Pyrenean foreland basin, northeast Spain. *Gelogical Society of America Bulletin*, **104**, 1101-1120. doi: 10.1130/0016-7606(1992)104<1101:TCOTET>2.3.CO;2

CASCELLA, A., DINARÈS-TURELL, J., (2009). Integrated calcareous nannofossil biostratigraphy and magnetostratigraphy from the uppermost marine Eocene deposits of the southeastern pyrenean foreland basin: evidences for marine Priabonian deposition. *Geological Acta*, **7**, 281-296. doi: 10.1344/105.000000282

COSTA, E., GARCÉS, M., LÓPEZ-BLANCO, M., BEAMUD, E., GÓMEZ-PACCARD, M., LARRASOAÑA, J.C., (2010). Closing and continentalization of the South Pyrenean foreland Basin (NE Spain): Magnetochronological constraints. *Basin Research*, **22**, 904-917. doi: 10.1111/j.1365-2117.2009.00452.x

COSTA, E., GARCÉS, M., LÓPEZ-BLANCO, M., SERRA-KIEL, J., BERNAOLA, G., CABRERA, L., BEAMUD, E., (*accepted*). The Bartonian-Priabonian marine record of the eastern South Pyrenean Foreland Basin (NE Spain): A new calibration of the larger foraminifers and calcareous nannofossil biozonation. *Geologica Acta*.

COSTA, E., GARCÉS, M., SÁEZ, A., CABRERA, L., LÓPEZ-BLANCO, M., (2011). The age of the "Grande Coupure" mammal turnover: New constraints from the Eocene-Oligocene record of the Eastern Ebro Basin (NE Spain). *Palaeogeography, Palaeoclimatology, Palaeoecology*, **301**, 97-107. doi: 10.1016/j.palaeo.2011.01.005

GÓMEZ-PACCARD, M., LÓPEZ-BLANCO, M., COSTA, E., GARCÉS, M., BEAMUD, E., LARRASOAÑA, J.C., (*submitted*). Tectonic and climatic controls on the sequential arrangement of an alluvial fan/fan-delta complex (Montserrat, Eocene, Ebro basin, NE Spain). *Basin Research*.

LÓPEZ-BLANCO, M., MARZO, M., BURBANK, D.W., VERGÉS, J., ROCA, E., ANADÓN, P., PIÑA, J., (2000). Tectonic and climatic controls on the development of foreland fan deltas: Montserrat and Sant Llorenç del Munt systems (Middle Eocene, Ebro Basin, NE Spain). *Sedimentary Geology*, **138**, 17-39. doi: 10.1016/S0037-0738(00)00142-1

RIBA, O., REGUANT, S., VILLENA, J., (1983). Ensayo de síntesis estratigráfica y evolutiva de la cuenca terciaria del Ebro. In: Comba, J.A., (Ed.). *Geología de España. Libro Jubilar J.M. Ríos, Tomo II*, pp. 131-159. Instituto Geológico y Minero de España, Madrid.

SOANES, C., STEVENSON, A., (2004). *Concise Oxford English Dictionary, 11th Edition*. Oxford University Press, Oxford. 1708pp.

TABERNER, C., DINARÈS-TURELL, J., GIMÉNEZ, J., DOCHERTY, C., (1999). Basin infill architecture and evolution from magnetostratigraphic cross-basin correlations in the southeastern Pyrenean foreland basin. *Geological Society of America Bulletin*, **111**, 1155-1174. doi: 10.1130/0016-7606(1999)111<1155:BIAAEF>2.3.CO;2

VERGÉS, J., FERNÀNDEZ, M., MARTÍNEZ, A., (2002). The Pyrenean orogen: pre-, syn-, and post-collisional evolution. In: Rousenbaum, G., Lister, G.S., (Eds.). Reconstruction of the Evolution of the Alpine-Himalayan Orogen. *Journal of the Virtual Explorer*, **8**, 55-74.

CHAPTER 1:

INTRODUCTION

Building an integrated basin-scale chronostratigraphy is a challenge that requires, first, an understanding of geologic time and how Earth scientists measure it. Second, an exhaustive update of the regional stratigraphic setting must be compiled, so that all previous litho-, bio-, and magnetostratigraphic data are conveniently interpreted, or re-interpreted, in the light of the new data before a new integrative proposal is put forward. In this chapter, a brief introduction to the Geologic Time Scale (GTS) and related dating methods, as well as the geological context of the Eastern Ebro Basin is provided.

1.1. Geologic Time and the Geologic Time Scale: an Essential Framework in Geology

Geology is a science which traditionally has been divided into two disciplines, the physical geology and the historical geology. Physical geology deals with the study of Earth-forming materials, and its goal is to understand the processes that take place both on the surface of the Earth and its interiors. On the other hand, the main objective of historical geology is to study the origin and evolution of the Earth through time, therefore to establish a chronology of the several physical, chemical, and biological changes which have taken place in the Earth during the past. The time variable in geological studies is thus an essential framework.

1.1.1. A Bit of History: Relative Dating

Current radioactive decay calculations assign an age of the Earth of *ca.* 4600 Ma. However, during the XIX century and before the development of the radiometric techniques (Holmes, 1937, 1947), a GTS was established by *Relative Dating* using laws and principles such as the *Law of Superposition* and the *Principle of Biotic Succession* (Tarbuck & Lutgens, 1999). Hutton, a Scottish geologist, first proposed formally the fundamental principle used to classify rocks according to their relative ages (Newman, 1997). After studying rocks at many outcrops, Hutton concluded that each layer represented a specific interval of geologic time. Further, he proposed that wherever untwisted layers were exposed, the bottom layer was deposited first, being thus the oldest layer. Therefore, each succeeding layer, up to the topmost one, was progressively younger. William Smith, a civil engineer and surveyor, was familiar with areas in Southern England where *"…limestone and shales are layered like slices of bread and butter"* (Newman, 1997). His hobby of collecting and cataloging fossil shells from these rocks led to the discovery that certain layers contained fossils unlike those in other layers. Using these index

fossils as markers, Smith could identify a particular layer of rock wherever it was exposed, establishing thus first biostratigraphic correlation exercises.

1.1.2. Linking Time and Rock: Chronostratigraphic Units, Geochronologic Units, and GSSP

The use of the fragmentary chapters in the history of life and the regional sediment facies ("rock-time" or *chronostratigraphic units*) gave rise to the succession of standard geologic periods and subdivisions of periods into stages that form the *chronostratigraphic time scale* (Gradstein *et al.*, 2004). In its classical usage, each geologic stage was delimited at a *stratotype* to indicate its idealized extent and fossil contents. The historical development of stratigraphy in old Europe favored the use of regional marginal marine to pelagic successions to define the chronostratigraphic units. This influence is still notable in their names (*e.g.* the term *Jura Kalkstein* was applied by Alexander von Humboldt in 1799 to a series of carbonate shelf deposits exposed in the northernmost Swiss region of Jura to distinguish them from the *German Muschelkalk*; Ogg, 2004). Noteworthy, the geologic record is discontinuous, and these stratotype-based chronostratigraphic units are an imperfect record of the continuum of geological time. Therefore, a distinction between the hierarchy of material chronostratigraphic units ("rock-time") and abstract *geochronological units* (Earth time), which are measured in years from the rock record by radioactive decay or by correlation of the observable cyclicity in the sedimentary record to the astronomical ephemeredes, was required.

In the Phanerozoic, geochronologic and chronostratigraphic scales are now united by formally establishing markers within continuous intervals on the stratigraphic record to define the beginning of each successive chronostratigraphic unit and their associate geochronological units by means of the *Global Stratotype Section and Point* (GSSP). Thus, synchronous events over the world such as geomagnetic reversals, a global change in a stable isotope value, or the evolutionary appearance/disappearance of one or more prominent widespread fossil taxa are used to define a GSSP. Each successive pair of GSSPs in the rock record precisely defines the associated subdivision of geological time, enhancing their value as standard units in chronostratigraphy and ultimately in geochronology. Therefore, the GSSP concept has actually replaced the earlier use of "stage stratotypes", and has enabled the standard globally applicable geological time-scale, which is cosponsored by the *International Comission on Stratigraphy* (Gradstein *et al.*, 2004; Gradstein & Ogg, 2005). Updated information on the location, definition, the global correlation events, and the status of the GSSP points can be found in the *International Comission on Stratigraphy* website (http://www.stratigraphy.org), as well as the requirements for establishing them.

1.1.3. Building the Geologic Time Scale

The ideal Phanerozoic time-scale is built from accurate radioisotopic ages, taken precisely at stage boundaries thorough the stratigraphic column (Gradstein & Ogg, 2005). Basically, two measuring tools exist to build the linear geological time-scale. These are stratigraphically meaningful radiometric dates, measured in millions of years (Myr), and the Earth-orbit-tunned sedimentary cycles, measured in thousands of years (kyr). Moreover, outcrop (or core) sections suitable for dating with the occurrence of index fossils, recorded geomagnetic reversals, and/or stable isotope anomalies, *etc.* are also required. Merging the obtained geochronometric and chronostratigraphic scales through a calibration process, results in the construction of a geological time-scale (Fig. 1.1).

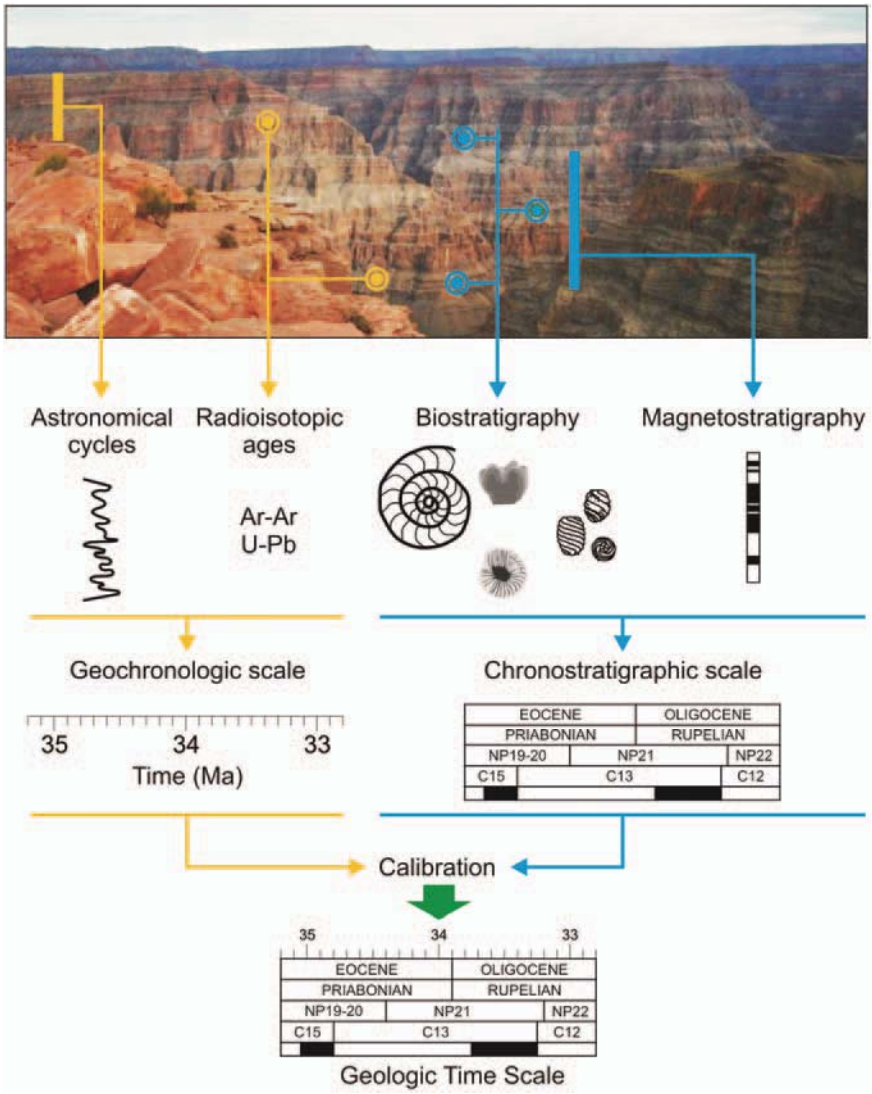

Figure 1.1. Geologic Time Scale. Its construction is the merger of a geochronologic (measured in years) and chronostratigraphic (formalized definitions of geologic stages, biostratigraphic zonation units, magnetic polarity zones, and other subdivisions of the rock record) scales.

First chapters of Gradstein *et al.* (2004) are focused on the process of building a geological time-scale and further provide an exhaustive description of the different techniques involved in the process. Also Gradstein & Ogg (2005) shortly summarize the steps required in modern geological time-scale construction, the behind work needed, and an historical perspective of how the procedures have evolved. These steps are the following:

i) construct an updated global chronostratigraphic scale of the Earth's rock record

ii) identify key linear-ages calibration levels for the chronostratigraphic scale using radioisotopic age dates

iii) apply Earth-orbit tuning to intervals with cyclic sediments or stable isotope sequences that have sufficient bio- or magnetostratigraphic ties

iv) interpolate the combined chronostratigraphic and chronometric scale when direct information is insufficient

v) calculate or estimate error bars on the combined chronostratigraphic and geochronometric information to obtain a geological time-scale with estimates of uncertainty on boundaries and on unit durations

vi) peer-review the resultant geological time-scale

Once all these steps are concluded a new GTS is born. However, this geological time-scale does not constitute the "definitive" geological time-scale. Instead the resultant GTS is under permanent evolution (Gradstein *et al.*, 2004; Hilgen, 2008). Improved updates of the Earth insolation curve solutions include now more geologically meaningful constraints, extending the astronomical scale back to the Oligocene and Eocene by applying a combination of cyclostratigraphy, magnetostratigraphy, and isotope stratigraphy (Pälike *et al.*, 2006; Jovane *et al.*, 2010; Laskar *et al.*, in press). Calibration of the decay constants or measurement standards can be enhanced by intercalibration to other radioisotopic methods, or by dating rocks of known age (*e.g.*, a volcanic ash within an astronomically tuned section; Kuiper *et al.*, 2008). Despite progress in the standardization and dating, occurrence of ash layers being able to provide accurate radioisotopic date from each stage boundary is sparse. Therefore, bio-, magneto-, and chronostratigraphy still play an important role by providing the principal fabric for stretching the relative time-scale between dated tie points on the loom of the linear time (Gradstein & Ogg, 2005).

1.2. Regional Setting

The present-day geology of NE Iberia (Fig. 1.2) has resulted from two successive plate-tectonic scenarios. First, the Late Cretaceous to Miocene convergence and continental collision between the Iberian and Eurasian plates (Anadón & Roca, 1996), which led to the growth of the Pyrenean thrust belt at the plate boundary as well as the growth of the intraplate Catalan Coastal Ranges and Iberian Range thrust belts, and the formation of the South Pyrenean Foreland Basin on the subducting Iberian plate (Anadón *et al.*, 1985a; Zoetemeijer *et al.*, 1990; Muñoz, 1992; Beaumont *et al.*, 2000; Vergés *et al.*, 2002). Second, the Oligocene-Miocene rift and opening of the Western Mediterranean Basin and related extension of the Eastern Iberian Margin (Roca *et al.*, 1999).

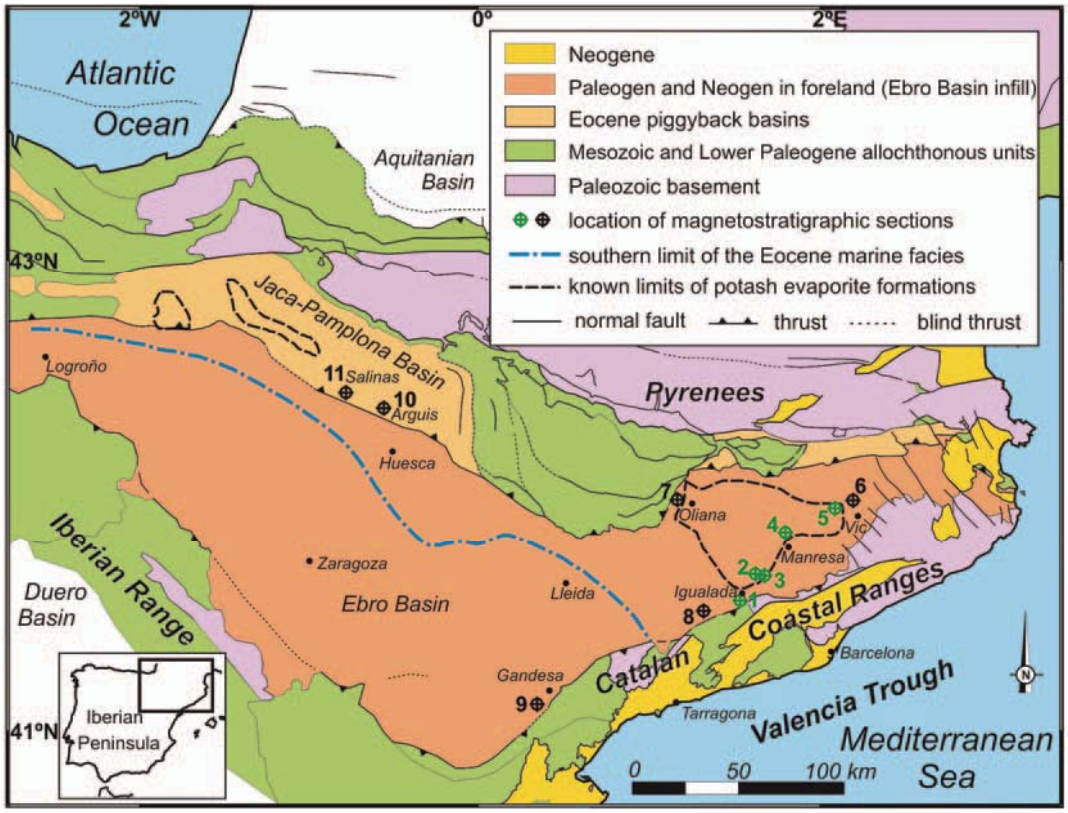

Figure 1.2. Geological map of the South Pyrenean Foreland Basin. Distribution of the Upper Eocene marine facies and evaporites based on outcrop, mine, and borehole data (simplified from Rosell & Pueyo, 1997). Location of new (previous) magnetostratigraphic sections are shown in green (black) symbols. (1) Miralles-La Tossa; (2) Maians-Rubió; (3) Montserrat; (4) Santpedor; (5) Moià; (6) Vic (Burbank *et al.*, [1992a,b]; Taberner *et al.*, [1999]; Cascella & Dinarès-Turell, [2009]); (7) Oliana (Vergés & Burbank, 1996); (8) Rocafort-Vinaixa (Barberà *et al.*, 2001); (9) Bot (Garcés *et al.*, 2008); (10) Arguis (Hogan & Burbank, 1996); (11) Salinas (Hogan & Burbank, 1996).

1.2.1.The Ebro Basin and the South Pyrenean Foreland Basin

The Ebro Basin is a triangular-shaped basin surrounded by three alpine ranges: the Pyrenees to the N, the Iberian Range to the SW and the Catalan Coastal Ranges to the SE (Fig. 1.2). This basin represents the latest evolutionary stage of the South Pyrenean foreland, whereas earlier stages of foreland basin were incorporated as piggy-back basins on top of allochtonous thrust nappes (Ori & Friend, 1984; Puigdefàbregas *et al.*, 1992). In this sense, the Ebro Basin is considered the autochthonous part of the South Pyrenean Foreland Basin (Riba *et al.*, 1983).

The Ebro Basin is filled with up to 5000 meters of marine and continental sediments ranging in age from Upper Cretaceous to Middle Miocene. Marine deposition was dominant along its northern margin, were subsidence was greater (Riba *et al.*, 1983). Paleogeographic reconstructions for the middle-Late Eocene (Meulenkamp & Sissingh, 2003) show that the South-Pyrenean region formed a narrow marine corridor connecting the Atlantinc and Tethyan oceanic domains. No precise constraint exists on the age of closure of its eastern gateway, presumably taking place during the Bartonian (Plaziat, 1981; Meulenkamp & Sissingh, 2003; Serra-Kiel *et al.*, 2003a), leading the basin to evolve into an elongated gulf, only connected with oceanic waters through the Bay of Biscay. The western marine communication of the South Pyrenean Foreland Basin was certainly maintained until the Late Eocene, when uplift in the Western Pyrenees (Muñoz *et al.*, 1986; Puigdefàbregas *et al.*, 1992) led to the final isolation from the Atlantic Ocean. Restricted marine conditions led to the deposition of evaporites and salts in two main depocentres (the Catalan and the Navarrese Potash sub-basins) now separated by the emplacement of the South Central Pyrenean thrust sheets (Rosell & Pueyo, 1997). No field or subsurface evidences exist on the continuity or isochrony of the marine salt deposition between the eastern (Catalan) and western (Navarrese) sub-basins. Nonetheless, the geochemical signature in both evaporite sequences indicates that they experienced a parallel evolution (Cendón *et al.*, 2003).

Following the basin closure, steady and continuous continental sedimentation took place from Late Eocene to the late Middle Miocene (Barberà *et al.*, 2001; Pérez-Rivarés *et al*., 2002; Larrasoaña *et al.*, 2006), rising the basin base level to nearly one thousand meters above sea level. This unusual and long-lasting endorheic stage led to the progressive basin filling and, eventually, backfilling of the thrust-belt margins with conglomerates (Riba *et al*., 1983; Coney *et al.*, 1996). Alluvial and fluvial sedimentation predominated in the basin margins (Anadón *et*

al., 1985a; López-Blanco *et al.*, 2000; Arenas *et al.*, 2001; López-Blanco, 2002); whereas in the inner parts fluvial and lacustrine systems were set up (Anadón *et al.*, 1989; Arenas & Pardo, 1999; Cuevas *et al.*, 2010). The end of sedimentation in the Ebro Basin (Middle-Late Miocene) occurred as a combined result of basin overfilling and escarpment erosion across the differentially rifted and uplifted Catalan Margin (Garcia-Castellanos *et al.*, 2003; Urgelés *et al.*, 2011). River incision allied with rift shoulder uplift and accelerated erosion of both the central Catalan Coastal Range and the Eastern Ebro Basin (Gaspar-Escribano *et al.*, 2004), bringing to surface the complete basin infill sequence with a smooth northwestward tilt.

1.2.2. The Paleogene Southern Margin of the Ebro Basin

The SE margin of the Ebro Basin is formed by the Catalan Coastal Ranges. This NE-SW range has a complex arrangement reflecting the superposition of compressive and extensional structures resulting from the growth of a Paleogene transpressive intraplate chain (Guimerà, 1984, 1988; Anadón *et al.*, 1985a; López-Blanco, 2002), which during the Late Oligocene, became the western passive margin of the extensional Valencia Trough (Roca & Guimerà, 1992; Roca *et al.*, 1999). The structure of the Paleogene transpressive intraplate chain is characterized by contractional deformation associated with the NW-verging Prelitoral Fault, a shortcut developed in the footwall of the Mesozoic Vallès-Penedès Fault during its Paleogene reactivation under transpressive conditions (Gaspar-Escribano *et al.*, 2004). The Prelitoral Fault crops out along the Prelitoral Range, a narrow zone of Paleozoic and Mesozoic rocks between the Paleogene Ebro Basin and the Miocene Vallès-Penedès half-graben (Fig 1.3).

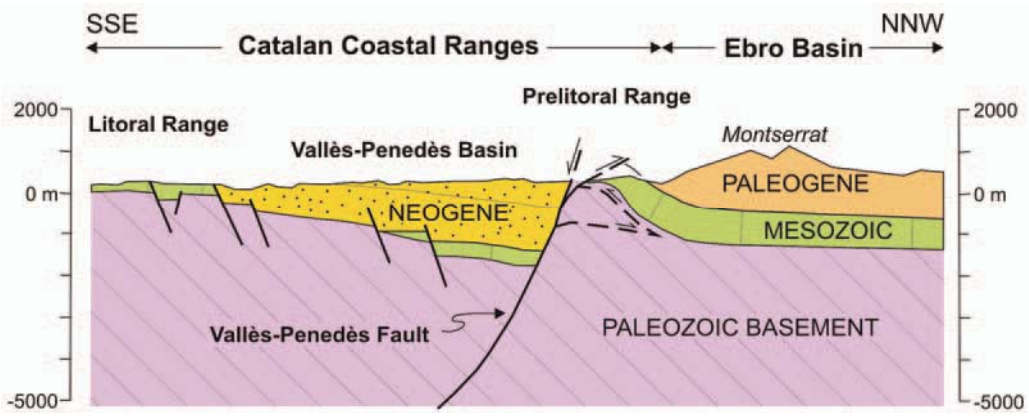

Figure 1.3. Cross section trough the Catalan Coastal Ranges and the Ebro Basin margin, showing the main structural units of the area and the superposition of compressive (Paleogene) and extensive (Neogene) structures. Redrawn from López-Blanco (2002).

A tectonosedimentary evolution of the central SE margin of the Ebro Basin has been proposed by López-Blanco (2002) based on the study of the different tectonic structures and stratigraphic units from this area. López-Blanco (2002) identified three main stages linked to the evolution of the Prelitoral Fault during the Paleogene. The first stage, associated to the emplacement of shallow thrust wedges, is represented by the deposition of growth strata of monomictic Triassic-derivated breccias onlapping erosive surfaces. This early deformation event was followed by a period of relative quiescence before the re-activation of the structures that controlled the second and third stages. The second stage is characterized by synsedimentary fold growth, leading to the development of several unconformities, related to the emplacement of deep intracutaneous thrust wedges. Finally, the third stage corresponds to major out-of-sequence thrusting of the Prelitoral Thrust, resulting in the development of the large alluvial fans and fan-deltas of Montserrat, Sant Llorenç del Munt and Sant Miquel de Montclar (Anadón *et al.*, 1985b; López-Blanco, 2002).

1.3. Stratigraphy of the Middle Eocene-Lower Oligocene Record of the SE Margin of the Ebro Basin

Historically, according to geological and geographical criteria, stratigraphic studies in the Eastern Ebro Basin have clearly distinguished three sectors. From SW to NE, these are the Igualada, Montserrat, and Vic-Manresa areas. In the following an introduction to the Middle Eocene-Lower Oligocene stratigraphic record of the SE margin of the Ebro Basin is provided. This description is mainly focused in the Igualada sector where a broader biostratigraphical record is available.

1.3.1. Lithostratigraphy of the Middle-Upper Eocene Record

The Middle-Upper Eocene record of the SE margin of the South Pyrenean Foreland Basin in the Igualada area consists of a 2000-m-thick transgressive-regressive sequence divided into three units (Figs. 1.4): a lower continental unit (Pontils Group), a middle marine unit (including the Santa Maria Group, the "Terminal Complex" and the Cardona Formation), and an upper continental succession (Artés Formation). All these three units laterally grade towards the margin into alluvial conglomeratic units such as Montserrat, Sant Llorenç del Munt, and Montclar Conglomerates. The Pontils Group (Ferrer 1971a; Anadón, 1978) consists of red mudstones with interbedded carbonatic and evaporitic sediments deposited in continental and transitional environments. These sediments were first attributed to Cuisian and Lutetian

ages as determined by charophyte assemblages (Rosell *et al.*, 1966; Ferrer, 1971a). They were subsequently attributed to the Lutetian and Bartonian according to the proposed charophyte biozonation of Anadón & Feist (1981) and Anadón *et al.* (1992).

In the Igualada area, the marine sediments of the Santa Maria Group (Ferrer, 1971a), comprise three main formations; the Collbàs Formation (limestones and marls levels with subordinated sandstones and fine conglomerates corresponding to the nearshore deposits), the offshore marls of the Igualada Formation, and the Tossa Formation, a coralline limestone unit that corresponds to reef and bioclastic bar environments. On top of these sediments the shallow water carbonate platforms of the "Terminal Complex" (Travé, 1992; Travé *et al.*, 1996), the halite-dominated Cardona Formation and its sulfate-dominated evaporitic Òdena Formation (Pueyo, 1974) represent the uppermost marine sediments deposited in the Ebro Basin.

No physical continuity exists between the marine sedimentary units recognized in the Igualada and Vic areas. However, in the Vic area (Fig. 1.4) the Middle-Upper Eocene record of the South Pyrenean Foreland Basin also consists of a 2000-m-thick succession of transgressive-regressive marine units that grade southwards, towards the SE margin, into the alluvial deposits of the Romagats Formation (Colombo, 1980). Offshore marine units (gray and blue marls) of the Vic area interfinger with carbonate platforms and transitional units (shallow water siliciclastic and reef and bioclastic constructions). From bottom to top, the following marine formations in the Vic area are: the Tavertet Limestones; the Banyoles or Coll de Malla Marls; the Folgueroles Sandsone; the Vic Marls, including its three members Manlleu Marls capped by the Orís Sandstone, La Guixa or Gurb Marls, and the Vespella Marls (Almela & Rios, 1943; Reguant, 1967; Clavell *et al.*, 1970; Taberner, 1983). As in the Igualada area, interfingered and on top of the uppermost Vic Marls sediments the Centelles Sandstones, the Sant Martí Xic Limestone, the "Terminal Complex", and the halite-dominated Cardona Formation and its sulphate-dominated evaporitic La Noguera formations represent the uppermost marine sediments deposited in the Ebro Basin (Pueyo, 1974; Taberner, 1983; Travé, 1992; Travé *et al.*, 1996). Finally, interfingering with these uppermost marine units and also overlying them the continental Artés Formation is also cropping out in the Vic-Manresa area (Ferrer, 1971a).

Serra-Kiel *et al.* (2003b) produced a litho- and biostratigraphical synthesis of the marine and transitional Middle-Upper Eocene units of the South Pyrenean Foreland Basin. In this

synthesis four transgressive-regressive cycles are described for the Lutetian units of the Vic area, while other two transgressive-regressive cycles are recognized in the Bartonian units of the Igualada and Vic areas (Serra-Kiel *et al.*, 2003b). In the Igualada area, the first Bartonian sedimentary cycle corresponds to the Collbàs Formation, and its maximum flooding surface is determined at the transition from marls with larger foraminifers and ahermatypical corals to marls. The second Bartonian sedimentary cycle includes the rest of the marine deposits of the Igualada area (Igualada and Tossa formations, the "Terminal Complex", and the Cardona Formation) and its maximum flooding surface is represented by a marker level that covers the Igualada area and has been interpreted as a condensation level, containing abundant *Discocyclina*, *Asterocyclina*, *Assilina,* and *Operculina*. In the Vic area, the transgressive system tract of the first Bartonian sedimentary cycle includes the Folgueroles Sandstone Formation and the lower part of the Manlleu Marls Member, while its regressive system tract is represented by the upper part of the Manlleu Marls Member and the Orís Sandstone. Finally, the second Bartonian sedimentary cycle includes the uppermost marine units of the Vic area, being the La Guixa (Gurb) Marl Members the transgressive system tract, and the rest of the marine units (Vespella Marl Member, the Sant Martí Xic Limestone Formation, the "Terminal Complex", and the La Noguera Formation) the regressive system tract of the second Bartonian sedimentary cycle.

1.3.2. Biostratigraphy of the Middle-Upper Eocene Marine Record

The pioneering studies in the Middle-Upper Eocene marine record of the Eastern Ebro Basin made the attempt to apply the Paris Basin chronology by ascribing Auversian, Bartonian, and/or Ledian ages to the marine Santa Maria Group (Ruiz de Gaona & Colom, 1950; Ruiz de Gaona, 1952). However, the description of the two new stages (Ilerdian and Biarritzian) in the Eocene of the Western Pyrenees by Hottinger & Schaub (1960) favored the adoption of these chronological units in later works (Rosell *et al.*, 1966; Reguant, 1967; Ferrer, 1971a; Caus, 1975; Schaub, 1981; Serra-Kiel, 1984). Subsequently, with a planktonic foraminifers and larger foraminifers biozonation, Ferrer (1971a) established a Biarritzian age (*Truncarotaloides rohri*, *Nummulites perforatus* and *Alveolina elongata* Biozones) to the Collbàs Formation and the lower part of the Igualada Formation. Ferrer (1971b) also attributed a lower Priabonian age

Figure 1.4. Lithostratigraphy of the central SE margin of the Ebro Basin. The lithostratigraphic sketch has no vertical scale. Previous biochronostratigraphic information comes from Hottinger & Schaub (1960), Ferrer (1971a,b), Caus (1973), and Serra-Kiel *et al.* (2003a,b).

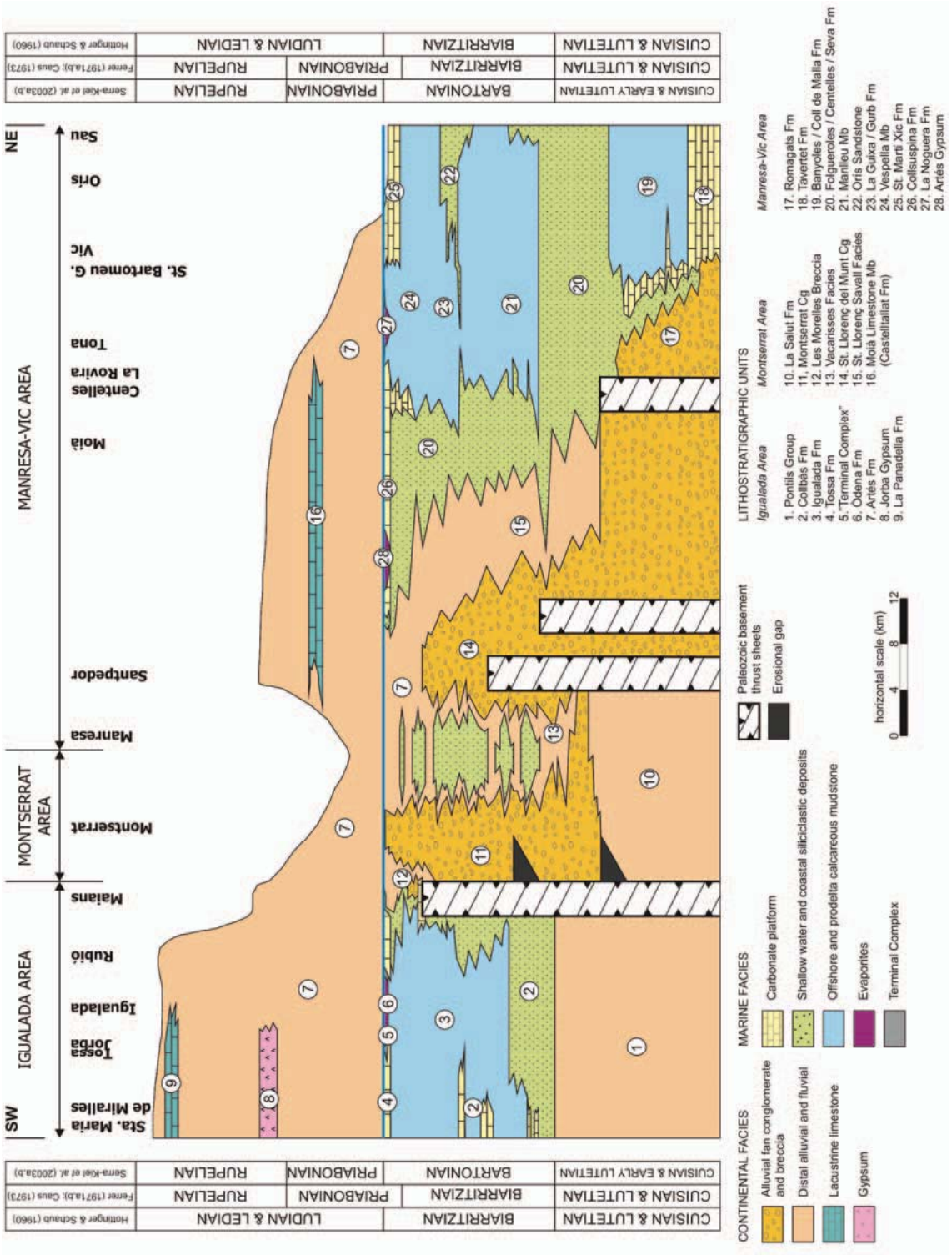
SW
NE
IGUALADA AREA
MONTSERRAT AREA
MANRESA-VIC AREA
Sta. Maria de Miralles
Torre Jorba
Igualada
Rubió
Mians
Montserrat
Manresa
Sanpedor
Moià
Centelles
La Rovira
Tona
St. Bartomeu G.
Vic
Oris
Sau
CUISIAN & EARLY LUTETIAN
CUISIAN & LUTETIAN
BARTONIAN
BIARRITZIAN
PRIABONIAN
LUDIAN & LEDIAN
RUPELIAN
Serra-Kiel et al. (2003a,b)
Ferrer (1971a,b); Caus (1973)
Hottinger & Schaub (1960)
CONTINENTAL FACIES
Alluvial fan conglomerate and breccia
Distal alluvial and fluvial
Lacustrine limestone
Gypsum
MARINE FACIES
Carbonate platform
Shallow water and coastal siliciclastic deposits
Offshore and prodelta calcareous mudstone
Evaporites
Terminal Complex
Paleozoic basement thrust sheets
Erosional gap
horizontal scale (km)
0
4
8
12
LITHOSTRATIGRAPHIC UNITS
Igualada Area
1. Pontils Group
2. Collbàs Fm
3. Igualada Fm
4. Tossa Fm
5. "Terminal Complex"
6. Òdena Fm
7. Artés Fm
8. Jorba Gypsum
9. La Panadella Fm
Montserrat Area
10. La Salut Fm
11. Montserrat Cg
12. Les Moneles Breccia
13. Vacarisses Facies
14. St. Llorenç del Munt Cg
15. St. Llorenç Savall Facies
16. Moià Limestone Mb (Castellfollit Fm)
Manresa-Vic Area
17. Romagats Fm
18. Tavertet Fm
19. Banyoles / Coll de Malla Fm
20. Folgueroles / Centelles / Seva Fm
21. Manlleu Mb
22. Oris Sandstone
23. La Guixa / Gurb Fm
24. Vespella Mb
25. St. Martí Xic Fm
26. Collsuspina Fm
27. La Noguera Fm
28. Artés Gypsum

(*Globigerinatheka semiinvoluta* and *Nummulites prefabianii* Biozones) to the upper parts of the Igualada Formation and to the Tossa Formation because of the presence of larger foraminifers *Pellatispira madaraszi* HANTKEN, 1875 and *Heterostegina reticulata* RÜTIMEYER, 1850 (=*Grzybowskia reticulate*). These results were challenged by Serra-Kiel *et al.* (1998a,b), who used the associations of larger foraminifers of the Igualada area, together with data from other alpine-belt regions, as the basis for the definition of the Zones SBZ17 and SBZ18. Currently accepted calibration of the larger foraminifer biostratigraphy indicates that Zones SBZ17 and SBZ18 correlate with the Bartonian stage (Serra-Kiel *et al.*, 1998a,b), in accordance with the occurrence of younger SBZ19 assemblages in the Priabonian type locality (Luciani *et al.*, 2002).

1.3.3.Litho- and Biostratigraphy of the Upper Eocene-Lower Oligocene Continental Record

Laterally equivalent to the uppermost marine sediments and also overlaying the top marine beds, the Artés Formation (Ferrer, 1971a), consists of alluvial and fluvial red beds with interbedded lacustrine limestone units (Moià Member) of the Castelltallat Formation (Sáez, 1987). In the Vic-Manresa area, Late Eocene (Sant Cugat de Gavadons) to Early Oligocene (Santpedor) vertebrate fossil assemblages have been reported in the sediments of the Artés Formation (Agustí *et al.*, 1987; Anadón *et al.,* 1987, 1992; Sáez, 1987; Arbiol & Sáez, 1988). Southwestwards of the Igualada area, younger units have provided a complete Oligocene magnetostratigraphic record which contributed to the age calibration of the Western Europe MP mammal biochronology (Barberà, 1999; Barberà *et al.*, 2001).

1.3.4.Magnetostratigraphy

A number of magnetostratigraphic studies spanning the Middle-Late Eocene record of the Eastern Ebro Basin were performed in the Vic, Oliana, and Montserrat areas during the 1990's (Burbank *et al.*, 1992a,b; Vergés & Burbank, 1996; Taberner *et al.*, 1999; López-Blanco *et al.*, 2000). These studies were unable to provide an independent match with the geomagnetic polarity time scale based on the magnetostratigraphic pattern. On the contrary, their correlations were built on the presumed "Bartonian" age of the foraminiferal assemblages of the top marine units. Recent studies, however, have challenged this view showing the presence of fossil assemblages of Priabonian age in the upper units of the Santa Maria Group (Cascella & Dinarès-Turell, 2009), in agreement with earlier findings of Ferrer (1971b).

1.4. References

AGUSTÍ, J., ANADÓN, P., ARBIOL, S., CABRERA, L., COLOMBO, F., SÁEZ, A., (1987). Biostratigraphical characteristics of the Oligocene sequences of North-Eastern Spain (Ebro and Campins Basins). *Münchner Geowissenschaftliche Abhandlungen*, **10**, 35-42.

ALMELA, A., RÍOS, J.M., (1943). Contribución al conocimiento de la zona surpirenaica catalana: Las edades de los yesos del Eoceno Catalán y algunas observaciones sobre la estratigrafía del mismo. *Boletín del Instituto Geológico y Minero de España*, **56**, 391-451.

ANADÓN, P., (1978). El Paleógeno continental anterior a la transgresión Biarritziense (Eoceno medio) entre los ríos Gaià y Ripoll (provincia de Tarragona y Barcelona). *Estudios Geológicos*, **34**, 341-440.

ANADÓN, P., CABRERA, L., CHOI, S.J., COLOMBO, F., FEIST, M., SÁEZ, A., (1992). Biozonación del Paleógeno continental de la zona oriental de la Cuenca del Ebro mediante carófitas; implicaciones en la biozonación general de carófitas de Europa occidental. *Acta Geologica Hispanica*, **27**, 69-94.

ANADÓN, P., CABRERA, L., COLLDEFORNS, B., SÁEZ, A., (1989). Los sistemas lacustres del Eoceno superior y Oligoceno del sector oriental de la Cuenca del Ebro. *Acta Geologica Hispanica*, **24**, 205-230.

ANADÓN, P., CABRERA, L., GUIMERÀ, J., SANTANACH, P., (1985a). Paleogene strike-slip deformation and sedimentation along the southeastern margin of the Ebro Basin. In: Biddle, K.T., Christie-Blick, N., (Eds.). Strike-slip tectonics and sedimentation. *Society of Economic Paleontology and Mineralogy, Special Publication*, **37**, 303-318.

ANADÓN, P., FEIST, M., (1981). Charophytes et Biostratigraphie du Paléogène Inférieur du bassin de l'Ebre oriental. *Palaeontographica, Abt. B*, **178**, 143-168.

ANADÓN, P., MARZO, M., PUIGDEFÀBREGAS, C., (1985b). The Eocene fan-delta of Montserrat (Southeastern Ebro Basin, Spain). In: Milà, M.D., Rosell, J., (Eds.). *6th European Meeting Excursion Guidebook*, pp. 109-146. Institut d´Estudis Ilerdencs, Lleida.

ANADÓN, P., ROCA, E., (1996). Geological setting of the Tertiary basins of the Northeastern Spain. In: Friend, P.F., Dabrio, C.J., (Eds.). *Tertiary basins of Spain. The stratigraphic record of crustal kinematics*, pp. 43-48. Cambridge University Press, Cambridge.

ANADÓN, P., VIANEY-LIAUD, M., CABRERA, L., HARTENBERGER, J.L., (1987). Gisements à vertébrés du paléogène de la zone orientale du bassin de l'Ebre et leur apport à la stratigraphie. *Paleontologia i Evolució*, **21**, 117-131.

ARBIOL, S., SÁEZ, A., (1988). Sobre la edad oligocénica inferior del yacimiento de Santpedor (Cuenca del Ebro, provincia de Barcelona). *Acta Geologica Hispanica*, **23**, 47-50.

ARENAS, C., MILLÁN, H., PARDO, G., POCOVÍ, A., (2001). Ebro Basin continental sedimentation associated with late compressional Pyrenean tectonics (north-eastern Iberia): controls on basin margin fans and fluvial systems. *Basin Research*, **13**, 65-89. doi: 10.1046/j.1365-2117.2001.00141.x

ARENAS, C., PARDO, G., (1999). Latest Oligocene-Late Miocene lacustrine systems of the north-central part of the Ebro Basin (Spain): sedimentary facies model and palaeogeographic synthesis. *Palaeogeography, Palaeoclimatology, Palaeoecology*, **151**, 127-143. doi: 10.1016/S0031-0182(99)00025-5

BARBERÀ, X., (1999). Magnetostratigrafia de l'Oligocè del sector sud-oriental de la Conca de l'Ebre: implicacions magnetobiocronológiques i seqüencials. PhD Thesis, Universitat de Barcelona. 247pp.

BARBERÀ, X., CABRERA, L., MARZO, M., PARÉS, J.M., AGUSTÍ, J., (2001). A complete terrestrial Oligocene magnetostratigraphy from the Ebro Basin, Spain. *Earth and Planetary Science Letters*, **187**, 1-16. doi: 10.1016/S0012-821(01)00270-9

BEAUMONT, C., MUÑOZ, J.A., HAMILTON, J., FULLSACK, P., (2000). Factors controlling the Alpine evolution of the Central Pyrenees inferred from the comparison of observations and

geodynamical models. *Journal of Geophysical Research*, **105**, 8121-8145. doi: 10.1029/1999JB900390

BURBANK, D.W., PUIGDEFÀBREGAS, C., MUÑOZ, J.A., (1992a). The chronology of the Eocene tectonic and stratigraphic development of the eastern Pyrenean foreland basin, northeast Spain. *Gelogical Society of America Bulletin*, **104**, 1101-1120. doi: 10.1130/0016-7606(1992)104<1101:TCOTET>2.3.CO;2

BURBANK, D.W., VERGÉS, J., MUÑOZ, J.A., BENTHAM, P., (1992b). Coeval hindward- and forward-imbricating thrusting in the south-central Pyrenees, Spain: Timing and rates of shortening and deposition. *Gelogical Society of America Bulletin*, **104**, 3-17. doi: 10.1130/0016-7606(1992)104<0003:CHAFIT>2.3.CO;2

CASCELLA, A., DINARÈS-TURELL, J., (2009). Integrated calcareous nannofossil biostratigraphy and magnetostratigraphy from the uppermost marine Eocene deposits of the southeastern pyrenean foreland basin: evidences for marine Priabonian deposition. *Geological Acta*, **7**, 281-296. doi: 10.1344/105.000000282

CAUS, E., (1973). Bioestratifrafía y micropaleontología del Eoceno medio y superior del Prepirineo Catalán. PhD-Thesis, Universitat Autònoma de Barcelona. 186pp.

CAUS, E., (1975). Bioestratigrafía del Eoceno medio y superior del Prepirineo Catalán (y la zona del transito entre esta unidad y la Cordillera Prelitoral Catalana). *Revista Española de Micropaleontologia*, **7**, 297-316.

CENDÓN, D.I., AYORA, C., PUEYO, J.J., TABERNER, C., (2003). The geochemical evolution of the Catalan potash subbasin, South Pyrenean foreland basin (Spain). *Chemical Geology*, **200**, 339-357. doi: 10.1016/S0009-2541(03)00195-5

CLAVELL, E., DEFALQUE, G., REGUANT, S., (1970). La situación estratigráfica de las Margas de Bañolas (Almela y Ríos, 1943). *Acta Geologica Hispanica*, **4**, 94-96.

COLOMBO, F., (1980). Estratigrafía y sedimentología del Terciario Inferior continental de los Catalánides. PhD-Thesis, Universitat de Barcelona. 609pp.

CONEY, P.J., MUÑOZ, J.A. MCCLAY, K.R., EVENCHICK, C.A., (1996). Syntectonic burial and post tectonic exhumation of southern Pyrenees foreland fold-thrust best. *Journal of Geological Society of London*, **153**, 9-16. doi: 10.1144/gsjgs.153.1.0009

CUEVAS, J.L., CABRERA, L., MARCUELLO, A., ARBUÉS, P., MARZO, M., BELLMUNT, F., (2010). Exhumated channel sandstone networks within fluvial fan deposits from the Oligo-Miocene Caspe Formation, South-east Ebro Basin (North-east Spain). *Sedimentology*, **57**, 162-189. doi: 10.1111/j.1365-3091.2009.01096.x

FERRER, J., (1971a). El Paleoceno y Eoceno del borde suroriental de la Depresión del Ebro (Cataluña). *Mémoires suisses de Paléontologie*, **90**, 1-70.

FERRER, J., (1971b). Presencia de macroforaminíferos priabonienses en el Eoceno de Igualada. *Acta Geolocica Hispanica*, **6**, 4-7.

GARCIA-CASTELLANOS, D., VERGÉS, J., GASPAR-ESCRIBANO, J., CLOETINGH, S., (2003). Interplay between tectonics, climate, and fluvial transport during the Cenozoic evolution of the Ebro Basin (NE Iberia). *Journal of Geophysical Research*, **108**, 2347-2364. doi: 10.1029/2002JB002073

GARCÉS, M., CABRERA, L., ROCA, E., GRATACÓS, O., (2008). Comment on "The diachroneity of alluvial-fan lithostratigraphy? A test case from southeastern Ebro basin magnetostratigraphy" by N. Swanson-Hysell and D. L. Barbeau, Jr. *Earth and Planetary Science Letters*, **275**, 181-186. doi: 10.1016/j.epsl.2008.07.024

GASPAR-ESCRIBANO, J., GARCIA-CASTELLANOS, D., ROCA, E., CLOETINGH, S., (2004). Cenozoic vertical motions of the Catalan Coastal Ranges (NE Spain): the role of tectonics, isostacy, and surface transport. *Tectonics*, **23**, 1-18. doi: 10.1029/2003TC001511

GRADSTEIN, F.M., OGG, J.G., (2005). Time Scale. In: Selly, R.C., Cocks, L.R.M., Plimer, I.R., (Eds.). *Encyclopedia of Geology,* pp. 503-520. Elsevier Academic Press, Amsterdam.

GRADSTEIN, F.M., OGG, J.G., SMITH, A.G., (2004). *A Geologic Time Scale 2004*. Cambridge University Press, Cambridge. 589pp.

GUIMERÀ, J., (1984). Paleogene evolution of deformation in the northeastern Iberian Peninsula. *Geological Magazine*, **121**, 413-420. doi: 10.1017/S0016756800029940

GUIMERÀ, J., (1988). Estudi estructural de l'enllaç entre la Serralada Ibèrica i la Serralada Costanera Catalana. PhD-Thesis, Universitat de Barcelona. 600pp.

HILGEN, F.J., (2008). Recent progress in the standardization and calibration of Cenozoic Time Scale. *Newsletters on Stratigraphy*, **43**, 15-22. doi: 10.1127/0078-0421/2008/0043-0015

HOGAN, P.J., BURBANK, D.W., (1996). Evolution of the Jaca piggyback basin and emergence of the External Sierra, southern Pyrenees. In: Friend, P.F., Dabrio, C.J., (Eds.). *Tertiary basins of Spain. The stratigraphic record of crustal kinematics*, pp. 153-160. Cambridge University Press, Cabridge.

HOLMES, A., (1937). *The Age of the Earth,2nd Edition*. Nelson, London.

HOLMES, A., (1947). The construction of a geological time-scale. *Transactions Geological Society of Glasgow*, **21**, 117-152.

HOTTINGER, L., SCHAUB, H., (1960). Zur Stufeneintelung des Paleocaens und des Eocaens. Einführung der Stufen Ilerdien und Biarritzien. *Eclogae geologicae Helvetiae*, **53**, 453-480.

JOVANE, L., SPROVIERI, M., COCCIONI, R., FLORINDO, F., MARSILI, A., LASKAR, J., (2010). Astronomical calibration of the middle Eocene Contesta Highway section. *Earth and Planetary Science Letters*, **298**, 77-88. doi: 10.1016/j.epsl.2010.07.027

LARRASOAÑA, J.C., MURELAGA, X., GARCÉS, M., (2006). Magnetobiochronology of Lower Miocene (Ramblian) continental sediments from the Tudela Formation (western Ebro basin, Spain). *Earth and Planetary Science Letters*, **243**, 409-423. doi: 10.1016/j.epsl.2006.01.034

LASKAR, J., FIENGA, A., GASTINEAU, M., MANCHE, H., (in press). La2010: A new orbital solution for long term motion of the Earth. *Astronomy & Astophysics*.

LÓPEZ-BLANCO, M., (2002). Sedimentary response to thrusting and fold growing on the SE margin of the Ebro basin (Paleogene, NE Spain). *Sedimentary Geology*, **146**, 133-154. doi: 10.1016/S0037-0738(01)00170-1

LÓPEZ-BLANCO, M., MARZO, M., BURBANK, D.W., VERGÉS, J., ROCA, E., ANADÓN, P., PIÑA, J., (2000). Tectonic and climatic controls on the development of foreland fan deltas: Montserrat and Sant Llorenç del Munt systems (Middle Eocene, Ebro Basin, NE Spain). *Sedimentary Geology*, **138**, 17-39. doi: 10.1016/S0037-0738(00)00142-1

LUCIANI, V., NEGRI, A., BASSI, D., (2002). The Bartonian-Priabonian transition in the Mossano section (Colli Berici, north-eastern Italy): a tentative correlation between calcareous plankton and shallow-water benthic zonations. *Geobios*, **35**, Supplement 1, 140-149. doi: 10.1016/S0016-6995(02)00055-4

KUIPER, K.F., DEINO, A., HILGEN, F.J., KRIJGSMAN, W., RENNE, P.R., WIJBRANS, J.R., (2008). Synchronizing rock clocks of Earth history. *Science*, **320**, 500-504. doi: 10.1126/science11.54339

MEULENKAMP, J.E., SISSINGH, W., (2003). Tertiary palaeogeography and tectonostratigraphic evolution of the Northern and Southern Peri-Tethys platforms and the intermediate domains of the African-Eurasian convergent plate boundary zone. *Palaeogeography, Palaeoclimatology, Palaeoecology*, **196**, 209-228. doi: 10.1016/S0031-0182(03)00319-5

MUÑOZ, J.A., (1992). Evolution of a continental collision belt: ECORS-Pyrenees crustal balanced cross-section. In: McClay, K.R., (Ed.). *Thrust tectonics*, pp. 235-246. Chapman & Hall, London.

MUÑOZ, J.A., MARTINEZ, A., VERGÉS, J., (1986). Thrust sequences in the eastern Spanish Pyrenees. *Journal Structural Geology*, **8**, 399-405. doi: 10.1016/0191-8141(86)90058-1

NEWMAN, W.L., (1997). Geologic Time. Online Edition. http://pubs.usgs.gov/gip/geotime/contents.html

OGG, J.G., (2004). The Jurassic Period. In: Gradstein, F.M., Ogg, J.G., Smith, A.G., (Eds.). *A Geologic Time Scale 2004*, pp. 307-343. Cambridge University Press, Cambridge.

ORI, G.G., FRIEND, P.F., (1984). Sedimentary basins formed and carried piggyback on active thrust sheets. *Geology*, **12**, 475-478. doi: 10.1130/0091-7613(1984)12<475:SBFACP>2.0.CO;2

PÄLIKE, H., NORRIS, R.D., HERRLE, J.O., WILSON, P.A., COXALL, H.K., LEAR, C.H., SHACKELTON, N.J., TRIPATI, A.K., WADE, B.S., (2006). The heartbeat of the Oligocene climate system. *Science*, **314**, 1894-1898. doi: 10.1126/science.1133822

PÉREZ-RIVARÉS, F.J., GARCÉS, M., ARENAS, C., PARDO, G., (2002). Magnetocronología de la sucesión miocena de la Sierra de Alcubierre (sector central de la Cuenca del Ebro). *Revista de la Sociedad Geológica de España*, 15: 211-225.

PLAZIAT, J.C., (1981). Late Cretaceous to Late Eocene paleogeographic evolution of southwest Europe. *Palaeogeography, Palaeoclimatology, Palaeoecology*, **36**, 263-320. doi: 10.1016/0031-0182(81)90110-3

PUEYO, J.J., (1974). Estudio petrológico y geoquímico de los yacimientos potásicos de Cardona, Súria, Sallent y Balsareny (Barcelona, España). PhD-Thesis, Universitat de Barcelona. 351pp.

PUIGDEFÀBREGAS, C., MUÑOZ, J.A., VERGÉS, J., (1992). Thrusting and foreland basin evolution in the Southern Pyrenees. In: McClay, K.R., (Ed.). *Thrust Tectonics*, pp. 247-254. Chapman and Hall, London.

REGUANT, S., (1967). *El Eoceno Marino de Vic (Bercelona)*. Memorias del Instituto Geológico y Minero de España, Tomo LXVIII. Instituto Geológico y Minero de España, Madrid. 350 pp.

RIBA, O., REGUANT, S., VILLENA, J., (1983). Ensayo de síntesis estratigráfica y evolutiva de la cuenca terciaria del Ebro. In: Comba, J.A., (Ed.). *Geología de España. Libro Jubilar J.M. Ríos, Tomo II*, pp. 131-159. Instituto Geológico y Minero de España, Madrid.

ROCA, E., GUIMERÀ, J., (1992). The Neogene structure of the eastern Iberian margin: Structural constraints on the crustal evolution of the Valencia trough (western Mediterranean). *Tectonophysics*, **203**, 203-218. doi: 10.1016/0040-1951(92)90224-T

ROCA, E., SANS, M., CABRERA, L., MARZO, M., (1999). Oligocene to Middle Miocene evolution of the central Catalan margin (northwestern Mediterranean). *Tectonophysics*, **315**, 209-233. doi: 10.1016/S0040-1951(99)00289-9

ROSELL, J., JULIÁ, R., FERRER, J., (1966). Nota sobre la estratigrafía de unos niveles con Carófitas existentes en el tramo rojo de la base del Eoceno al S de los Catalánides (Provincia de Barcelona). *Acta Geologica Hispanica*, **1**, 17-20.

ROSELL, L., PUEYO, J.J., (1997). Second Marine Evaporitic Phase in the South Pyrenean foredeep: The Priabonian Potash Basin (Late Eocene: Autochthonous-Allochthonous Zone). In: Busson, G., Schreiber, B.C., (Eds.). *Sedimentary Deposition in Rift and Foreland Basins in France and Spain. (Paleogene and Lower Neogene)*, pp. 358-387. Columbia University Press, New York.

RUIZ DE GAONA, M., (1952). Resultado del estudio de los foraminíferos del Nummulítico de Montserrat y regiones limítrofes. *Estudios Geológicos*, **15**, 21-28.

RUIZ DE GAONA, M., COLOM, G., (1950). Estudios sobre las sinencias de los foraminíferos eocénicos de la vertiente meridional del Pirineo (Cataluña-Vizcaya). *Estudios Geológicos*, **12**, 293-434.

SÁEZ, A., (1987). Estratigrafía y sedimentología de las formaciones lacustres del tránsito Eoceno-Oligoceno del noreste de la cuenca del Ebro. PhD-Thesis, Universitat de Barcelona. 353pp.

SCHAUB, H., (1981). Nummulites et Assilines de la Tethys Paléogène. Taxonomie, phylogénèse et biostratigraphie. *Mémoires suisses de Paléontologie*, **104/105/106**, 1-236.

SERRA-KIEL, J., (1984). Estudi del *Nummulites* del grup *N. perforatus* (Montfort). *Treballs de la Institució Catalans d'Història Natural*, **11**, 1-244.

SERRA-KIEL, J., HOTTINGER, L., CAUS, E., DROBNE, K., FERRÀNDEZ-CAÑADELL, C., JAUHRI, A.K., LESS, G., PAVLOVEC, R., PIGNATTI, J., SAMSÓ, J.M., SCHAUB, H., SIREL, E., STROUGO, A., TAMBAREAU, Y.,

TOSQUELLA, J., ZAKREVSKAYA, E., (1998a). Larger Foraminiferal Biostratigraphy of the Tethyan Paleocene and Eocene. *Bulletin de la Societé géologique de France*, **169**, 281-299.

SERRA-KIEL, J., HOTTINGER, L., DROBNE, K., FERRÀNDEZ-CAÑADELL, C., JAUHRI, A.K., LESS, G., PIGNATTI, J., SAMSÓ, J.M., SCHAUB, H., SIREL, E., TAMBAREAU, Y., TOSQUELLA, J., ZAKREVSKAYA, E., (1998b). Larger benthic foraminifera. In: Thierry, J., Farley, M.B., Jacquin, Th., Graciansky, P.C., Vail, P.R., (Eds.). *Mesozoic-Cenozoic sequence stratigraphy of European basins.* Society of Economic Paleontologist and Mineralogist, Special Publication, **60**, 767pp., chart 3.

SERRA-KIEL, J., MATÓ, E., SAULA, E., TRAVÉ, A., FERRÀNDEZ-CAÑADELL, C., BUSQUETS, P., SAMSÓ, J.M., TOSQUELLA, J., BARNOLAS, A., ÀLVAREZ-PÉREZ, G., FRANQUÈS, J., ROMERO, J., (2003a). An inventory of the marine and transitional Middle/Upper Eocene deposits of the Southeastern Pyrenean Foreland Basin (NE Spain). *Geologica Acta*, **1**, 201-229. doi: 10.1344/105.000001610

SERRA-KIEL, J., TRAVÉ, A., MATÓ, E., SAULA, E., FERRÀNDEZ-CAÑADELL, C., BUSQUETS, P., TOSQUELLA, J., VERGÉS, J., (2003b). Marine and Transitional Middle/Upper Eocene Units of the Southeastern Pyrenean Foreland Basin (NE Spain). *Geologica Acta*, **1**, 177-200. doi: 10.1344/105.000001609

TABERNER, C., (1983). Evolución ambiental y diagenética de los depósitos del Terciario inferior (Paleoceno y Eoceno) de la Cuenca de Vic. PhD-Thesis, Universitat de Barcelona. 1400pp.

TABERNER, C., DINARÈS-TURELL, J., GIMÉNEZ, J., DOCHERTY, C., (1999). Basin infill architecture and evolution from magnetostratigraphic cross-basin correlations in the southeastern Pyrenean foreland basin. *Geological Society of America Bulletin*, **111**, 1155-1174. doi: 10.1130/0016-7606(1999)111<1155:BIAAEF>2.3.CO;2

TARBUCK, E.J., LUTGENS, F.K., (1999). *Ciencias de la Tierra. Una introducción a la geología física*. Pearson, Prentice Hall. 616pp.

TRAVÉ, A., (1992). Sedimentologia, petrologia i geoquímica (elements traça i isòtops) dels estromatòlits de la Conca Eocena Sudpirinenca. PhD-Thesis, Universitat de Barcelona. 396pp.

TRAVÉ, A., SERRA-KIEL, J., ZAMARREÑO, I., (1996). Paleoecological interpretation of transitional enviroments in Eocene carbonates (NE Spain). *Palaios*, **11**, 141-160.

URGELÉS, R., CAMERLENGHI, A., GARCIA-CASTELLANOS, D., DE MOL, B., GARCÉS, M., VERGÉS, J., HASLAM, I., HARDMAN, M., (2011). New constraints on the Messinian sealevel drawdown from 3D seismic data of the Ebro Margin, western Mediterranean. *Basin Research*, **23**, 123-145. doi: 10.1111/j.1365-2117.2010.00477.x

VERGÉS, J., BURBANK, D.W., (1996). Eocene-Oligocene thrusting and basin configuration in the eastern and central Pyrenees (Spain). In: Friend, P.F., Dabrio, C.J., (Eds.). *Tertiary basins of Spain. The stratigraphic record of crustal kinematics*, pp. 120-133. Cambridge University Press, Cambridge.

VERGÉS, J., FERNÀNDEZ, M., MARTÍNEZ, A., (2002). The Pyrenean orogen: pre-, syn-, and post-collisional evolution. In: Rousenbaum, G., Lister, G.S., (Eds.). Reconstruction of the Evolution of the Alpine-Himalayan Orogen. *Journal of the Virtual Explorer*, **8**, 55-74. doi: 10.3809/jvirtex.2002.00058

ZOETEMEIJER, R., DESEGAULX, P., CLOETINGH, S., ROURE, F., MORETTI, I., (1990). Lithospheric dynamics and tectonic-stratigraphic evolution of the Ebro Basin. *Journal of Geophysical Research*, **95**, 2701-2711. doi: 10.1029/JB095iB03p02701

http://www.stratigraphy.org

CHAPTER 2:

METHODOLOGY

This PhD-Thesis aims to obtain an independent chronology of the Paleogene sedimentary units of the Ebro Basin by means of magnetostratigraphy combined with available biostratigraphic constraints. Magnetostratigraphy refers to the application of the stratigraphic principles to the polarity reversal pattern recorded in stratified rock sequences by means of magnetic acquisition processes. This requires that rocks properly recorded the ancient magnetic field at the time of its formation, a prerequisite that must be checked in the laboratory using paleomagnetic and rock magnetic techniques. In the following, an introduction to magnetostratigraphy as a dating tool is given.

2.1. The Earth Magnetic Field: Fundamentals and Concepts

A dynamo capable of generating a magnetic field appears to be a general property of planets and stars that possess a relatively large electrical conducting region that is rotating and convecting (Merrill *et al.*, 1996). Fluid motions of the Earth's outer core generate a global magnetic field (*geomagnetic field*) that approximates in a 90% a geocentric dipole field aligned with the rotation axis of the Earth (Fig 2.1). The remaining 10% derives from higher order terms including the non-centered dipolar fields, non-dipolar fields, and external origin magnetic fields. This dipole has an irregular drift or secular variation about the Earth's rotational axis such that the time averaged field over several thousand years roughly coincides with the Earth's rotational poles (Merrill *et al.*, 1996). The geomagnetic field on any point of the Earth's surface is a vector (F) which possesses a component in the horizontal plane called the horizontal component (H) which makes an angle (Dec) with the geographical meridian. The *declination* (Dec) is an angle from north measured eastward ranging from 0° to 360°. The *inclination* (Inc) is the angle made by the magnetic vector with the horizontal. By convention, it is positive if the north-seeking vector points downward and negative if it points upward (Fig. 2.1).

In the Earth's surface, magnitude and direction of the geomagnetic field changes with time, ranging from milliseconds, hours, or days (*pulsations* or *short-term fluctuations*, *daily magnetic variations*, or *magnetic storms*) to centuries, thousands of years, or millions of years (*secular variations*, *magnetic excursions*, and *polarity reversals*). While the short-term behaviors are atmospheric or ionospheric in origin, the longer term behaviors are produced in

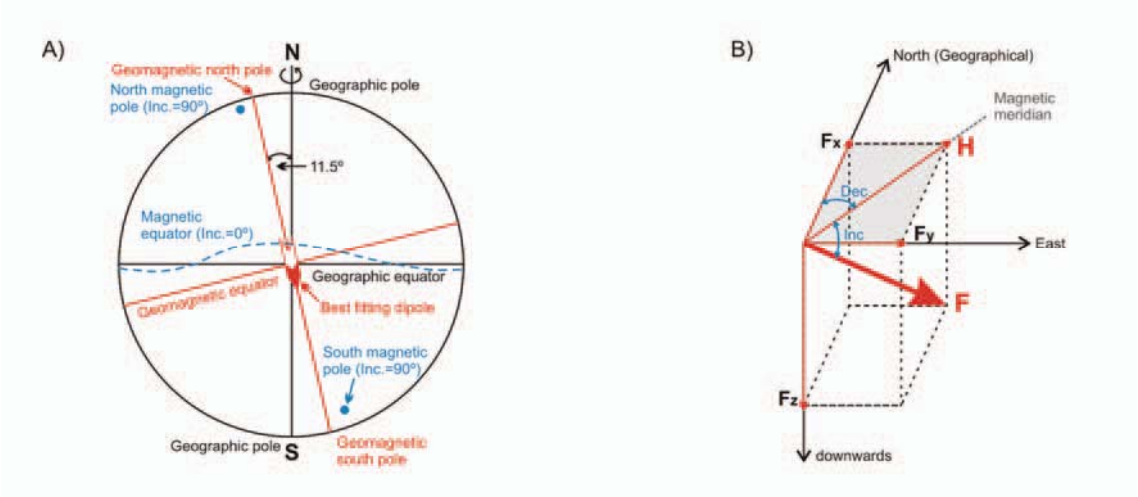

Figure 2.1. (A) Graphical sketch of the magnetic, geomagnetic, and geographical poles and equators. (B) The magnetic field on any point of the Earth's surface is a vector (F) which possesses a component in the horizontal plane (horizontal component, H) which makes an angle (Dec) with the geographical meridian. The inclination (Inc) is the angle made by the magnetic vector with horizontal plane. Redrawn from Opdike & Channell (1996).

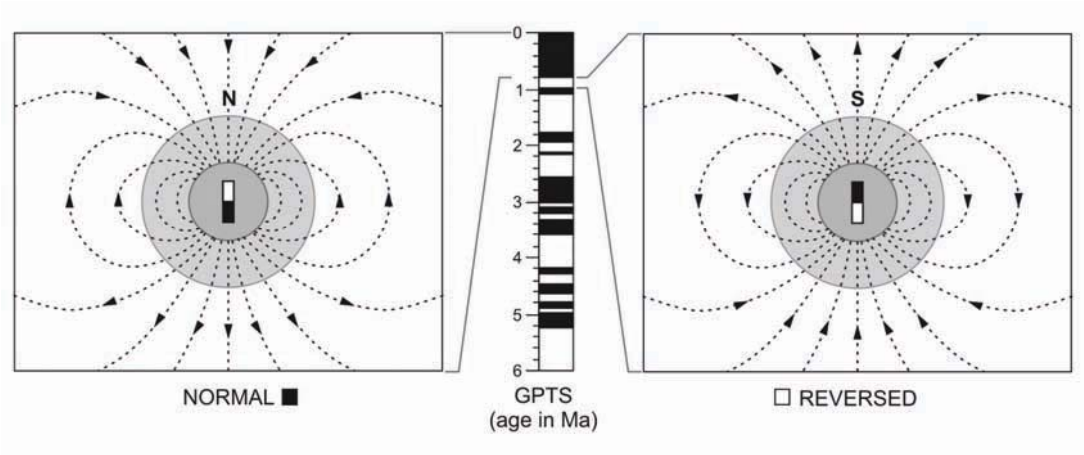

Figure 2.2. Schematic representation of the geomagnetic field of a geocentric axial dipole. During normal polarity of the field the average magnetic north pole is at the geographic north pole, and compass aligns along magnetic field lines. During normal polarity, the inclination is positive (downward directed) in the northern hemisphere and negative (upward directed) in the southern hemisphere. On the contrary, during reversed polarity, the compass needle points south, being the inclination negative in the northern hemisphere and positive in the southern one. In the geomagnetic polarity time scale, periods of normal (reversed) polarity are conventionally represented by black (withe) intervals. Modified from Langereis *et al.* (2010).

the Earth's interior (Opdyke & Channell, 1996). Among the longer term variations of the geomagnetic field the polarity reversals, with durations ranging from thousands of years to million years, are the switch of north and south magnetic poles. Polarity reversals have occurred randomly trough the Earth history, taking typically less than 5000 years to occur (Ogg & Smith, 2004), fast enough to be considered globally synchronous on geologic time scales. By convention, in paleomagnetism, present day configuration with the north magnetic pole close to the north geographic pole is considered a *normal polarity interval*, while opposite configuration is considered a *reversed polarity interval* (Fig. 2.2). Intervals of geological time having a constant geomagnetic field polarity delimitated by reversals are defined as *polarity chrons*, while a *polarity zone* is the corresponding interval in a stratigraphic section deposited during the polarity chron (Ogg & Smith, 2004).

2.2. Natural Remanent Magnetization: Origin and Types

The geomagnetic field can be registered in rocks at the time of their formation because of the presence of ferromagnetic minerals in their internal structure. During the rock-forming processes the magnetic moment of these minerals statistically align with the ambient field, and are subsequently "locked in" the rock system, thus preserving the direction of the field as a *Natural Remanent Magnetization* (NRM). In this sense, the NRM is considered the paleomagnetic signal. Principal minerals contributing to the NRM are usually iron oxydes such as magnetite, hematite, and maghemite; iron hydroxides (goethite); or iron sulphides including the pyrrhotite and the greigite. Other common minerals such as phyllosilicates (*e.g.*, ilmenite), pyroxenes, and amphiboles can significantly contribute to the induced magnetization. However, they do not have the capability to carry a NRM.

Depending on the mechanism of the paleomagnetic signal acquisition, three basic types of NRM are distinguished:

i) *Thermoremanent Magnetization* (TRM) is the magnetization acquired when a rock cools below the *Curie temperature* of its magnetic minerals, thereby "locking" the magnetic domains of these minerals along positions statistically aligned with the ambient field and producing a magnetic remanence that at room temperature may be stable for millions of years. TRM is characteristic of iron oxides present in igneous rocks.

ii) *Chemical Remanent Magnetization* (CRM) is the magnetization acquired when a magnetic mineral grows at low temperature (*authigenesis*) through a critical "blocking

volume" or grain size at which the field is locked in and the acquired remanence can, again, be stable for millions of years. Besides the CRM is characteristic of authigenic minerals, it is also carried by hematitic and goethitic cement formed as diagenetic minerals during soil alteration processes.

iii) *Detrital Remanent Magnetization* (DRM) is the magnetization acquired when magnetic grains of detrital origin are deposited, or when they are formed directly in the water column as *magnetosomes* (intra-cellular chains of magnetic minerals made by magnetotactic bacteria; *e.g.*, Vasiliev *et al.*, 2008). Detrital magnetic grains statistically align with the ambient field as long as they are in the water column or in the soft water-saturated topmost layer of the sediment. Upon compaction and dewatering, the grains are mechanically fixated in a *lock-in depth zone* and will preserve the direction of the ambient field.

Sedimentary rocks may carry a complex NRM, made of a DRM component carried by the terrigenous fraction of the sediment, fixed at specific lock-in depth, and a CRM component, carried by authigenic or diagenetic magnetic minerals. Both the DRM and the CRM acquisitions may occur in an early stage, but also well after deposition, deeper within the sediment. In the latter case, an apparent delay of one component of the NRM with respect to the other may be observed, which distorts the magnetic record. In order to unravel the complexity of the NRM of rocks it is fundamental to carry out a component analysis by means of stepwise NRM demagnetization techniques.

2.3. Demagnetization Techniques and Display of the NRM

Frequently, the total NRM of rock or sediments is the vector sum of different magnetic components. This is because the *primary NRM* (the one which is originated at the time of rock formation) may be overprinted by subsequent magnetic components acquired later in geologic history through processes such as weathering reactions, and/or other thermochemical reactions due to tectonic or burial processes. These *overprint components* can be removed through "magnetic cleaning" techniques, which primarily are the *thermal demagnetization technique* and the *alternating magnetic field* (AF) *demagnetization technique* (*e.g.*, Zijderveld, 1967; Butler, 1992; Opdyke & Channell, 1996; Tauxe, 1998). During demagnetization experiments, paleomagnetic samples are subjected to stepwise increasing values of temperature or alternating field in a zero magnetic field space. After each demagnetization step, the residual magnetization is measured and the resultant changes in direction and

intensity are displayed and analyzed in order to reconstruct the complete component structure of the NRM.

The results of stepwise demagnetization are commonly visualized and analyzed using the so-called *Zijderveld diagrams* (Zijderveld, 1967), also known as *vector end-point demagnetization diagrams* (Fig. 2.3). In these diagrams, both the intensity and directional changes of the NRM occurring during demagnetization are displayed at the same time. Magnetic components are then extracted from the Zijderveld diagrams using least-square analysis (Kirschvink, 1980), and the most stable and consistent component that can be isolated is referred to as the *Characteristic Remanent Magnetization* (ChRM). This ChRM is further investigated to establish if it represents a record of the geomagnetic field at, or close to, the time of rock formation, or a *secondary magnetization* acquired later in geologic history by post-depositional processes.

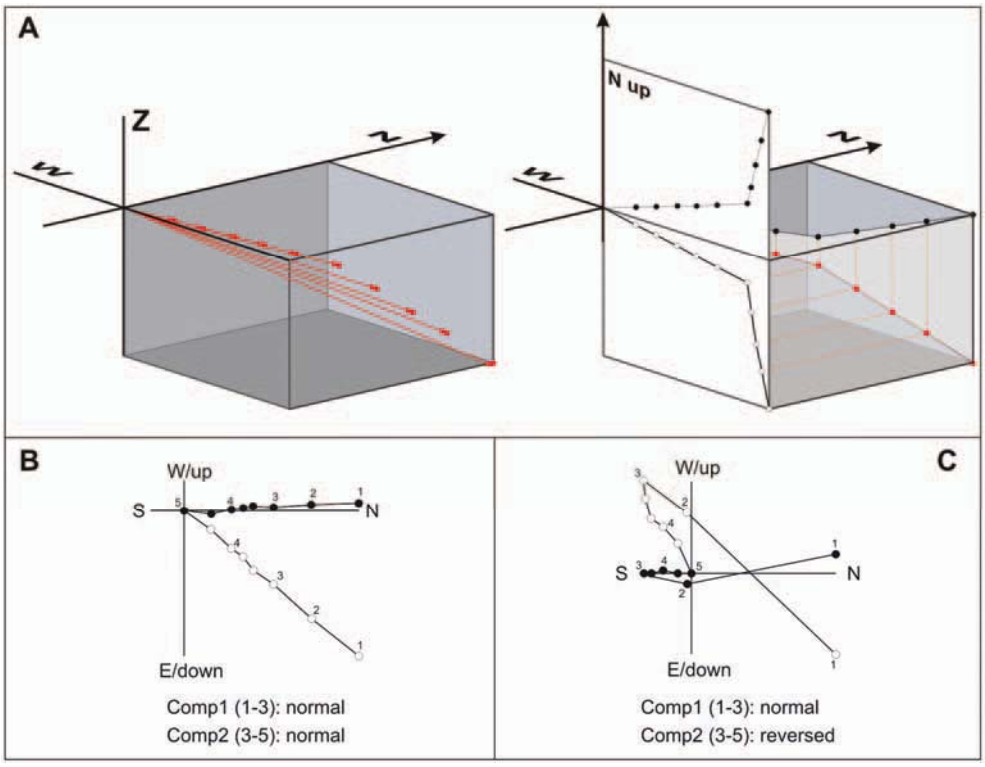

Figure 2.3. (A) Changes in the magnetization vector during demagnetization involve both its direction and its intensity, and orthogonal vector diagrams show the changes in both. The endpoint of the vector measured after each demagnetization step is projected both onto the horizontal plane (closed symbols) and onto the vertical plane (open symbols). Difference vectors (lines between end points) then show the behavior of the total vector upon stepwise removal of the magnetization. (B) and (C) Examples of Zijderveld diagrams. Conventionally, the solid points are these endpoints when projected onto the horizontal plane containing axes NS and EW, whereas the open points are these endpoints when projected onto the vertical plane containing axes NS (or EW), and up-down. Although many variations exist in literature, the only sensible projected axes combinations are W/up vs. NS and N/up vs. EW.

To assess the primary nature of the ChRM, and hence its suitability for magnetostratigraphic studies, rock magnetic experiments and reliability tests are usually carried out. Rock magnetic experiments are aimed at determining the fundamental characteristics such as type, grain size, *etc.* of the minerals bearing the magnetic remanence. A review of these methods can be found in appropriate text books (*e.g.*, Butler, 1992; Opdyke & Channell, 1996; Tauxe, 1998). However, a short description of the three more important reliability tests used in magnetostratigraphy is here given:

i) *Consistency test:* A natural remanent magnetization component is considered primary in origin when it defines a sequence of polarity reversals that is laterally traceable by independent means (*e.g.*, lithostratigraphy) between distant sections from different parts of the basin.

ii) *Reversal test:* The observation of ChRM directions with different polarity and, in particular, the occurrence of antiparallel (within statistical error) directions is taken as a strong indication for the primary origin of that ChRM. This test is greatly enhanced if a polarity zonation can be established, and if this zonation is independent of possible changes in the composition of the rock.

iii) *Fold test:* If the ChRM directions from differently tilted beds converge after correction for the dip of the strata, this remanence was acquired before tilting. Strictly speaking, this fold test does not directly prove a primary origin of this component, but only that it dates from before tilting.

From the above listed reliability tests, the consistency test has been the one applied in this PhD-Thesis to assess the primary nature of the observed ChRM directions of all the magnetostratigraphic sections.

2.4. The Geomagnetic Polarity Time Scale and Magnetostratigraphic Correlation

The sequence of geomagnetic polarity reversals, providing a unique global "bar-code" recorded in Earth's rocks of different ages, constitutes the *Geomagnetic Polarity Time Scale* (GPTS). For the construction of the GPTS geophysicists fundamentally rely on, first, the sea-floor magnetic anomaly record, and, second, the higher-resolution but fragmentary magnetostratigraphic record. Both records can be linked by means of radiometric and biostratigraphical constraints (Ogg & Smith, 2004; Langereis, *et al.*, 2010).

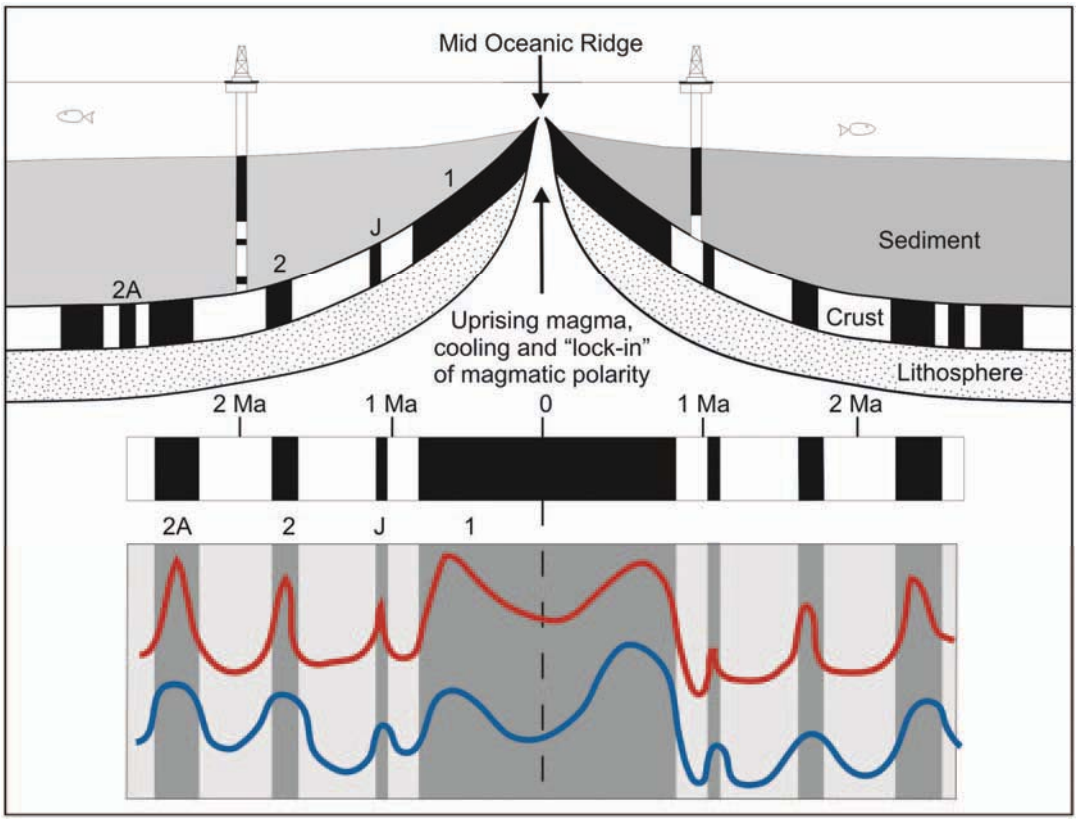

Figure 2.4. Formation of marine magnetic anomalies during seafloor spreading. The oceanic crust is formed at the ridge crest, and while spreading away from the ridge it is covered by an increasing thickness of oceanic sediments. The black (white) blocks of oceanic crust represent the original normal (reversed) polarity of the Thermoremanent Magnetization (TRM) acquired upon cooling at the ridge. The black and white blocks in the drill holes represent normal and reversed polarity Depositional Remanent Magnetization (DRM) acquired during deposition of the marine sediments. Normal polarity anomalies are given numbers and refer to anomaly 1 (Brunhes Chron), 2 (Olduvai subchron), and 2A (Gauss Chron); J = Jaramillo subchron. Redrawn from Langereis *et al.* (2010).

Oceanic surveys carried out during the 1950's and 1960's and equipped with shipboard magnetometers found linear magnetic anomalies parallel to the mid-oceanic ridges (Cox *et al.*, 1963; Heirtzler *et al.*, 1968). These anomalies resulted from the remanent magnetization of the oceanic crust, acquired during the process of seafloor spreading. As the uprising magma beneath the axis of the oceanic ridges cools down through the Curie temperatures of its constituent ferromagnetic minerals and in presence of the ambient geomagnetic field, the oceanic crust acquires the direction and polarity of this ambient field. The spreading process results in the magnetization of the crust in alternating normal and reverse polarity, which produces a slight increase or decrease of the measured field (*i.e.*, the *marine magnetic anomalies*; Fig. 2.4). It was also found that the magnetic anomaly pattern is generally symmetric on both sides of the ridge providing a remarkably continuous record of the geomagnetic reversal sequence. The template of magnetic anomaly patterns from the ocean

floor has remained central for constructing the GPTS from Early Cretaceous onward (*ca.* 124.5 Ma to 0 Ma; Ogg & Smith, 2004; Langereis *et al.*, 2010). Combined magnetostratigraphic, biostratigraphic, and radioisotopic results of deep-sea sediments and land-based sections have confirmed and refined the general validity and accuracy of the GPTS (*e.g.*, LaBreque *et al.*, 1977; Berggren *et al.*, 1985; Harland *et al.*, 1990; Cande & Kent, 1992), reflecting increasing detail and gradually improved age control.

The latest development in constructing a GPTS comes from orbital tuning of the sedimentary record, the so-called astronomically calibrated polarity time scale. First geological time scale including astronomical ages was that of Cande & Kent (1995) time scale, and the GPTS used in this PhD-Thesis provides a fully astronomically tuned Neogene time scale (Lourens *et al.*, 2004; Gradstein *et al.*, 2004). It essentially differs from the conventional GPTS, in the sense that each reversal boundary and any other geological boundary (*e.g.*, biostratigraphic datum levels or stage and epoch boundaries) is dated individually rather than interpolated between radioisotopic calibration points.

2.5. References

BERGGREN, W.A., KENT, D.V., FLYNN, J.J., (1985). Cenozoic geochronology. *Geological Society of America Bulletin*, **96**, 1407-1418. doi: 10.1130/0016-7606(1985)96<1407:CG>2.0.CO;2

BUTLER, R.F., (1992). *Paleomagnetism: Magnetic Domains to Geologic Terranes*. Blackwell Scientific Publications, Boston. 319pp.

CANDE, S.C., KENT, D.V., (1992). A new geomagnetic polarity time scale for the Late Cretaceous and Cenozoic. *Journal of Geophysical Research*, **97**, 13917-13951. doi: 10.1029/92JB01202

CANDE, S.C., KENT, D.V., (1995). Revised calibration of the geomagnetic polarity time scale for the Late Cretaceous and Cenozoic. *Journal of Geophysical Research*, **100**, 6093-6095. doi: 10.1029/94JB03098

COX, A.V., DOELL, R.R., DALRYMPLE, G.B., (1963). Geomagnetic polarity epochs and Pleistocene geochronometry. *Nature*, **198**, 1049-1051. doi: 10.1038/1981049a0

GRADSTEIN, F.M., OGG, J.G., SMITH, A.G., (2004). *A Geologic Time Scale 2004*. Cambridge University Press, Cambridge. 589pp.

HARLAND, W.B., ARMSTRONG, R.L., COX, A.V., CRAIG, L.E., SMITH, A.G., SMITH, D.G., (1990). *A Geologic Time Scale 1989*. Cambridge University Press, Cambridge. 263pp.

HEIRTZLER, J.R., DICKSON, G.O., HERRON, E.M., PITMAN III, W.C., LEPICHON, X., (1968). Marine Magnetic Anomalies, Geomagnetic Field Reversals, and Motions of the Ocean Floor and Continents. *Journal of Geophysical Research*, **73**, 2119-2136. doi: 10.1029/JB073i006p02087

KIRSCHVINK, J.L., (1980). The least-squares line and plane and the analysis of paleomagnetic data. *Geophysical Journal of the Royal Astronomical Society*, **62**, 699-718. doi: 10.1111/j.1365-246X.1980.tb02601.x

LANGEREIS, C.G., KRIJGSMAN, W., MUTTONI, G., MENNING, M., (2010). Magnetostratigraphy - concepts, definitions, and applications. *Newsletter on Stratigraphy*, **43**, 207-233. doi: 10.1127/0078-0421/2010/0043-0207

LABREQUE, J.L., KENT, D.V., CANDE, S.C., (1977). Revised magnetic polarity time scale for Late Cretaceous and Cenozoic time. *Geology*, **5**, 330-335. doi: 10.1130/0091-7613(1977)5<330:RMPTSF>2.0.CO;2

LOURENS, L., HILGEN, F.J., SCHACKELTON N.J., LASKAR, J., WILSON, D., (2004). The Neogene Period. In: Gradstein, F.M., Ogg, J.G., Smith, A.G., (Eds.). *A Geologic Time Scale 2004*, pp. 409-440. Cambridge University Press, Cambridge.

MERRIL, R.T., MCELHINNY, M.W., MCFADDEN, P.L., (1996). *The Magnetic Field of the Earth: Palaeomagnetism, the Core, and the Deep Mantle*. Internacional Geophysical Series, **63**, Academic Press, San Diego. 531pp.

OGG, J.G., SMITH, A.G., (2004). The geomagnetic polarity time scale. In: Gradstein, F.M., Ogg, J.G., Smith, A.G., (Eds.). *A Geologic Time Scale 2004*, pp. 63-86. Cambridge University Press, Cambridge.

OPDYKE, N.D., CHANNELL, J.E.T., (1996). *Magnetic Stratigraphy*. Internacional Geophysical Series, **64**, Academic Press, San Diego. 346pp.

TAUXE, L., (1998). *Paleomagnetic Principles and Practice*. Kluwer Academic Publisher, Dordrecht. 299pp.

VASILIEV, I., FRANKE, C., MEELDIJK, J.D., DEKKERS, M.J., LANGEREIS, C.G., KRIJGSMAN, W., (2008). Putative greigite magnetofossils from the Pliocene epoch. *Nature Geosciences*, **1**, 782-786. doi: 10.1038/ngeo335

ZIJDERVELD, J.D.A., (1967). A.C. demagnetization rocks: Analysis of results. In: Collinson, D.W., Creer, K.M., Runcorn, S.K., (Eds.). *Methods in Palaeomagnetism*, pp. 254-286. Elsevier, Amsterdam.

CHAPTER 3:

RESULTS

CHAPTER 3.1:

CHRONOLOGY OF THE MARINE UNITS OF THE IGUALADA AREA: *"THE BARTONIAN-PRIABONIAN MARINE RECORD OF THE EASTERN SOUTH PYRENEAN FORELAND BASIN (NE SPAIN): A NEW CALIBRATION OF THE LARGER FORAMINIFERS AND CALCAREOUS NANNOFOSSIL BIOZONATION"*

Chapter 3.1 constitutes the first scientific paper of this PhD-Thesis: *Costa, E., Garcés, M., López-Blanco, M., Serra-Kiel, J., Bernaola, G., Cabrera, L., Beamud, E., (accepted). The Bartonian-Priabonian marine record of the Eastern South Pyrenean Foreland Basin (NE Spain): A new calibration of the larger foraminifers and calcareous nannofossil biozonation. Geologica Acta.*

The Bartonian-Priabonian marine record of the eastern South Pyrenean Foreland Basin (NE Spain): A new calibration of the larger foraminifers and calcareous nannofossil biozonation.

E. COSTA (1,4) M. GARCÉS (1,4) M. LÓPEZ-BLANCO (1,4) J. SERRA-KIEL (1,4) G. BERNAOLA (2) L. CABRERA (1,4) and E. BEAMUD (3,4)

(1) Departament d'Estratigrafia, Paleontologia i Geociències Marines. Facultat de Geologia. Universitat de Barcelona. c/ Martí i Franquès s/n, 08028-Barcelona, Spain. Costa E-mail: elicosta@ub.edu; Garcés E-mail: mgarces@ub.edu; López-Blanco E-mail: m.lopezblanco@ub.edu; Serra-Kiel E-mail: josepserra@ub.edu; Cabrera E-mail: lluis.cabrera@ub.edu

(2) Departamento de Ingeniería Minera y Metalúrgica y Ciencia de los Materiales. EUIT de Minas y Obras Públicas. UPV/EHU Colina de Beurko s/n, 48902-Barakaldo, Spain. Bernaola E-mail: gilen.bernaola@ehu.es

(3) Laboratori de Paleomagnetisme UB-CSIC. Centres Científics i Tecnològics UB (CCiTUB). Institut de Ciències de la Terra "Jaume Almera" (CSIC). c/ Solé i Sabarís s/n, 08028-Barcelona, Spain. Beamud E-mail: betbeamud@ub.edu

(4) Institut GEOMODELS. Grup de recerca consolidat Geodinàmica i Anàlisi de Conques (GGAC). Barcelona Knowledge Campus.

ABSTRACT

This study presents a combined biostratigraphic (calcareous nannofossil, larger foraminifers) and magnetostratigraphic study of the Middle and Late Eocene marine units of the Igualada area, eastern Ebro Basin. The studied sections of Santa Maria de Miralles and La Tossa encompass the complete marine succession of the Santa Maria Group, where rich larger foraminifers assemblages have been studied since the early 1950's. A total of 224 paleomagnetic sites and 62 biostratigraphic samples were collected along a 1350-m-thick section that ranges from chron C20n to chron C16n (~43 Ma to ~36 Ma). The resulting magnetostratigraphy-based chronology challenges existing chronostratigraphic interpretations of these units and results in a new calibration of the biostratigraphic zonations. The base of calcareous nannofossil Zone NP19-20 is pinned down to an older age than its presently accepted attribution, whereas the time span assigned to Zone NP18 is significantly reduced. A revised calibration of larger foraminifers indicates that Zone SBZ18, formerly assigned exclusively to late Bartonian, extends its range to the earlymost Priabonian, being the Bartonian stage almost entirely represented by Zone SBZ17. A division of Zone SBZ18 into two subzones is proposed.

KEYWORDS: Middle/Late Eocene. Chronostratigraphy. Magnetostratigraphy. Biostratigraphy. Time Scale.

INTRODUCTION

Providing a robust high-resolution chronostratigraphic scheme of the geological record is essential for the advance of earth-science research (Gradstein et al., 2004). Age control is the key to calculate rates of change in geodynamic systems and to unravel cause-effect relationships. Magnetostratigraphy has been successfully proved to constitute an effective dating tool of stratigraphic successions (Langereis et al., 2010), capable of integrating disparate records in a global basis. In combination with biostratigraphic methods, it provides the means for increasing resolution of the geological time scale (Langereis et al., 2010; Agnini et al., 2011).

The South Pyrenean Foreland Basin (in NE Spain) has for long awaked the curiosity of geologists because of its exceptional sedimentary record (Virgili, 2007). The present level of erosion of the basin infill and its surrounding mountain ranges is at an optimal stage for studying tectonostratigraphic relationships on surface, making this region a natural laboratory for the study of collision belts and their adjacent foreland systems. A biochronological framework of the South Pyrenean Foreland Basin has been developed since the early 1950's (Ruiz de Gaona and Colom, 1950; Ruiz de Gaona, 1952; Hottinger, 1960; Hottinger and Schaub, 1960; Reguant, 1967; Colom, 1971; Ferrer, 1971a, 1971b; Kapellos and Schaub, 1973; Caus, 1973 and 1975; Schaub, 1981; Serra-Kiel, 1984; Tosquella, 1995; Papazzoni and Sirotti, 1995; Romero et al., 1999; Romero, 2001; Hottinger et al., 2001), which was later combined with magnetostratigraphic studies (Burbank et al., 1992a). All the available literature on the biostratigraphy and magnetostratigraphy of the Paleocene and Eocene Tethys were integrated in a general chronostratigraphic framework, used to define and calibrate the larger foraminifer biozonation (Shallow Benthic Zones, SBZ) (Serra-Kiel et al., 1998a, 1998b).

A recent study has challenged the Middle-Late Eocene chronostratigraphy of the South Pyrenean Foreland Basin, showing that the youngest marine deposits in the Vic region, of presumed Bartonian age, yield calcareous nannofossils assigned to the Priabonian Zone NP19-20 (Cascella and Dinarès-Turell, 2009). Furthermore, a magnetostratigraphic study focused in the overlying continental units of the Artés Formation (Costa et al., 2010) confirmed these results, dating the marine-continental transition in the Ebro Basin within chron C16n (i.e. Priabonian).
In this paper we present a new integrated biomagnetostratigraphic study of the Eocene marine units in the Igualada area, close to the SE margin of the South Pyrenean Foreland Basin. The results provide a revised chronology of these stratigraphic units, and a new calibration of the Late Eocene marine standard biozonation.

GEOLOGICAL SETTING

The present geology of NE Iberia has resulted from two successive plate-tectonic scenarios. First, the Late Cretaceous to Miocene convergence and continental collision between the Iberian and Eurasian plates (Anadón and Roca, 1996), which led to the growth of the Pyrenean thrust belt at the plate boundary, and the formation of the South Pyrenean Foreland Basin on the subducting Iberian plate (Zoetemeijer et al., 1990; Muñoz, 1992; Beaumont et al., 2000; Vergés et al., 2002). Second, the Oligocene-Miocene rift and opening of the Western Mediterranean basin and related extension of the eastern Iberian margin (Roca et al., 1999).

The South Pyrenean Foreland Basin (Fig. 1) is filled with up to 5000 meters of marine and continental sediments ranging in age from Upper Cretaceous to Middle Miocene. Marine deposition was dominant along its northern margin, were subsidence was greater (Riba et al., 1983). Paleogeographic reconstructions for the middle-Late Eocene (Meulenkamp and Sissingh, 2003) show that the South-Pyrenean region formed a narrow marine corridor connecting the Atlantinc and Tethyan oceanic domains. No precise constraint exists on the age of closure of its eastern gateway, presumably taking place during the Bartonian (Plaziat, 1981; Meulenkamp and Sissingh, 2003; Serra-Kiel et al., 2003a), leading the basin to evolve into an elongated gulf, only connected with oceanic waters through the Bay of Biscay. Marine sedimentation in the foreland basin ended in the Priabonian (Costa et al., 2010), after the tectonic uplift and closure of its western marine gateway.

The latest evolutionary stage of the South Pyrenean Foreland Basin, namely Ebro Basin (Riba et al., 1983), is bounded to the SE and SW by the Catalan Coastal Ranges and the Iberian Chain, respectively. In addition to the

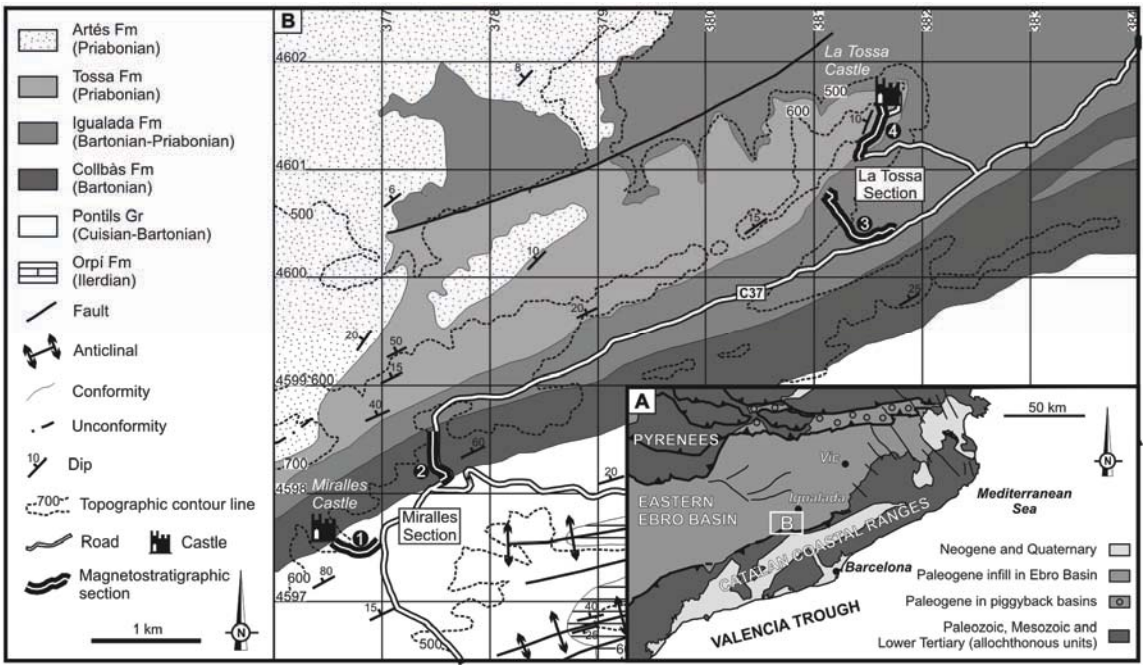

Figure 1 Geological setting of the Miralles and La Tossa sections. (A) Main geological units in the NE Iberian Peninsula. B: location of the detailed geological map of the study area. (B) Detailed geological map of the study area with indication of the Miralles (1 and 2) and La Tossa (3 and 4) sections. Map coordinates are in UTM projection, ED50 / zone 31N.

South-Pyrenean foredeep, the eastern margin of the Ebro Basin also developed a secondary foredeep zone as a consequence of thrusting and uplift of the Catalan Coastal Range from the Early Eocene until Late Oligocene (Guimerà, 1984; Anadón et al., 1985a). In the central sector of the Catalan Coastal Range, maximum deformation occurred in the Middle-Late Eocene, as recorded by the syntectonic development of alluvial-fan and fan-delta systems (López-Blanco, 2002). In the eastern Ebro Basin, two important transgressive events of Ilerdian and Bartonian age are recognized. Following the basin closure, steady and continuous continental sedimentation took place from Late Eocene to the late Middle Miocene (Barberà et al., 2001; Pérez-Rivarés et al., 2002), rising the basin base level to nearly one thousand meters above sea level. Alluvial and fluvial sedimentation predominated in the basin margins (Anadón et al., 1985a; López-Blanco et al., 2000; López-Blanco, 2002); whereas in the inner parts fluvial and lacustrine systems were set up (Anadón et al., 1989; Cuevas et al., 2010).

The end of sedimentation in the Ebro Basin (Middle-Late Miocene) occurred as a combined result of basin overfilling and escarpment erosion across the differentially rifted and uplifted Catalan margin (Garcia-Castellanos et al., 2003; Urgelés et al., 2011). River incision allied with rift shoulder uplift and accelerated erosion of both the central Catalan Coastal Range and the eastern Ebro Basin (Gaspar-Escribano et al., 2004), bringing to surface the complete basin infill sequence with a smooth northwestward tilt.

STRATIGRAPHY OF THE MIDDLE-UPPER EOCENE RECORD OF THE EASTERN EBRO BASIN

The Middle-Upper Eocene record of the SE margin of the South Pyrenean Foreland Basin in the Igualada area consists of a 2000-

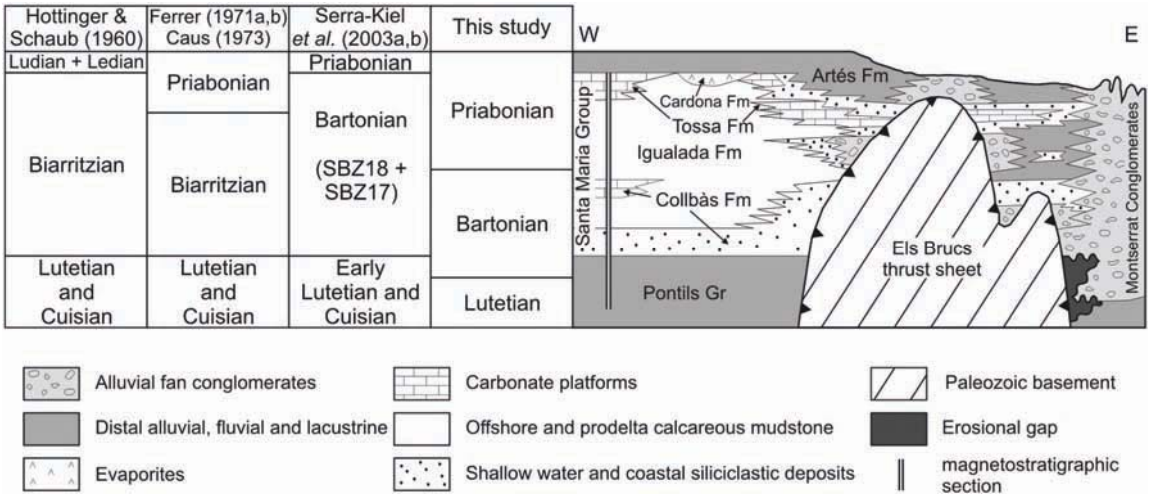

Figure 2 Litho- and biochronostratigraphy of the Igualada area. The lithostratigraphic sketch has no vertical scale and it has been modified from Anadón et al. (1985b). Previous biochronostratigraphic information comes from Hottinger and Schaub (1960), Ferrer (1971a, 1971b), Caus (1973) and Serra-Kiel et al. (2003a, 2003b).

-m-thick transgressive-regressive sequence divided into three units (Figs. 2 and A1): a lower continental unit (Pontils Group), a middle marine unit (including the Santa Maria Group, the "Terminal Complex" and the Cardona Formation), and an upper continental succession (Artés Formation). All these three units laterally grade towards the margin into alluvial conglomeratic units such as Montserrat, Sant Llorenç del Munt, and Montclar Conglomerates.

The Pontils Group (Ferrer 1971a; Anadón, 1978) consists of red mudstones with interbedded carbonatic and evaporitic sediments deposited in continental and transitional environments. These sediments were first attributed to Cuisian and Lutetian ages as determined by charophyte assemblages (Rosell et al., 1966; Ferrer, 1971a). They were subsequently attributed to the Lutetian and Bartonian according to the proposed charophyte biozonation of Anadón and Feist (1981) and Anadón et al. (1992).

The marine sediments of the Santa Maria Group (Ferrer, 1971a), comprise three main formations; the Collbàs Formation (limestones and marls levels with subordinated sandstones and fine conglomerates corresponding to the nearshore deposits), the offshore marls of the Igualada Formation, and the Tossa Formation, a coralline limestone unit that corresponds to reef and bioclastic bar environments. On top of these sediments the shallow water carbonate platforms of the "Terminal Complex" (Travé, 1992; Travé et al., 1996; Fig A1), the halite-dominated Cardona Formation and its sulfated-dominated evaporitic Òdena and La Noguera formations (Pueyo, 1974) represent the uppermost marine sediments deposited in the Ebro Basin.

Two transgressive-regressive cycles were earlier described in the Middle-Upper Eocene marine deposits of the Igualada area (Serra-Kiel et al., 2003b). The first sedimentary cycle corresponds to the Collbàs Formation, and its maximum flooding surface is determined at the transition from marls with larger foraminifers and ahermatypical corals to marls. The second sedimentary cycle includes the rest of the marine deposits of the Igualada area (Igualada and Tossa formations, the "Terminal Complex" and the Cardona Formation) and its maximum flooding surface is represented by a marker level that covers the Igualada area and has

been interpreted as a condensation level, containing abundant *Discocyclina, Asterocyclina, Assilina* and *Operculina*.

The pioneering studies in the Middle-Upper Eocene marine record of the eastern Ebro Basin made the attempt to apply the Paris Basin chronology by ascribing Auversian, Bartonian and/or Ledian ages to the marine Santa Maria Group (Ruiz de Gaona and Colom, 1950; Ruiz de Gaona, 1952). However, the description of the two new stages (Ilerdian and Biarritzian) in the Eocene of the western Pyrenees by Hottinger and Schaub (1960) favored the adoption of these chronological units in later works (Rosell et al., 1966; Reguant, 1967; Ferrer, 1971a; Caus, 1975; Schaub, 1981; Serra-Kiel, 1984). Subsequently, with a planktonic foraminifers and larger foraminifers biozonation, Ferrer (1971a) established a Biarritzian age (*Truncarotaloides rohri, Nummulites perforatus* and *Alveolina elongata* Biozones) to the Collbàs Formation and the lower part of the Igualada Formation. Ferrer (1971b) also attributed a lower Priabonian age (*Globigerinatheka semiinvoluta* and *Nummulites prefabianii* Biozones) to the upper parts of the Igualada Formation and to the Tossa Formation because of the presence of larger foraminifers *Pellatispira madaraszi* Hantken, 1875 and *Heterostegina reticulata* Rütimeyer, 1850 (=*Grzybowskia reticulate*). These results were challenged by Serra-Kiel et al. (1998a, 1998b), who used the associations of larger foraminifers of the Igualada area, together with data from other alpine-belt regions, as the basis for the definition of the Zones SBZ17 and SBZ18. Currently accepted calibration of the larger foraminifer biostratigraphy indicates that Zones SBZ17 and SBZ18 correlate with the Bartonian stage (Serra-Kiel et al., 1998a, 1998b), in accordance with the occurrence of younger SBZ19 assemblages in the Priabonian type locality (Luciani et al., 2002).

Laterally equivalent to the uppermost marine sediments and also overlaying the top marine beds, the Artés Formation (Ferrer, 1971a), consists of alluvial red beds with interbedded lacustrine limestone units. The basal members of the Artés Formation have yielded scarce biostratigraphic information, reporting a Late Eocene to Early Oligocene vertebrate fossil assemblages (Agustí et al., 1987; Anadón et al., 1987, 1992; Sáez, 1987; Arbiol and Sáez, 1988).

A number of magnetostratigraphic studies spanning the Middle-Late Eocene record of the eastern Ebro Basin were performed in the Vic and Oliana areas during the 1990's (Burbank et al., 1992a, 1992b; Vergés and Burbank, 1996; Taberner et al., 1999). These studies were unable to provide an independent match with the geomagnetic polarity time scale based on the magnetostratigraphic pattern. On the contrary, their correlations were built on the presumed "Bartonian" age of the foraminiferal assemblages of the top marine units. Recent studies, however, have challenged this view showing the presence of fossil assemblages of Priabonian age in the upper units of the Santa Maria Group (Cascella and Dinarès-Turell, 2009), in agreement with earlier findings of Ferrer (1971b). In support of this scenario, a recent magnetostratigraphic study has independently shown that the marine-continental transition took place in the chron C16n.2n, during the Priabonian (Costa et al., 2010).

NEW DATA FROM THE MIRALLES-LA TOSSA COMPOSITE SECTION

Two stratigraphic sections, spanning the Middle-Upper Eocene record of the Igualada area were sampled for magnetostratigraphy and biostratigraphy (Fig. 1B). The Miralles section (1 and 2 in Fig. 1B) covers the continental sediments of the Pontils Group and the marine Collbàs Formation of the Santa Maria Group. The La Tossa section (3 and 4 in Fig. 1B) covers the Igualada and Tossa formations and has its top in the La Tossa de Montbui Castle, 4 km south of Igualada. At the top of the La Tossa section and above the patch reef facies that constitutes the Tossa Formation, yellowish

marine sandstones occur. These transitional sandstones are lateral equivalent to the "Terminal Complex" and the Òdena Gypsum Formation (sulfated belt of the halite-dominated Cardona Formation) and constitute the uppermost marine deposits of the South Pyrenean foreland basin (Fig. 2). Correlation between the Miralles and La Tossa sections yields a total thickness of 1350 meters, which includes a non-outcropping stratigraphic gap of 100 meters at the base of the Igualada Formation.

Larger foraminifers

Recorded assemblages

Along the Miralles-La Tossa composite section 14 samples were collected for the study of larger foraminifers, 9 samples in the Collbàs Formation, 4 samples in the Igualada Formation, and 1 sample in the Tossa Formation. In addition, 3 samples were collected from the "Terminal Complex" outcropping in the nearest Puig Aguilera (Fig. A1). All the samples were studied by means of isolated specimens, which allowed us to observe the external characters as well as to obtain equatorial and axial sections. The samples from the "Terminal Complex" of the Puig Aguilera were studied in thin section.

A complete distribution of the identified larger foraminifers specimens along the Miralles-La Tossa composite section and Puig Aguilera is shown in Fig. 3. Some remarks regarding the biostratigraphical content of the samples, and their correspondence to type localities are detailed below.

Sample BM005, at the bottom of the Collbàs Formation, contains *Nummulites biarritzensis* De La Harpe in Rozlozsnik 1926*, Nummulites beaumonti* D'Archiac and Haime 1853 and *Nummulites praegarnieri* Schaub 1981 (Figs. A7 1 and 2).

Sample BM010 corresponds to a stratigraphical level characterized as a monospecific bank of *Nummulites perforatus* De Montfort 1808 (Figs. A3 4 to 7; A10 6 to 10) by Serra-Kiel and Reguant (1984) and Teixell and Serra-Kiel (1988). The top of this level also contains *Alveolina fragilis* Hottinger 1960.

Sample MM004 corresponds to the type locality of *Nummulites hottingeri* Schaub 1981 (Figs. A3 1; A10 5) associated with *N. biarritzensis* (Figs. A2 5 to 7; A9 9 to 12) and *N. beaumonti*.

Sample MM007 contains *N. biarritzensis, N. beaumonti* and *Assilina schwageri* Silvestri 1928 (Figs. A11 11 and 12).

Sample MM008 corresponds to the type locality of *N. praegarnieri* associated with *N. beaumonti* (Figs. A2 1 and 2; A9 1 to 8)*, A. schwageri* (Fig. A11 11) and *Operculina roselli* Hottinger 1977.

Sample MM022 contains *N. hottingeri* (Figs. A3 2 and 3; A10 1 to 4), *N. biarritzensis* (Figs. A2 8; A9 11) and *N. beaumonti* (Figs. A2 3 and 4; A9 7 and 8).

Sample MM024 contains *Nummulites vicaryi* Schaub 1981, *A. schwageri* (Fig. A11 12) and *O. roselli* (Fig A11 10).

Sample MM028-29 contains *Nummulites striatus* Bruguière 1792, *N. vicaryi* (Figs. A4 1 to 5; A11 1 to 6), and *A. schwageri.*
Sample MM050, at the top of the Collbàs Formation, contains *N. striatus* (Figs. A5 2; A12 1 and 3).

Sample LT000, at the lower part of the Igualada Formation, contains *Nummulites stellatus* Roveda 1961 (Figs. A4 6 and 7; A11 7 and 8) and *Nummulites orbignyi* Galeotti 1837.

Sample LT104 contains *N. striatus* (Figs. A5 1 and 3; A12 2, 4 and 5)*, N. stellatus* (Figs. A4 8 and 9), and *N. orbignyi*.

Sample LT157 contains *N. orbignyi* (Figs. A4 10; A11 9).

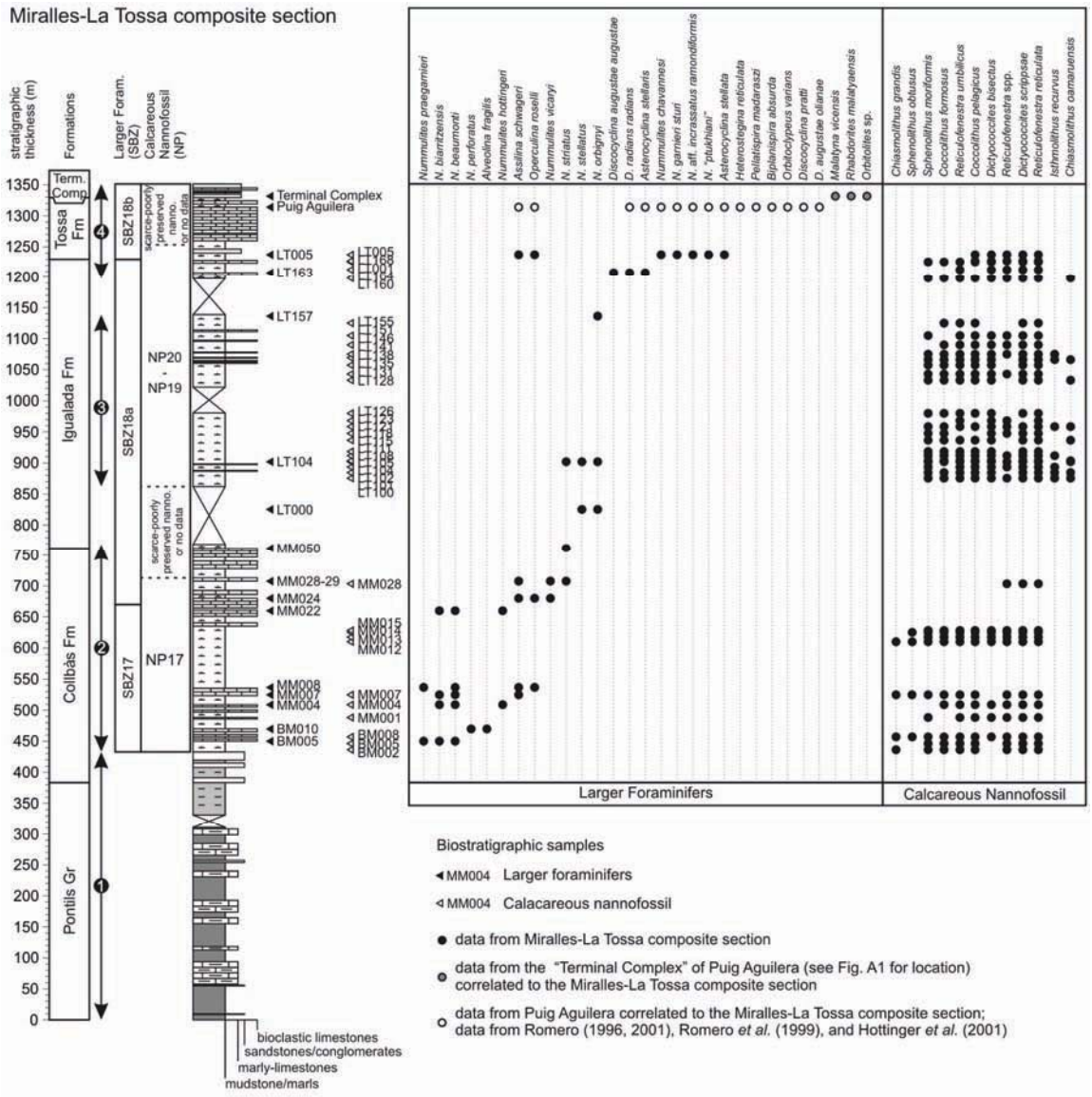

Figure 3 Biostratigraphy of the Miralles-La Tossa composite section (larger foraminifers and calcareous nannofossil). Larger foraminifers from the Tossa Formation and the "Terminal Complex" cropping out in Puig Aguilera (Fig. A1) are added as gray dots. Only the most significant calcareous nannofossil species have been plotted in the figure, for a complete list see appendix Table A1. Larger foraminifers zonation in the Miralles-La Tossa composite section is based in Serra-Kiel et al. (1998a) but modified in this work. Calcareous nannofossil zonation from Martini (1971). 1 to 4 correspond to subsections shown in Fig. 1B.

*S*ample LT163 contains *Discocyclina augustae augustae* Weijden 1840, *Discocyclina radians radians* D'Archiac 1850, and *Asterocyclina stellaris* Brünner 1848 in Rütimeyer 1850.

Sample LT005, from the Tossa Formation, contains *Assilina schwageri, O. roselli, Asterocyclina stellata* D'Archiac 1846, *Nummulites chavannesi* De La Harpe 1878 (Figs. A6 1 to 9; A13 6 to 11), *Nummulites garnieri sturi* Vanova 1972 (Figs. A7 14 to 18; A13 1 to 5), *Nummulites "ptukhiani"*

sensu Papazonni (1998), and *Nummulites* aff. *incrassatus ramondiformis* De La Harpe 1883 (Figs. A8 1 to 5; A13 12 to 26).

In the nearest Puig Aguilera area (Fig. A1), the Tossa Formation contains *Nummulites* aff. *incrassatus ramondiformis, N. chavanesi, N. garnieri sturi, N. "ptukhiani", Operculina roselli, Assilina schwageri, Heterostegina reticulata* Rütimeyer 1850, *Discocyclina pratti* Michelin 1846, *D. radians radians, D. augustae olianae, Asterocyclina stellaris, A. stellata, Orbitoclypeus varians* Kaufmann 1867*, Pellatispira madaraszi* Hantken 1875, and *Biplanispira absurda* Umgrove 1938. A detailed stratigraphical distribution of all this forms (white dots in Fig. 3) at the Puig Aguilera section is presented in Serra-Kiel et al. (2003a). Finally, the study of the thin sections of the samples collected in the "Terminal Complex" of Puig Aguilera (Fig. A1) has revealed the presence of *Malatyna vicensis* Sirel and Açar 1998*, Rhabdorites malatyaensis* Sirel 1976, and *Orbitolites* sp. (marked as grey dots in Fig. 3).

Larger foraminifers from the Miralles-La Tossa composite section were well described and illustrated by previous authors (e.g. Hottinger, 1960; Schaub, 1981; Papazzoni and Sirotti, 1995; Romero et al., 1999; Romero, 2001; Hottinger et al., 2001; Serra-Kiel et al., 2003a). However, some forms as *Nummulites chavannesi*, *N. garnieri sturi*, and *N.* aff. *incrassatus ramondiformis* of the Tossa Formation need an accurate description. With that purpose a Larger Foraminifers Systematic Remarks chapter has been added at the end of this paper.

Biostratigraphy

From the study of the Miralles-La Tossa composite section a larger foraminifer biozonation can be established. The Zone SBZ17 is represented by the occurrence of *Alveolina fragilis*, *Nummulites biarritzensis, N. perforatus, N. beaumonti, N. hottingeri,* and *N. praegarnieri* in the interval covering from sample BM005 and sample MM022, within the Collbàs Formation (Fig. 3). The first occurrence of the *N. vicaryi* in sample MM024 and *N. striatus* in sample MM028-029 indicates the bottom of the Zone SBZ18. The top of this zone is not recognized because of the absence of the typical Zone SBZ19 forms such as *N. fabianii, N. cunialensis* and *N. garnieri garnieri.* It is noticeable, however, the occurrence of *Nummulites stellatus* (samples LT000 and LT104 in Fig. 3) and the *Nummulites chavannesi* (sample LT005 in Fig. 3), forms of Priabonian age according to Roveda (1961) and Herb and Hekel (1975).

Special attention should be given to the fossil assemblage of the sample LT005, which contains *Nummulites* aff. *incrassatus ramondiformis*, *N. garnieri sturi*, and *N. chavannesi* (Figs. 3 and A6, A7, and A8). This assemblage was characterized by Papazzoni and Sirotti (1995) as *Nummulites variolarius/incrassatus Biozone*, and was considered to be located close to the Bartonian-Priabonian boundary. Characteristic of this interval is the first occurrence of the *Pellatispira madaraszi, Biplanispira absurda* and *Heterostegina reticulata*, and the absence of *N. striatus, N. vicaryi, N. boulangeri*, and *N. cyrenaicus.* In Fig. 3 this zone has been denoted as larger foraminifer Zone SBZ18b and it comprises the entire Tossa Formation.

Calcareous nannofossil

Recorded assemblages

For the calcareous nannofossil analysis 47 samples were studied from the marine units of the Miralles-La Tossa composite section, 12 from the Collbàs Formation, 25 from the Igualada Formation, and 10 from the Tossa Formation (Fig. 3). All the samples were processed following the micropipette method of Bown (1998) and studied under a Leica petrographic microscope at 1500 and 2000 magnification. For the quantitative analysis, at least 300 species per sample were counted in a randomly selected field of view. In order to detect rare species with key biostratigraphic value additional 8 mm^2 were analyzed in each sample. The results of the quantitative analysis, summarized in Table

A1, include the preservation degree of the assemblage, the presence of reworked assemblages, the total species abundance (in number of specimens per field of view), and the relative abundance of single species (%).

The total abundance and preservation of calcareous nannofossil assemblages varies along the section. At the base of the Collbàs Formation the reworked cretaceous species are abundant and the preservation and abundance of autochthonous species is poor. Up in the succession the total abundance of calcareous nannofossils increase and the preservation changes from poor to moderate-good. At the upper 50 meters of the Collbàs Formation the autochthonous species are almost absent and their preservation is very poor, making impossible the assignment of a calcareous nannofossil zone to this stratigraphic interval. In the lowest samples of the Igualada Formation calcareous nannofossils are again abundant and well preserved. However, from sample LT141 upward the total abundance decreases distinctly and preservation gets worse. From sample LT155 up to the top of the Igualada Formation very rare and poorly preserved autochthonous calcareous nannofossil has been recorded. Finally, at the Tossa Formation calcareous nannofossils are absent.

In the Miralles-La Tossa composite section the calcareous nannofossil diversity is relatively low (about 15 species per sample), especially when compared to that registered in lower and middle Eocene of classical Pyrenean sections, such as Zumaia or Gorrondatxe sections (Orue-Etxebarria et al., 2004; Bernaola et al., 2006). Throughout the Collbàs Formation the assemblage is dominated by *Reticulofenestra reticulata, Dictyococcites scrippsae, Reticulofenestra umbilicus*, and in lesser extent *Coccolithus pelagicus* and *Coccolithus formosus*. At the Igualada Formation the calcareous nannofossil assemblage is mainly defined by the same species that dominate the Collbàs Formation with the exception of *Dictyococcites bisectus* that change from being rare at the base of the Collbàs Formation to be abundant in the Igualada Formation. *Discoaster, Sphenolithus*, and *Chiasmolithus* are scarce throughout the whole section.

Biostratigraphy and main bioevents

Following the standard biostratigraphic zonation of Martini (1971) the studied interval spans from the upper part of Zone NP17 to the undifferentiated Zone NP19-NP20 (Fig. 3). Zones NP19 and NP20 are combined because the First Appearance Datum (FAD) of *Sphenolithus pseudoradians*, the marker of the base of Zone NP20, is an unreliable marker (Aubry, 1983; Gradstein et al., 2004). The Zone NP18, defined by the stratigraphic interval between the FAD of *Chiasmolithus oamaruensis* to the FAD of *Isthmolithus recurvus*, has not been recorded at the Miralles-La Tossa composite section. In the present study these two biomarkers first occur together from the lowest sample of the Igualada Formation. The lack of record of Zone NP18 in this study could be due to the almost absence and very poor preservation of calcareous nannofossil in the upper 50 meters of the Collbàs Formation and the non-outcropping 100-m-thick interval at the base of the Igualada Formation.

Calcareous nannofossil biostratigraphy of the Miralles-La Tossa section allows recognition of 6 relevant bioevents (Fig. 3) as described below.

- FOs of *Dictyococcites scrippsae* and *Dictyococcites bisectus*

D. scrippsae has been recorded from the lowest sample of the studied interval whereas *D. bisectus* has its First Occurrence (FO) in sample BM008. The FO of *D. bisectus* is not easy to pinpoint precisely in this section since it is rare in the lower part of its range and the preservation of the calcareous nannofossil assemblages in the lower portion of the Collbàs Formation is poor. The FOs of *D. scrippsae* and *D. bisectus* has been used by many authors to mark the base and middle part of NP17 respectively. However, recent studies carried out at ODP Legs 198 (Shatsky

Rise, Pacific Ocean), ODP Site 1052 (Blake Nose, northwestern Atlantic Ocean), Agost section (southeastern Spain), and Alano section (northern Italy) show that the FO of both species occur earlier in Zones NP15 and NP16 (Bralower, 2005; Larrasoaña et al., 2008; Fornaciari et al., 2010; Agnini et al., 2011).

- LO of *Chiasmolithus grandis*
The presence of *C. grandis* in the Miralles-La Tossa composite section is rare and shows a discontinuous distribution. In the present study the Last Occurrence (LO) of this species has been recorded at sample MM012 in the meter 610. Due to the scarcity of *C. grandis* at the section this could be considered an unreliable marker. However, the absence of both *C. grandis* and *C. oamaruensis* from sample MM013 to sample MM028 suggest that this part of the section corresponds to the upper part of Zone NP17. It is important to pinpoint that the scarcity of *Chiasmolithus* is a generalized feature in the upper Eocene of the South Pyrenean Foreland Basin (Cascella and Dinarès-Turell, 2009) and Mediterranean area (Nocchi et al., 1988; Luciani et al., 2002) and thus it is complex to accurately locate the base of Zone NP18 in these areas.

- LO of *Sphenolithus obtusus*
Together with the LO of *C. grandis*, the LO of *S. obtusus* is used to mark the uppermost part of Zone NP17. In the Miralles-La Tossa composite section the LO of *S. obtusus* has been recorded in sample MM014. This event confirms that from the sample MM015 upward the section corresponds, at least, to the uppermost part of Zone NP17.

- FO of *Chiasmolithus oamaruensis*
The FO of *C. oamaruensis* marks the base of Zone NP18. At the Miralles-La Tossa composite section this event has been recorded at sample LT100, located approximately 100 meters above the base of the Igualada Formation. Although *Chiasmolithus* specimens are scarce throughout the whole section *C. oamaruensis* has been continuously recorded from sample LT100 upward.
- FO of *Isthmolithus recurvus*
The FO of *I. recurvus* marks the base of Zone NP19. At the Miralles-La Tossa composite section the FO of *I. recurvus* has been recorded together with the FO of *C. oamaruensis* at sample LT100 and as a result the record of Zone NP18 is missing. However, Zone NP18 could still be present in the upper 50 meters of the Collbàs Formation with scarce and poor preserved calcareous nannofossil and/or the non-outcropping 100-m-thick interval of the base of the Igualada Formation.

Magnetostratigraphy

In the 1350-m-thick composite section of Miralles-La Tossa a total of 224 paleomagnetic sites were collected. The mean sampling resolution obtained was of 6 meters in the Miralles section and of 4 meters in the La Tossa section, enough to allow a complete identification of this time period geomagnetic polarity reversals considering mean accumulation rates of 20-25 cm/kyr reported along the eastern Ebro Basin (Burbank et al., 1992a, 1992b; Vergés and Burbank, 1996; Taberner et al., 1999; Costa et al., 2010). Sampling was focused in fine-grained fraction lithologies, mudstones and micritic limestones in the continental Pontils Group and gray marls, limestones and fine sandstones in the marine Igualada and Tossa formations and in the "Terminal Complex". Two oriented cores per site were taken with an electrical portable drill at most sites. Samples were oriented in situ using a magnetic compass coupled to a core-orienting fixture.

The paleomagnetic analysis consisted in stepwise thermal demagnetization of the natural remanent magnetization (NRM) on at least one sample per site. Measurements of the NRM were performed using a 2G superconducting rock magnetometer at the Paleomagnetic Laboratory of the Universitat de Barcelona (CCiTUB-CSIC). Stepwise thermal demagnetization was conducted in a

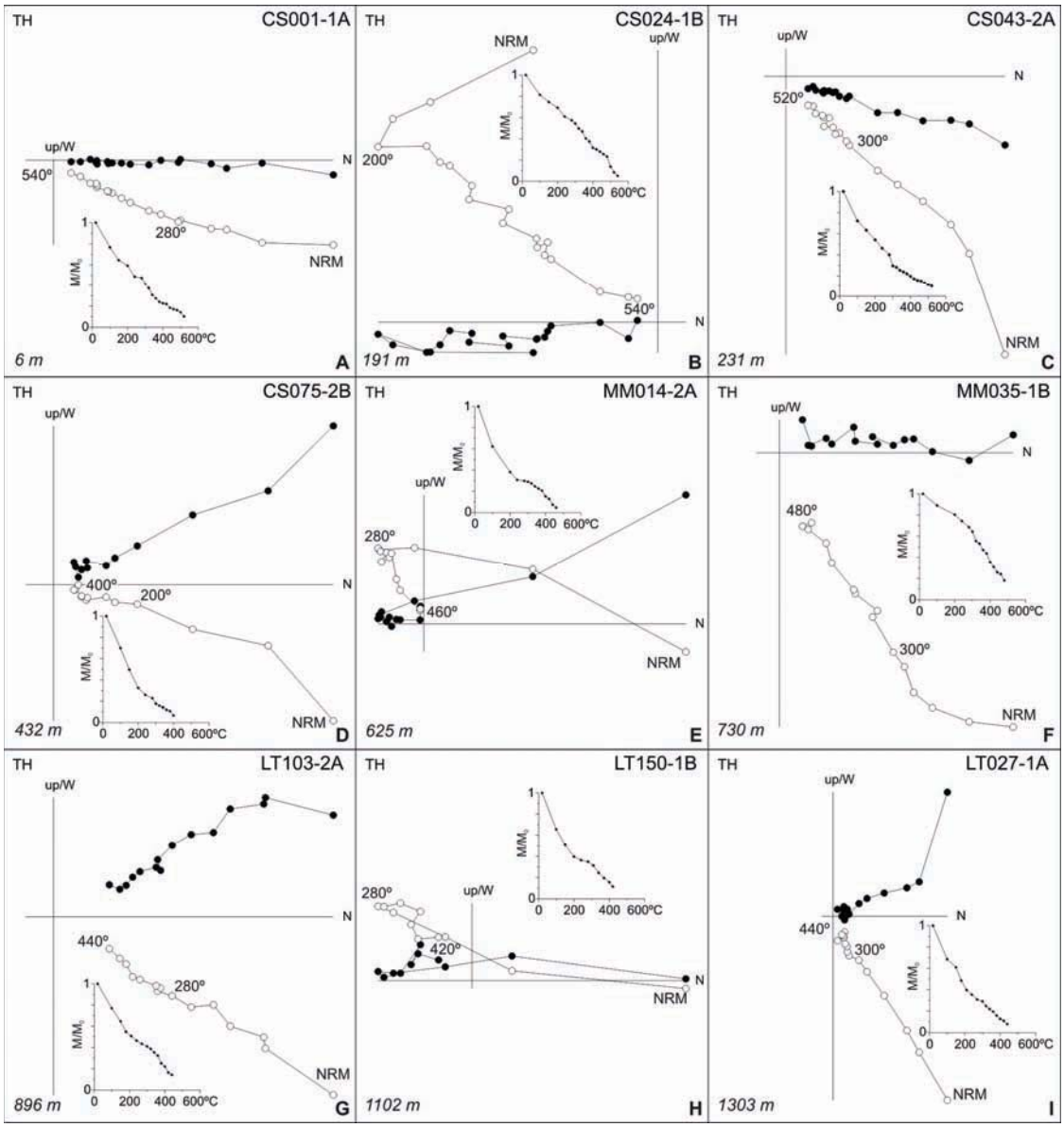

Figure 4 Representative Zijderveld demagnetization diagrams from the Miralles-La Tossa composite section. All the projections are in tectonic corrected coordinates. The NRM decay plots (squared curve) are obtained after the normalization of the vector subtraction module. The stratigraphic position is shown in meters (lower left). (A to F) Samples from the Miralles section and (G to I) are samples from the La Tossa section.

Schönstedt TSD-1 and a Magnetic Measurements MMTD-80 thermal demagnetizers at intervals ranging between 100ºC and 20ºC and up to a maximum temperature of 540ºC.

Paleomagnetic components were determined from visual inspection of the Zijderveld diagrams (Fig. 4). In all the specimens, a viscous magnetization component which parallels the present day field and represents up to 70% of the initial NRM is unblocked at temperatures below 240ºC to 280ºC. Above this temperature, a characteristic remanent magnetization (ChRM) of either normal or reversed polarity can be identified. The ChRM shows maximum unblocking temperatures above 300ºC, which suggests that the ChRM is carried by iron oxides such as magnetite and hematite. ChRM directions were calculated from the demagnetization diagrams by means of principal components analysis (Kirschvink, 1980). Reliable ChRM directions were calculated for 186 paleomagnetic sites (Table A2), which represents the 83% of the total number of the sampled levels. The normal and reversed ChRM directions yield antipodal Fisherian means after the bedding correction (Fig. 5) and the obtained values conform to the paleomagnetic references for the Middle-Upper Eocene (Burbank et al., 1992a; Taberner et al., 1999).

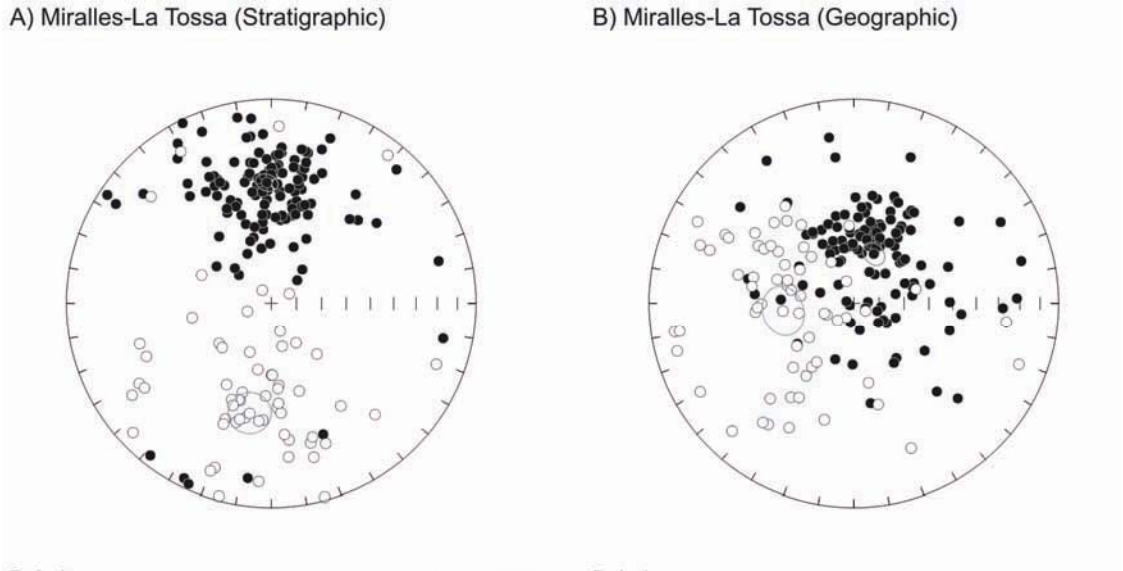

Polarity	N	Dec	Inc	k	α95
Normal	127	357.9	40.5	9.9	4.2
Reversed	61	191.0	-44.1	5.8	8.3

Polarity	N	Dec	Inc	k	α95
Normal	126	21.9	68.7	8.9	4.5
Reversed	62	263.8	-61.5	5.0	9.0

Figure 5 Stereonet projections of the ChRM of the Miralles-La Tossa composite section with calculated Fisherian statistics and mean. (A) Stratigraphic and (B) Geographic coordinates.

ChRM directions were used to compute the latitude of the virtual geomagnetic pole (VGP) in order to obtain a local magnetostratigraphy of the Miralles-La Tossa composite section (see Table A2). Magnetozones were defined by at least two adjacent paleomagnetic sites with the same polarity. Single-site reversals were denoted as

half-bar magnetozones in the local magnetostratigraphic section, but were not considered for magnetostratigraphic correlation purposes. After the exclusion of these unreliable short magnetic reversals, a total of 7 normal and 5 reversed polarity magnetozones have been recognized along the composite Miralles-La Tossa magnetostratigraphic section (Fig. 6).

CORRELATION OF THE MIRALLES-LA TOSSA MAGNETOSTRATIGRAPHIC SECTION TO THE GEOMAGNETIC POLARITY TIME SCALE

A correlation of the local magnetostratigraphic section of Miralles-La Tossa with the Geomagnetic Polarity Time Scale (GPTS) 2004 (Gradstein et al., 2004) can be put forward on the basis of the available biostratigraphic constraints and the obtained polarity reversal pattern (Fig. 6). Biostratigraphic data discussed above clearly indicates that the marine units of the Miralles-La Tossa composite section span from Bartonian to Priabonian age. Taken biostratigraphy as a first-order coarse constraint, a good fit of the composite Miralles-La Tossa magnetostratigraphy with the GPTS (Gradstein et al., 2004) is achieved by correlating the long reversed magnetozones R1 and R2 with the chrons C19r and C18r, and the long normal magnetozones N4, N5+N6, and N7 with chrons C18n, C17n, and C16n respectively (Fig. 6). Correlation of the top normal magnetozone N7 with chron C16n.2n is in agreement with the calcareous nannofossil data reporting a NP19-20 age, and best fits with the age of the marine-continental transition in the basin (Costa et al., 2010). Following this solution, shorter chrons C17n.2n, C17n.1r, and C17n.2r must have been missed in the non outcropping gap corresponding to the lower part of the Igualada Formation. A short normal magnetozone at the transition from the continental Pontils Group to the Collbàs Formation (N3) is ignored in the proposed correlation. A delayed magnetization associated to this transition is suggested given the correspondence between polarity and sedimentary facies changes. Samples recording N3 correspond to lagoonal grey mudstones of the top Pontils Group, while samples recording R3 correspond to the transgressive coarse sediments of the basal Collbàs Formation.

The biomagnetostratigraphy-based chronology of the Miralles-La Tossa composite section allows establishing a reliable chronostratigraphy of the Middle-Upper Eocene marine record of the eastern Ebro Basin. The resulting absolute chronology, ranging from chron C20n to chron C16n (~43 Ma to ~36 Ma), challenges existing chronostratigraphic interpretations of the Pontils and Santa Maria groups (Fig. 2). While earlier studies attributed to these units a Bartonian age according to its fossil contents (Serra-Kiel et al., 2003b), the new magnetostratigraphy of Miralles-La Tossa sections demonstrates that the Igualada Formation embraces a large part of the Priabonian stage.

CALIBRATION OF THE BARTONIAN-PRIABONIAN SBZ AND NP BIOZONES

The Bartonian-Priabonian boundary as defined in the historical type section of Priabona (northern Italy) is loosely characterized because it corresponds to a transition from continental to marine facies (Luciani et al., 2002; Gradstein et al., 2004; Cascella and Dinarès-Turell, 2009; Agnini et al., 2011). For that reason, biomagnetostratigraphic calibrations of the Priabonian stage have been to date based on the classic pelagic sections in Umbria, central Italy (Lowrie et al., 1982; Monechi and Thierstein, 1985; Monechi, 1986), as well as Ocean Drilling Program (ODP), Deep Sea Drilling Project (DSDP) and Integrated Ocean Drilling Program (IODP) Sites (Poore et al., 1982; Backman, 1987; Wei and Wise, 1989; Wei, 1991; Wei and Thiesrstein, 1991; Chanell et al., 2003). More recently, detailed biomagnetostratigraphic data from the ODP Site 1052 (northwestern Atlantic Ocean) and

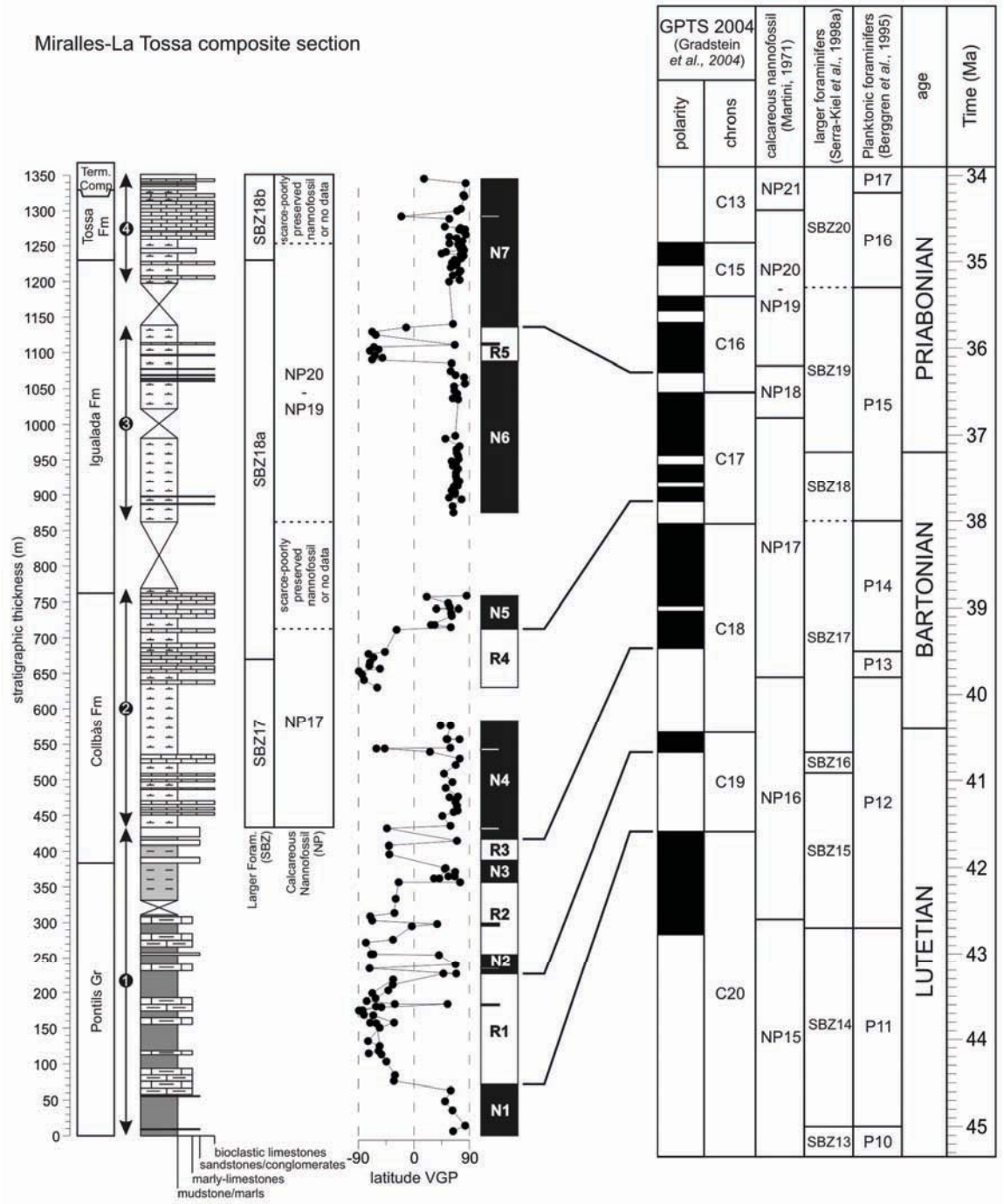

Figure 6 Local magnetostratigraphic section of the Miralles-La Tossa and correlation to the GPTS (Gradstein et al., 2004). Circles show the VGP latitude. Stable magnetozones were defined by at least 2 adjacent paleomagnetic sites showing the same polarity. Half-bar zones denote single-site reversals. Calcareous nannofossil, larger foraminifers and planktonic foraminifers zonations come from Martini (1971), Serra-Kiel et al. (1998a) and Berggren et al. (1995), respectively. 1 to 4 correspond to subsections shown in Fig. 1B.

the Alano section (northern Iatly) have provided new insights in the calibration of the calcareous nannofossil zonation of the middle-late Eocene (Fornaciari et al., 2010; Agnini et al., 2011). Larger foraminifer data is absent in these pelagic records, so that calibration of the SBZ scale has remained elusive to most recent calibration efforts of marine biostratigraphy. The new biomagnetostratigraphic data from the Miralles-La Tossa composite section allows an improved intercalibration between larger foraminifers and calcareous nannofossils as well as a new correlation with the geomagnetic polarity time scale.

Larger foraminifers

The current calibration of the larger foraminifer biostratigraphy correlates Zones SBZ17 and SBZ18 with the Bartonian (Serra-Kiel et al., 1998a), the two Zones being well represented in the fossil record of the Ebro Basin. According to Serra-Kiel et al. (1998a), Zone SBZ17 is defined by the biostratigraphic range of *Alveolina elongata, A. fragilis, A. fusiformis, Nummulites brongniarti, N. perforatus, N. hottingeri, N. puschi, N. biarritzensis, N. lyelli,* and *Discocyclina pulcra baconica*. It is worth noting that during the thorough revision of the larger foraminiferal assemblages of the Miralles section, a transcription error in the later work of Serra-Kiel et al. (2003a, 2003b) was detected, which lead to an incorrect attribution of *Nummulites cyrenaicus, N. vicary,* and *N. striatus* to Zone SBZ17. Zone SBZ18 is defined by the biostratigraphic range of *Nummulites biedai, N. cyrenaicus, N. vicaryi,* and *N. boulangeri* (Serra-Kiel et al., 1998a). The absence of these species in the Upper Eocene series of the northern Italy has to date supported a correspondence of Zone SBZ18 with the late Bartonian. The Zone SBZ19, correlated with early Priabonian, is defined by the biostratigraphic range of *Nummulites fabianii, N. garnieri garnieri, N. cunialensis, Discocyclina pratti minor,* and *Asterocyclina alticostata danubica*.

In the GTS 2004 (Gradstein et al., 2004) no correlation of the Paleogene larger foraminifers zonation with the geomagnetic polarity time scale is provided, therefore the only calibration is the one proposed by Serra-Kiel et al. (1998a). These authors correlated the Zones SBZ17 and SBZ18 to the GPTS (Berggren et al., 1995) according to the magnetostratigraphic data of Burbank et al. (1992a) in the equivalent marine units of the Vic area (Fig. 1A for location). The Vic magnetostratigraphy, however, was questioned by new biostratigraphic data from the same area (Cascella and Dinarès-Turell, 2009), and its correlation with the GPTS re-interpreted in the light of new magnetostratigraphic constraints (Costa et al., 2010). Therefore, a new calibration of the larger foraminifers zonation is required.

The results of the present study (Fig. 3) provide further constraints for a revised calibration of Zones SBZ17, SBZ18, and SBZ19 (Figs. 6 and 7). It is shown that the entire Zone SBZ17 correlates with the Bartonian (Fig. 7). Zone SBZ18 spans from late Bartonian to early Priabonian, in contrast to its currently accepted late Bartonian age. This new attribution is coherent with the presence of *N. stellatus* in the lowermost part of the Igualada Formation, a form which has been found in the Priabonian record of the Monte Cavro, Nago, Mossano (Papazzoni and Sirotti, 1995) and in the Marne di Possagno in northern Italy (Herb and Hekel, 1975). As a consequence, a division of Zone SBZ18 into two Subzones (SBZ18a and SBZ18b) is here proposed. Subzone SBZ18a is characterized by the presence of *Nummulites vicaryi*, *Nummulites cyrenaicus*, *Nummulites biedai,* and *Nummulites boulangeri*. Subzone SBZ18b is characterized by the presence of *Nummulites* aff. *incrassatus ramondiformis*, *Nummulites garnieri sturi*, *Nummulites chavannesi*, *Asterocyclina stellata, Pellatispira madaraszi*, *Heterostegina reticulate,* and *Biplanispira absurda*, being this Subzone equivalent to the *Nummulites variolarius/incrassatus* Biozone of Papazzoni and Sirotti (1995).

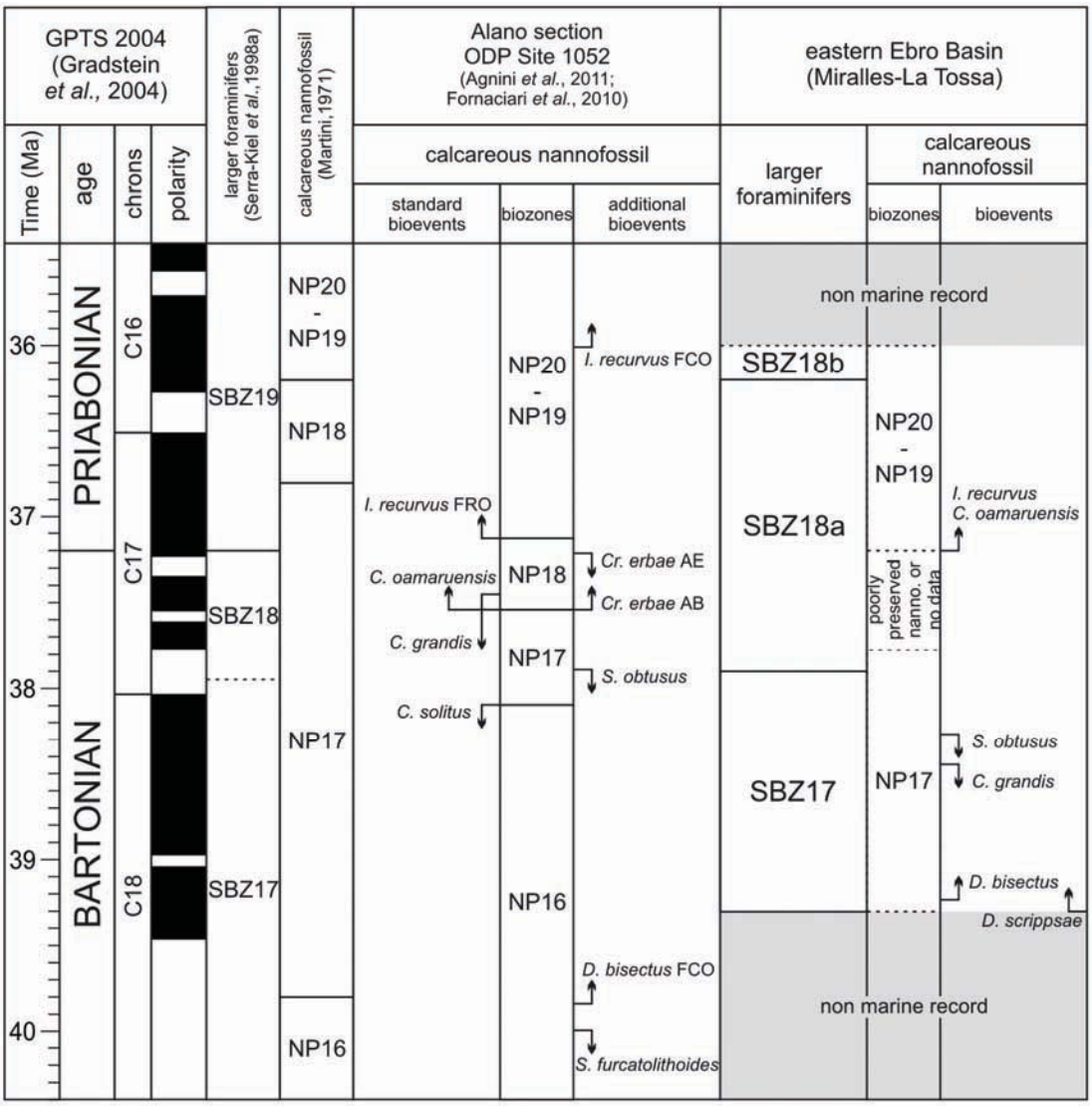

Figure 7 New calibration of the Miralles-La Tossa larger foraminifers and calcareous nanofossil zones to the GPTS (Gradstein et al., 2004). Previous calibrations of these zonations (Martini, 1971; Serra-Kiel et al., 1998a; Fornaciari et al., 2010; Agnini et al., 2011) are also shown to contrast. Discontinuous line indicates indeterminate zone boundary and gray colour indicates lack of marine record in the eastern Ebro Basin. FRO, First Rare Occurrence. FCO, First Common Occurrence. AB, Acme Beginning. AE, Acme End.

The newly defined Subzone SBZ18b, spanning the Tossa Formation and the "Terminal Complex", correlates to the mid-Priabonian (chron C16n). The fossil assemblage found in the "Terminal Complex" contains an association of *Malatyna vicensis*, *Orbitolites* sp., and *Rhabdorites malatyaensis*. Remarkably, this fossil assemblage is not known in the Priabonian type sections of northern Italy, probably related to paleoenvironmental issues.

Calcareous nannofossil

The Bartonian and Priabonian Stages include the calcareous nannofossil Zones NP17, NP18, and NP19-20 (Martini, 1971). The current calibration of the NP zones (Gradstein

et al., 2004) is largely based on the biomagnetostratigraphic correlations of Berggren et al. (1995). Following this scheme, the base of Zone NP17 (LO of the *Chiasmolithus solitus*) correlates with the reversed chron C18r (early Bartonian), the base of Zone NP18 (FO of the *Chiasmolithus oamaurensis*) with chron C17n.1n (early Priabonian), and the base of Zone NP19-20 (FO of the *Isthmolithus recurvus*) with chron C16n.2n (Priabonian). Regarding the age of this last bioevent, debate has persisted in the literature. In Umbria, the FO of *I. recurvus* was first correlated with chron C15 (Lowrie et al., 1982; Monechi and Thierstein, 1985), but latter found to occur at an older age, within chron C16n.2n (Monechi, 1986), such discrepancy being attributed to the poor preservation or scarcity of *I. recurvus* in the Umbrian sections (Monechi, 1986). In oceanic sections of the Southern Ocean, the same event was found either in chron C15n in Site 522 (Poore et al., 1982), or chron C16n (in Sites 522 and 523 Backman, 1987; Sites 699A and 703A Wei, 1991; Site 744A Wei and Thiesrstein, 1991; Site 1090 Channell et al., 2003), this diachrony being attributed to its cool water affinity (Backman, 1987; Wei and Wise, 1989; Wei, 1991).

In the eastern Ebro Basin, the new biomagnetostratigraphy of Miralles-La Tossa indicates a correlation of FO of *I. recurvus* with chron C17n.1n, an age which is considerably older than the records discussed above. Noteworthy, a correlation of this event with chron C17n was already reported from Site 516 (Wei and Wise, 1989), and Site 523 (Backman, 1987), both records regarded as unreliable: Site 516 was considered to yield poor-quality magnetostratigraphy (Chanell et al., 2003), while data from Site 523 was rejected arguing downhole contamination (Backman, 1987). But, recent results from the ODP Site 1052 in NW Atlantic Ocean (Fornaciari et al., 2010) and the Alano section in the Possagno area, northern Italy, (Agnini et al., 2011) firmly supports a correlation of the first rare occurrence of *I. recurvus* with chrons C17n.1r and C17n.1n (Fig. 7), in agreement with results from the Ebro Basin.

Extending the range of Zone NP19-20 down to chrons C17n.1n or C17n.1r, would lead to a complete overlap with the range of Zone NP18 (Fig. 7). This raises the question on whether FO of *I. recurvus* is a reliable long-distance chronostratigraphic marker, a question which is in agreement with the highlighted need to revise the present Middle-Late Eocene calcareous nannofossil biochronology pointed by Fornaciari et al. (2010) and Agnini et al. (2011).

CONCLUSIONS

The combined biostratigraphic (calcareous nannofossil, larger foraminifers) and magnetostratigraphic study of the Middle-Late Eocene marine units of the Igualada area (NE Spain) allows establishing a reliable chronostratigraphy of the Middle-Upper Eocene marine record of the eastern Ebro Basin. The resulting new chronology, that ranges from chron C20n to chron C16n (Bartonian-Priabonian), challenges existing chronostratigraphic attributions of the Igualada and Tossa formations (Santa Maria Group). As a result, a revised calibration of the late Eocene larger foraminifers and calcareous nannofossil biozonation is proposed. The traditional division of the Bartonian stage into two complete larger foraminifers zones, SBZ17 and SBZ18, is challenged. Zone SBZ17 embraces most of the Bartonian, while Zone SBZ18 extends from late Bartonian to early Priabonian. In addition, a new Subzone (SBZ18b = *N. variolarius/incrassatus* Biozone), recognized in both the Ebro Basin and the Priabonian type sections of Italy, is proposed, while the Subzone SBZ18a is equivalent to the former Zone SBZ18 of Serra-Kiel et al. (1998a). Magnetostratigraphic calibration of calcareous nannofossil in the Ebro Basin reveals a mismatch with the current calibration of Zone NP19-20, suggesting that FO of *I. recurvus* is a diachronic event, of low reliability for long-distance correlations. The calcareous nannofossil Zone NP19-20 correlates to the larger foraminifers Zone

SBZ18 (uppermost Bartonian-early Priabonian).

ACKNOWLEDGEMENTS

This paper has been developed in the framework of the Spanish MCI projects: CENOCRON CGL2004-00780, REMOSS 3D-4D CGL2007-66431-C02-02/BTE and INTERBIOSTRAT CGL2008-0809/BTE. This research was supported by the Research Group of "Geodinàmica i Anàlisi de Conques" (2009 GGR 1198-Comissionat d'Universitats i Recerca de la Generalitat de Catalunya) and the Research Institute GEOMODELS. We are grateful to Vanesa Pulido and Ruth Soto who assisted during field work and laboratory analysis. The discussion, comments and suggestions of an Anonymous Reviewer, Jaume Dinarès-Turell, and Simonetta Monechi have significantly improved this paper. EC was funded by a PhD grant of the MCI.

REFERENCES

Agnini, C., Fornaciari, E., Giusberti, L., Grandesso, P., Lanci, L., Luciani, V., Muttoni, G., Pälike, H., Rio, D., Spofforth, D.J.A., Stefani, C., 2011. Integrated biomagnetostratigraphy of the Alano section (NE Italy): A proposal for defining the middle-late Eocene boundary. Geological Society of American Bulletin, 123, 841-872. doi: 10.1130/B30158.1

Agustí, J., Anadón, P., Arbiol, S., Cabrera, L., Colombo, F., Sáez, A., 1987. Biostratigraphical characteristics of the Oligocene sequences of North-Eastern Spain (Ebro and Campins Basins). Münchner Geowissenschaftliche Abhandlungen, 10, 35-42.

Anadón, P., 1978. El Paleógeno continental anterior a la transgresión Biarritziense (Eoceno medio) entre los ríos Gaià y Ripoll (provincia de Tarragona y Barcelona). Estudios Geológicos, 34, 341-440.

Anadón, P., Feist, M., 1981. Charophytes et Biostratigraphie du Paléogène Inférieur du bassin de l'Ebre oriental. Palaeontographica Abt. B, 178, 143-168.

Anadón, P., Roca, E., 1996. Geological setting of the Tertiary basins of the Northeaste Spain. In: Friend, P.F., Dabrio, C.J. (eds.). Tertiary basins of Spain. The stratigraphic record of crustal kinematics, Cambridge, Cambridge University Press, World and Regional Geology, 6, 43-48.

Anadón, P., Cabrera, L., Guimerà, J., Santanach, P., 1985a. Paleogene strike-slip deformation and sedimentation along the southeastern margin of the Ebro Basin. In: Biddle, K.T., Christie-Blick, N. (eds.). Strike-slip tectonics and sedimentation. Society of Economic Paleontology and Mineralogy. Special Publication, 37, 303-318.

Anadón, P., Marzo, M., Puigdefàbregas, C., 1985b. The Eocene fan-delta of Montserrat (Southeastern Ebro basin, Spain). In: Milà, M.D., Rosell, J. (eds.). 6th European Meeting Excursion Guidebook, Lleida, IAS/Institut d´estudis Ilerdencs, 109-146.

Anadón, P., Vianey-Liaud, M., Cabrera, L., Hartenberger, J.L., 1987. Gisements à vertébrés du paléogène de la zone orientale du bassin de l'Ebre et leur apport à la stratigraphie. Paleontologia i Evolució, 21, 117-131.

Anadón, P., Cabrera, L., Colldeforns, B., Sáez, A., 1989. Los sistemas lacustres del Eoceno superior y Oligoceno del sector oriental de la Cuenca del Ebro. Acta Geologica Hispanica, 24(3-4), 205-230.

Anadón, P., Cabrera, L., Choi, S.J., Colombo, F., Feist, M., Sáez, A., 1992. Biozonación del Paleógeno continental de la zona oriental de la Cuenca del Ebro mediante carófitas; implicaciones en la biozonación general de carófitas de Europa occidental. Acta Geologica Hispanica, 27(1-2), 69-94.

Arbiol, S., Sáez, A., 1988. Sobre la edad oligocénica inferior del yacimiento de Santpedor (Cuenca del Ebro, provincia de Barcelona). Acta Geologica Hispanica, 23(1), 47-50.

Aubry, M.P., 1983. Biostratigraphie du Paléogène de l'Europe épicontinentale du Nord-Ouest, etude fondée sur les nannofossiles calcaires. Documents des Laboratoires de Géologie de Lyon, 89, 1-317.

Backman, J., 1987. Quantitative calcareous nannofossil biochronology of middle Eocene through early Oligocene sediment from DSDP Sites 522 and 523. Abhandlungen der Geologische Bundesanstalt, 39, 21-32.

Barberà, X., Cabrera, L., Marzo, M., Parés, J.M., Agustí, J., 2001. A complete terrestrial Oligocene magnetostratigraphy from the Ebro Basin, Spain. Earth and Planetary Science Letters, 187, 1-16.

Beaumont, C., Muñoz, J.A., Hamilton, J., Fullsack, J., 2000. Factors controlling the Alpine evolution of the Central Pyrenees inferred from the comparison of observations and geodynamical models. Journal of Geophysical Research, 105, 8121-8145.

Berggren, W.A., Kent, D.V., Swicher III, C.C., Aubry, M.P., 1995. A revised Cenozoic geochronology and chronostratigraphy. In: Berrgren, W.A., Kent, D.V., Aubry, M.P., Hardenbol, P. (eds.). Geochonology, Time Scales and Global Stratigraphic Correlations. Tulsa, Society for Sedimentary Geology, SEMP Special Publication, 129-212.

Bernaola, G., Orue-Etxebarria, X., Payros, A., Dinarès-Turell, J., Tosquella, J., Apellaniz, E., Caballero, F., 2006. Biomagnetostratigraphic analysis of the Gorrondatxe section (Basque Country, Western Pyrenees): Its significance for definition of the Ypresian/Lutetian boundary startotype. Neues Jahrbuch für Geologie und Paläontologie Abhandlungen, 241, 67-109.

Bown, P.R., 1998. Calcareous Nannofossil Biostratigraphy. London, Chapman Hall Ltd. Kluwer Academic Publisher, 385 pp.

Bralower, T.J., 2005. Data Report: Paleocene-early Oligocene calcareous nannofossil biostratigraphy, ODP Leg 198, Sites 1209, 1210, and 1211 (Shatsky Rise, Pacific Ocean). In: Bralower, T.J., Premoli-Silva, I., Malone, M.J. (eds.). Proceedings of the Ocean Drilling Project. Scientific Results, 198, 1-15.

Burbank, D.W., Puigdefabregas, C., Muñoz, J.A., 1992a. The chronology of the Eocene tectonic and stratigraphic development of the eastern Pyrenean foreland basin, northeast Spain. Gelogical Society of America Bulletin, 104, 1101-1120.

Burbank, D.W., Vergés, J., Muñoz, J.A., Bentham, P., 1992b. Coeval hindward- and forward-imbricating thrusting in the south-central Pyrenees, Spain: Timing and rates of shortening and deposition. Gelogical Society of America Bulletin, 104, 3-17.

Cascella, A., Dinarès-Turell, J., 2009. Integrated calcareous nannofossil biostratigraphy and magnetostratigraphy from the uppermost marine Eocene deposits of the southeastern pyrenean foreland basin: evidences for marine Priabonian deposition. Geological Acta, 7(1-2), 281-296.

Caus, E., 1973. Bioestratigrafía y micropaleontología del Eoceno medio y superior del Prepirineo Catalán. Doctoral thesis. Universitat Autònoma de Barcelona, 186pp.

Caus, E., 1975. Bioestratigrafía del Eoceno medio y superior del Prepirineo Catalán (y la zona del tránsito entre esta unidad y la Cordillera Prelitoral Catalana). Revista Española de Micropaleontologia, 7(2), 297-316.

Channell, J.E.T., Galeotti, S., Martin, E.E., Billups, K., Scher, H.D., Stoner, J.S., 2003. Eocene to Miocene magnetostratigraphy, biostratigraphy, and chemostratigraphy at ODP Site 1090 (sub-Antarctic South Atlantic). Gelogical Society of America Bulletin, 115(5), 607-623.

Colom, G., 1971. Micropaleontología de las séries eocénicas de Santa Coloma de Queralt (Tarragona). Memórias de la Real Académia de Ciencias y Artes de Barcelona, 51(4), 73-135.

Costa, E., Garcés, M., López-Blanco, M., Beamud, E., Gómez-Paccard, M.,

Larrasoaña, J.C., 2010. Closing and continentalization of the South Pyrenean foreland Basin (NE Spain): Magnetochronological constraints. Basin Research, 22, 904-917.

Cuevas, J.L., Cabrera, L., Marcuello, A., Arbués, P., Marzo, M., Bellmunt, F., 2010. Exhumated channel sandstone networks within fluvial fan deposits from the Oligo-Miocene Caspe Formation, South-east Ebro Basin (North-east Spain). Sedimentology, 57, 162-189.

Ferrer, J., 1971a. El Paleoceno y Eoceno del borde suroriental de la Depresión del Ebro (Cataluña). Mémoires Suisses de Paléontologie, 90, 1-70.

Ferrer, J., 1971b. Presencia de macroforaminíferos priabonienses en el Eoceno de Igualada. Acta Geologica Hispanica, 6(1), 4-7.

Fornaciari, E., Agnini, C., Catanzariti, R., Rio, D., Bolla, E.M., Valvasoni, E., 2010. Mid-Latitude calcareous nannofossil biostratigraphy and biochronology across the middle to late Eocene transition. Stratigraphy, 7(4), 229-264.

Garcia-Castellanos, D., Vergés, J., Gaspar-Escribano, J., Cloetingh, S., 2003. Interplay between tectonics, climate, and fluvial transport during the Cenozoic evolution of the Ebro Basin (NE Iberia). Journal of Geophysical Research, 108(B7), 2347-2364.

Gaspar-Escribano, J., Garcia-Castellanos, D., Roca, E., Cloetingh, S., 2004. Cenozoic vertical motions of the Catalan Coastal Ranges (NE Spain): the role of tectonics, isostacy, and surface transport. Tectonics, 23, 1-18.

Gradstein, F.M., Ogg, J.G., Smith, A.G., 2004. A Geologic Time Scale 2004. Cambridge, Cambridge University Press, 589pp.

Guimerà, J., 1984. Paleogene evolution of deformation in the northeastern Iberian Peninsula. Geological Magazine, 121(5), 413-420.

Herb, R., Hekel, H., 1975. Nummulites aus dem Obereocaen von Possagno. Schweizerische Paläontologische Abhandlungen, 97, 113-211.

Hottinger, L., 1960. Recherches sur les Alvéolines du Paléocène et de l'Éocène. Mémoires Suisses de Paléontologie, 75/76, 1-243.

Hottinger, L., Schaub, H., 1960. Zur Stufeneintelung des Paleocaens und des Eocaens. Einführung der Stufen Ilerdien und Biarritzien. Eclogae geologicae Helvetiae, 53, 453-480.

Hottinger, L., Romero, J., Caus, E., 2001. Architecture and revision of the Pellatispirines planispiral canaliferous foraminifera from the Late Eocene Tethys. Micropaleontology, 47(2), 35-77.

Kapellos, C., Schaub, H., 1973. Zur Korrelation von Biozonierungen mit Grossforaminiferen und Nannoplankton im Paläogen der Pyrenäen. Eclogae geologicae Helvetiae, 66, 687-737.

Kirschvink, J.L., 1980. The least-squares line and plane and the analysis of paleomagnetic data. Geophysical Journal of the Royal Astronomical Society, 62, 699-718.

Langereis, C.G., Krijgsman, W., Muttoni, G., Menning, M., 2010. Magnetostratigraphy - concepts, definitions, and applications. Newsletter on Stratigraphy, 43(3), 207-233.

Larrasoaña, J.C., Gonzalvo, C., Molina, E., Monechi, S., Ortiz, S., Tori, F., Tosquella, J., 2008. Integrated magnetobiochronology of the Early/Middle Eocene transition at Agost (Spain): Implications for defining the Ypresian/Lutetian boundary stratotype. Lethaia, 41, 395–415. doi: 10.1111/j.1502-3931.2008.00096.x

Lowrie, W., Alvarez, W., Napoleone, G., Perch-Nielsen, K., Premoli-Silva, I., Toumarkine, M., 1982. Paleogene magnetic stratigraphy in Umbrian pelagic carbonate rocks: The Contessa sections, Gubbio. Gelogical Society of America Bulletin, 93, 414-432.

López-Blanco, M., 2002. Sedimentary response to thrusting and fold growing on the SE margin of the Ebro basin (Paleogene, NE Spain). Sedimentary Geology, 146, 133-154.

López-Blanco, M., Marzo, M., Burbank,

D.W., Vergés, J., Roca, E., Anadón, P., Piña, J., 2000. Tectonic and climatic controls on the development of foreland fan deltas: Montserrat and Sant Llorenç del Munt systems (Middle Eocene, Ebro Basin, NE Spain). Sedimentary Geology, 138, 17-39.

Luciani, V., Negri, A., Bassi, D., 2002. The Bartonian-Priabonian transition in the Mossano section (Colli Berici, north-eastern Italy): a tentative correlation between calcareous plankton and shallow-water benthic zonations. Geobios, 35 (M.S. 24), 140-149.

Martini, E., 1971. Standard Tertiary and Quaternary calcareous nannofossil zonation. In: Farinaci, A. (ed.). Proceedings of the II Planktonic Conference, Roma 1970, vol. 2, Roma, Edizioni Tecnoscienza, 739-785.

Meulenkamp, J.E., Sissingh, W., 2003. Tertiary palaeogeography and tectonostratigraphic evolution of the Northern and Southern Peri-Tethys platforms and the intermediate domains of the African-Eurasian convergent plate boundary zone. Palaeogeography, Palaeoclimatology, Palaeoecology, 196, 209-228.

Monechi, S., 1986. Calcareous nannofossil events around the Eocene-Oligocene Boundary in the Umbrian Apennines (Italy). Palaeogeography, Palaeoclimatology, Palaeoecology, 57, 61-69.

Monechi, S., Thierstein, H.R., 1985. Late Cretaceous-Eocene nannofossil and magnetostratigraphic correlations near Gubbio, Italy. Marine Micropaleontology, 9, 419-440.

Muñoz, J.A., 1992. Evolution of a continental collision belt: ECORS-Pyrenees crustal balanced cross-section. In: McClay, K.R. (ed.). Thrust Tectonics, London, Chapman & Hall, 235-246.

Nocchi, M., Parisi, G., Monaco, P., Monechi, S., Madile, M., 1988. Eocene and Early Oligocene micropaleontology and paleoenvironments in SE Umbria, Italy. Palaeogeography, Palaeoclimatology, Palaeoecology, 67, 181-244.

Orue-Etxebarria, X., Bernaola, G., Baceta, J.I., Angori, E., Caballero, F., Monechi, S., Pujalte, V., Dinarès-Turell, J., Apellaniz, E., Payros, A., 2004. New constraints on the evolution of planktic foraminifera and calcareous nannofossils accross the Paleocene-Eocene boundary interval: The Zumaia section revisited. Neues Jahrbuch für Geologie und Paläontologie Abhandlungen, 234, 223-259.

Papazzoni, C.A., 1998. Biometric analysis of *Nummulites "ptukhiani"* (Z.D. KACHAREVA 1969) and *Nummulites fabianii* (Prever in FABIANI, 1905). Journal of Foraminiferal Research, 28(3), 161-176.

Papazzoni, C.A., Sirotti, A., 1995. Nummulite boistratigraphy at the Middle/Upper Eocene boundary in the northern Mediterranean area. Rivista Italiana di Paleontologia e Stratigrafia, 101(1), 63-80.

Pérez-Rivarés, F.J., Garcés, M., Arenas, C., Pardo, G., 2002. Magnetocronología de la sucesión miocena de la Sierra de Alcubierre (sector central de la Cuenca del Ebro). Revista de la Sociedad Geológica de España, 15, 211-225.

Plaziat, J.C., 1981. Late Cretaceous to Late Eocene paleogeographic evolution of southwest Europe. Palaeogeography, Palaeoclimatology, Palaeoecology, 36, 263-320.

Poore, R.Z., Tauxe, L., Percival Jr., S.F., LaBrecque, J.L., 1982. Late Eocene-Oligocene magnetostratigraphy and biostratigraphy at South Atlantic DSDP Site 522. Geology, 10, 508-511.

Pueyo, J.J., 1974. Estudio petrológico y geoquímico de los yacimientos potásicos de Cardona, Súria, Sallent y Balsareny (Barcelona, España). Doctoral thesis. Universitat de Barcelona, 351pp.

Reguant, S., 1967. El Eoceno Marino de Vic (Bercelona). Memorias del Instituto Geológico y Minero de España, Tomo LXVIII, Madrid, Instituto Geológico y Minero de España, 350 pp.

Riba, O., Reguant, S., Villena, J., 1983. Ensayo de síntesis estratigráfica y

evolutiva de la cuenca terciaria del Ebro. In: Comba, J.A. (ed.). Geología de España. Libro Jubilar J.M. Ríos, Tomo II., Madrid, Instituto Geológico y Minero de España, 131-159.

Roca, E., Sans, M., Cabrera, L., Marzo, M., 1999. Oligocene to Middle Miocene evolution of the central Catalan margin (northwestern Mediterranean). Tectonophysics, 315, 209-233.

Romero, J., 1996. Estudio de los foraminíferos bentónicos del límite Eoceno Medio-Eoceno Superior de la Cuenca de Igualada. Master Degree thesis. Universitat de Barcelona, 184pp.

Romero, J., 2001. Los macroforaminíferos del Eoceno Medio del borde suroriental de la Cuenca Paleógena Surpirenaica. Doctoral thesis. Univeristat Autònoma de Barcelona, 349pp.

Romero, J., Hottinger, L., Caus, E., 1999. Early appearence of larger foraminifera supposedly characteristic for Late Eocene in the Igualada Basin, NE Spain. Revista Española de Paleontología, 14(1), 79-92.

Rosell, J., Juliá, R., Ferrer, J., 1966. Nota sobre la estratigrafía de unos niveles con Carófitas existentes en el tramo rojo de la base del Eoceno al S de los Catalánides (Provincia de Barcelona). Acta Geologica Hispanica, 1(5), 17-20.

Roveda, V., 1961. Contributo allo studio di alcuni macroforaminiferi di Priabona. Rivista Italiana di Paleontologia, 67(2), 153-225.

Ruiz de Gaona, M., 1952. Resultado del estudio de los foraminíferos del Nummulítico de Montserrat y regiones limítrofes. Estudios Geológicos, 15, 21-28.

Ruiz de Gaona, M., Colom, G., 1950. Estudios sobre las sinencias de los foraminíferos eocénicos de la vertiente meridional del Pirineo (Cataluña-Vizcaya). Estudios Geológicos, 12, 293-434.

Sáez, A., 1987. Estratigrafía y sedimentología de las formaciones lacustres del tránsito Eoceno-Oligoceno del noreste de la cuenca del Ebro. Doctoral thesis. Universitat de Barcelona, 353pp.

Schaub, H., 1981. Nummulites et Assilines de la Tethys Paléogène. Taxonomie, phylogénèse et biostratigraphie. Mémoires Suisses de Paléontologie, 104/105/106, 1-236.

Serra-Kiel, J., 1984. Estudi dels *Nummulites* del grup *N. perforatus* (Montfort). Treballs de la Institució Catalans d'Història Natural, 11, 1-244.

Serra-Kiel, J., Reguant, S., 1984. Paleoecological conditions and morphological variation in monospecific banks of Nummulites: an example. Benthos'83, 2nd International Symposium on Benthic Foraminifera. Bulletin des Centres de Recherches Exploration-Production Elf-Aquitanie, 6, 557-563.

Serra-Kiel, J., Hottinger, L., Caus, E., Drobne, K., Ferràndez-Cañadell, C., Jauhri, A.K., Less, G., Pavlovec, R., Pignatti, J., Samsó, J.M., Schaub, H., Sirel, E., Strougo, A., Tambareau, Y., Tosquella, J., Zakrevskaya, E., 1998a. Larger Foraminiferal Biostratigraphy of the Tethyan Paleocene and Eocene. Bulletin de la Societé géologique de France, 169(2), 281-299.

Serra-Kiel, J., Hottinger, L., Drobne, K., Ferràndez-Cañadell, C., Jauhri, A.K., Less, G., Pignatti, J., Samsó, J.M., Schaub, H., Sirel, E., Tambareau, Y., Tosquella, J., Zakrevskaya, E., 1998b. Larger benthic foraminifera. In: Thierry, J., Farley, M.B., Jacquin, Th., Graciansky, P.C., Vail P.R. (eds.). Mesozoic-Cenozoic sequence stratigraphy of European basins. Society of Economic Paleontologist and Mineralogist. Special Publication, 60, 767pp., chart 3.

Serra-Kiel, J., Mató, E., Saula, E., Travé, A., Ferràndez-Cañadell, C., Busquets, P., Samsó, J.M., Tosquella, J., Barnolas., A., Àlvarez-Pérez, G., Franquès, J., Romero, J., 2003a. An inventory of the marine and transitional Middle/Upper Eocene deposits of the Southeastern Pyrenean Foreland Basin (NE Spain). Geologica Acta, 1(2), 201-229.

Serra-Kiel, J., Travé, A., Mató, E., Saula, E., Ferràndez-Cañadell, C., Busquets, P.,

Tosquella, J., Vergés, J., 2003b. Marine and Transitional Middle/Upper Eocene Units of the Southeastern Pyrenean Foreland Basin (NE Spain). Geologica Acta, 1(2), 177-200.

Taberner, C., Dinarès-Turell, J., Giménez, J., Docherty, C., 1999. Basin infill architecture and evolution from magnetostratigraphic cross-basin correlations in the southeastern Pyrenean foreland basin. Geological Society of America Bulletin, 111(8), 1155-1174.

Teixell, A., Serra-Kiel, J., 1988. Sedimentología y distribución de foraminiferos en medios litorales y de plataforma mixta (Eoceno Medio y Superior, Cuenca del Ebro Oriental). Boletín Geológico y Minero; 94, 871-885.

Tosquella, J., 1995. Els Nummulitinae del Paleocè-Eocè inferior de la conca sudpirinenca. Doctoral thesis. Universitat de Barcelona, 581pp.

Travé, A., 1992. Sedimentologia, petrologia i geoquímica (elements traça i isòtops) dels estromatòlits de la Conca Eocena Sudpirinenca. Doctoral thesis. Universitat de Barcelona, 396pp.

Travé, A., Serra-Kiel, J., Zamarreño, I., 1996. Paleoecological interpretation of transitional enviroments in Eocene carbonates (NE Spain). Palaios, 11, 141-160.

Urgelés, R., Camerlenghi, A., Garcia-Castellanos, D., De Mol, B., Garcés, M., Vergés, J., Haslam, I., Hardman, M., 2011. New constraints on the Messinian sealevel drawdown from 3D seismic data of the Ebro Margin, western Mediterranean. Basin Research, 23(2), 123-145. doi: 10.1111/j.1365-2117.2010.00477.x

Vergés, J., Burbank, D.W., 1996. Eocene-Oligocene thrusting and basin configuration in the eastern and central Pyrenees (Spain). In: Friend, P.F., Dabrio, C.J. (eds.) Tertiary basins of Spain. The stratigraphic record of crustal kinematics. Cambridge, Cambridge University Press. World and Regional Geology, 6, 120-133.

Vergés, J., Fernàndez, M., Martínez, A., 2002. The Pyrenean orogen: pre-, syn-, and post-collisional evolution. In: Rousenbaum, G., Lister, G.S. (eds.). Reconstruction of the Evolution of the Alpine-Himalayan Orogen. Journal of the Virtual Explorer, 55-74.

Virgili, C., 2007. Lyell and the Spanish Geology. Geologica Acta, 5(1), 119-126.

Wei, W., 1991. Middle Eocene-lower Miocene calcareous nannofossil magnetobiochronology of ODP Holes 699A and 703A in the subantartic South Atlantic. Marine Micropaleontology, 18, 143-165.

Wei, W., Thierstein H.R., 1991. Upper Cretaceous and Cenozoic calcareous nannofossils of the Kerguelen Plateau (Southern Indian Ocean) and Prydz Bay (East Antarctica). Proceedings of the Ocean Drilling Program, Scientific Results, 119, 467-493.

Wei, W., Wise, S.W., 1989. Paleogene Calcareous Nannofossil Magnetobiochronology: Results from South Atlantic DSDP Site 516. Marine Micropaleontology, 14, 119-152.

Zoetemeijer, R., Desegaulx, P., Cloetingh, S., Roure, F., Moretti, I., 1990. Lithospheric dynamics and tectonic-stratigraphic evolution of the Ebro Basin. Journal of Geophysical Research, 95(3), 2701-2711.

APPENDIX: LARGER FORAMINIFERS SYSTEMATIC REMARKS

An accurate description of *Nummulites chavannesi*, *Nummulites garnieri sturi,* and *Nummulites* aff. *incrassatus ramondiformis* from the Miralles-La Tossa composite section is provided in order to help comparison with specimens of these forms described in Priabona and Mossagno areas in Italy, Upper Horn Depression in Slovakia, and the Western Alps in France (Roveda, 1961; Vanova, 1972; Herb and Hekel, 1973 and 1975; Schaub, 1981; Papazzoni and Sirotti, 1995) (Figs. A6, A7, and A8).

Family *Nummulitidae* De Blainville, 1825
Genus *Nummulites* Lamark, 1801
Nummulites chavannesi De La Harpe 1878
Figs. A6 1 to 9; A13 6 to 11
1961 *Nummulites chavanessi* De La Harpe, Roveda (1961), 177-181pp.; Pl. 14, Figs. 1-8.
1975 *Nummulites chavanessi* De La Harpe, Herb and Hekel (1975), 123-125pp.; Pl. 2, Figs. 1-3; Text-Fig. 14-21.
2002 *Nummulites chavannesi* De La Harpe, Luciani et al. (2002), Fig. 4 (2-4) and Fig. 6.

Material: 16 specimens in the sample LT005 (Miralles-La Tossa composite section).
Description: Test lenticular flattened in the external zone with sharp periphery. The external view permits to observe the last marginal cord. The chambers are subromboidal in outline, with an aspect ratio (height/length) > 1, and with arcuate ceiling. Septa are gently inclined to perpendicular and recurved towards periphery. The ornamentation consists of a coarse granule at the polar zone with radial filaments sinuous with S-form in the external zone. The spiral is thin and the growth is slightly irregular. The diameter of the proloculus in A-forms is between 0.140-0.230 mm (mean 0.180 mm).

Dimensions of the B-Form in mm (4 specimens measured)

	Max	Min	Mean
Diameter	4.74	4.28	4.50

Equatorial section (mean values)

Whorld	1	2	3	4	5	6
Radius	0.30	0.50	0.78	1.15	1.60	2.00
Chambers	11	14	21	25	28	29

Dimensions of the A-Form in mm (12 specimens measured)

	Max	Min	Mean
Diameter	3.00	2.60	2.90

Equatorial section (mean values)

Whorld	1	2	3	4	5
Radius	0.30	0.50	0.70	1.15	1.35
Chambers	7	14	17	22	26

Remarks: With the exception of the specimen illustrated in Fig. A6 13, the forms from the Priabona area (Roveda, 1961), reproduced in Figs. A6 10 to 13, have the test and the proloculus in A-Form greater than the specimens from the Tossa Formation (Figs. A6 1 to 9; A13 6 to 11). The A-Form from the Marne di Possagno (Herb and Hekel, 1975) reproduced in Figs. A6 14 to 17, in the

lowermost part of the Cunial-Santa Giustina-Col dell'Asse section, have test and proloculus of smaller in diameter than the specimens from the Tossa Formation. On the other hand, the A- and B-Form from the Calcare di Santa Giustina and Marne siltose (Herb and Hekel, 1975), at the middle and lowermost part of the Cunial-Santa Giustina-Col dell'Asse section (Figs. A6 18 to 20), are of greater size and shown a spiral growth less closed than our material. Whether this variability is intraspecific or corresponds to different chronospecies within the same lineage is not determined. Unfortunately, we have not enough material to clarify this question, and we prefer to use the specific terminology as evolutive species.

Nummulites chavannesi differs from the *Nummulites* aff. *incrassatus ramondiformis* for having sinuous filaments, thinner marginal cord, higher chambers and curved and more irregular spiral growth. *Nummulites chavannesi* differs from *Nummulites garnieri garnieri* for the type of the ornamentation, pattern of the spiral growth, and the size and outline of the chambers.

Nummulites garnier sturi Boussac 1911
Figs. A7 14 to 18; A13 1 to 5
1972 *Nummulites garnieri sturi* n. sp. Vanova (1972), 56-59 pp.; Pl. 6, Figs. 5-9; Pl. 7 Figs. 1-9; Pl. 8 Figs. 1-8
1995 *Nummulites garnieri garnieri* De La Harpe, Papazzoni and Sirotti (1995), Pl. 2, Figs. 6-7

Material: 12 specimens in the sample LT005 (Miralles-La Tossa composite section).
Description: Test lenticular with rounded periphery. The ornamentation consists of granules and filaments. The filaments are sinuous curved in S form in the periphery. The granules are distributed at the polar zone and over the filaments towards the periphery. The chambers have an aspect ratio > 1, with rhomboidal outline and arcuate ceiling. The septa are straight, slightly inclined towards the periphery. The spiral growth is regular, but slightly irregular in B-Form. The diameter of the proloculus is between 0.090-0.140 mm (mean 0.125 mm).

Dimensions of the B-Form in mm (4 specimens measured)

	Max	Min	Mean
Diameter	4.90	3.64	4.35

Equatorial section (mean values)						
Whorld	1	2	3	4	5	6
Radius	0.25	0.47	0.75	1.00	1.50	2.00
Chambers	10	15-16	19-20	24	29-30	35

Dimensions of the A-Form in mm (8 specimens measured)

	Max	Min	Mean
Diameter	2.70	2.20	2.50

Equatorial section (mean values)						
Whorld	1	2	3	4	5	6
Radius	0.25	0.45	0.60	0.90	1.25	1.65
Chambers	11-12	17	22-23	25	28-30	30

Remarks: We consider the specimens of the sample LT005 as *Nummulites garnieri sturi* (Figs. A7 14 to 18; A13 1 to 5). They have a test size and the diameter of the proloculus (0.090-0.140 mm) greater than *Nummulites praegarnieri* (0.100-0.120 mm) (Figs. A7 1 to 4), and similar to the forms

described by Vanova (1972) (Figs. A7 5 to 7). *Nummulites garnieri sturi* from the Tossa Formation have smaller test and proloculus diameter than *Nummulites garnieri* (0.150-0.200 mm) described by Schaub (1981) (Figs. A7 19 and 20) and *Nummulites garnieri garnieri* described by Herb and Hekel (1973) (Figs. A7 21 and 22). We consider *Nummulites garnieri garnieri* (Figs. A7 8 to 13) illustrated by Herb and Hekel (1975) as a synonymy of *Nummulites garnieri sturi* (Figs. A7 5 to 7, and 14 to 18) because it yields the same test size and proloculus diameter. Finally, the succession of chronospecies of the *Nummulites garnieri* lineage, from Bartonian to uppermost Priabonian, consists of *Nummulites praegarnieri* Schaub 1981*, Nummulites garnieri sturi* Vanova 1972*, Nummulites garnieri* sensu Schaub (1981) and *Nummulites garnieri inaequalis* Herb and Hekel 1975 (Figs. A7 23 to 26).

Nummulites aff. *incrassatus ramondiformis* De La Harpe 1883
Figs. A8 1 to 5; A13 12 to 26

Material: 14 specimens in the sample LT005 (Miralles-La Tossa composite section).
Description: Test inflated lenticular with rounded periphery. The chambers are subromboidal in outline, isometric or with aspect ratio slightly larger than 1, and flattened ceiling. Septa are inclined. The ornamentation consists of a big granule at the polar zone with radial filaments. The spiral growth is regular. The diameter of the proloculus is 0.140-0.180 mm (mean 0.160 mm).

Dimensions of the B-Form in mm (4 specimens measured)

	Max	Min	Mean			
Diameter	4.90	3.85	4.37			
Equatorial section (mean values)						
Whorld	1	2	3	4	5	6
Radius	0.20	0.47	0.75	1.15	1.60	2.00
Chambers	13	13	17	22	24	29

Dimensions of the A-Form in mm (10 specimens measured)

	Max	Min	Mean		
Diameter	2.70	2.20	2.50		
Equatorial section (mean values)					
Whorld	1	2	3	4	5
Radius	0.25	0.50	0.70	1.00	1.35
Chambers	5-6	13	18	20	22

Remarks: *Nummulites* aff. *incrassatus ramondiformis* from the sample LT005 (Figs. A8 1 to 5; A13 12 to 26) have a test and proloculus diameter of smaller size than the *Nummulites incrassatus* (Figs A8 6 to 9) from the Boro-Granella section (Priabona area, Roveda, 1961) and the *Nummulites incrassatus ramondiformis* (Figs. A8 10 to 14) from Cunial-Santa Giustina-Col dell'Asse section (Possagno area, Herb and Hekel, 1975). *Nummulites incrassatus incrassatus* (Fig. A8 15) illustrated by Herb and Hekel (1975) have a greater size of the test and the diameter of the proloculus than the specimens from Tossa Formation. Thus, we use the terminology affinis because we consider the specimens from Tossa Formation (sample LT005) a primitive chronospecies within the lineage *Nummulites incrassatus ramondiformis*.

References

Herb, R., Hekel, H., 1973. Biostratigraphy, Variability and Facies Relations of some Upper Eocene Nummulites from Northern Italy. Eclogae geologicae Helvetiae, 55(2), 419-445.

Herb, R., Hekel, H., 1975. Nummulites aus dem Obereocaen von Possagno. Schweizerische Paläontologische Abhandlungen, 97, 113-211.

Luciani, V., Negri, A., Bassi, D., 2002. The Bartonian-Priabonian transition in the Mossano section (Colli Berici, north-eastern Italy): a tentative correlation between calcareous plankton and shallow-water benthic zonations. Geobios, 35 (M.S. 24), 140-149.

Papazzoni, C.A., Sirotti, A., 1995. Nummulite biostratigraphy at the Middle/Upper Eocene boundary in the northern Mediterranean area. Rivista Italiana di Paleontologia e Stratigrafia, 101(1), 63-80.

Roveda, V., 1961. Contributo allo studio di alcuni macroforaminiferi di Priabona. Rivista Italiana di Paleontologia, 67(2), 153-225.

Schaub, H., 1981. Nummulites et Assilines de la Tethys Paléogène. Taxonomie, phylogénèse et biostratigraphie. Mémoires Suisses de Paléontologie, 104/105/106, 1-236.

Vanova, M., 1972. Nummulites from the area of Bojnice, the Upper Horn Depression, and the Budín paleogene around Stúrovo. Zbor. Geol. vied Západné Karpaty, 17, 5-104.

APPENDIX OF CHAPTER 3.1:

SUPPORTING ELECTRONIC INFORMATION

Figure A1 Larger foraminifers samples location of the "Terminal Complex" in Puig Aguilera (Igualada area, eastern Ebro Basin). (A) Geographic location of the Puig Aguilera and La Tossa section. (B) Detailed geological map with the location of the larger foraminifers samples of the "Terminal Complex" of Puig Aguilera. A sketched lithostratigraphic panel showing lateral and vertical relationship between the marine and continental facies in the eastern part of the Igualada area is also shown. The black (white) dots correspond to normal (reversed) paleomagnetic sites of the lowermost Maians-Rubió section (Costa et al., 2010). (C) UTM coordinates (ED50 / zone 31N).

A)

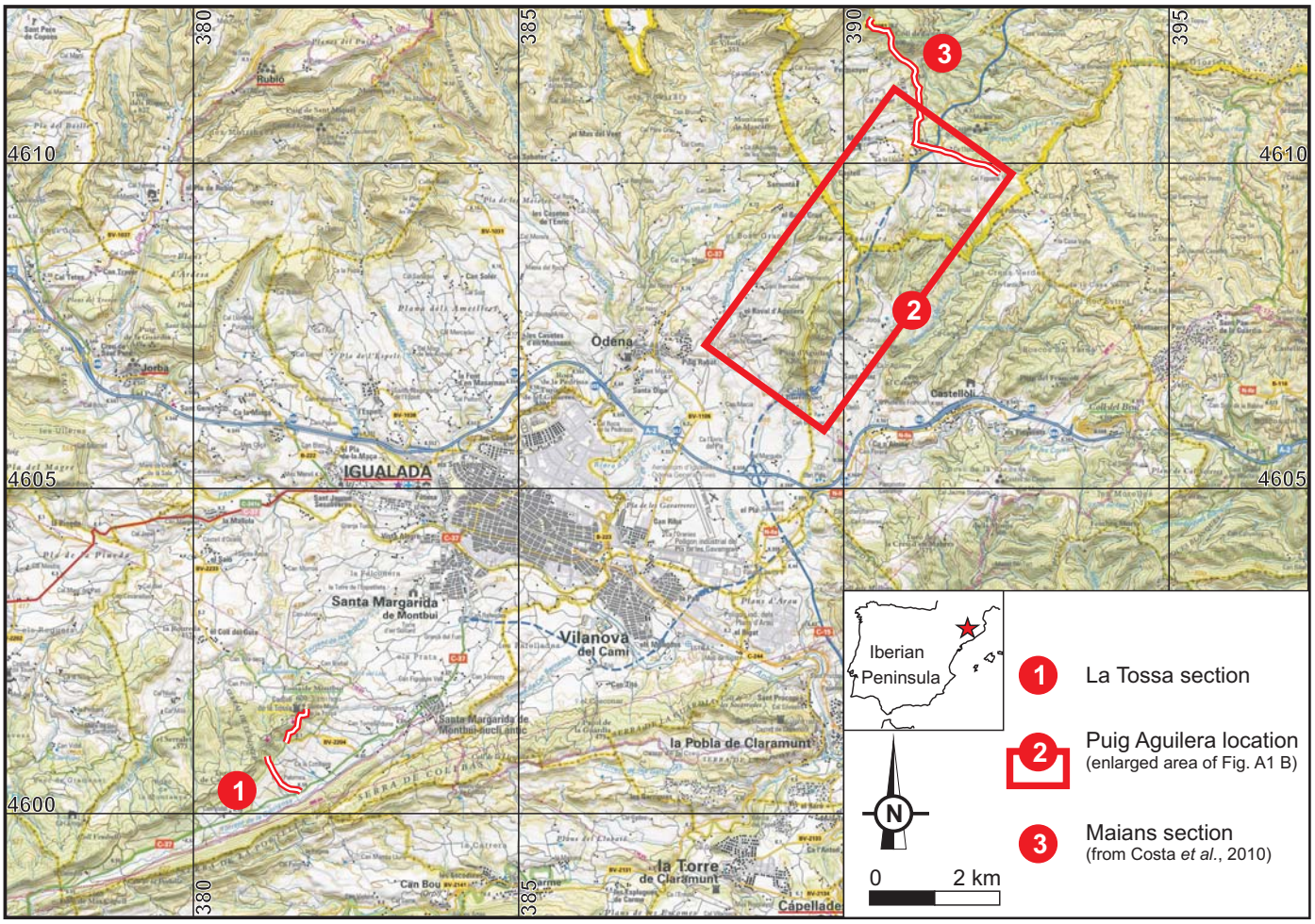

B)

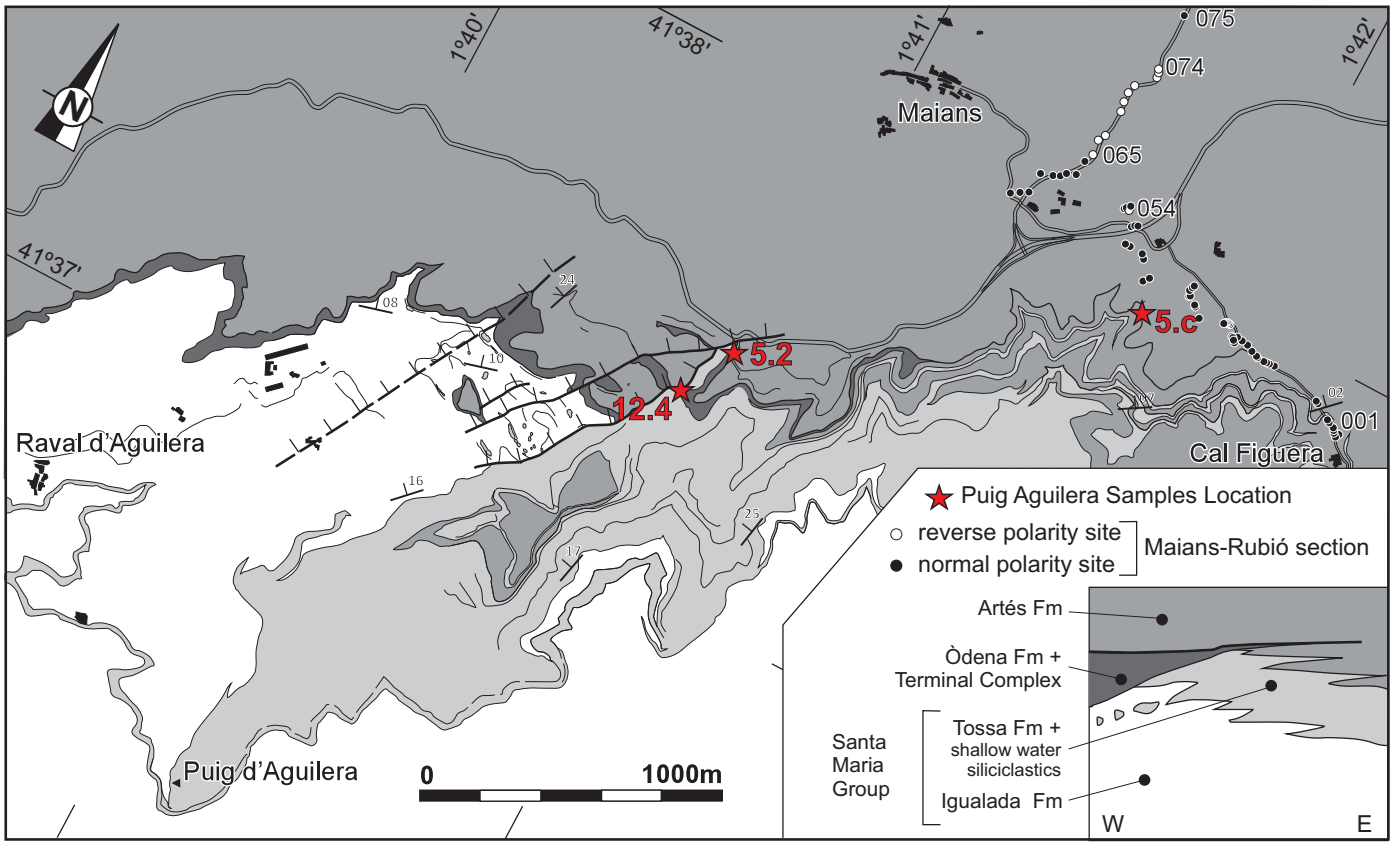

C)

			UTM coordinates (ED50 / zone 31N)		
Sample	**Unit**	**Facies**	**x**	**y**	**z**
5.2	Terminal Complex	marine limestone / larger foraminifers	390318.1214	4609173.713	556
5.c	Terminal Complex	marine limestone / larger foraminifers	391515.1564	4609982.287	544
12.4	Terminal Complex	marine limestone / larger foraminifers	390220.9346	4608940.702	565

Figure A2 Drawings of *Nummulites beaumonti* D'ARCHIAC and HAIME 1853 and *N. biarritzensis* DE LA HARPE in ROZLOZSNIK 1926 from the Miralles-La Tossa composite section. *N. beaumonti* (1-4). 1: B-Form from sample MM008; 2: A-Form from sample MM008; 3 and 4: A-Forms from sample MM022. *N. biarritzensis* (5-8). 5: B-Form from sample MM004; 6 and 7: A-Forms from sample MM004; 8: A-Form from sample MM022.

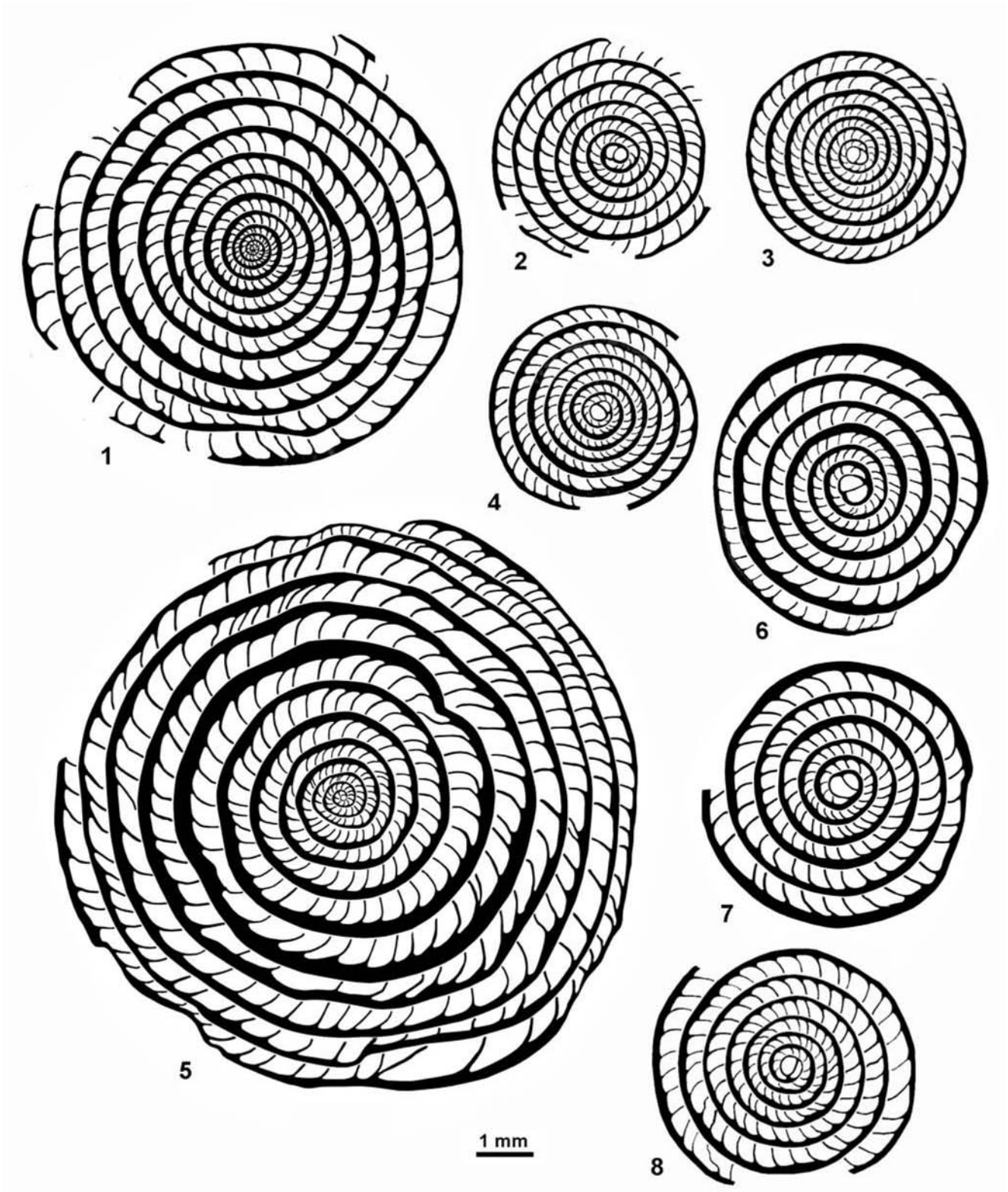
1
2
3
4
5
6
7
8
1 mm

Figure A3 Drawings of *Nummulites hottingeri* SCHAUB 1981 and *Nummulites perforatus* DE MONTFORT 1808 from the Miralles-La Tossa composite section. *N. hottingeri* (1-3). 1: B-Form from sample MM004; 2 and 3: A-Forms from sample MM022. *N. perforatus* (4-7). 4, 5, and 6: A-Forms from sample BM010; 7: B-Form from sample BM010.

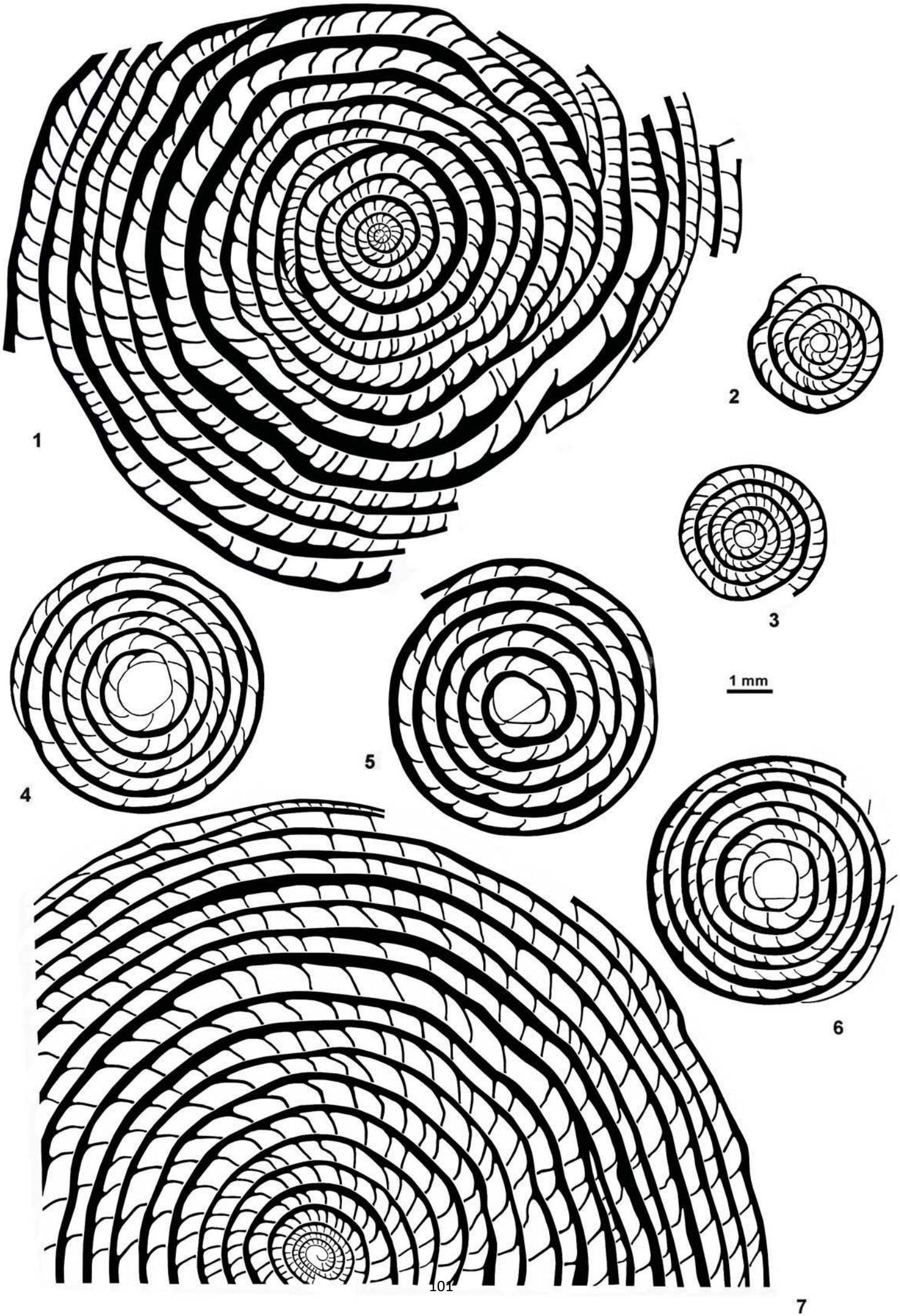
1
2
3
1 mm
4
5
6
7

Figure A4 Drawings of *Nummulites vicaryi* SCHAUB 1981, *Nummulites stellatus* ROVEDA 1961 and *Nummulites orbignyi* GALEOTTI 1837 from the Miralles-La Tossa composite section. *N vicaryi* (1-5). 1 and 2: B-Forms from sample MM028-29; 3 to 5: A-Forms from sample MM028-29. *N. stellatus* (6-9). 6 and 7: A-Forms from sample LT000; 8 and 9: A-Forms from sample LT104. *N. orbignyi* (10). 10: A-Form from sample LT157.

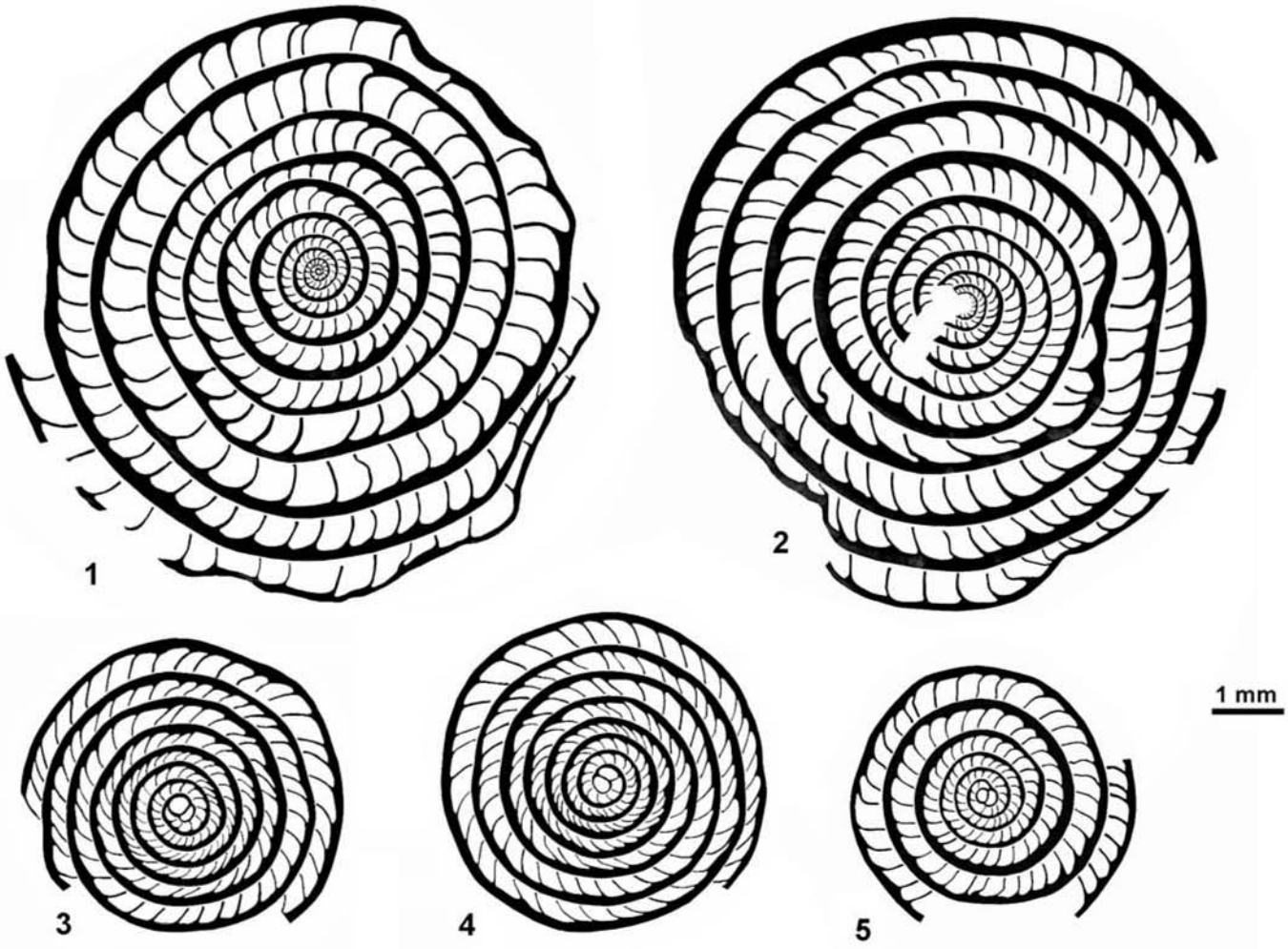
1
2
3
4
5
1 mm

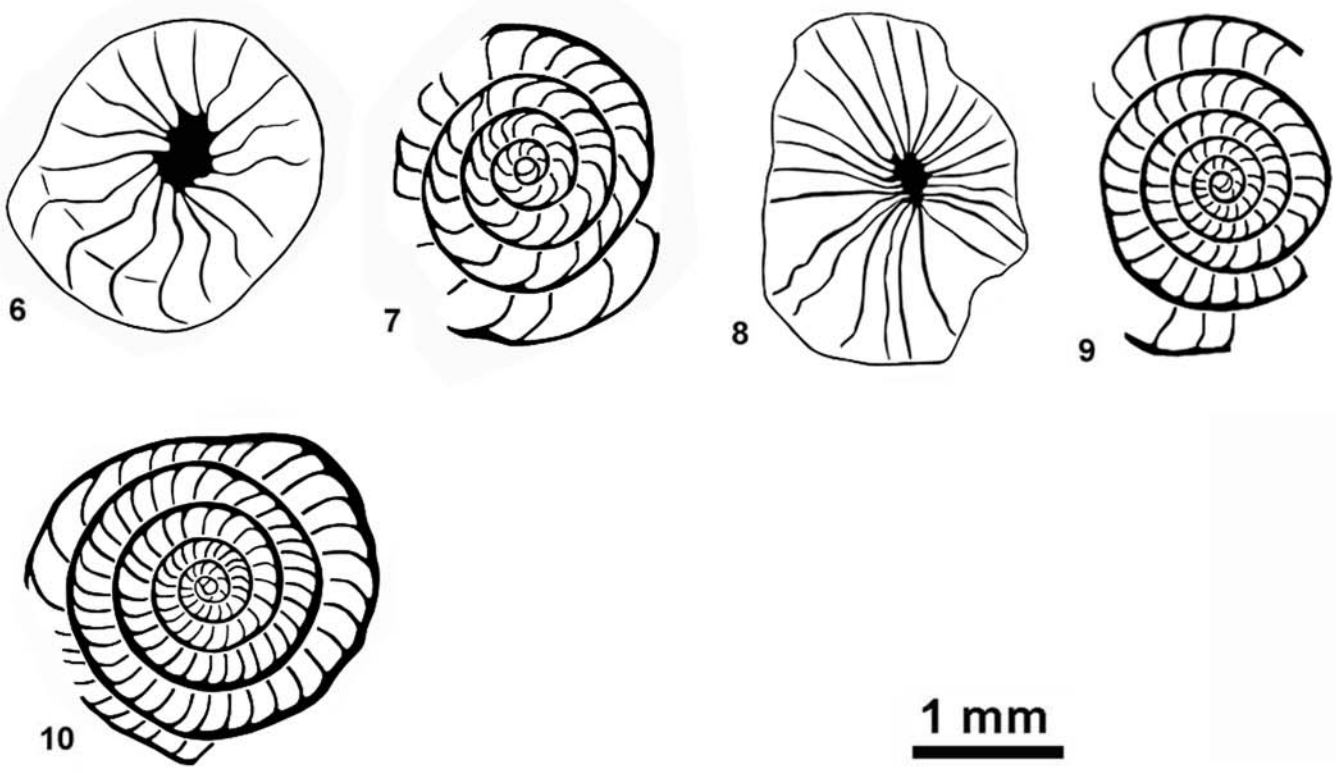
6
7
8
9
10
1 mm

Figure A5 Drawings of *Nummulites striatus* BRUGUIÈRE 1792 from the Miralles-La Tossa composite section. 1: B-Form from sample LT104; 2: A-Form from sample MM050; 3: A-Form from sample LT104.

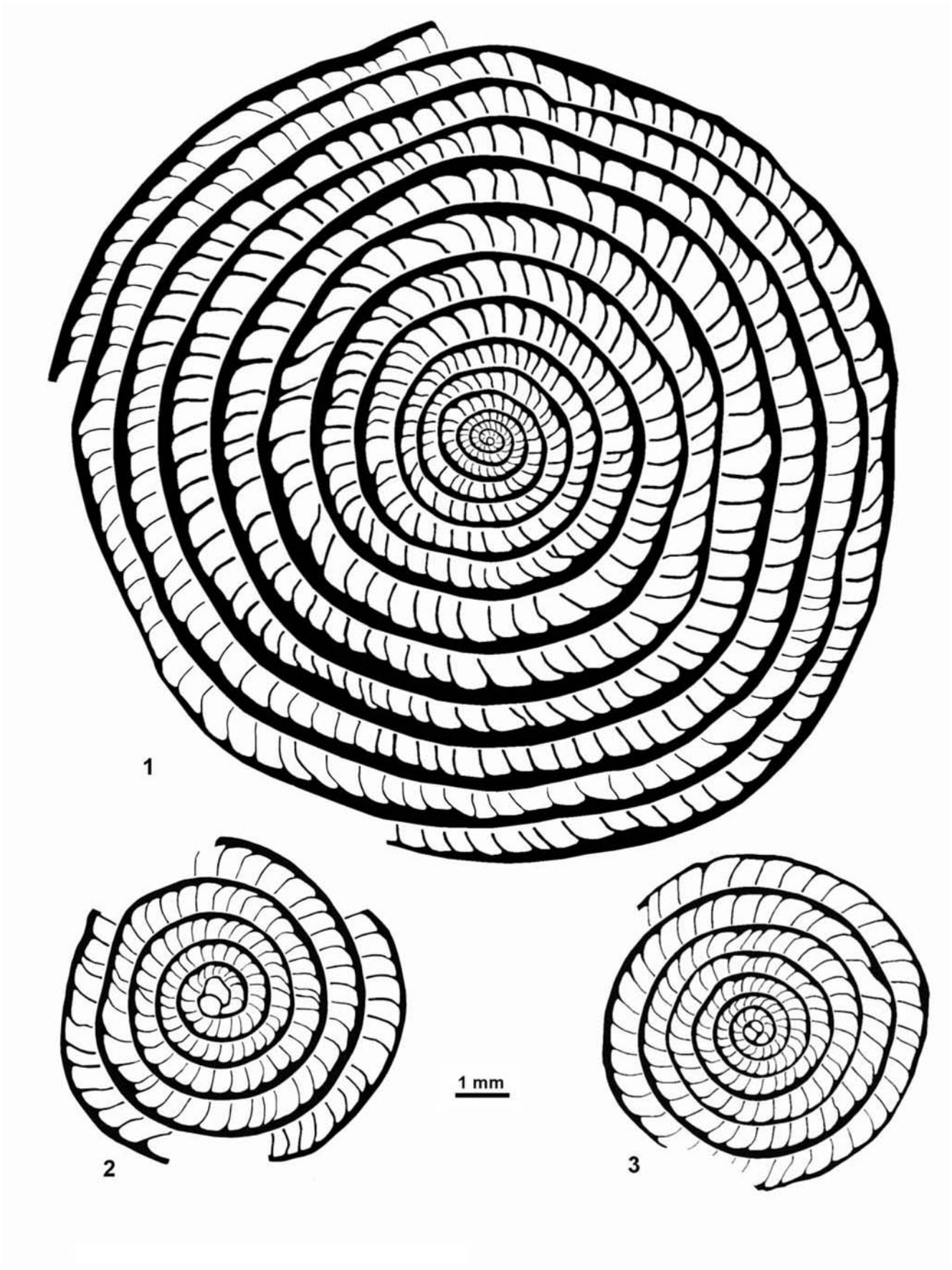
1
2
1 mm
3

Figure A6 Drawings of *Nummulites chavannesi* DE LA HARPE 1978.

1 to 9: *N. chavannesi* from the sample LT005 in the Miralles-La Tossa composite section. 1, 3, 5, and 6: A-Form equatorial sections; 2, 4, and 7: A-Form external views; 8 and 9: equatorial section and external view respectively of a B-Form.

10 to 13: drawings after Roveda (1961) of *N. chavannesi* from the Boro-Granella section in the Priabona area. 10: B-Form equatorial section; 11 and 13: A-Form equatorial sections; 12: B-Form external view.

14 to 20: drawings after Herb and Hekel (1975) of *N. chavannesi* from the Cunial-Santa Giustina-Col dell'Asse section in the Possagno area. 14 to 17: equatorial section of A-Forms from the Marne di Possagno Formation; 18: equatorial section from Calcare di Santa Giustina Formation; 19: equatorial section of A-Form from the Marne siltose Formation; 20: equatorial section of B-Form from the Marne siltose Formation.

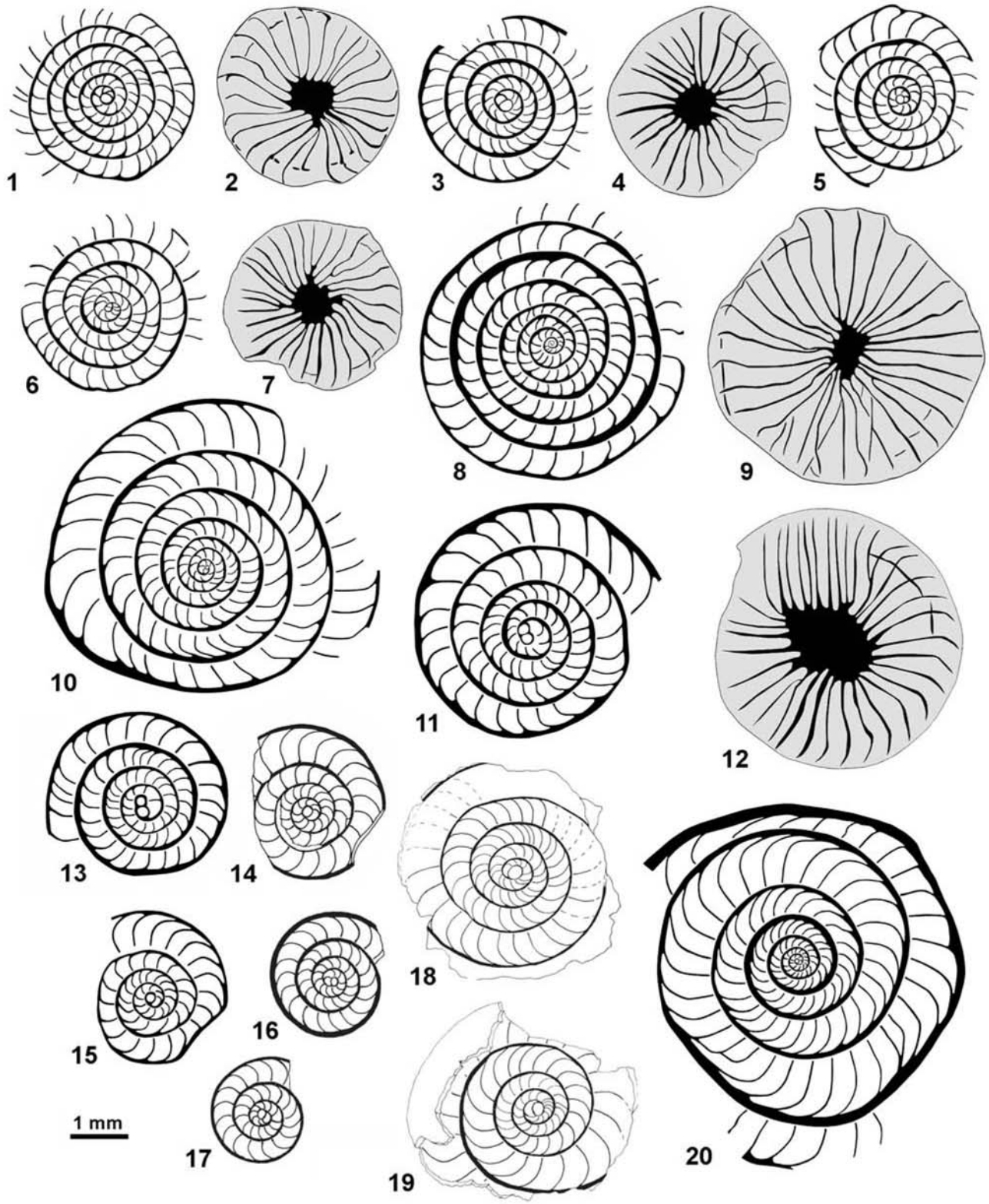
1
2
3
4
5
6
7
8
9
10
11
12
13
14
15
16
17
18
19
20
1 mm

Figure A7 Drawings of *Nummulites praegarnieri* SCHAUB 1981 (1-4), *N. garnieri sturi* VANOVA 1972 (5-7 and 14-18), *N. garnieri garnieri* DE LA HARPE in BOUSSAC 1911 (8-13 and 21-22), *N. garnieri* DE LA HARPE in BOUSSAC 1911 (19-20), and *N. garnieri inaequalis* HERB and HEKEL 1973 (23-26).

1 and 2: *Nummulites praegarnieri* from sample BM005 in the Collbàs Formation (Miralles-La Tossa composite section). 1: A-Form equatorial section; 2: A-Form external view.

3 and 4: *Nummulites praegarnieri* from the Collbàs Formation. Holotype drawings after Schaub (1981). 3: A-Form equatorial section; 4: A-Form external view.

5 to 7: *Nummulites garnieri sturi* from the Upper Horn Depression (Slovakia). Figure drawings after Vanova (1972). 5: equatorial section of the holotype; 6: external view of the holotype; 7: A-Form equatorial section.

8 to 13: *Nummulites garnieri garnieri* from the Marne di Possagno in Cunial-Santa Giustina-Col dell'Asse section (Possagno area, Italy). Figure drawings after Herb and Hekel (1975). 8 to 12: A-Form equatorial sections; 13: A-Form external view.

14 to 18: *Nummulites garnieri sturi* from sample LT005 in the Tossa Formation (Miralles-La Tossa composite section). 14: A-Form equatorial section; 15: A-Form external view; 16 and 17: B-Form equatorial sections; 18: B-Form external view.

19 and 20: *Nummulites garnieri* from Châteaugarnier (Western Alps, France). Figure drawings after Schaub (1981). 19: B-Form equatorial section; 20: A-Form equatorial section.

21 and 22: *Nummulites garnieri garnieri* from Châteaugarnier (Western Alps, France). Figure drawings after Herb and Hekel (1973). 21: B-Form equatorial section; 22: A-Form equatorial section.

23 to 26: *Nummulites garnieri inaequalis* from the Marne siltose in Cunial-Santa Giustina-Col dell'Asse section (Possagno section, Italy). Figure drawings after Herb and Hekel (1975). 23 and 24: A-Form equatorial sections; 25: A-Form external view; 26: B-Form equatorial section.

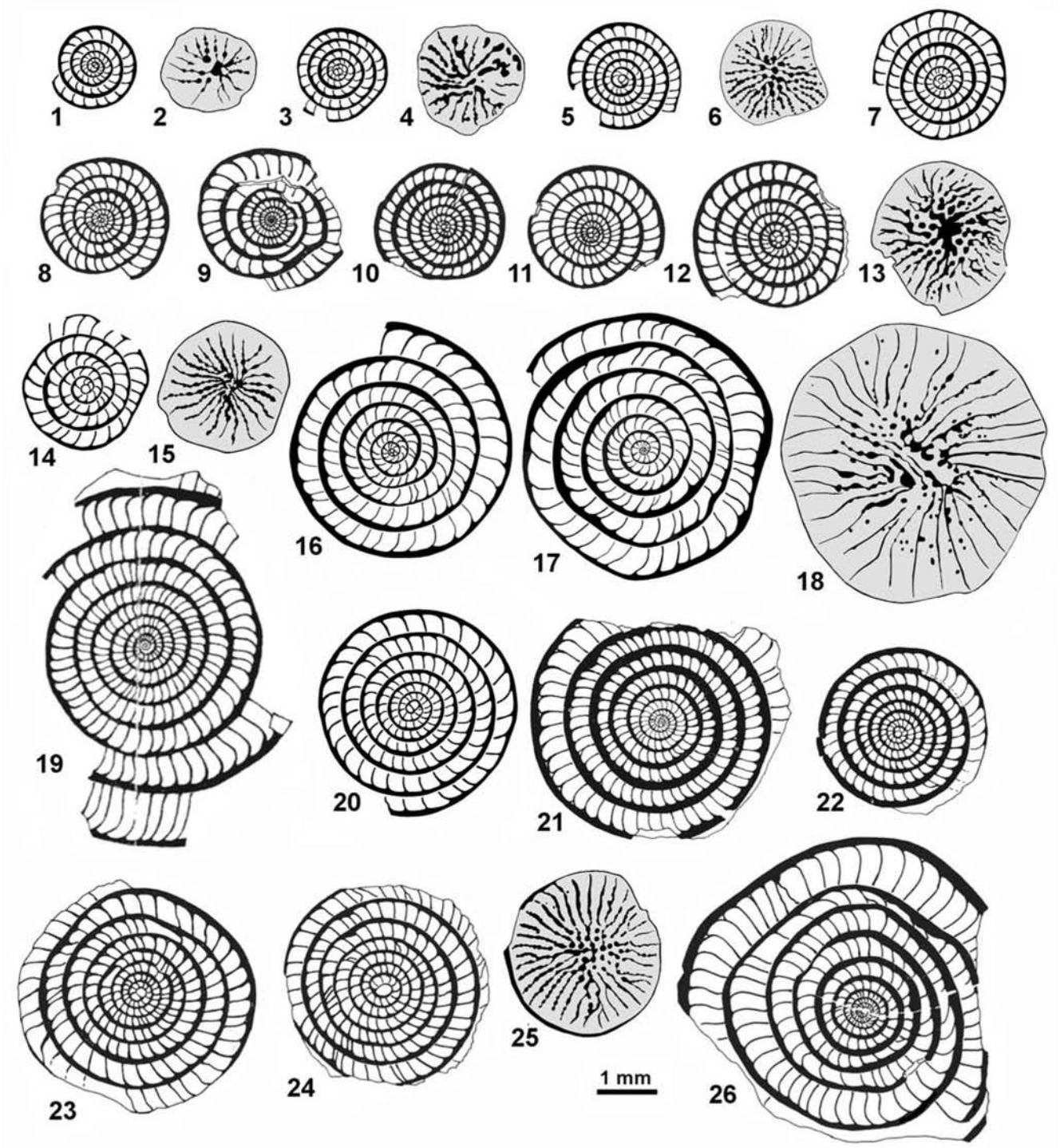
1
2
3
4
5
6
7
8
9
10
11
12
13
14
15
16
17
18
19
20
21
22
23
24
25
1 mm
26

Figure A8 Drawings of *Nummulites* aff. *incrassatus ramondiformis* DE LA HARPE in ROZLOZSNIK 1926 (1-5), *N. incrassatus* DE LA HARPE 1883 (6-9), *N. ramondiformis* DE LA HARPE in ROZLOZSNIK 1926 (10-14), and *N. incrassatus incrassatus* DE LA HARPE 1883 (15).

1 to 5: *N.* aff. *incrassatus ramondiformis* from sample LT005 in the Miralles-La Tossa composite section. 1 and 3: B-Form equatorial sections; 2 and 4: B-Form external views; 5: A-Form equatorial section.

6 to 9: drawings after Roveda (1961) of *N. incrassatus* from the Boro-Granella section in the Priabona area. 6 and 8: A-Form equatorial sections; 7: A-Form external view; 9: B-Form equatorial section.

10 to 14: drawings after Herb and Hekel (1975) of *N. ramondiformis* from the Cunial-Santa Giustina-Col dell'Asse section in the Possagno area. 10: A-Form equatorial section from the Marne di Possagno; 11: B-Form equatorial section from the Marne di Possagno; 12: equatorial section of an A-Form from the Calcaria di Santa Giustina; 13: equatorial section of an A-Form from the Marne Siltose; 14: equatorial section of a B-Form from the Marne Siltose.

15: a drawing after Herb and Hekel (1975) of an A-Form equatorial section of an *N. incrassatus incrassatus* from the Cunial-Santa Giustina-Col dell'Asse section in the Possagno area.

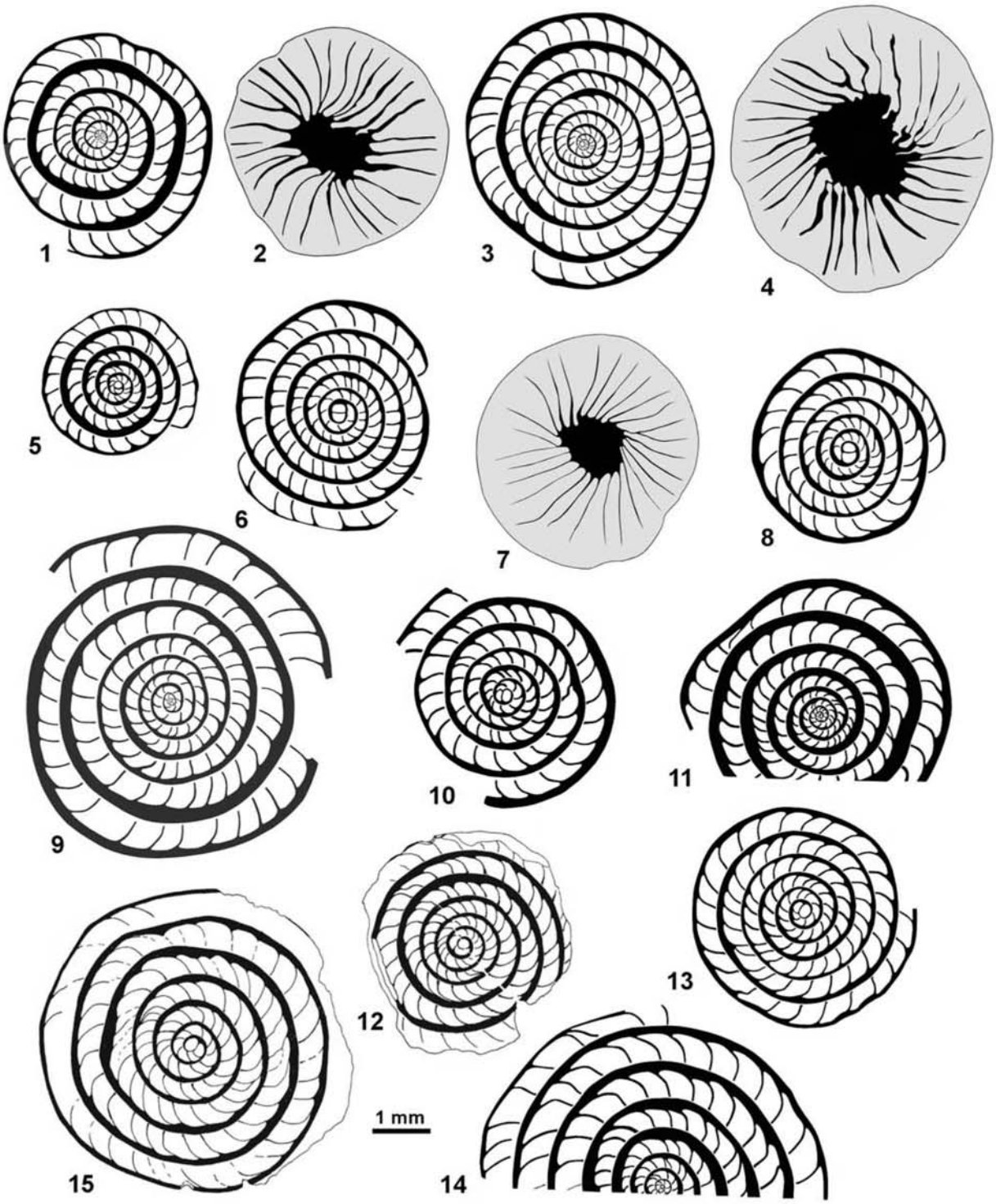
1
2
3
4
5
6
7
8
9
10
11
12
13
14
15
1 mm

Figure A9 *Nummulites beaumonti* D'ARCHIAC and HAIME 1853 and *N. biarritzensis* DE LA HARPE in ROZLOZSNIK 1926 from the Miralles-La Tossa composite section. *N. beaumonti* (1-8). 1 and 2: B-Forms from sample MM008; 3 to 8: A-Forms from sample MM008. *N. biarritzensis* (9-13). 9 and 10: B-Form from sample MM004; 11 and 12: A-Forms from sample MM004; 13: A-Form from sample MM022.

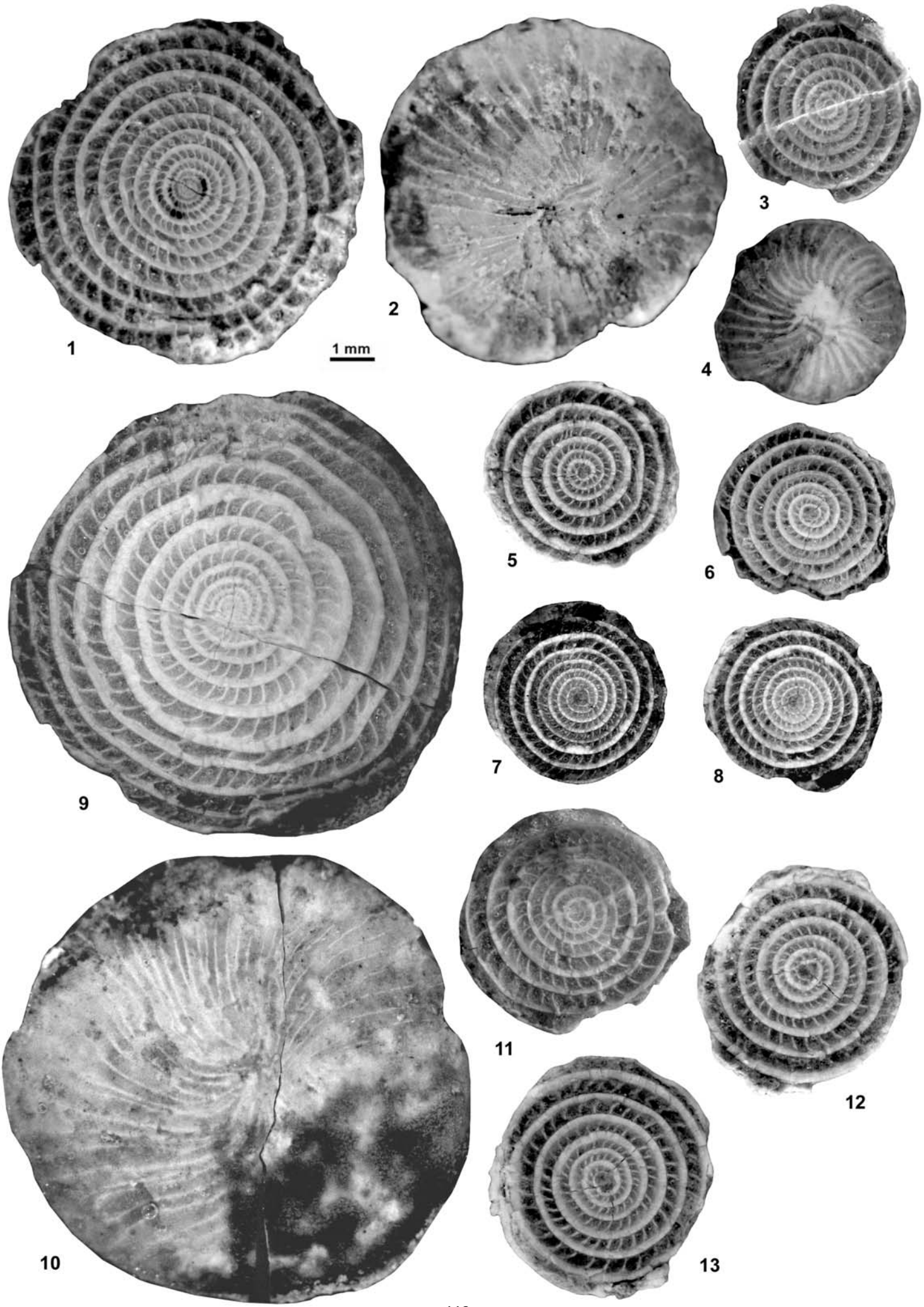
1
1 mm
2
3
4
5
6
7
8
9
10
11
12
13

Figure A10 *Nummulites hottingeri* SCHAUB 1981 and *Nummulites perforatus* DE MONTFORT 1808 from the Miralles-La Tossa composite section. *N. hottingeri* (1-5). 1 to 4: A-Forms from sample MM022; 5: B-Form from sample MM004. *N. perforatus* (6-10). 6 to 9: A-Forms from sample BM010; 10: B-Form from sample BM010.

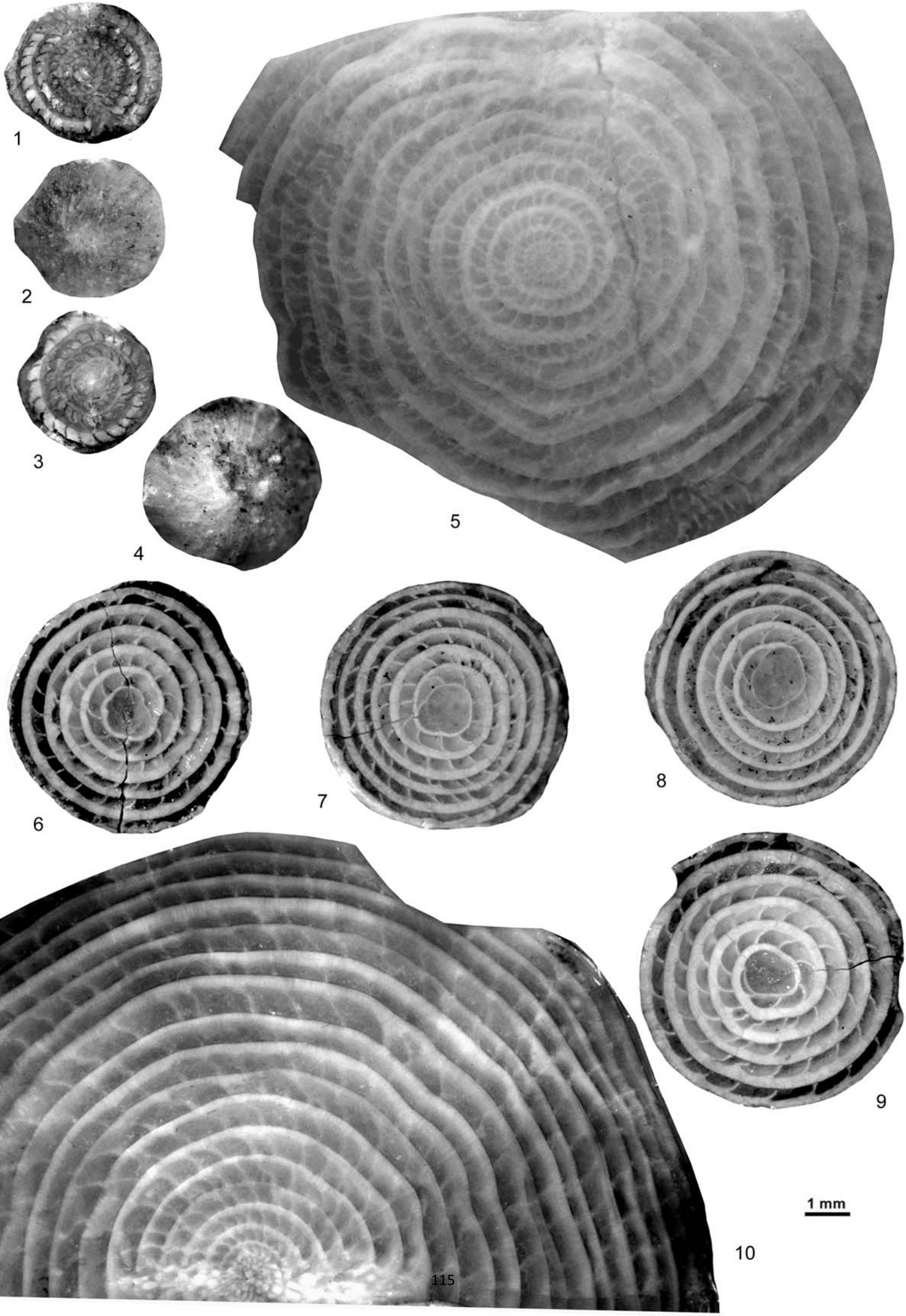
1
2
3
4
5
6
7
8
9
10
1 mm

Figure A11 *Nummulites vicaryi* SCHAUB 1981, *Nummulites stellatus* ROVEDA 1961, *Nummulites orbignyi* GALEOTTI 1837, *Operculina roselli* HOTTINGER 1977, and *Assilina schwageri* SILVESTRI 1928 from the Miralles-La Tossa composite section. *N vicaryi* (1-6). 1 to 3: B-Forms from sample MM028-29; 4 to 6: A-Forms from sample MM028-29. *N. stellatus* (7-8). 7 and 8: A-Forms from sample LT000. *N. orbignyi* 9: A-Form from sample LT157. *O. roselli* 10: A-Form from sample MM024. *A. schwageri* (11-12). 11 and 12: A-Forms from sample MM008.

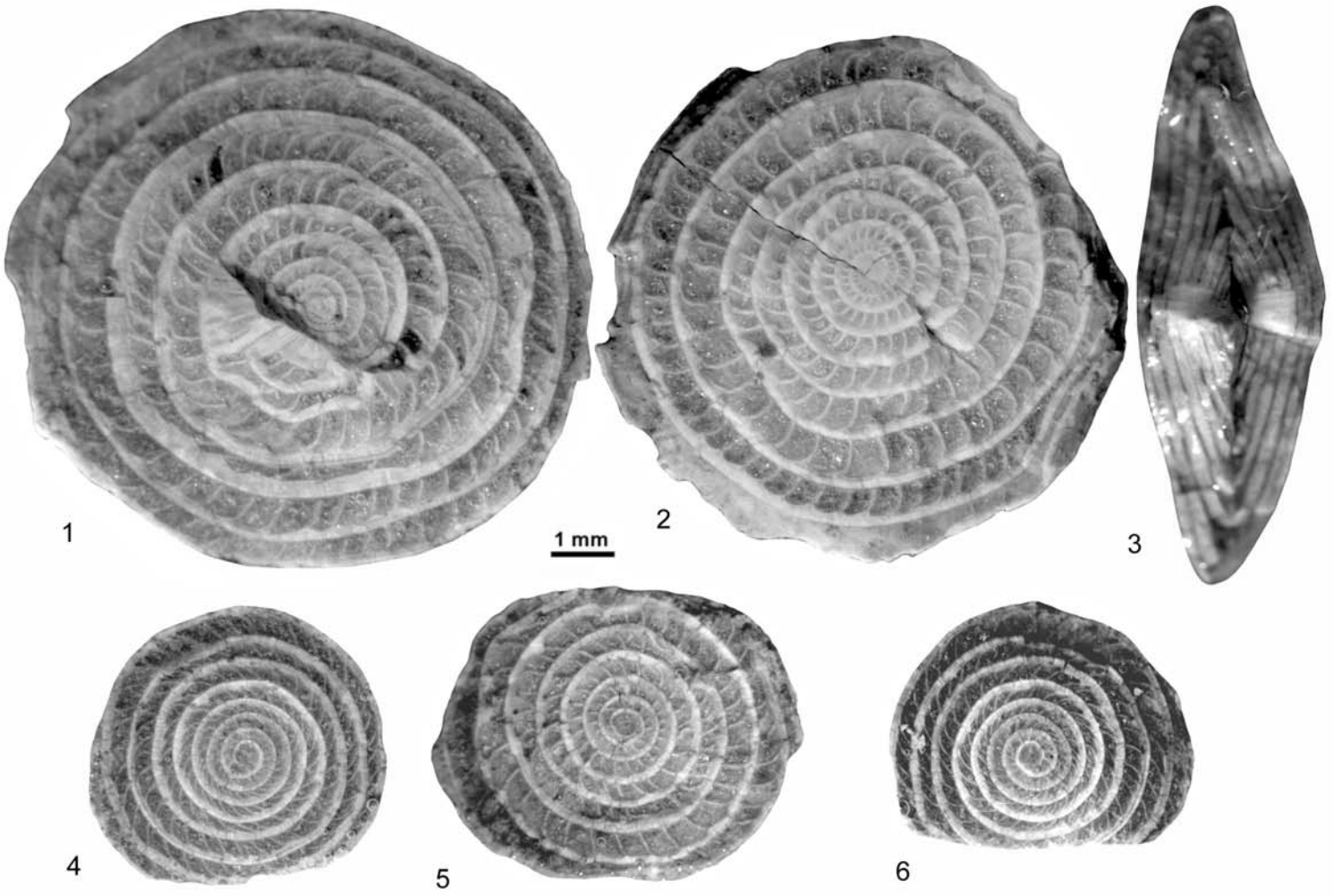
1
1 mm
2
3
4
5
6

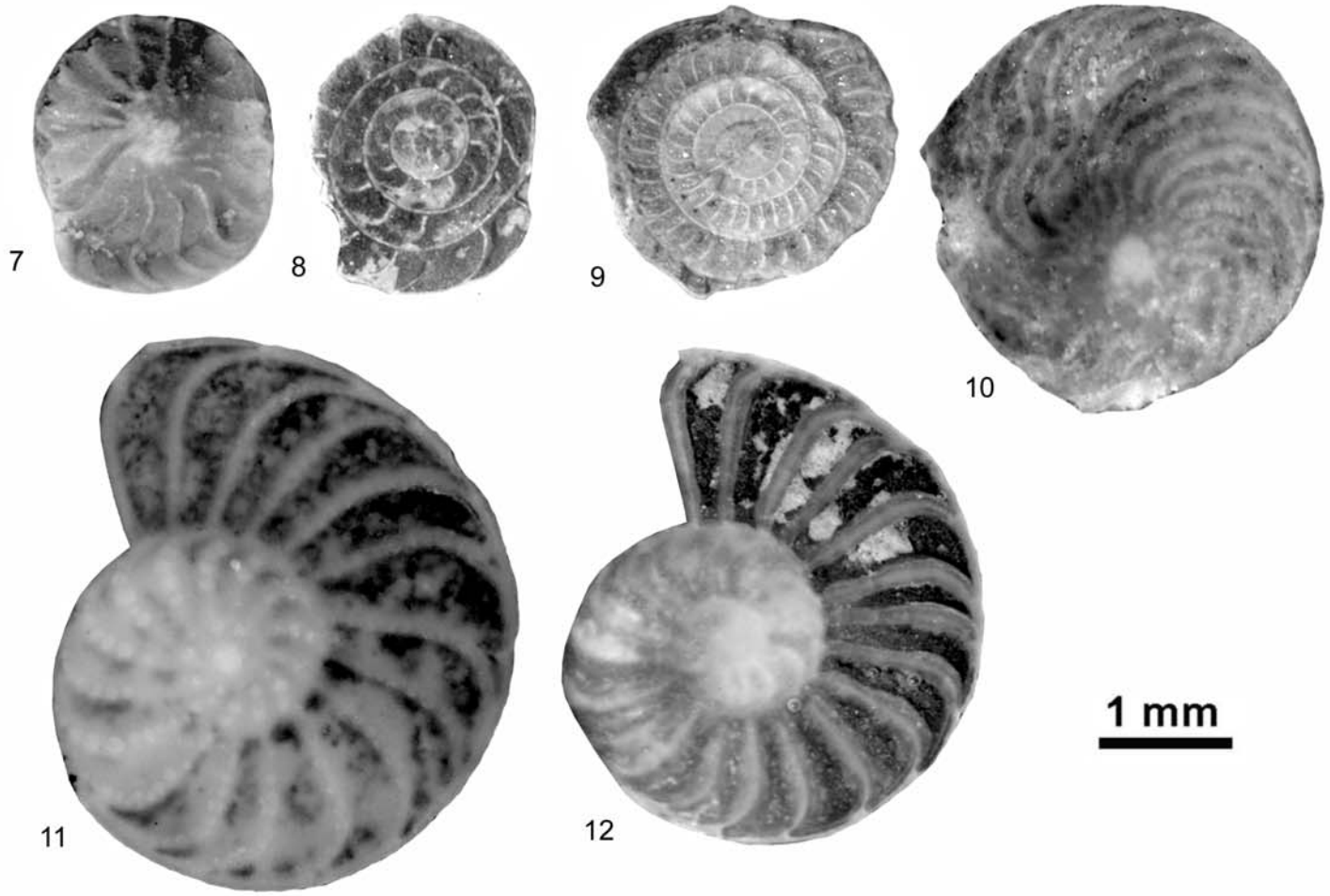
7
8
9
10
11
12
1 mm

Figure A12 *Nummulites striatus* BRUGUIÈRE 1792 from the Miralles-La Tossa composite section. 1 and 3: A-Forms from sample MM050; 2: A-Form from sample LT104; 4 and 5: B-Forms from sample LT104.

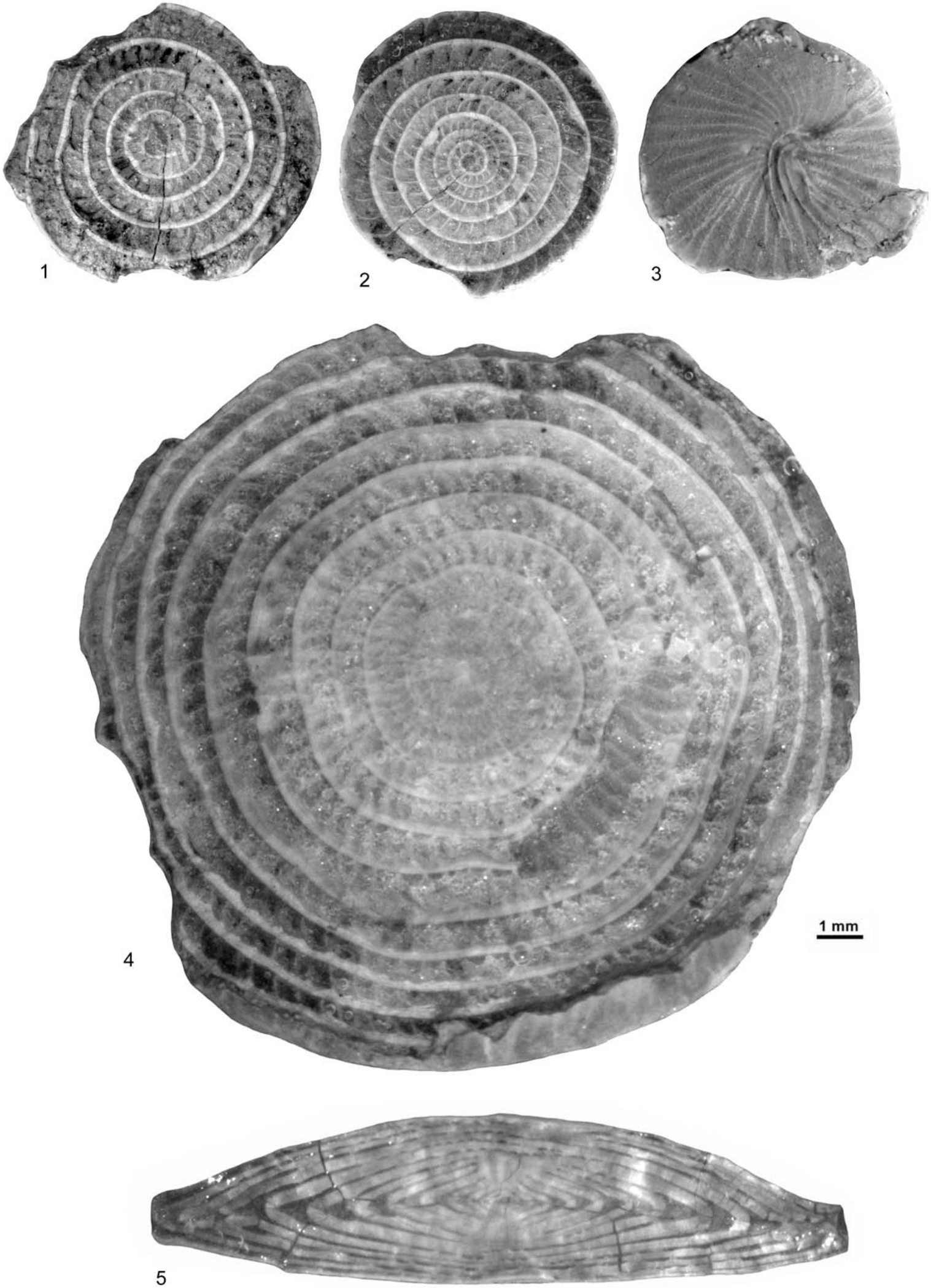
1
2
3
4
1 mm
5

Figure A13 *Nummulites garnieri sturi* VANOVA 1972, *Nummulites chavannesi* DE LA HARPE 1978, and *Nummulites* aff. *incrassatus ramondiformis* DE LA HARPE IN ROZLOZSNIK 1926 from the Miralles-La Tossa composite section. *N. garnieri sturi* (1-5). 1 to 4: A-Forms from sample LT005; 5: B-Form from sample LT005. *N. chavannesi* (6-11). 6 to 10: A-Forms from sample LT005; 11: B-Form from sample LT005. *N.* aff. *incrassatus ramondiformis* (12-26). 12 to 15: B-Forms from sample LT005; 16 to 26: A-Forms from sample LT005.

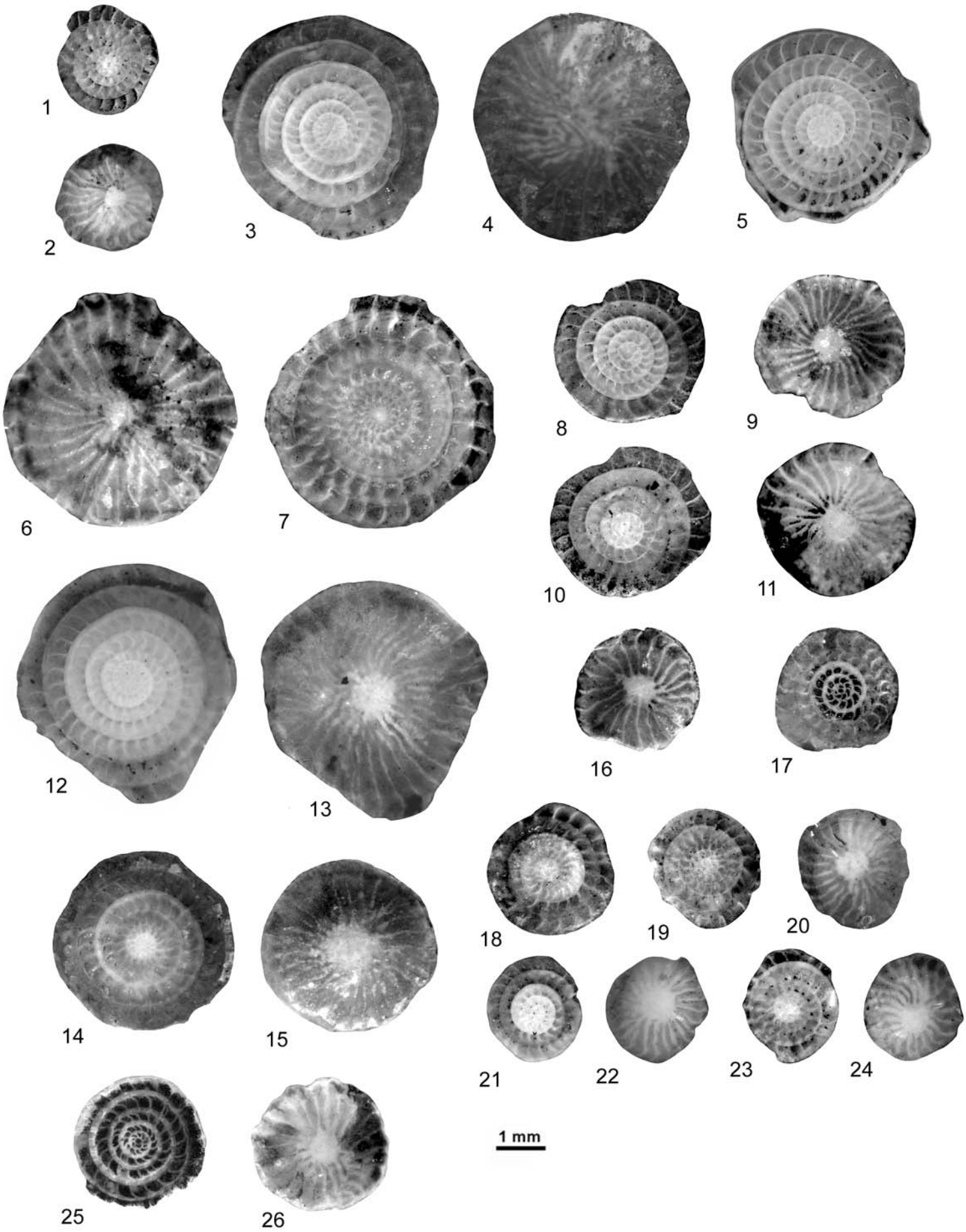
1
2
3
4
5
6
7
8
9
10
11
12
13
16
17
18
19
20
21
22
23
24
25
26
1 mm

Table A1 Results of the calcareous nannofossil quantitative analysis of the Miralles-La Tossa composite section. PDE, preservation degree of the assemblage; PRA, presence of reworked assemblages; TSA, total species abundance in number of specimens per field of view; and RASS, relative abundance of single species (%). Indididual and Total Abundance of nannofossil: A (abundant) more than 20 specimens per field of view (spp/fv); C (common) 10-20 spp/fv; F (few) 1-10 spp/fv; R (rare) 0,1-1 spp/fv; P (presence) less than 0,1 spp/fv; B (barren of nannofossil). Preservation Degree and Reworked Assemblages: G (good) individual specimens exhibit little or no dissolution or overgrowth, diagnostic characteristic are preserved, and nearly all of the species can be identified; M (moderate) individual specimens show evidence of dissolution or owergrowth, some spices can not be identified to the species level; P (poor) individual specimens exhibit considerable dissolution or overgrowth, many specimens cannot be identified to the species level.

Formations	Sample	meters	Total abundance	Preservation	Reworking	*Braarudosphaera bigelowii*	*Bramletteius serraculoides*	*Calcidiscus protoanulus*	*Calciduscus spp.*	***Chiasmolithus grandis***	***Chiasmolithus oamaruensis***	*Chiasmolithus* spp.	*Coccolithus formosus*	*Coccolithus pelagicus*	*Coronocyclus bramlettei*	*Cyclicargolithus florindanus*	***Dictyococcites bisectus***	*Dictyococcites scrippsae*	*Discoaster barbadiensis*	*Discoaster saipanensis*	*Discoaster tani*	*Helicosphaera spp.*	***Isthmolithus recurvus***	*Lanternitus minutus*	*Pemma basquensis*	*Pemma papillatum*	*Pemma ssp.*	*Pontosphaera* spp.	*Postospharea exilis*	*Postosphaerea multipora*	*Reticulofenestra dyctioda*	*Reticulofenestra reticulata*	*Reticulofenestra* spp.	*Reticulofenestra umbilicus*	*Sphenolithus cf. anharropus*	*Sphenolithus moriformis*	***Sphenolithus obtusus***	*Zygrhablithus bijugatus*	NANNOFOSSIL ZONES
TOSSA FORMATION	LT034	1345.1	B	-	-	-	-	-	-	-	-	-	-	-	-	-	-	-	-	-	-	-	-	-	-	-	-	-	-	-	-	-	-	-	-	-	-	-	-
	LT031	1322.1	B	-	-	-	-	-	-	-	-	-	-	-	-	-	-	-	-	-	-	-	-	-	-	-	-	-	-	-	-	-	-	-	-	-	-	-	-
	LT027	1302.7	B	-	-	-	-	-	-	-	-	-	-	-	-	-	-	-	-	-	-	-	-	-	-	-	-	-	-	-	-	-	-	-	-	-	-	-	-
	LT020	1275.8	B	-	-	-	-	-	-	-	-	-	-	-	-	-	-	-	-	-	-	-	-	-	-	-	-	-	-	-	-	-	-	-	-	-	-	-	-
	LT016	1266.6	B	-	-	-	-	-	-	-	-	-	-	-	-	-	-	-	-	-	-	-	-	-	-	-	-	-	-	-	-	-	-	-	-	-	-	-	-
	LT014	1261.3	B	-	-	-	-	-	-	-	-	-	-	-	-	-	-	-	-	-	-	-	-	-	-	-	-	-	-	-	-	-	-	-	-	-	-	-	-
	LT012	1253.3	B	-	-	-	-	-	-	-	-	-	-	-	-	-	-	-	-	-	-	-	-	-	-	-	-	-	-	-	-	-	-	-	-	-	-	-	-
	LT010	1248.1	B	-	-	-	-	-	-	-	-	-	-	-	-	-	-	-	-	-	-	-	-	-	-	-	-	-	-	-	-	-	-	-	-	-	-	-	-
	LT009	1246.1	B	-	-	-	-	-	-	-	-	-	-	-	-	-	-	-	-	-	-	-	-	-	-	-	-	-	-	-	-	-	-	-	-	-	-	-	-
	LT007	1241.4	B	-	-	-	-	-	-	-	-	-	-	-	-	-	-	-	-	-	-	-	-	-	-	-	-	-	-	-	-	-	-	-	-	-	-	-	-
IGUALADA FORMATION	LT005	1237.5	P	P	-	-	-	-	-	-	-	-	-	-	-	-	-	P	-	-	-	-	-	-	-	-	-	-	-	-	-	-	-	-	-	-	-	-	-
	LT001	1225.8	F	M	-	-	-	-	-	-	-	-	-	P	P	P	-	F	R	-	-	-	-	-	-	-	-	-	-	-	-	-	-	-	-	-	-	-	-
	LT168	1226.0	P	P	-	-	-	-	-	-	-	-	-	P	P	P	-	P	R	-	-	-	-	-	-	-	-	-	-	-	-	-	-	-	-	-	-	-	-
	LT164	1212.0	R	P	-	-	-	-	-	-	-	-	-	-	-	-	-	F	R	P	-	-	-	-	-	-	-	-	-	-	-	-	-	-	-	-	-	-	-
	LT160	1199.5	F	P	-	-	-	-	-	-	-	-	cf.	-	-	-	-	F	R	P	-	-	-	-	-	-	-	-	-	-	-	-	-	-	-	-	-	-	-
	LT155	1124.7	R	P	-	-	-	-	-	-	-	-	-	P	R	-	-	-	R	-	-	-	-	-	-	-	-	-	-	-	-	-	-	-	-	-	-	-	-
	LT151	1104.4	F	M	-	-	-	-	-	-	-	-	-	-	F	-	-	F	R	cf.	-	-	-	-	-	-	-	-	-	-	-	-	-	-	-	-	-	-	-
	LT146	1090.2	F	P	P	-	-	-	-	-	-	-	-	P	F	-	-	F	R	R	P	-	-	-	-	-	-	-	-	-	-	-	-	-	-	-	-	-	-
	LT141	1074.5	F	M	-	-	-	-	-	-	-	-	-	R	R	-	-	F	R	-	-	-	-	-	-	-	-	-	-	-	-	-	-	-	-	-	-	-	-
	LT138	1066.0	C	G	-	-	-	-	-	-	-	-	P	-	R	F	-	F	R	P	-	-	-	-	-	-	-	-	-	-	-	-	-	-	-	-	-	-	-
	LT135	1057.2	F	M	-	-	-	-	-	-	-	-	-	R	R	R	-	F	R	-	-	-	-	-	-	-	-	-	-	-	-	-	-	-	-	-	-	-	-
	LT131	1042.7	C	G	-	-	-	-	-	-	-	-	R	F	F	-	-	F	R	-	-	-	-	-	-	-	-	-	-	-	-	-	-	-	-	-	-	-	-
	LT128	1032.0	C	M	-	-	-	-	-	-	-	-	P	F	F	-	-	F	R	-	-	-	-	-	-	-	-	-	-	-	-	-	-	-	-	-	-	-	-
	LT126	979.8	F	G	P	-	-	-	-	-	-	-	P	F	F	-	-	F	R	P	-	-	-	-	-	-	-	-	-	-	-	-	-	-	-	-	-	-	-
	LT123	969.1	P	M	-	-	-	-	-	-	-	-	-	-	-	-	-	F	R	P	-	-	-	-	-	-	-	-	-	-	-	-	-	-	-	-	-	-	-
	LT121	959.6	C	M	P	-	-	-	-	-	-	-	P	R	R	F	-	F	R	P	-	-	-	-	-	-	-	-	-	-	-	-	-	-	-	-	-	-	-
	LT118	948.0	F	M	-	-	-	-	-	-	-	-	-	P	R	-	-	F	R	P	-	-	-	-	-	-	-	-	-	-	-	-	-	-	-	-	-	-	-
	LT115	937.3	C	G	P	-	-	-	-	-	-	-	R	P	R	R	-	F	R	P	-	-	-	-	-	-	-	-	-	-	-	-	-	-	-	-	-	-	-
	LT111	919.5	F	G	P	-	-	-	-	-	-	-	-	-	R	R	-	F	R	P	-	-	-	-	-	-	-	-	-	-	-	-	-	-	-	-	-	-	-
	LT108	911.3	F	M	-	-	-	-	-	-	-	-	-	-	P	R	-	F	R	P	-	-	-	-	-	-	-	-	-	-	-	-	-	-	-	-	-	-	-
	LT105	903.4	C	G	P	-	-	-	-	-	-	-	-	-	-	F	-	F	R	-	-	-	-	-	-	-	-	-	-	-	-	-	-	-	-	-	-	-	-
	LT104	901.3	C	M	-	-	-	-	-	-	-	-	P	-	R	F	-	F	R	-	-	-	-	-	-	-	-	-	-	-	-	-	-	-	-	-	-	-	-
	LT102	893.8	F	G	-	-	-	-	-	-	-	-	-	P	R	F	-	F	R	-	-	-	-	-	-	-	-	-	-	-	-	-	-	-	-	-	-	-	-
	LT101	884.1	C	G	-	-	-	-	-	-	-	-	-	-	R	R	-	F	R	-	-	-	-	-	-	-	-	-	-	-	-	-	-	-	-	-	-	-	-
	LT100	875.3	C	G	-	-	-	-	-	-	-	R	R	-	R	F	-	F	R	P	-	-	-	-	-	-	-	-	-	-	-	-	-	-	-	-	-	-	-
	MM028	703.5	P	P	-	-	-	-	-	-	-	-	-	-	-	-	-	F	R	-	-	-	-	-	R	-	-	-	-	-	-	-	-	-	-	-	-	-	-
	MM015	628.9	A	G	P	-	-	-	-	-	-	-	-	-	-	-	-	-	P	-	-	-	-	-	-	-	-	-	-	-	-	-	-	-	-	-	-	-	-
	MM014	624.5	C	G	P	-	-	-	P	-	-	-	-	R	R	F	-	R	F	R	-	-	-	P	-	-	-	-	-	-	-	-	-	-	-	-	-	-	-
	MM013	617.0	F	M	-	-	-	-	-	-	-	-	-	R	R	F	cf.	-	R	-	-	-	-	-	-	-	-	-	-	-	-	-	-	-	-	-	-	-	-
	MM012	610.0	A	G	P	-	-	-	-	P	-	-	-	R	R	F	-	-	R	-	-	-	-	-	-	-	-	-	-	-	-	-	-	-	-	-	-	-	-
	MM007	524.5	F	M	R	-	-	-	-	-	-	-	-	R	F	R	-	-	R	-	-	-	-	-	-	-	-	-	-	-	-	-	-	-	-	-	-	-	-
	MM004	509.8	F	M	P	-	-	-	-	-	-	-	-	P	P	F	-	-	R	P	-	-	-	-	-	-	-	-	-	-	-	-	-	-	-	-	-	-	-
	MM001	489.5	F	P	R	-	-	-	-	-	-	-	-	R	-	R	-	-	R	P	-	-	-	-	-	-	-	-	-	-	-	-	-	-	-	-	-	-	-
	BM010	470.2	B	-	-	-	-	-	-	-	-	-	-	-	-	-	-	-	R	P	-	-	-	-	-	-	-	-	-	-	-	-	-	-	-	-	-	-	-
	BM008	457.5	C	M	F	P	-	-	-	-	-	-	-	-	-	-	-	-	R	R	-	-	-	-	-	-	-	-	-	-	-	-	-	-	-	-	-	-	-
	BM005	446.0	F	P	F	P	-	-	-	-	-	-	-	-	-	-	-	-	R	R	-	-	-	-	-	-	-	-	-	-	-	-	-	-	-	-	-	-	-
	BM002	437.5	C	P	C	-	-	-	-	-	-	-	-	-	-	-	-	-	R	P	-	-	-	-	-	-	-	-	-	-	-	-	-	-	-	-	-	-	-
COLLBÀS FORMATION																																							
NP17																																							
NP19 - NP20																																							
NANNOFOSSIL ZONES																																							

Table A2 ChRM directions of the Miralles and La Tossa magnetostratigraphic sections. Site No., name and number of paleomagnetic site and specimen code; Stratigraphic level, stratigraphic position of the paleomagnetic site in the Miralles-La Tossa composite section; Dec. and Inc., declination and inclination in geographic (in situ) and stratigraphic coordinates (after bedding correction); Dip. Az. and Dip., azimuth of down dip direction of local bedding and angle of dip of local bedding; VGP Lat., latitude of the Virtual Geomagnetic Pole used to build the local magnetostratigraphy of Miralles and La Tossa sections (see Fig. 6).

Site No.	Stratigraphic level (m)	Geographic coordinates Dec. (º)	Geographic coordinates Inc. (º)	Stratigraphic coordinates Dec. (º)	Stratigraphic coordinates Inc. (º)	Dip az. (º)	Dip. (º)	VGP Lat. (º)
Miralles Section								
CS001-1A	6.0	391.1	47.8	361.8	28.2	315	40	63.5
CS002-2A	13.6	435.7	58.5	366.5	56.2	315	40	83.1
CS003-1B	34.0	391.7	45.5	363.9	26.9	315	40	62.5
CS004-2B	46.3	340.7	67.5	325.2	29.3	315	40	50.5
CS006-2A	60.8	369.1	69.8	334.4	36.4	315	40	59.7
CS008-1A	73.3	326.3	-51.8	421.6	-81.8	315	40	-32.6
CS009-1B	81.0	315.6	-43.8	326.0	-83.7	315	40	-30.9
CS012-1A	99.3	301.3	-44.7	251.2	-80.1	315	40	-44.8
CS013-1C	108.8	215.1	-28.1	198.8	-16.0	315	40	-52.7
CS027-2A	110.3	284.7	-48.0	197.8	-52.0	330	60	-73.3
CS028-1C	113.5	223.3	-80.6	158.9	-27.1	330	60	-57.3
CS029-1A	120.0	297.8	-31.5	227.5	-63.4	330	60	-55.7
CS030-1A	126.8	282.0	-64.5	175.0	-45.0	330	60	-74.5
CS031-1A	144.8	341.5	-80.7	146.1	-39.0	330	60	-55.6
CS016-1D	150.8	232.1	-67.5	173.6	-25.1	330	60	-61.1
CS017-1B	151.5	305.6	-40.4	203.5	-68.5	330	60	-71.0
CS032-2B	151.8	260.9	-12.5	238.5	-25.3	330	60	-32.2
CS033-1A	161.5	264.8	-50.1	196.4	-38.9	330	60	-66.1
CS019-1B	162.3	301.4	-47.5	191.3	-62.7	330	60	-81.3
CS034-1C	168.0	304.5	-53.0	179.2	-61.0	330	60	-89.2
CS020-1B	168.3	299.4	-58.3	175.5	-55.3	330	60	-83.3
CS021-1B	172.5	298.2	-29.6	231.9	-63.6	330	60	-52.7
CS035-1C	173.4	251.0	-77.7	162.9	-31.9	330	60	-61.7
CS022-1B	176.8	132.7	31.5	408.2	76.2	330	60	54.6
CS022-2A	176.8	297.7	-14.9	259.7	-57.8	330	60	-31.1
CS023-2B	180.8	285.3	-62.4	176.7	-47.3	330	60	-76.7
CS036-1C	184.5	325.0	-41.4	162.6	-78.3	330	60	-62.3
CS024-1B	191.5	259.8	-67.9	174.3	-35.5	330	60	-67.6
CS037-1A	195.3	217.2	-27.4	204.5	3.0	330	60	-41.6
CS038-1C	203.0	260.8	-14.9	236.0	-26.3	330	60	-34.3
CS026-3C	210.0	223.4	-14.7	218.3	5.4	330	60	-33.8
CS039-1A	218.0	91.9	28.0	406.1	40.8	330	60	47.7
CS039-2A	218.0	449.3	51.3	374.9	41.7	330	60	68.6
CS042-1A	225.2	321.1	-46.8	166.0	-72.1	330	60	-72.0
CS043-2A	230.8	95.9	46.2	381.7	46.3	330	60	67.5
CS044-2B	244.5	448.2	21.4	412.6	35.5	330	60	40.6
CS045-1B	245.8	269.6	-52.8	192.8	-41.8	330	60	-69.6
CS045-1C	245.8	284.0	-41.5	208.5	-52.4	330	60	-65.9
CS047-1A	261.5	289.4	-61.9	175.8	-49.1	330	60	-78.0
CS049-1B	265.5	239.8	-14.4	226.7	-8.1	330	60	-34.0
CS051-1A	283.8	97.1	-25.9	101.7	15.4	330	60	-3.4
CS052-1A	286.8	420.9	19.1	403.0	11.3	330	60	37.7
CS053-1E	291.5	267.5	-51.1	195.1	-40.6	330	60	-67.8
CS056-1A	297.3	279.6	-48.2	198.4	-48.6	330	60	-70.9
CS057-1B	301.8	254.7	-11.6	236.3	-19.5	330	60	-31.7
CS058-2A	321.0	290.4	-25.9	246.6	-34.0	354	66	-29.6
CS060-2B	343.3	290.8	-20.9	252.6	-33.2	354	66	-24.8
CS060-1B	343.3	146.4	61.0	371.7	48.8	354	66	74.9
CS065-2A	348.5	412.0	35.0	398.1	-8.6	354	66	32.5
CS065-1B	348.5	367.7	50.6	362.5	-14.2	354	66	41.2
CS062-1A	351.3	442.2	66.5	378.1	21.7	354	66	55.8
CS062-1B	351.3	128.7	77.5	363.0	32.6	354	66	66.1
CS063-2A	357.3	198.1	66.2	338.6	44.8	354	66	66.8
CS064-1B	361.5	106.1	49.7	397.7	33.0	354	66	50.2
CS066-1A	362.5	233.8	62.1	322.9	34.5	354	66	51.3
CS067-2B	381.0	221.0	-37.8	206.4	4.8	347	60	-40.0
CS068-3A	392.4	194.1	-40.7	187.6	14.6	347	60	-40.6
CS069-1B	398.6	124.2	55.6	382.4	51.2	347	60	69.7
CS072-1A	415.5	437.1	-64.6	137.2	-26.3	347	60	-43.8
CS073-2B	419.0	431.3	64.7	373.7	25.1	347	60	59.3
CS075-2B	432.3	289.7	68.4	327.2	16.7	347	60	46.1
BM002-2A	437.5	435.1	65.6	372.3	33.3	344	54	64.4
BM003-1A	439.5	97.5	79.1	355.6	39.9	344	54	70.8
BM005-1A	446.0	167.6	79.0	341.4	46.9	344	54	69.8
BM006-1B	451.0	444.7	84.4	349.6	37.0	344	54	67.4

Site No.	Stratigraphic level (m)	Geographic coordinates Dec. (º)	Geographic coordinates Inc. (º)	Stratigraphic coordinates Dec. (º)	Stratigraphic coordinates Inc. (º)	Dip az. (º)	Dip. (º)	VGP Lat. (º)
BM007-1B	454.5	112.4	85.0	347.7	39.1	344	54	68.0
BM008-1A	457.5	382.0	68.0	357.2	18.1	344	54	57.7
BM009-1A	458.5	108.4	80.2	353.3	41.3	344	54	71.4
BM010-1A	470.2	357.3	61.6	349.7	8.3	344	54	51.6
BM011-1C	478.0	395.8	75.8	355.4	26.8	344	54	62.4
MM001-1A	489.5	337.2	66.3	338.1	10.3	340	56	48.8
MM003-1A	501.2	437.3	73.0	359.3	34.8	340	56	67.7
MM004-1A	509.8	109.3	72.4	357.4	44.1	340	56	74.2
MM005-1A	519.0	283.1	46.0	303.6	4.4	340	56	26.1
MM006-1A	523.5	213.6	-43.7	195.1	-2.4	340	56	-47.5
MM006-2A	523.5	207.3	-83.5	164.3	-29.5	340	56	-61.0
MM007-2A	524.5	137.0	40.3	402.4	71.7	340	56	59.1
MM008-1B	536.0	320.9	80.4	335.5	24.8	340	56	54.4
MM008-2B	536.0	121.6	74.7	351.8	45.5	340	56	74.0
MM009-1A	536.2	371.9	62.1	353.8	9.8	340	56	53.0
MM010-1A	554.8	420.5	59.0	372.8	24.7	340	56	59.4
MM010-2A	554.8	329.7	57.6	333.9	1.9	340	56	43.1
MM011-1A	606.8	356.6	-58.7	138.4	-62.5	340	56	-59.7
MM013-1C	617.0	302.2	-64.6	183.4	-52.3	340	56	-81.0
MM014-2A	624.5	317.8	-64.8	174.7	-56.6	340	56	-84.0
MM015-2A	628.9	318.4	-59.8	179.8	-61.0	340	56	-89.4
MM016-1B	632.2	213.1	-59.2	184.0	-13.5	340	56	-55.2
MM017-1A	636.3	278.2	-68.6	184.0	-42.0	340	56	-72.4
MM018-1A	640.9	287.4	-57.8	197.6	-48.5	340	56	-71.4
MM019-1A	647.5	246.5	-78.4	172.6	-32.8	340	56	-65.5
MM020-1A	652.2	331.6	-71.2	162.5	-52.6	340	56	-73.8
MM021-1A	654.9	169.6	-57.3	164.6	-1.8	340	56	-47.1
MM025-1A	684.9	158.5	-24.6	158.5	31.4	340	56	-28.2
MM026-1B	688.3	246.4	88.2	336.6	34.1	340	56	59.7
MM027-1A	691.5	326.7	40.6	329.3	-14.6	340	56	33.6
MM027-2A	691.5	275.3	49.8	302.7	10.8	340	56	27.8
MM028-1A	703.5	189.1	82.1	333.4	40.7	340	56	61.3
MM029-1A	707.1	181.1	65.3	322.2	55.9	340	56	60.4
MM030-1A	713.0	120.0	76.5	350.4	44.0	340	56	72.4
MM030-1C	713.0	273.0	60.8	310.7	18.8	340	56	36.4
MM031-1B	714.8	285.8	87.0	335.9	32.2	340	56	58.3
MM032-1A	720.5	170.5	48.7	311.4	72.9	340	56	55.5
MM034-1A	728.9	310.4	28.0	311.7	-22.4	340	56	20.8
MM035-1B	730.3	142.5	62.1	353.9	60.1	340	56	85.4
La Tossa Section								
LT100-1A	875.3	376.0	56.8	351.5	30.9	320	35	64.1
LT101-1A	884.1	364.2	68.5	338.4	37.8	320	35	62.7
LT102-1A	893.8	408.3	65.4	357.5	47.8	320	35	77.2
LT103-2A	896.0	349.3	64.4	334.0	31.6	320	35	57.0
LT104-1A	901.3	380.3	61.2	350.5	35.7	320	35	66.8
LT105-1A	903.4	391.6	53.4	362.3	33.6	320	35	66.8
LT106-2A	906.0	359.3	67.3	337.2	35.8	320	35	61.0
LT107-2A	908.5	378.3	56.5	352.9	31.3	320	35	64.7
LT108-2B	911.3	367.2	53.0	358.2	30.0	340	25	64.5
LT109-2A	913.0	395.3	61.8	371.9	43.4	340	25	71.1
LT110-2A	916.0	374.1	59.3	360.7	37.1	340	25	69.2
LT111-1A	919.5	384.6	64.7	364.2	43.8	340	25	73.8
LT112-1A	922.9	366.6	61.2	355.6	37.8	340	25	69.4
LT113-1A	927.1	379.6	57.3	364.9	36.1	340	25	68.1
LT114-1A	931.8	393.6	58.3	373.1	39.9	340	25	68.2
LT115-2C	937.3	390.3	61.9	369.0	42.4	340	25	71.5
LT116-1A	941.8	381.7	49.9	369.2	29.5	340	25	63.1
LT117-1A	945.0	373.3	58.0	360.7	35.7	340	25	68.2
LT118-1A	948.0	348.4	54.0	345.4	29.2	340	25	61.2
LT119-1A	951.3	402.2	64.4	373.8	47.2	340	25	72.7
LT120-2B	955.5	372.5	63.3	358.2	40.6	340	25	71.6
LT121-2A	959.6	364.6	62.0	354.1	38.4	340	25	69.5
LT122-2A	964.7	368.5	60.1	357.0	37.0	340	25	69.0
LT123-2B	969.1	374.9	66.3	358.2	43.7	340	25	74.0
LT126-1B	979.8	428.8	49.1	402.9	43.0	340	25	51.0

Site No.	Stratigraphic level (m)	Geographic coordinates Dec. (º)	Geographic coordinates Inc. (º)	Stratigraphic coordinates Dec. (º)	Stratigraphic coordinates Inc. (º)	Dip az. (º)	Dip. (º)	VGP Lat. (º)
LT127-1B	983.8	371.5	56.5	360.1	33.9	340	25	67.1
LT129-1A	1035.0	408.8	64.4	377.3	48.8	340	25	71.7
LT130-1B	1036.5	397.7	52.5	379.0	35.8	340	25	63.0
LT131-1A	1042.7	409.1	63.0	378.8	47.8	340	25	70.2
LT132-1B	1047.0	391.7	54.9	373.7	36.4	340	25	65.8
LT133-2A	1053.2	383.7	53.0	369.3	32.8	340	25	65.1
LT135-1A	1057.2	386.3	76.0	356.8	54.1	340	25	82.7
LT138-1A	1066.0	406.5	72.7	367.6	54.8	340	25	81.4
LT139-2A	1069.1	390.9	57.0	372.2	38.1	340	25	67.4
LT141-1A	1074.5	381.6	44.3	371.2	24.1	340	25	59.5
LT145-1B	1085.2	372.5	46.5	363.8	24.4	340	25	61.1
LT146-1A	1090.2	232.7	-61.4	202.1	-47.6	340	25	-67.9
LT147-1A	1092.7	207.3	-31.8	199.9	-13.7	340	25	-51.2
LT148-2A	1096.2	223.1	-54.3	201.5	-38.8	340	25	-63.3
LT150-1B	1102.5	212.0	-62.0	186.0	-41.4	340	25	-71.6
LT151-1A	1104.4	166.6	-47.6	164.6	-22.7	340	25	-57.4
LT152-1B	1107.7	122.8	-84.5	148.3	-71.2	339	14	-65.0
LT153-2B	1110.9	332.3	63.2	334.2	49.2	339	14	66.3
LT155-1B	1124.7	210.0	-45.5	201.5	-36.4	339	14	-62.0
LT159-1B	1129.2	213.0	-54.8	200.4	-45.5	339	14	-67.8
LT157-1A	1135.2	304.9	-49.1	292.2	-59.9	339	14	-12.6
LT158-2A	1140.2	380.7	43.3	373.8	32.4	339	14	63.3
LT160-1A	1199.5	325.5	56.4	329.8	36.8	340	20	57.0
LT161-1B	1202.0	365.6	63.0	355.6	44.3	340	20	74.1
LT163-1B	1208.3	369.8	45.5	363.0	27.6	340	20	63.0
LT164-1A	1212.0	343.4	72.2	341.3	52.2	340	20	72.9
LT165-1A	1214.7	380.5	63.1	364.8	46.2	340	20	75.5
LT166-1C	1219.7	393.4	45.6	381.3	32.1	340	20	59.8
LT167-1A	1223.0	428.5	68.1	388.5	60.5	340	20	68.8
LT001-2A	1225.8	336.4	57.7	340.0	48.1	355	10	69.6
LT168-2A	1226.0	383.7	45.2	373.9	29.6	340	20	61.7
LT002-1B	1230.3	330.1	56.9	334.9	47.6	355	10	66.0
LT003-1A	1232.2	379.7	62.7	373.6	53.5	355	10	76.9
LT004-2A	1236.0	375.2	64.9	369.7	55.4	355	10	80.6
LT005-1A	1237.5	377.7	60.0	372.5	50.7	355	10	75.8
LT006-2B	1239.1	328.7	19.3	329.8	10.3	355	10	44.8
LT007-2A	1241.4	381.2	24.2	379.6	15.2	355	10	52.0
LT008-1A	1243.8	371.4	63.9	367.0	54.3	355	10	81.3
LT009-1B	1246.1	381.6	61.9	375.2	52.7	355	10	75.4
LT010-1A	1248.1	340.1	72.5	345.1	62.7	355	10	78.8
LT011-1A	1251.6	364.6	51.0	362.9	41.1	355	10	71.9
LT012-1B	1253.3	352.8	28.7	352.9	18.7	355	10	57.5
LT013-1B	1257.3	356.7	59.8	356.2	49.8	355	10	78.7
LT014-1B	1261.3	360.9	46.9	359.9	36.9	355	10	69.1
LT015-1A	1263.3	287.7	76.0	314.2	69.9	355	10	57.4
LT016-1A	1266.6	353.9	67.2	354.0	57.2	355	10	84.1
LT017-1A	1272.6	349.9	67.7	349.9	67.7	0	0	78.5
LT018-1A	1273.6	381.6	65.7	381.6	65.7	0	0	73.4
LT019-1B	1273.8	359.0	66.1	359.0	66.1	0	0	83.0
LT020-1A	1275.8	342.2	56.5	342.2	56.5	0	0	75.6
LT021-1B	1277.7	304.2	63.6	304.2	63.6	0	0	50.1
LT023-1A	1288.8	351.5	19.0	351.5	19.0	320	25	57.4
LT024-1A	1292.1	110.5	-15.0	110.5	-15.0	320	25	-20.4
LT026-2A	1299.8	334.5	68.0	334.5	68.0	320	7	70.1
LT027-1A	1302.7	341.5	63.7	341.5	63.7	320	7	76.1
LT030-1B	1320.1	354.2	54.0	354.2	54.0	320	7	81.7
LT031-1A	1322.1	347.8	58.6	347.8	58.6	340	25	80.4
LT033-1A	1338.8	362.9	55.3	362.9	55.3	320	7	83.9
LT034-1B	1345.1	435.8	16.8	435.8	16.8	320	7	16.3

CHAPTER 3.2:

CHRONOLOGY OF THE MARINE-CONTINENTAL TRANSITION IN THE IGUALADA AREA: *"CLOSING AND CONTINENTALIZATION OF THE SOUTH PYRENEAN FORELAND BASIN (NE SPAIN): MAGNETOCHRONOLOGICAL CONSTRAINTS"*

Chapter 3.2 constitutes the second scientific paper of this PhD-Thesis: *Costa, E., Garcés, M., López-Blanco, M., Beamud, E., Gómez-Paccard, M., Larrasoaña, J.C., (2010). Closing and continentalization of the South Pyrenean foreland basin (NE Spain): magnetochronological constraints. Basin Research, 22, 904-917.* doi: 10.1111/j.1365-2117.2009.00452.x

Basin Research

IAS EAGE

Basin Research (2010) **22**, 904–917, doi: 10.1111/j.1365-2117.2009.00452.x

Closing and continentalization of the South Pyrenean foreland basin (NE Spain): magnetochronological constraints

Elisenda Costa*, Miguel Garcés*, Miguel López-Blanco*, Elisabet Beamud†, Miriam Gómez-Paccard* and Juan Cruz Larrasoaña‡[1]

*Grup de Geodinàmica i Anàlisis de Conques (GGAC), Universitat de Barcelona. Departament d'Estratigrafia, Paleontologia i Geociències Marines, Facultat de Geologia, Martí i Franquès s/n, 08028 Barcelona, Spain

†Laboratori de Paleomagnetisme (UB-CSIC), Serveis de Suport a la Recerca UB, Istitute of Earth Sciences 'Jaume Almera', CSIC. Solé i Sabarís s/n, 08028 Barcelona, Spain

‡Institute of Earth Sciences 'Jaume Almera', CSIC. Solé i Sabarís s/n, 08028 Barcelona, Spain

ABSTRACT

This paper presents new magnetostratigraphic results from a 1100-m-thick composite section across the marine to continental sediments of the central part of the SE margin of the Ebro basin (NE Spain). Integration with existing marine and continental biochronological data allows a robust correlation with the geomagnetic polarity time scale. The resulting absolute chronology ranges from 36.3 to 31.1 Ma (Priabonian to Rupelian), and yields an interpolated age of ~36.0 Ma (within chron C16n.2n) for the youngest marine sediments of the eastern Ebro basin. This age is in concordance with a reinterpretation of earlier magnetostratigraphic data from the western South Pyrenean foreland basin, and indicates that continentalization of the basin occurred as a rapid and isochronous event. The basin continentalization, determined by the seaway closure that resulted from the uplift of the western Pyrenees, was probably coincident with a mid-amplitude eustatic sea level low with a maximum at 36.2 Ma. The base level drop that followed the basin closure and desiccation does not appear associated to a significant sedimentary hiatus along the margins, suggesting a late Eocene shallow marine basin that rapidly refilled and raised its base level after the seaway closing. Rapid basin filling following continentalization predates the phase of rapid exhumation of the Central Pyrenean Axial Zone from 35.0 to 32.0 Ma, determined from the thermochronology data. It is possible then that sediment aggradation at the front of the fold-and-thrust belt could have contributed to a decrease in the taper angle, triggering growth of the inner orogenic wedge through break-back thrusting and underplating. Contrasting sedimentation trends between the western and eastern sectors of the South Pyrenean foreland indicate that basin closing preferentially affected those areas subjected to sediment bypass towards the ocean domain. As a result, sediment ponding after basin closure is responsible for a two-fold increase of sedimentation rates in the western sector, while changes of sedimentation rates are undetected in the more restricted scenario of the eastern Ebro basin.

INTRODUCTION

Peripheral foreland basins are wedge-shaped elongated troughs that form as a flexural response of tectonic plates to continental collision. By way of the lithospheric flexure, a strong dynamic link exists between the foreland basin and its adjacent orogen (Beaumont, 1981), such that geodynamic processes related to the orogenic belt and its associated subduction systems determine the evolution of the foreland basin (DeCelles & Giles, 1996). This coupling is bi-directional, because sediment load in the infilling foreland can influence the deformation style in the orogenic belt (Stori & McClay, 1995; Mugnier *et al.*, 1997). As a result, a comprehension of the overall collision setting demands an integrated approach, with kinematics of the fold-and-thrust belt and basin stratigraphy being conveniently included in a tectonostratigraphic frame.

The evolution of peripheral foreland basins often includes an early phase of rapid deepening of basin floor as subsidence greatly surpasses sediment yield. Ongoing

Correspondence: E. Costa, Departament d'Estratigrafia, Paleontologia i Geociències Marines, Facultat de Geologia, Martí i Franquès s/n, 08028-Barcelona, Spain. E-mail: elicosta@ub.edu

[1]Present address: Instituto Geológico y Minero de España (IGME). Oficina de Proyectos de Zaragoza, Manuel Lasala 44, 9B, 50006 Zaragoza, Spain

plate convergence drives widening and thickening of the orogenic wedge, with subsequent increase of surface processes and of sediment erosion and transport into the foreland. In consequence, a late evolution of peripheral foreland basins often culminates with a transition from an underfilled to a filled or an overfilled depositional state as sediment supply surpasses accommodation in the foredeep zone. In ancient settings, the reference frame for the filling state is the sea level, so that transition from marine to continental sedimentation normally equates with the overfilled stage (Sinclair, 1997).

The timing and rates at which continentalization occurs in a foreland basin are dependent on the interplay of a number of factors such as the rate of thrust wedge propagation, the flexural rigidity of the underlying plate and the rate of sediment supply from the mountain range (Sinclair, 1997). Marine–continental transition is often thought to be diachronous, achieved by filling of the basin along its axis and following the regional depositional gradient. However, if continental collision ultimately leads to a land-locked palaeogeographic configuration, the transition from open to closed drainage may result into a basin-wide isochronous continentalization.

It reveals that unravelling the palaeogeographic scenario and driving mechanism of basin continentalization is of relevance for constraining geodynamic models of the thrust wedge-foreland basin system. Achieving this goal requires a basin-wide correlation of the stratigraphic units associated to the marine–continental transition, which can be accomplished through accurate dating. Difficulties often arise, however, when searching for age constraints in shallow marine to continental sedimentary environments (Bera *et al.*, 2008). Restricted marine environments preceding continentalization often fail to provide reliable biostratigraphic markers, while vertebrate fossil findings in continental sediments are typically scarce. Also, if sedimentary gaps or sudden changes in sediment accumulation occurred during the continentalization process, magnetostratigraphic analysis may lead to uncertain correlations with the time scale.

The South Pyrenean foreland basin in NE Spain is a particular case among the alpine foreland basins because it is limited by active margins that underwent sufficient uplift to cause isolation of the basin from the open ocean. The continentalization of the basin was preceded by a phase of progressive restriction of its marine connections, leading to precipitation of relatively thick salt deposits in two distinct depocentres. In this paper, we provide constraints on the evolution of the South Pyrenean foreland basin by establishing a precise chronology for its complete continentalization. We contribute with new magnetostratigraphic data from the eastern Ebro basin, and integrate our results with a reinterpretation of existing magnetostratigraphic records along the South Pyrenean foreland basin. We analyse the timing and the sedimentation trends across the marine–continental transition and discuss the overall scenario of basin continentalization within the tectonostratigraphic framework of the South Pyrenean fold-and-thrust belt.

GEOLOGICAL SETTING

The Ebro basin is a triangular-shaped basin surrounded by three alpine ranges: the Pyrenees to the N, the Iberian Range to the SW and the Catalan Coastal Ranges to the SE (Fig. 1). This basin represents the latest evolutionary stage of the South Pyrenean foreland, whereas earlier stages of foreland basin evolution are now incorporated as piggyback basins on top of allochtonous thrust nappes (Ori & Friend, 1984; Puigdefàbregas *et al.*, 1992). In this sense, the Ebro basin is considered the autochthonous part of the

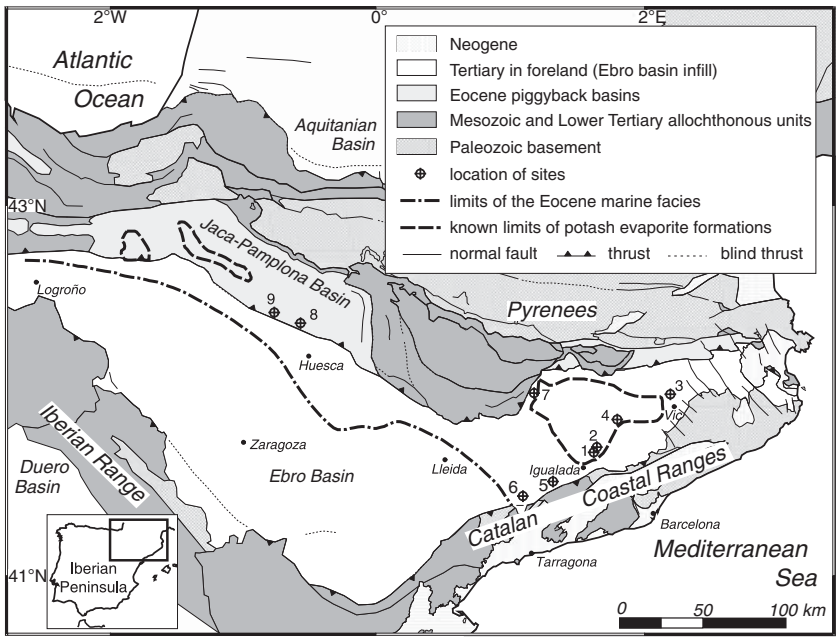

Fig. 1. Geological map of the South Pyrenean foreland basin. Distribution of the Upper Eocene evaporites based on outcrop, mine and borehole data (simplified from Rosell & Pueyo, 1997). Locations of sites: (1) Maians–Rubió composite magnetostratigraphic section; (2) Castellfollit del Boix hydrocarbon borehole (IGME, 1987); (3) Vic magnetostratigraphic section (Burbank *et al.*, 1992; Taberner *et al.*, 1999; Cascella & Dinarès-Turell, 2009); (4) Santpedor fossil locality (Sáez, 1987; Arbiol & Sáez, 1988; Anadón *et al.*, 1992); (5) Jorba–La Panadella section (Feist *et al.*, 1994); (6) Rocafort–Vinaixa composite magnetostratigraphic section of Barberà *et al.* (2001); (7) Oliana magnetostratigraphic section (Vergés & Burbank, 1996); (8) Arguis magnetostratigraphic section (Hogan & Burbank, 1996); and (9) Salinas magnetostratigraphic section (Hogan & Burbank, 1996).

South Pyrenean foreland basin (Riba *et al*., 1983). The South Pyrenean foreland evolved from Late Cretaceous to Miocene times in response to flexural subsidence related to the growth of its margins driven by convergence and continental collision between the Iberian and European plates (Zoetemeijer *et al*., 1990; Vergés *et al*., 2002).

The South Pyrenean foreland basin infill includes marine and continental sediments that range from upper Cretaceous to middle Miocene in age. Sea way connections with marginal oceanic basins were feasible to the east (Tethys domain) and west (Atlantic Ocean). Palaeogeographic reconstructions of the circum-Pyrenean region (Plaziat, 1981; Meulenkamp & Sissingh, 2003) indicate that the eastern marine gateway underwent an early progressive restriction during the middle-late Eocene. No precise age constraint exists on the closure of this connection due to the scarcity of preserved sedimentary record after the uplift and erosion of the Catalan margin during the neogene rifting of the western Mediterranean. The conclusion is that no evidence exists of marine sedimentation younger than Bartonian age along the crustal blocks that formed this eastern corridor (Plaziat, 1981; Meulenkamp & Sissingh, 2003; Serra-Kiel *et al*., 2003a).

The western marine communication of the South Pyrenean foreland basin was certainly maintained until the Late Eocene, when uplift in the western Pyrenees (Muñoz *et al*., 1986; Puigdefàbregas *et al*., 1992) led to the final isolation from the Atlantic Ocean. Restricted marine conditions led to the deposition of evaporites and salts in two main depocentres (the Catalan and the Navarrese Potash sub-basins), now separated by the emplacement of the South Central Pyrenean thrust sheets (Rosell & Pueyo, 1997). No field or subsurface evidences exist on the continuity or isochrony of the marine salt deposition between the eastern (Catalan) and western (Navarrese) sub-basins. Nonetheless, the geochemical signature in both evaporite sequences indicates that they experienced a parallel evolution (Cendón *et al*., 2003). The closure of the basin was followed by uninterrupted upper Eocene to middle Miocene sedimentation of a thick alluvial–lacustrine sequence (Anadón *et al*., 1989; Arenas & Pardo, 1999). This unusual and long-lasting endorheic stage led to the progressive basin filling and, eventually, backfilling of the thrust-belt margins with conglomerates (Riba *et al*., 1983; Coney *et al*., 1996). Finally, the opening of the Ebro basin towards the Mediterranean occurred between 13.0 and 8.5 Ma as a combined result of both lake overfilling and escarpment erosion (Garcia-Castellanos *et al*., 2003).

The eastern margin of the Ebro basin also developed a foredeep zone as a consequence of thrusting and uplift of the Catalan Coastal Ranges from the Early Eocene until Oligocene (Guimerà, 1984; Anadón *et al*., 1985). In the central sector of the Catalan Coastal Ranges, maximum deformation occurred in the Middle to Late Eocene, as recorded by the syntectonic development of alluvial-fan and fan-delta systems (López-Blanco, 2002). These marginal alluvial deposits graded basinwards into shallow marine clastic sediments and carbonates. Biostratigraphic studies in the marine successions of the Igualada area (Figs 1 and 2) have yielded a complete Bartonian succession based on the recognition of the Shallow Benthic Zones SBZ17 and SBZ18 (Serra-Kiel *et al*., 2003b).

The top marine sedimentation in the Igualada area (Fig. 2) is represented from base to top by offshore marls (Igualada Formation), prograding bioclastic and reefal limestones (Tossa Formation) both forming part of the Santa Maria Group (Ferrer, 1971; Pallí, 1972), the shallow water carbonate platforms of the 'Terminal Complex' (Travé, 1992), and the Òdena Gypsum Formation, the marginal equivalent of the central-basin salt deposits of the Cardona Formation. In a laterally equivalent position and above the marine units, the alluvial and lacustrine beds of the Artés Formation (Ferrer, 1971) were deposited. The continental Artés Formation has yielded a complete Oligocene sequence of rodent fossil assemblages (Barberà *et al*., 2001). The basal members of the Artés Formation have yielded scarce biostratigraphic information, but Late Eocene (Sant Cugat de Gavadons) to Early Oligocene (Santpedor) vertebrates fossil assemblages have been reported (Agustí *et al*., 1987; Anadón *et al*., 1987, 1992; Sáez, 1987; Arbiol & Sáez, 1988).

Previous magnetostratigraphic studies provided absolute age constraints for the deposition of the marine Eocene succession in the eastern Ebro basin (Burbank *et al*., 1992; Vergés & Burbank, 1996; Taberner *et al*., 1999; López-Blanco *et al*., 2000), assigning a Bartonian age for the youngest marine sediments in this region. All these studies based their chronology on existing biostratigraphic constraints, which have been recently challenged (Cascella & Dinarès-Turell, 2009). In the present study, we aim at focusing on the age of the transition from marine to continental sedimentation by integrating new magnetostratigraphic results with the available marine and continental biostratigraphic information.

MAGNETOSTRATIGRAPHY OF THE MAIANS-RUBIÓ SECTION

Two overlapping stratigraphic successions in the Artés Formation, corresponding to the distal parts of the Montserrat alluvial-fan and fan-delta systems, were sampled for magnetostratigraphy. The Maians and Rubió sections consist of red alluvial and fluvial beds with some interbedded lacustrine limestones. Detailed lithostratigraphic correlation indicates that the lower 50 m of the Maians section grade basinwards into the marine Santa Maria Group, the overlying 'Terminal Complex', and the Òdena Gypsum Formation (Fig. 2). The correlated stratigraphic position of the Òdena Gypsum Formation in the Maians section (Fig. 2) is fully concordant with the depth at which the salts of the Cardona Formation were penetrated in the exploratory hydrocarbon borehole of Castellfollit del Boix (IGME, 1987), located 0.5 km north from the top of the Maians section (see Supporting Information, Fig. S1 for borehole location).

A total of 255 palaeomagnetic sites were sampled spanning about 1135 m in the Maians (Fig. S1) and Rubió (Fig. S2) sections. Two oriented cores per site were taken with an electrical portable drill at most sites. Samples were oriented using a magnetic compass coupled to a core-orienting fixture. Sampling was focused on red silts and very fine sandstones and avoided coarse-grained lithologies. The occurrence of suitable lithologies determined a sampling resolution of 2–3 m, with the exception of the uppermost intervals of the Maians and Rubió sections, where the abundance of conglomerates and coarse sandstones limited the sampling resolution to 5–8 m. According to previous age constraints, the given sampling frequency yields a time resolution of < 10 kyr, sufficient to allow a complete identification of the Upper Eocene–Lower Oligocene geomagnetic polarity reversals.

The palaeomagnetic analysis consisted of stepwise thermal demagnetization and subsequent measurement of the natural remanent magnetization (NRM) at intervals ranging between 50 °C and 10 °C. This was carried out on at least one sample per site up to a maximum temperature of 680 °C. Remanent magnetization was measured using superconducting rock magnetometers (2G Enterprises) at the Palaeomagnetic Laboratories of the Universitat de Barcelona (Serveis de Suport a la Recerca UB-CSIC), the 'Fort Hoofddijk' (Utrecht University, The Netherlands), and the Scripps Institution of Oceanography (University of California San Diego, USA). Magnetic susceptibility was also measured after each demagnetization step using a KLY-2 magnetic susceptibility bridge (Geofizika, Brno).

Palaeomagnetic components were determined from visual inspection of the vector endpoint demagnetization diagrams (Fig. 3). In all the specimens, a viscous magnetization representing up to 50% of the initial NRM was removed after heating to 250 to 300 °C. Above this temperature, a characteristic remanent magnetization (ChRM) of either normal or reversed polarity can be identified (Fig. 3). In most samples, the ChRM shows maximum unblocking temperatures ranging from 560 to 680 °C, which suggests that it is carried by the iron oxides magnetite and haematite. Occasionally, an intermediate component of exclusively reversed polarity and unblocking temperatures ranging from 500 °C to 590 °C to 620 °C has been identified in samples of the Maians section (Fig. 3d and e). This intermediate component was likely acquired during the Early Oligocene, because younger units studied by Barberà *et al.* (2001) have not shown secondary magnetizations of such nature. The ChRM directions were calculated from the demagnetization diagrams by means of principal component analysis (Kirschvink, 1980). Reliable ChRM directions were calculated for 221 samples (supporting information, Table S1), which represent 87% of the total number of the sampled levels. The stereonet projection of ChRM directions shows a large scatter (Fig. 4), which is particularly seen in samples from the Maians section. It is possible that scattered directions may relate with lithology as sampled levels in Maians often correspond to massive mottled-reddish siltstones likely affected by the postdepositional randomizing processes of bioturbation, palaeosoil formation, and desiccation

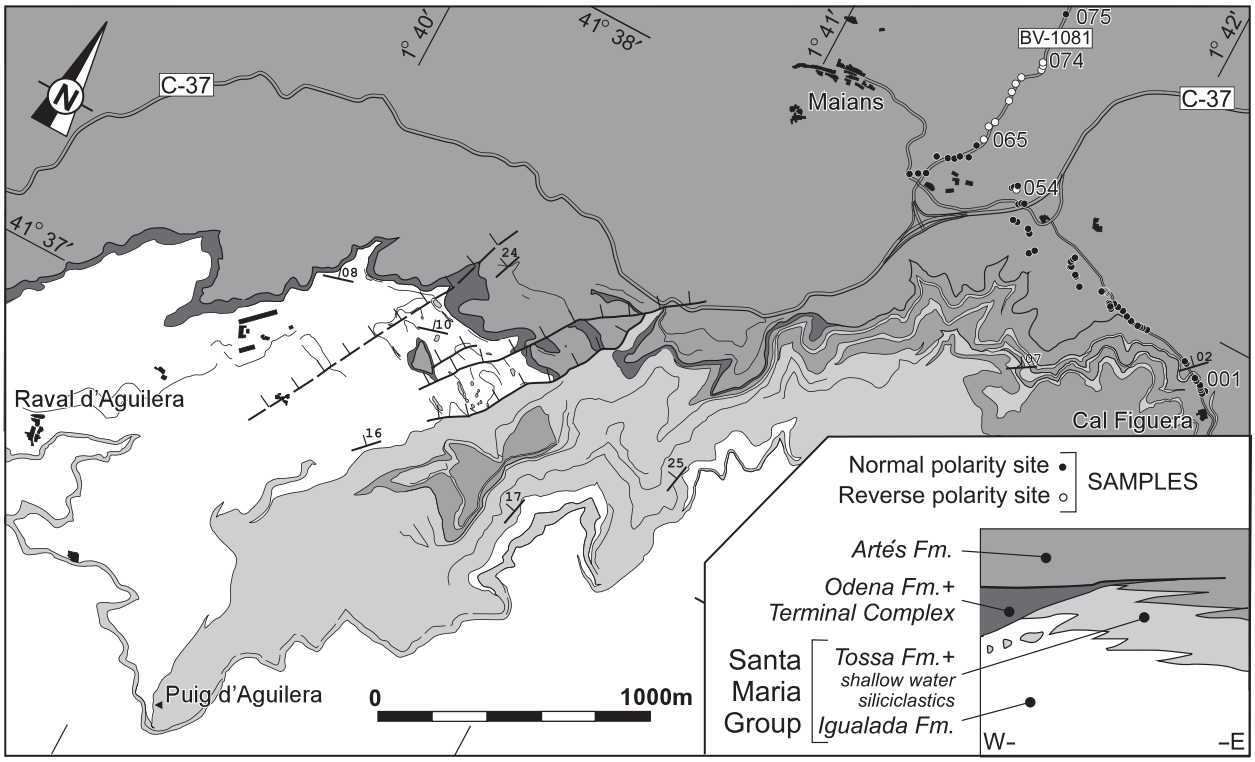

Fig. 2. Detailed geological map with sampled sites and sketched lithostratigraphic panel showing lateral and vertical relationship between the marine and continental facies in the western part of the Igualada area. The black (white) dots correspond to normal (reversed) palaeomagnetic sites of the lowermost Maians section (see Supporting Fig. S1 and S2 for a full location of all sampled sites).

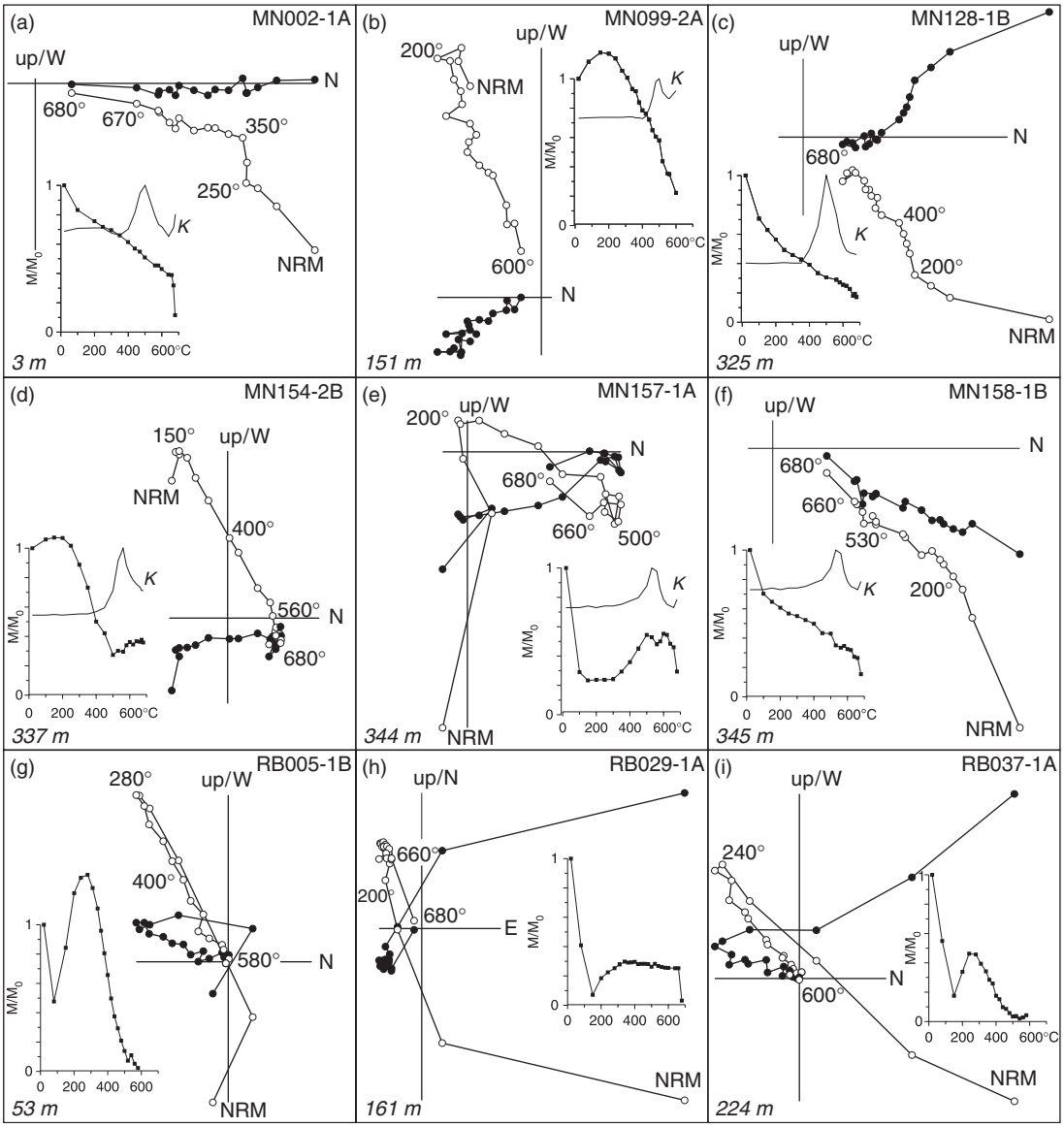

Fig. 3. Zijderveld demagnetization diagrams of representative samples from the Maians–Rubió section. NRM decay plots (squared curve) and magnetic susceptibility (*K*). The stratigraphic position of each sample is shown in metres (lower left). (a–c and f) samples from the Maians section displaying normal and reversed polarities. (d and e) Samples from the top of the Maians section carrying a high-temperature normal polarity magnetization and a reversed-polarity intermediate component. (g–i) Samples from the Rubió section yielding normal and reversed polarities.

cracks. In addition, partial overlap of a reversed-polarity secondary magnetization as seen in Maians (Fig. 3d and e) cannot be excluded as a source of directional dispersion. Nevertheless, the normal and reversed polarity sets yield antipodal Fisherian means (Fig. 4) that conform with the expected palaeomagnetic declination for the Eocene (Taberner *et al*., 1999). However, the inclination values obtained at the Maians and Rubió sections are about 10° shallower than those reported by Taberner *et al*. (1999), which could obey the presence of different magnetic carriers. In the continental red beds of the Maians and Rubió sections, the dominant magnetic carrier is haematite, which may yield higher inclination flattening than the magnetite and/or maghaemite present in the marine marly deposits of the Igualada Formation (Taberner *et al*., 1999). We applied the elongation/inclination method (Tauxe & Kent, 2004; Tauxe, 2009) to the samples of the Maians and Rubió sections in order to unflatten the systematic inclination error. The corrected inclination obtained is 56.2° with a 95% confidence interval ranging from 48.4° to 64.2° (Fig. S3), which agrees with the palaeolatitude of the Iberian plate predicted by plate kinematic reconstructions (Rosenbaum *et al*., 2002).

A local magnetic stratigraphy of the Maians and Rubió sections has been produced after computing the latitude of the virtual geomagnetic poles (VGP). Normal and reversed magnetozones were defined by at least two adjacent palaeomagnetic sites of the same polarity. One site rever-

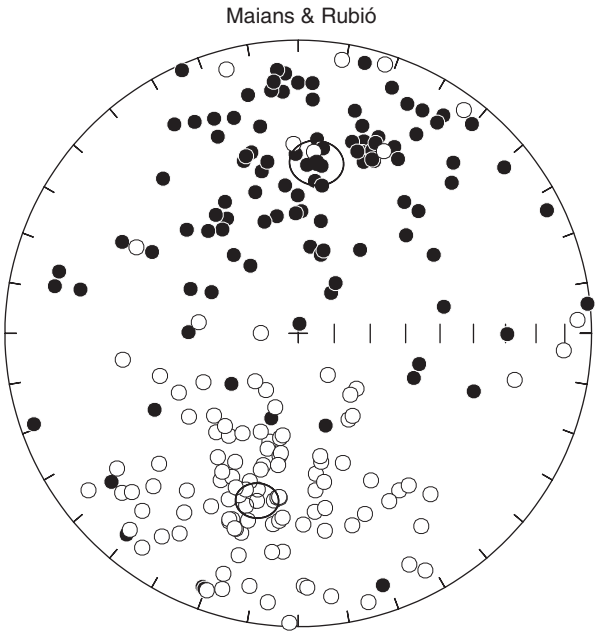

Polarity	N	Dec	Inc	k	α95
Normal	108	006.2	41.1	4.4	7.3
Reverse	113	193.8	–40.9	6.9	5.5

Fig. 4. Stereonet projection of the ChRM directions of the Maians and Rubió sections with calculated Fisherian statistics.

sals were denoted as half bar magnetozone in the local magnetostratigraphic logs, but were not considered for magnetostratigraphic correlation purposes. After an exclusion of unreliable short magnetic reversals, a total of five and two magnetozones have been recognized in the Maians and Rubió sections, respectively (Fig. 5). A straightforward physical correlation between the Maians and Rubió sections is feasible because the conglomerate strata at the top of the Maians section constitute a competent continuous horizon of regional significance (Fig. S4) that can be traced for tens of kilometres along the central SE margin of the Ebro basin. The resulting Maians–Rubió composite magnetostratigraphy yields a total of 1135 m and consists of six magnetozones (Fig. 5).

CHRONOLOGY OF THE FINAL MARINE REGRESSION IN THE SE MARGIN OF THE EBRO BASIN

The local magnetic stratigraphy of the Maians–Rubió composite section can be correlated with the geomagnetic polarity time scale (GPTS) 2004 (Gradstein *et al.*, 2004) considering the available marine and continental biochronological information (Fig. 6). Earlier biostratigraphic studies focused on the benthic foraminiferal assemblages of

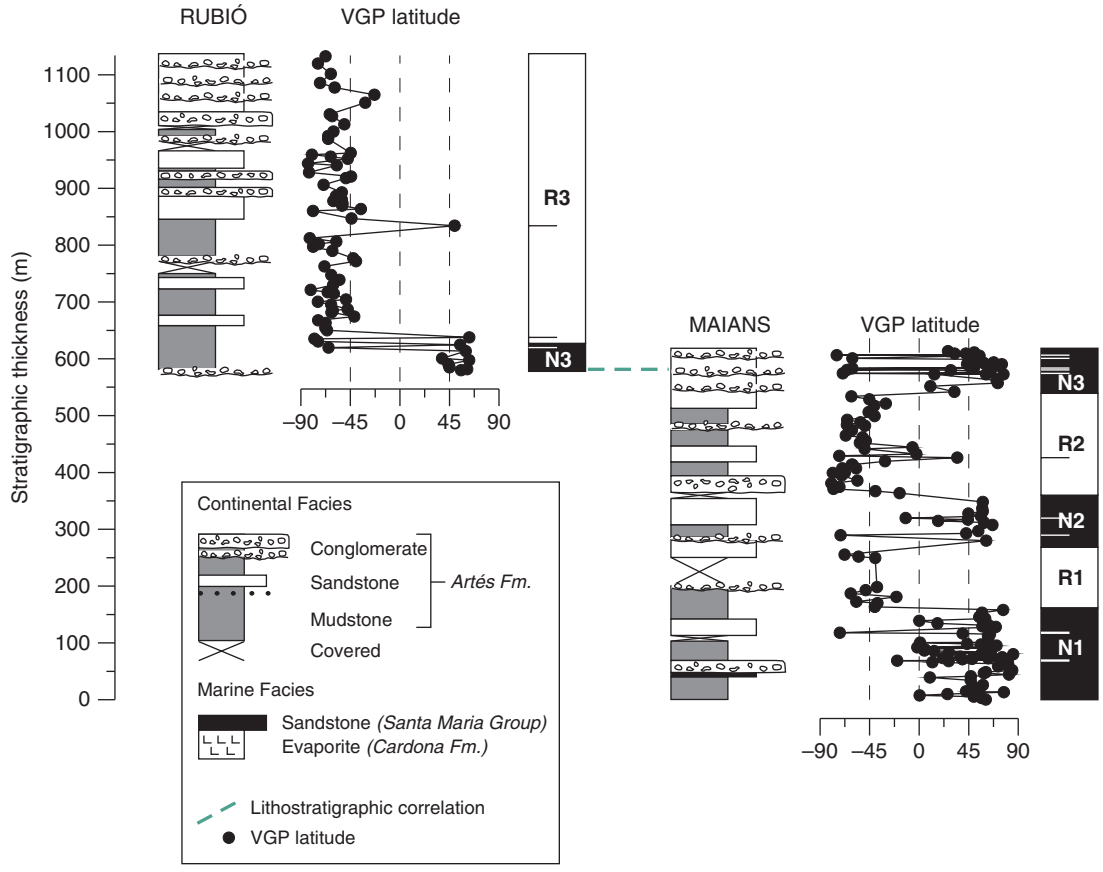

Fig. 5. Local litho- and magnetostratigraphic sections of Maians and Rubió. Stratigraphic correlation between the sections is shown with a dashed line (see text and Supporting Fig. S4 for further details on correlation). Stable magnetozones were defined by at least two adjacent palaeomagnetic sites of the same polarity. Half bar magnetozones denote one site reversals.

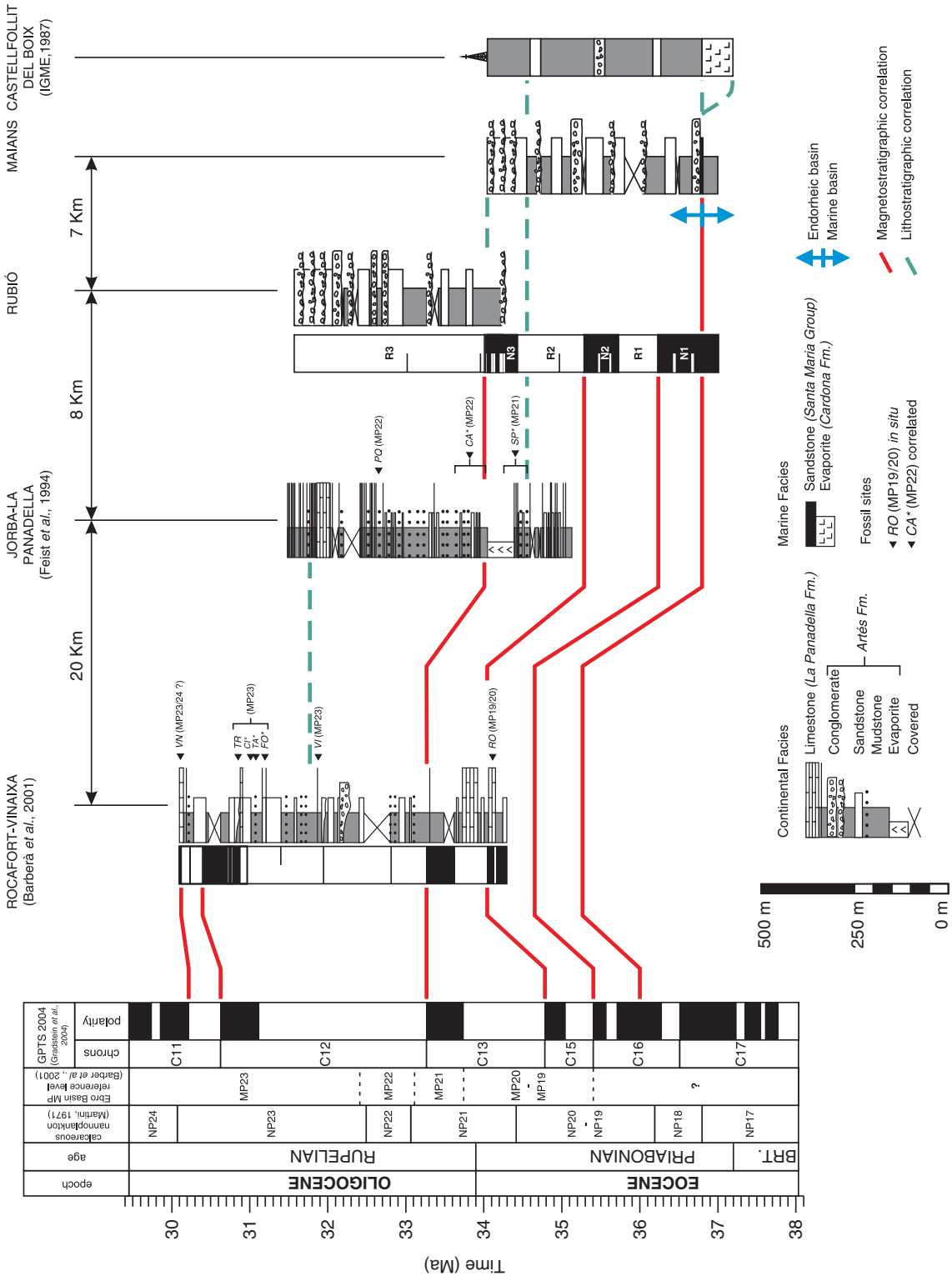

Fig. 6. Correlation of the local magnetostratigraphic section of Maians–Rubió to the GPTS (Gradstein *et al.*, 2004) with indication of the vertebrate localities and their corresponding MP reference level (Arbiol & Sáez, 1988; Anadón *et al.*, 1992; Barberà *et al.*, 2001). RO, Rocafort de Queralt. SP, Santpedor. CA, Calaf. PQ, Porquerisses. VI, Vimbodí. FO, Forés. TA, Tàrrega. CI, Ciutadilla. TR, Tàrrés. VN, Vinaixa. Asterisk indicates mammal fossil site correlated to the magnetostratigraphic section. The Rocafort–Vinaixa log is a composite section from the Rocafort, Sarral, Solivella, Tàrrés and Vinaixa magnetostratigraphic sections of Barberà *et al.* (2001) Hydrocarbon borehole of Castellfollit del Boix from IGME (1987). The Jorba–La Panadella lithostratigraphic section of Feist *et al.* (1994) correlates the Maians–Rubió composite section with the Rocafort–Vinaixa composite section of Barberà *et al.* (2001).

the marine sediments in the Igualada and Vic areas, reported a late Bartonian to lower Priabonian age for the 'Terminal Complex' underlying the Òdena Gypsum Formation (Serra-Kiel *et al.*, 2003b). More recently, a study based on calcareous nannoplankton (Cascella & Dinarès-Turell, 2009) further refined this chronology by providing evidence of a Priabonian age (NP19 zone) for the top marine sedimentation in the Vic area (site 3 in Fig. 1).

Biochronological constraints for the continental sedimentary units overlying the Cardona Formation are limited to a few mammal fossil sites. The oldest known vertebrate fossil assemblage in the Vic area is the locality of Sant Cugat de Gavadons, which indicates a late Eocene age (Mammal Palaeogene MP19-20 reference level) for the basal part of the red bed sequence (Anadón *et al.*, 1987, 1992). More relevant for our proposed correlation is the existence of early Oligocene (MP21) fauna at Santpedor (Sáez, 1987; Arbiol & Sáez, 1988; Anadón *et al.*, 1992). The Santpedor locality (site 4 in Fig. 1) is overlying the same competent sandstone and conglomerate unit used as the regional reference level to correlate the Maians and Rubió sections (Fig. S4). This unit can be traced to the SE to the basal levels of the Jorba–La Panadella stratigraphic section (Feist *et al.*, 1994; see Fig. 6 for correlation and site 5 in Fig. 1 for location). On top of the Jorba–La Panadella section, the La Panadella limestone Formation can be traced to the composite Rocafort–Vinaixa magnetostratigraphic section of Barberà *et al.* (2001) which, as part of a complete Oligocene magnetochronology, have yielded a robust correlation with the GPTS.

The resulting magnetostratigraphic correlation between the Maians–Rubió and the Rocafort–Vinaixa composite sections is supported by the mammal biochronological information from the same sections. Of particular relevance is the Rocafort de Queralt mammal site (RO in Fig. 6). This locality, interpreted as Priabonian based on its attribution to the MP 19-20 Mammal Paleogene level (Agustí *et al.*, 1987; Anadón *et al.*, 1987, 1992), underlies the approximate position of the levels of Santpedor (MP21), of an assumed Oligocene age (Sáez, 1987; Arbiol & Sáez, 1988; Anadón *et al.*, 1992).

Following the constraints described above, a good fit of the Maians–Rubió composite section with the GPTS (Gradstein *et al.*, 2004) results from anchoring the reversed magnetozone R3 with the chron C12r, and correlating normal magnetozones N1, N2 and N3 with chrons C16n, C15n and C13n, respectively. We reject the alternate correlation of the normal magnetozones N1, N2 and N3 with chrons C16n.2n, C16n.1n and C15n respectively; first, on the basis of the established physical correlation between the Maians–Rubió and the Rocafort–Vinaixa composite sections; and second, on the Oligocene age of a number of mammal sites found to correlate with the Rubió section (Fig. 6).

In our preferred correlation, we do not convincingly identify the chron C16n.1r. It is possible that chron C16n.1r could be represented by one of the short reversed polarity events, or by the distinct interval of low VGP latitudes within the magnetozone N1 (Fig. 5). Alternatively, it is also plausible that a short hiatus exists in relation with the shift from marine to continental sedimentation, which also occurs within the magnetozone N1.

As a conclusion of this magnetostratigraphic study, a reliable chronostratigraphy of the late Eocene to early Oligocene has been established for the SE margin of the Ebro foreland basin, based upon faunal marine and continental constraints and the distinctive pattern of local magnetozones. These results indicate that the final marine–continental transition in the eastern Ebro basin (found in magnetozone N1) correlates with the chron C16n, yielding an interpolated age of ~36.0 Ma (Priabonian).

DISCUSSION

The magnetostratigraphic results of the Maians–Rubió composite section are concordant with the nannoplankton data of Cascella & Dinarès-Turell (2009) and support a Priabonian age for the youngest marine sediments in the eastern Ebro basin, as were first indicated by the pioneering study of planktonic foraminifera of Ferrer (1971). Our correlation of the Maians–Rubió local magnetic stratigraphy with the GPTS (Gradstein *et al.*, 2004) allows dating the marine–continental transition in the eastern Ebro basin at ~36.0 Ma. This age is significantly older than the 35.1 ± 0.4 to 33.8 ± 0.2 Ma previously assigned to the Cardona Formation on the basis of $^{87}Sr/^{86}Sr$ ratios in anhydrite samples (Taberner *et al.*, 1999). Note, however, that $^{87}Sr/^{86}Sr$ ratios are only relevant for chronological purposes if they are in equilibrium with the global ocean signature. The environment during the deposition of the Cardona Formation likely corresponded to a highly restricted water mass, with isotopic ratios largely influenced by incoming continental waters (Ayora *et al.*, 1994; Cendón *et al.*, 2003). Therefore, continental isotopic signatures in the latest marine sediments of the Ebro basin could explain the observed discrepancy between the derived $^{87}Sr/^{86}Sr$ ages and the magnetostratigraphy-based chronology proposed here.

The results presented in this study call for a reinterpretation of earlier magnetostratigraphic studies spanning the middle to late Eocene sequences of the eastern Ebro basin in Vic (Burbank *et al.*, 1992; Taberner *et al.*, 1999) and Oliana (Vergés & Burbank, 1996; site 7 in Fig. 1). All these studies based their correlations on the presumed Bartonian age of the shallow benthic foraminiferal assemblages of the top marine units (Serra-Kiel *et al.*, 1998). However, assuming the age of ~36.0 Ma for the marine–continental transition in the eastern Ebro basin, a convincing alternate correlation of the Vic and Oliana sections can be put forward (Figs. S5 and S6). Correlating the normal magnetozone across the marine–continental transition with chron C16n.2n yields a better fit with the GPTS (Gradstein *et al.*, 2004) and smooth the sediment accumulation rates matching the long-term trends observed in other records (Fig. 8).

Of relevance for the palaeogeographic and tectonostratigraphic setting of the marine–continental transition in the South Pyrenean foreland basin is the correlation of the eastern Ebro basin record (described above) with the central and western regions (Jaca–Pamplona basin) of the foreland system. In this regard, it must be noticed that in the Jaca-Pamplona basin, the marine–continental transition is markedly diachronous. In this E–W elongated trough, a progressive westward retreat of marine environments is observed as the basin evolved from an underfilled to an overfilled stage. As a result, in the eastern sector of this trough the marine–continental transition occurred in the Late Lutetian, at about 41.5 Ma based on magnetostratigraphy (Bentham *et al.*, 1992), while in the western sector, the Navarrese Potash sequence is overlain by littoral-sandy facies yielding pollen (Ortí *et al.*, 1986) and scarce benthic foraminifera of a probable Priabonian age (Payros *et al.*, 2000). What is remarkable here is that this stepwise filling of the basin culminated with a far-reaching progradational pulse, likely representing a forced regression caused by a high-amplitude base level drop. The magnetostratigraphic records that best cover the final marine–continental transition in the Jaca–Pamplona piggy-back basin are the Arguis and Salinas sections (sites 8 and 9 in Fig. 1) of Hogan & Burbank (1996), where the prograding deltaic system of the Belsué–Atarés Formation is overlain by the continental red beds of the Campodarbe Formation. In their study, Hogan & Burbank (1996) concluded that the sedimentation of the Campodarbe Formation started in the Bartonian (chron C17n). However, a more feasible correlation with the GPTS can be put forward (Fig. 7) when considering that a number of magnetozones in the Arguis section are supported by only one site. Note that these short magnetozones (marked as a half bar magnetozone in Fig. 7) were not detected in the Salinas section, despite having a higher sampling resolution and yielding better quality directional data (Hogan & Burbank, 1996). Given such discordant results, it is likely that one site normal magnetozones represent recent overprints. Discarding unreliable magnetozones from the Arguis and Salinas sections allows a better match of the resulting composite magnetostratigraphy with the GPTS (Gradstein *et al.*, 2004), which yields a correlation of the Belsué–Atarés sandstone with chron C16n. This, in turn, gives an age of ~36.0 Ma for the marine to continental transition in the Jaca–Pamplona basin, which is consistent with biostratigraphic data from its western sector (Ortí *et al.*, 1986; Payros *et al.*, 2000). The proposed correlation allows identifying

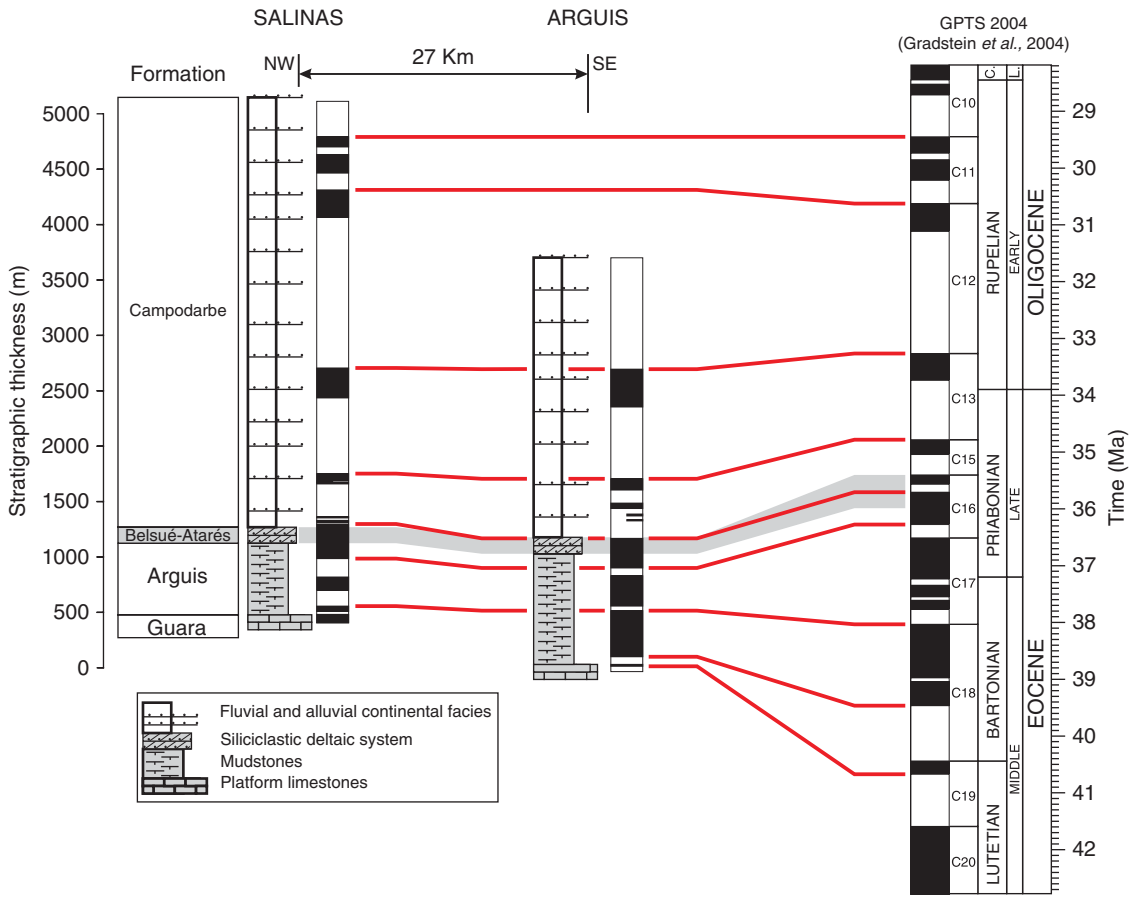

Fig. 7. Magnetostratigraphy of the Arguis and Salinas sections in the Jaca–Pamplona basin (Hogan & Burbank, 1996) with the GPTS (Gradstein *et al.*, 2004) after reinterpretation in this study (see Discussion for details). The reinterpreted correlation of the Belsué–Atarés sandstone with chron C16n yields an age of ~36.0 Ma for the marine–continental transition in the Jaca–Pamplona basin.

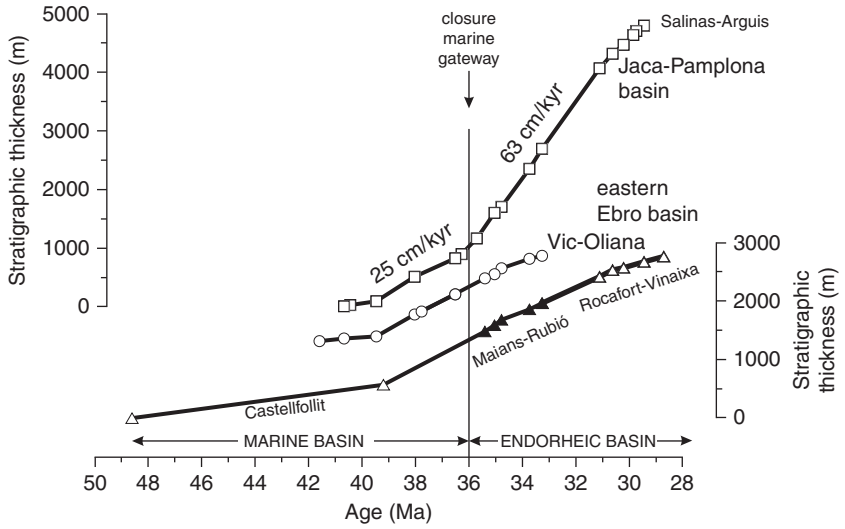

Fig. 8. Trends of sedimentation rates in the western (Jaca–Pamplona basin) and eastern South Pyrenean foreland basin across the marine–continental transition. Data from Salinas and Arguis sections as derived from the reinterpretation of magnetostratigraphic work of Hogan & Burbank (1996) (see Fig. 7). Data from the Vic and Oliana sections after the reinterpretation of Burbank *et al.* (1992), Taberner *et al.* (1999) and Vergés & Burbank (1996) magnetostratigraphic correlations (Supporting Figs. S5 and S6). Solid triangles correspond to the Maians–Rubió magnetostratigraphic section, and open triangles to data from Castellfollit del Boix hydrocarbon borehole (IGME, 1987) and the Rocafort–Vinaixa magnetostratigraphic sections of Barberà *et al.* (2001). A very important increase of sedimentation rates occurs in the western sector at the time of transition from an open to a closed basin, while no changes are observed in the eastern regions.

a sudden, two-fold increase of sedimentation rates that occurs at the time of the marine–continental transition (Fig. 8).

The above results led us to the conclusion that a marine–continental transition is recorded at ~36.0 Ma in both the western and eastern regions of the South Pyrenean foreland basin. No diachrony is detected within the resolution limits of magnetostratigraphy, thus supporting a scenario of rapid overall regression following disconnection from the open ocean. Basin closure resulted from the progressive tectonic uplift of the western Pyrenees from the Middle Eocene (Riba *et al.*, 1983; Puigdefàbregas *et al.*, 1992). Facies and thickness distribution of the top marine Liedena Sandstones unit (Payros *et al.*, 2000) evidences the tectonic uplift of the basinal domain during the Late Eocene, resulting from the southward translation of the Jaca–Pamplona basin on top of the South Pyrenean basal thrust (Payros *et al.*, 2000; Larrasoaña *et al.*, 2003). The tectonic uplift probably concurred with a mid-amplitude eustatic fall (Miller *et al.*, 2005) peaking at 36.2 Ma (i.e. cycles TA4.3-4.4, Haq *et al.*, 1987), to eventually cause the disconnection of the basin from the open ocean.

Basin closure was followed by a drop of base level to desiccation and the simultaneous precipitation of evaporites and salts in two separated depocentres in the west (Navarresse sub-basin) and east (Catalan sub-basin). The possibility of a short sedimentary hiatus associated to the drop of base level is uncertain, but could explain the lack of record of chron C16n.1r in all the magnetostratigraphic sections discussed here. However, if present, this hiatus must be of very short duration (< 200 kyr), suggesting a scenario of a shallow marine basin that after desiccation rapidly recovered its base level. The shift from marine to continental sedimentation did not equate with the overfilling stage in the sense of Sinclair (1997), because it was preceded by the disconnection from the reference sea level.

The evolution of the South Pyrenean foreland basin after closure was characterized by continuous aggradation of clastic sediments, giving rise to a progressive backfilling and burial of the orogenic front (Coney *et al.*, 1996; Lawton *et al.*, 1999). The increased sedimentation rates in the Jaca-Pamplona basin during the Oligocene (Fig. 8) might be tentatively linked with the accelerated exhumation of the Central Pyrenean Axial Zone from 35.0 to 32.0 Ma (Fitzgerald *et al.*, 1999; Sinclair *et al.*, 2005). However, an interpretation of the rise in accumulation rates as a function of increased sediment flux from the rejuvenated orogen is not supported by the chronological data, because the change in the accumulation rates at 36.0 Ma preceded the phase of rapid exhumation of the source area. On the contrary, the synchronicity with the shift from an open to a closed basin led us to envisage an alternate scenario where the sudden, two-fold increase of sediment accumulation resulted from the interruption of sediment bypass towards the oceanic basin. Sediment ponding in the South Pyrenean foreland basin since 36.0 Ma may have further contributed to a change in the redistribution of crustal loads, changing the taper angle of the orogenic wedge and thus potentially perturbing the system (Davis *et al.*, 1983). Sediment aggradation and burial of the frontal thrust favoured the stabilization of the outer orogenic wedge simultaneously to a growth of the inner orogenic wedge, through break-back thrusting and underplating (Puigdefàbregas *et al.*, 1992; Vergés & Burbank, 1996; Sinclair *et al.*, 2005). It

results that the progressive filling of the Ebro basin could have forced deformation to migrate hindward toward the interior of the orogen (Beaumont *et al.*, 2000), a plausible picture coherent with the foreland basin chronostratigraphy and the exhumation history derived from thermochronology.

It is shown that while in the western South Pyrenean foreland basin, the sedimentation rates are linked to basin-scale changes in base level; in the eastern Ebro basin, the sedimentation trends do not show appreciable changes across the marine–continental transition (Fig. 8). We interpret that connectivity between the eastern Ebro basin and the rest of the South Pyrenean foreland was limited to the water column, while sediments accumulated in their respective foredeep zones. It must be noted that by the late Eocene times, the restricted palaeogeographic configuration of the eastern Ebro basin was probably accentuated by the rising of the South Pyrenean Central Units, enhancing sediment trapping. Because sediment bypassing was not a relevant term of the equation, closure of the marine gateway had little influence on the sedimentation trends in the eastern Ebro basin.

CONCLUSIONS

Integration of magnetostratigraphic data from opposite margins in the South Pyrenean foreland basin indicates that the transition from marine to continental sedimentation was a rapid, likely isochronous, event occurring at ~36.0 Ma (late Priabonian). This result contrasts with the time-transgressive nature of lithostratigraphic units in foreland systems, but is coherent with a scenario of basin continentalization that resulted from seaway closure driven by the tectonic uplift of its margins. Coinciding with the marine to continental transition, the South Pyrenean foreland basin experienced a sudden increase in sedimentation rates, from 25 cm kyr^{-1} during marine deposition to 63 cm kyr^{-1} during continental deposition. We interpret this change as a consequence of the interruption of sediment bypass towards the oceanic domain after seaway closure. During this process, the Jaca–Pamplona trough evolved from an efficient sediment transfer zone to a sediment trap for all the erosion products of the Central Pyrenean Axial Zone. In the eastern Ebro basin, the change from open to closed basin drainage did not have significant effects on sedimentation rates due to the already restricted palaeogeographic configuration and its limited connectivity with the open ocean.

Results from the South Pyrenean foreland basin illustrate the extent to which restricted palaeogeographic configurations, such as those often found in the circum-Mediterranean Alpine belt, can influence the rates of sediment bypass towards the marginal ocean basins. The sediment involved represents a relevant term in the crustal-scale orogenic mass balance, feasibly contributing to the geodynamic evolution of the overall fold-and-thrust belt.

ACKNOWLEDGEMENTS

This paper has been developed in the framework of the MCI projects: CENOCRON CGL2004-00780 and REMOSS 3D-4D CGL2007-66431-C02-02/BTE. This research was supported by the Research Group of 'Geodinàmica i Anàlisi de Conques' (2009 GGR 1198 - Comissionat d'Universitats i Recerca de la Generalitat de Catalunya) and 'Centre Mixt d'Investigació GEOMODELS (UB-UPC-IGME). The authors wish to thank Dr. Cor Langereis from the Paleomagnetic Laboratory 'Fort Hoofddijk' (Utrecht Universiteit) and Dr. Lisa Tauxe from the Paleomagnetic Laboratory at Scripps Institution of Oceanography (University of California San Diego). The comments and suggestions of Guillaume Dupont-Nivet, Andrew Meigs and an Anonymous Reviewer have considerably improved the paper content and presentation. E.C. was founded by a PhD grant of MCI.

SUPPORTING INFORMATION

Additional Supporting Information may be found in the online version of this article:

Fig. S1. Location of palaeomagnetic sites along the Maians section. Normal (reverse) polarity of the palaeomagnetic sites are indicated by a solid (open) circles. The Castellfollit del Boix hydrocarbone borehole is located 0.5 km north from the top of the Maians section. The conglomerate strata used to correlate Maians with Rubió sections (Fig. S4) is also shown.

Fig. S2. Location of palaeomagnetic sites along the Rubió section. Normal (reverse) polarity of the palaeomagnetic sites are indicated by a solid (open) circles. The conglomerate strata used to correlate Maians with Rubió sections is also shown (Fig. S4).

Fig. S3. a) Equal area plots of the unflattened directions of the Maians-Rubió composite section. Red circles (white squares) indicates northern (southern) directions. Fisher statistics are listed in the table below. **b)** Elongation vs. inclination as a function of increasing unflattening (*f*). Green line is elongation vs. inclination trend from the model TK03.GDA (Tauxe *et al.*, 2008). Red line is evolution of directional data from a) when unflattened with ranging from 1 (no correction) to 0.6. Yellow lines show behaviour of 25 representative bootstrap samples. When the yellow curve crosses the green line, the elongation vs. inclination pair is consistent with the TK03 paleosecular variation model and the inclination is taken as the "correct inclination". **c)** Cummulative distribution of corrected inclinations from 5000 bootstrapped samples. Dashed blue lines are the confidence bounds containing the central 95% of the "corrected inclinations" from 5000 curves like those yellow shown in b). The crossing of the original data (red line in b)) is shown as the solid line. (PmagPy software package kindly provided by Dr. Lisa Tauxe can be found at: http://magician.ucsd.edu/ ~ltauxe)

Fig. S4. Correlation of Maians and Rubió sections. The conglomerate strata used to correlate the Maians (Fig. S1) and Rubió (Fig. S2) sections constitute a regional reference level that can be traced tens of kilometres along the central SE margin of the Ebro basin. This competent layer is well depicted in the topography by a change of gradient from the steep slopes of the "Solella de Can Vila" to the flattened area surrounding the Castellfollit del Boix village. Moreover, these conglomerate strata can be physically traced on the field into the Rubió section, resulting in a composite stratigraphy (Fig. 5). The distance between sections is 7 km.

Fig. S5. Magnetostratigraphy of the Vic section after Burbank *et al*. (1992) and alternate correlation assumed an age of the marine-continental transition in the eastern Ebro Basin at 36.0 Ma (this paper).

Fig. S6. Magnetostratigraphy of the Oliana section (eastern Ebro Basin) after Vergés & Burbank (1996) and alternate correlation assumed an age of the marine-continental transition in the eastern Ebro Basin at 36.0 Ma (this study).

Table S1. ChRM directions of the Maians and Rubió magnetostratigraphic sections. Site No., name and number of paleomagnetic site; Strat. level, stratigraphic position of the paleomagnetic site in the Mains-Rubió composite section; Dec. and Inc., declination and inclination in geographic (in situ) and stratigraphic coordinates (after bedding correction); Dip. Az. and Dip., azimuth of down dip direction of local bedding and angle of dip of local bedding; VGP Lat., latitude of the Virtual Geomagnetic Pole used to build the local magnetostratigraphy of Mains and Rubió sections (see Fig. 5).

Please note: Wiley-Blackwell are not responsible for the content or functionality of any supporting materials supplied by the authors. Any queries (other than missing material) should be directed to the corresponding author for the article.

REFERENCES

Agustí, J., Anadón, P., Arbiol, S., Cabrera, L., Colombo, F. & Sáez, A. (1987) Biostratigraphical characteristics of the Oligocene sequences of North-Eastern Spain (Ebro and Campins Basins). *Münchner Geowissenschaftliche Abhandlungen*, **10**, 35–42.

Anadón, P., Cabrera, L., Choi, S.J., Colombo, F., Feist, M. & Sáez, A. (1992) Biozonación del Paleógeno continental de la zona oriental de la Cuenca del Ebro mediante carófitas: implicaciones en la biozonación general de carófitas de Europa occidental. *Acta Geol Hispan*, **27**, 69–94.

Anadón, P., Cabrera, L., Colldeforns, B. & Sáez, A. (1989) Los sistemas lacustres del Eoceno superior y Oligoceno del sector oriental de la Cuenca del Ebro. *Acta Geol Hispan*, **24**, 205–230.

Anadón, P., Cabrera, L., Guimerà, J. & Santanach, P. (1985) Paleogene strike-slip deformation and sedimentation along the southeastern margin of the Ebro Basin. In: *Strike-Slip Tectonics and Sedimentation* (Ed. by K.T. Biddle & N. Christie-Blick), *Spec. Publ. Soc. Econ. Paleont. and Min.*, **37**, 303–318.

Anadón, P., Vianey-Liaud, M., Cabrera, L. & Hartenberger, J.L. (1987) Gisements à vertébrés du paléogène de la zone orientale du bassin de l'Ebre et leur apport à la stratigraphie. *Paleontol Evol*, **21**, 117–131.

Arbiol, S. & Sáez, A. (1988) Sobre la edad oligocénica inferior del yacimiento de Santpedor (Cuenca del Ebro, provincia de Barcelona). *Acta Geol Hispan*, **23**, 47–50.

Arenas, C. & Pardo, G. (1999) Latest Oligocene-Late Miocene lacustrine systems of the north central part of the Ebro Basin (Spain): sedimentary facies model and palaeogeographic synthesis. *Palaoegeogra, Palaeoclimatol, Palaeoecol*, **151**, 127–148.

Ayora, C., García-Veigas, J. & Pueyo, J.J. (1994) The chemical and hydrological evolution of an ancient potash-forming evaporite basin as constrained by mineral sequence, fluid inclusion composition, and numerical simulation. *Geochem Cosmochim Acta*, **58**, 3379–3394.

Barberà, X., Cabrera, L., Marzo, M., Parés, J.M. & Agustí, J. (2001) A complete terrestrial Oligocene magnetostratigraphy from the Ebro Basin, Spain. *Earth Planet Sci Lett*, **187**, 1–16.

Beaumont, C. (1981) Foreland basins. *J Roy Astronom Soc*, **65**, 291–329.

Beaumont, C., Muñoz, J.A., Hamilton, J. & Fullsack, P. (2000) Factors controlling the Alpine evolution of Central Pyrenees inferred from the comparison of observations and geodynamical models. *J Geophys Res*, **105**, 8121–8145.

Bentham, P.A., Burbank, D.W. & Puigdefàbregas, C. (1992) Temporal and spatial controls on the alluvial architecture of an axial drainage system: late Eocene Escanilla Formation, southern Pyrenean foreland basin, Spain. *Basin Res*, **4**, 335–352.

Bera, M.K., Sarkar, A., Chakraborty, P.P., Loyal, R.S. & Sanyal, P. (2008) Marine to continental transition in Himalaya foreland. *Geol Soc Am Bull*, **120**, 1214–1232.

Burbank, D.W., Puigdefabregas, C. & Muñoz, J.A. (1992) The chronology of the Eocene tectonic and stratigraphic development of the eastern Pyrenean foreland basin, northeast Spain. *Geol Soc Am Bull*, **104**, 1101–1120.

Cascella, A. & Dinarès-Turell, J. (2009) Integrated calcareous nannofossil biostratigraphy and magnetostratigraphy from the uppermost marine Eocene deposits of the southeastern pyrenean foreland basin: evidences for marine Priabonian deposition. *Geol Acta*, **7**, 281–296.

Cendón, D.I., Ayora, C., Puedo, J.J. & Taberner, C. (2003) The geochemical evolution of the Catalan potash subbasin, South Pyrenean foreland basin (Spain). *Chem Geol*, **200**, 339–357.

Coney, P.J., Muñoz, J.A., Mcclay, K.R. & Evenchick, C.A. (1996) Syntectonic burial and post tectonic exhumation of southern Pyrenees foreland fold-thrust best. *J Geol Soc Lond*, **153**, 9–16.

Davis, D., Suppe, J. & Dahlen, F.A. (1983) Mecanics of fold-and-thrust belts and accretionary wedges. *J Geophys Res*, **88**, 1153–1172.

Decelles, P.G. & Giles, K.A. (1996) Foreland basin systems. *Basin Res*, **8**, 105–123.

Feist, M., Anadón, P., Cabrera, L., Choi, S.J., Colombo, F. & Sáez, A. (1994) Upper Eocene-Lowermost Miocene charophyte succession in the Ebro Basin (Spain). Contribution to the charophyte biozonation in Western Europe. *Newslett Stratigr*, **30**, 1–32.

Ferrer, J. (1971) El Paleoceno y Eoceno del borde suroriental de la Depresión del Ebro (Cataluña). *Memor Suisses Paleontol*, **90**, 1–70.

Fitzgerald, P.G., Muñoz, J.M., Coney, P.J. & Baldwin, S.L. (1999) Asymmetric exhumation across the Pyrenean orogen: implications for the tectonic evolution of a collisional orogen. *Earth Planet Sci Lett*, **173**, 157–170.

Garcia-Castellanos, D., Vergés, J., gaspar-Escribano, J. & Cloetingh, S. (2003) Interplay between tectonics, climate, and fluvial transport during the Cenozoic evolution of the Ebro Basin (NE Iberia). *J Geophys Res*, **108**, 2347–2364.

Gradstein, F.M., Ogg, J. & Smith, A. (2004) *A Geologic Time Scale 2004*. Cambridge University Press, Cambridge.

Guimerà, J. (1984) Paleogene evolution of deformation in the northeastern Iberian Peninsula. *Geol Mag*, **121**, 413–420.

Haq, B.U., Hardenbol, J. & Vail, P.J. (1987) Chronology of fluctuating sea levels since the Triassic. *Science*, **235**, 1156–1167.

Hogan, P.J. & Burbank, D.W. (1996) Evolution of the Jaca piggyback basin and emergence of the External Sierra, southern Pyrenees. In: *Tertiary Basins of Spain. The Stratigraphic Record of Crustal Kinematics* (Ed. by P.F. Friend & C.J. Dabrio), pp. 153–160. Cambridge University Press, Cambridge.

IGME. (1987) *Contribución de la exploración petrolífera al conocimiento de la geología de España*. Instituto Geológico y Minero de España, Madrid.

Kirschvink, J.L. (1980) The least-squares line and plane and the analysis of palaeomagnetic data. *Geophys J Roy Astronom Soc*, **62**, 699–718.

Larrasoaña, J.C., Parés, J.M., Millán, H., del Valle, J. & Pueyo, E.L. (2003) Paleomagnetic, structural and stratigraphic constraints on transverse fault kinematics during basin inversion: the Pamplona Fault (Pyrenees, N Spain). *Tectonics*, **22**, 1071.

Lawton, T.F., Roca, E. & Guimerà, J. (1999) Kinematic-stratigraphic evolution of growth syncline and its implications for tectonic development of the proximal foreland basin, southeastern Ebro Basin, Catalunya, Spain. *Geol Soc Am Bull*, **111**, 412–431.

López-Blanco, M. (2002) Sedimentary response to thrusting and fold growing on the SE margin of the Ebro basin (Paleogene, NE Spain). *Sediment Geol*, **146**, 133–154.

López-Blanco, M., Marzo, M., Burbank, D.W., Vergés, J., Roca, E., Anadón, P. & Piña, J. (2000) Tectonic and climatic controls on the development of foreland fan deltas: Montserrat and San Llorenç del Munt systems (Middle Eocene, Ebro Basin, NE Spain). *Sediment Geol*, **138**, 17–39.

Meulenkamp, J.E. & Sissingh, W. (2003) Tertiary palaeogeography and tectonostratigraphic evolution of the Northern and Southern Peri-Tethys platforms and the intermediate domains of the African-Eurasian convergent plate boundary zone. *Palaeogeogr, Palaeoclimatol, Palaeoecol*, **196**, 209–228.

Miller, K.G., Kominz, M.A., Browning, J.V., Wright, J.D., Mountain, G.S., Katz, M.E., Sugarman, P.J., Cramer, B.S., Christie-Blick, N. & Pekar, S.F. (2005) The Phanerozoic record of global sea-level change. *Science*, **310**, 1293–1298.

Mugnier, J.L., Baby, P., Colletta, B., Vinour, P., Bale, P. & Leturmy, P. (1997) Thrust geometry controlled by erosion and sedimentation: a view from analogue models. *Geology*, **25**, 427–430.

Muñoz, J.A., Martínez, A. & Vergés, J. (1986) Thrust sequences in the eastern Spanish Pyrenees. *J Struct Geol*, **8**, 399–405.

Ori, G.G. & Friend, P.F. (1984) Sedimentary basins formed and carried piggyback on active thrust sheets. *Geology*, **12**, 475–478.

Ortí, F., Salvany, J.M., Rosell, L., Pueyo, J.J. & Inglés, M. (1986) evaporitas antiguas (Navarra) y actuales (Los Monearos) de la Cuenca del Ebro. In: *Guía de las Excursiones del XI Congreso Español de Sedimentologia* (Ed. by P. Anadón & L. Cabrera), pp. 2.1–2.40. Generalitat de Catalunya, Comissió Interdepartamental de Recerca i Innovació Tecnològica (CIRIT), Barcelona.

Pallí, L. (1972) Estratigrafía del Paleógeno del Empordà y zonas limítrofes. PhD Thesis, Universitat Autònoma de Barcelona.

Payros, A., Astibia, H., Cearreta, A., Pereda-Suberbiola, X., Muelaga, X. & Badiola, A. (2000) The Upper Eocene South Pyrenean coastal deposits (Liedena Sandstone, Navarre): sedimentary facies, benthic foraminifera and avian ichnology. *Facies*, **42**, 19–23.

Plaziat, J.C. (1981) Late Cretaceous to Late Eocene palaeogeographic evolution of southwest Europe. *Palaeogeogr, Palaeoclimatol, Palaeoecol*, **36**, 263–320.

Puigdefàbregas, C., muñoz, J.A. & Vergés, J. (1992) Thrusting and foreland basin evolution in the Southern Pyrenees. In: *Thrust Tectonics* (Ed. by K.R. McClay), pp. 247–254. Chapman & Hall, London.

Riba, O., Reguant, S. & Villena, J. (1983) Ensayo de síntesis estratigráfica y evolutiva de la cuenca terciaria del Ebro. In: *Geología de España. Libro Jubilar J.M. Ríos*, **vol. II** (Ed. by IGME.), pp. 131–159. Instituto Geológico y Minero de España, Madrid.

Rosell, L. & Pueyo, J.J. (1997) Second marine evaporitic phase in the South Pyrenean foredeep: The Priabonian Potash Basin (Late Eocene: autochthonous-allochthonous zone). In: *Sedimentary Deposition in Rift and Foreland Basins in France and Spain. (Paleogene and Lower Neogene)* (Ed. by G. Busson & B.C. Schreiber), pp. 358–387. Columbia University Press, New York.

Rosenbaum, G., Lister, G.S. & Duboz, C. (2002) Relative motions of Africa, Iberia and Europe during Alpine orogeny. *Tectonophysics*, **359**, 117–129.

Sáez, A. (1987) Estratigrafía y sedimentología de las formaciones lacustres del tránsito Eoceno-Oligoceno del noreste de la cuenca del Ebro. PhD thesis, Universitat de Barcelona, Barcelona.

Serra-Kiel, J., Hottinger, L., Caus, E., Drobne, K., Ferràndez, C., Jauhri, A.K., Less, G., Pavlovec, R., Pignatti, J., Samsó, J.M., Schaub, H., Sirel, E., Strougo, A., Tambareau, Y., Tosquella, J. & Zakrevskaya, E. (1998) Larger foraminiferal biostratigraphy of the Tethyan Paleocene and Eocene. *Bull Soc Geol France*, **169**, 281–299.

Serra-Kiel, J., Mató, E., Saula, E., Travé, A., Ferràndez-Cañadell, C., Àlvarez-Pérez, G., Busquets, P., Samsó, J.M., Tosquella, J., Franquès, J., Romero, J. & Barnolas, A. (2003a) An inventory of the marine and transitional middle/upper Eocene deposits of the Southeastern Pyrenean foreland basin (NE Spain). *Geol Acta*, **1**, 201–229.

Serra-Kiel, J., Travé, A., Mató, E., Saula, E., Ferràndez-Cañadell, C., Busquets, P., Tosquella, J. & Vergés, J. (2003b) Marine and transitional Middle/Upper Eocene units of the southeastern Pyrenean foreland basin (NE Spain). *Geol Acta*, **1**, 177–200.

Sinclair, H.D. (1997) Tectonostratigraphic model for underfilled peripheral foreland basins: an Alpine perspective. *Geol Soc Am Bull*, **109**, 324–346.

Sinclair, H.D., Gibson, M., Naylor, M. & Morris, R.G. (2005) Asymmetric growth of the Pyrenees revealed through measurement and modelling of orogènic fluxes. *Am J Sci*, **305**, 369–406.

Stori, F. & Mcclay, K.R. (1995) Influence of syntectonic sedimentation on thrust wedges in analogue models. *Geology*, **23**, 999–1002.

Taberner, C., Dinarès-Turell, J., Giménez, J. & Docherty, C. (1999) Basin infill architecture and evolution from magnetostratigraphic cross-basin correlations in the southeastern Pyrenean foreland basin. *Geol Soc Am Bull*, **111**, 1155–1174.

Tauxe, L. (2009) *Essentials of Paleomagnetism*. University of California Press, La Jolla, CA.

Tauxe, L. & Kent, D.V. (2004) A simplified statistical model for the geomagnetic field and the detection of shallow bias in paleomagnetic inclinations: was the ancient magnetic field dipolar? In: *Timescales of the Paleomagnetic Field* (Ed. by J.E.T. Channell, D.V. Kent, W. Lowrie & J. Meert), pp. 101–116. American Geophysical Union, Washington, DC.

Travé, A. (1992) Sedimentologia, petrologia i geoquímica (elements traça i isòtops) dels estromatòlits de la Conca Eocena Sudpirinenca. PhD Thesis, Universitat de Barcelona.

Vergés, J. & Burbank, D.W. (1996) Eocene–Oligocene thrusting and basin configuration in the eastern and central Pyrenees (Spain). In: *Tertiary Basins of Spain. The Stratigraphic Record of Crustal Kinematics* (Ed. by P.F. Friend & C.J. Dabrio), pp. 120–133. Cambridge University Press, Cambridge.

Vergés, J., Fernàndez, M. & Martínez, A. (2002) The Pyrenean orogen: pre-, syn-, and post-collisional evolution. In: *Reconstruction of the Evolution of the Alpine-Himalayan Orogen* (Ed. by G. Rousenbaum & G.S. Lister), *Journal of the Virtual Explorer*, pp. 55–74.

Zoetemeijer, R., Desegaulx, P., Cloetingh, S., Roure, F. & Moretti, I. (1990) Lithospheric dynamics and tectonic-stratigraphic evolution of the Ebro Basin. *J Geophys Res*, **95**, 2701–2711.

Manuscript received 31 March 2009; Manuscript accepted 1 November 2009.

APPENDIX OF CHAPTER 3.2:

SUPPORTING ELECTRONIC INFORMATION

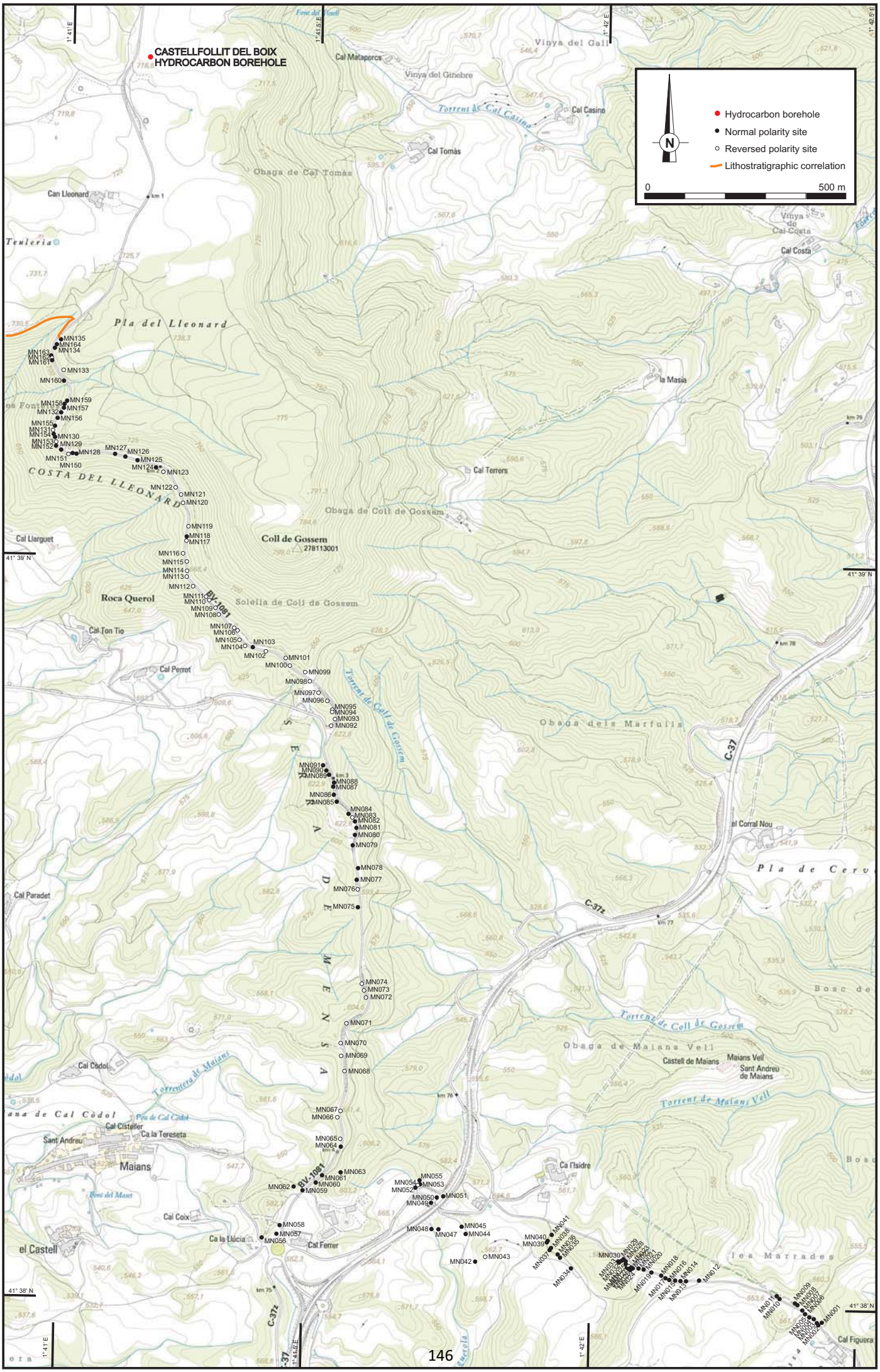

Supporting Fig. 1 Location of palaeomagnetic sites along the Maians section. Normal (reverse) polarity of the palaeomagnetic sites are indicated by a solid (open) circles. The Castellfollit del Boix hydrocarbone borehole is located 0.5 Km north from the top of the Maians section. The conglomerate strata used to correlate Maians with Rubió sections (Supporting Fig. 4) is also shown.

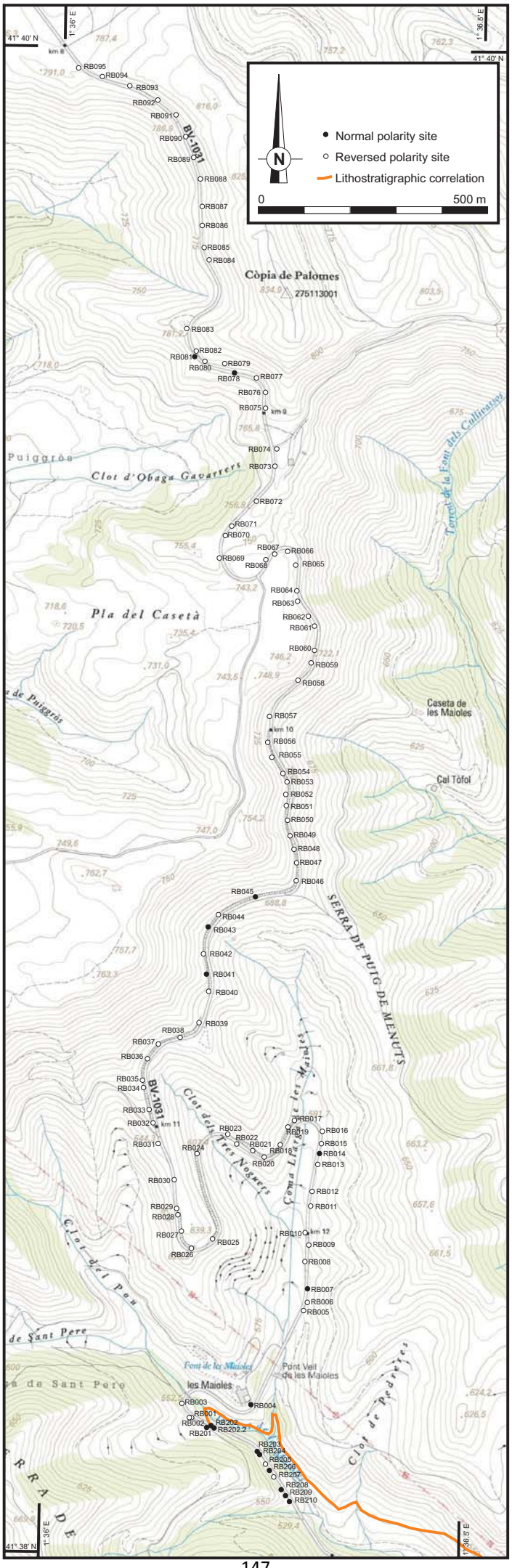

Supporting Fig. 2 Location of palaeomagnetic sites along the Rubió section. Normal (reverse) polarity of the palaeomagnetic sites are indicated by a solid (open) circles. The conglomerate strata used to correlate Maians with Rubió sections is also shown (Supporting Fig. 4).

a)

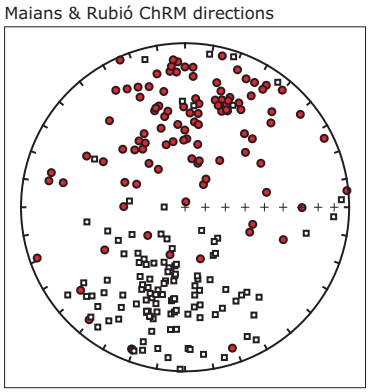

Polarity	N	dec	inc	k	a95
Normal	108	006.2	41.1	4.4	7.3
Reverse	113	193.8	-40.9	6.9	5.5

b)

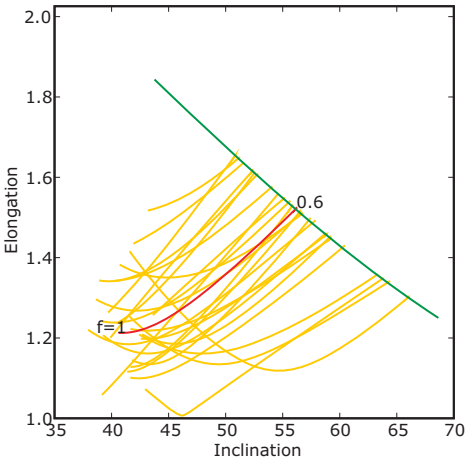

c)

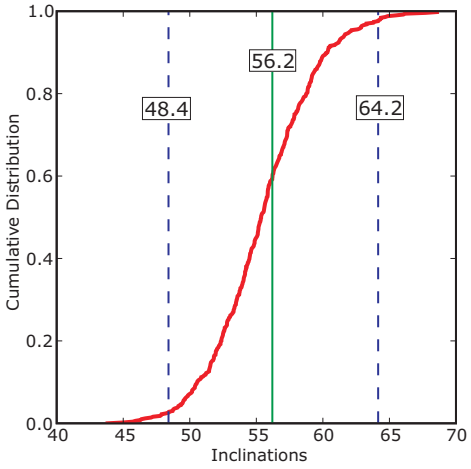

Supporting Fig. 3 a) Equal area plots of the unflattened directions of the Maians-Rubió composite section. Red circles (white squares) indicates northern (southern) directions. Fisher statistics are listed in the table below. **b)** Elongation vs. inclination as a function of increasing unflattening (*f*). Green line is elongation vs. inclination trend from the model TK03.GDA (Tauxe *et al.*, 2008). Red line is evolution of directional data from a) when unflattened with *f* ranging from 1 (no correction) to 0.6. Yellow lines show behaviour of 25 representative bootstrap samples. When the yellow curve crosses the green line, the elongation vs. inclination pair is consistent with the TK03 paleosecular variation model and the inclination is taken as the "correct inclination". **c)** Cummulative distribution of corrected inclinations from 5000 bootstrapped samples. Dashed blue lines are the confidence bounds containing the central 95% of the "corrected inclinations" from 5000 curves like those yellow shown in b). The crossing of the original data (red line in b)) is shown as the solid line.

(PmagPy software package kindly provided by Dr. Lisa Tauxe can be found at: **http://magician.ucsd.edu/~ltauxe/**)

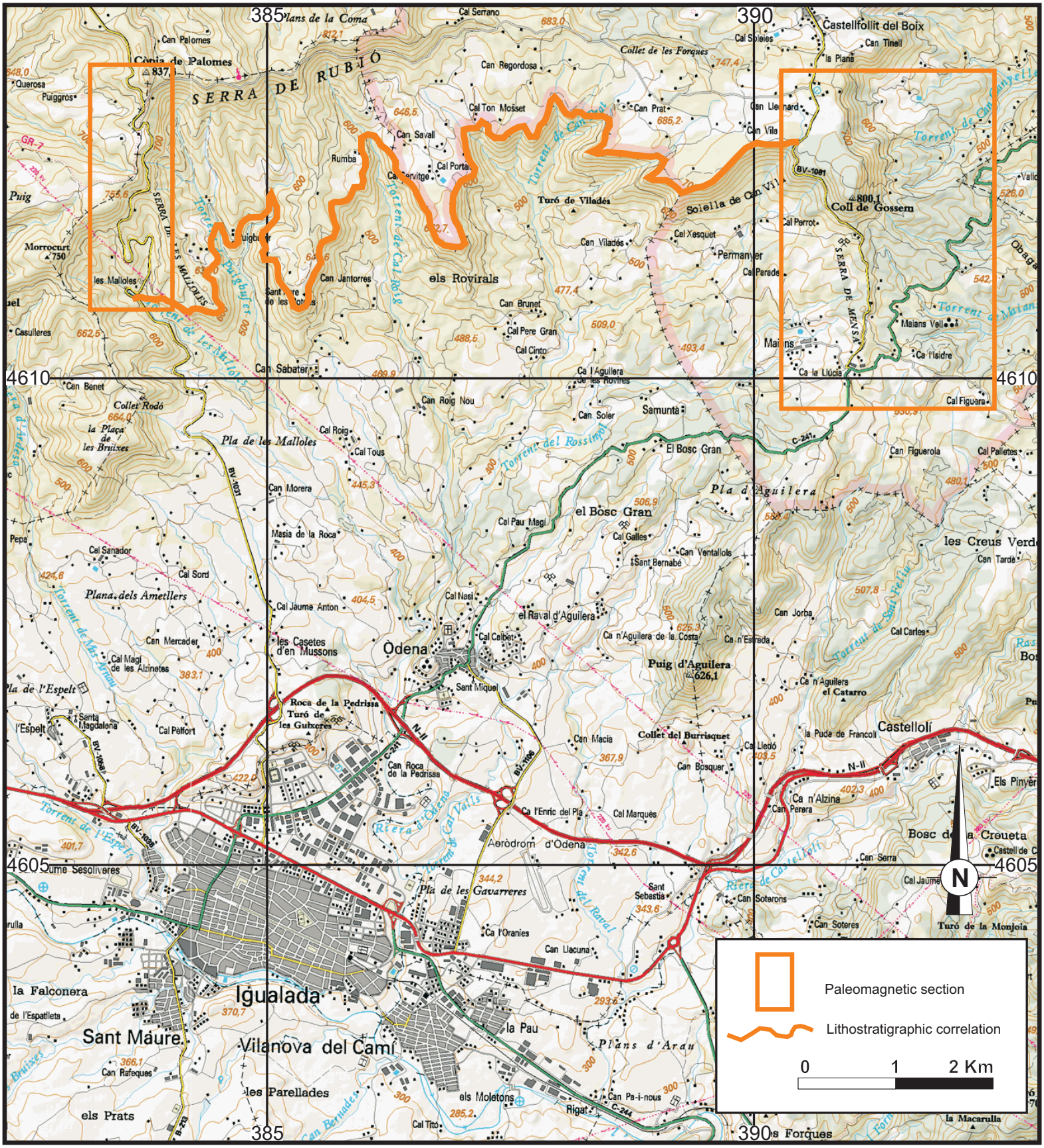

Supporting Fig. 4. Correlation of Maians and Rubió sections. The conglomerate strata used to correlate the Maians (Supporting Fig. 1) and Rubió (Supporting Fig. 2) sections constitute a regional reference level that can be traced tens of kilometres along the central SE margin of the Ebro basin. This competent layer is well depicted in the topography by a change of gradient from the steep slopes of the "Solella de Can Vila" to the flattened area surrounding the Castellfollit del Boix village. Moreover, these conglomerate strata can be physically traced on the field into the Rubió section, resulting in a composite stratigraphy (Fig. 5). The distance between sections is 7 Km.

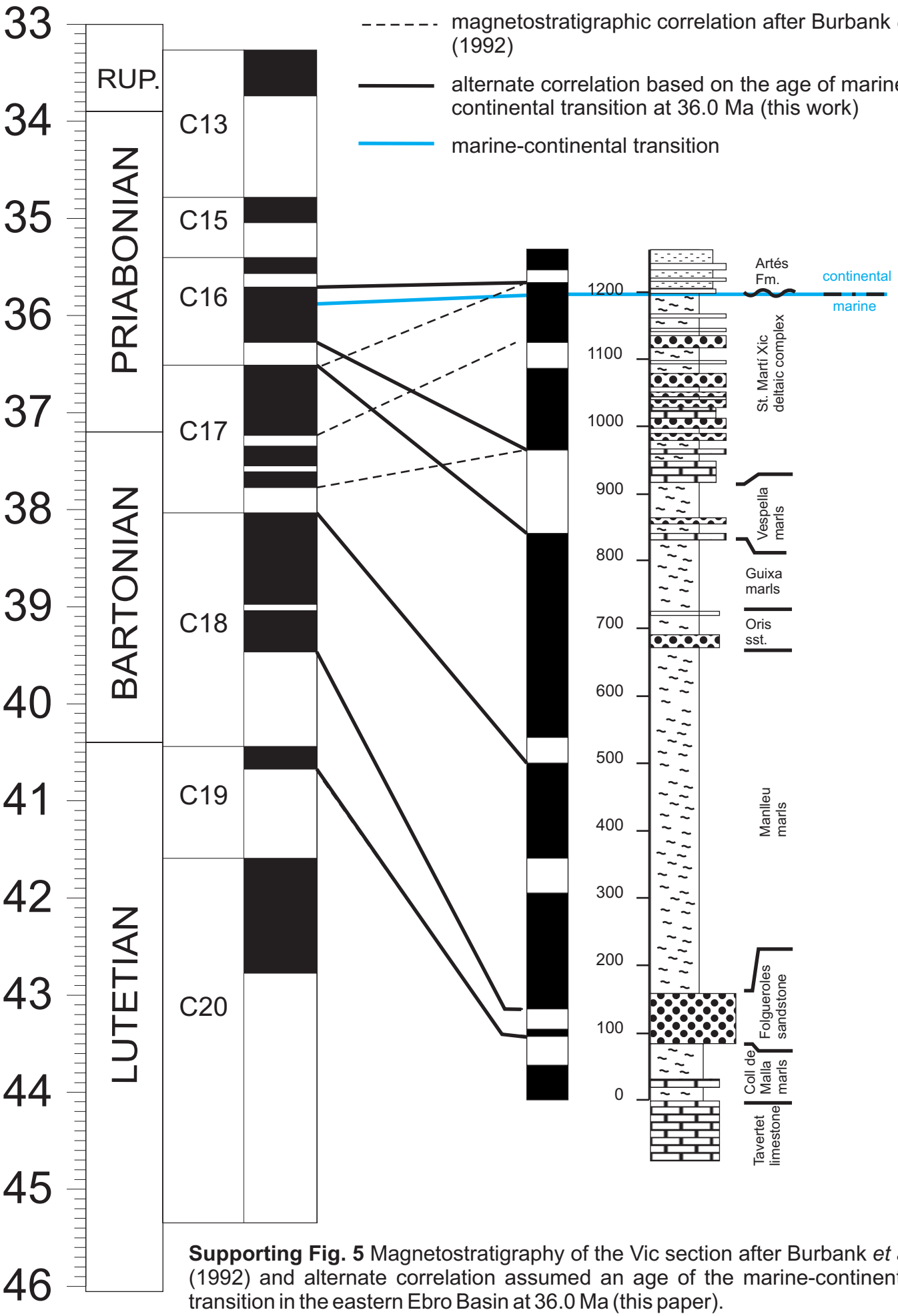

Supporting Fig. 5 Magnetostratigraphy of the Vic section after Burbank *et al.* (1992) and alternate correlation assumed an age of the marine-continental transition in the eastern Ebro Basin at 36.0 Ma (this paper).

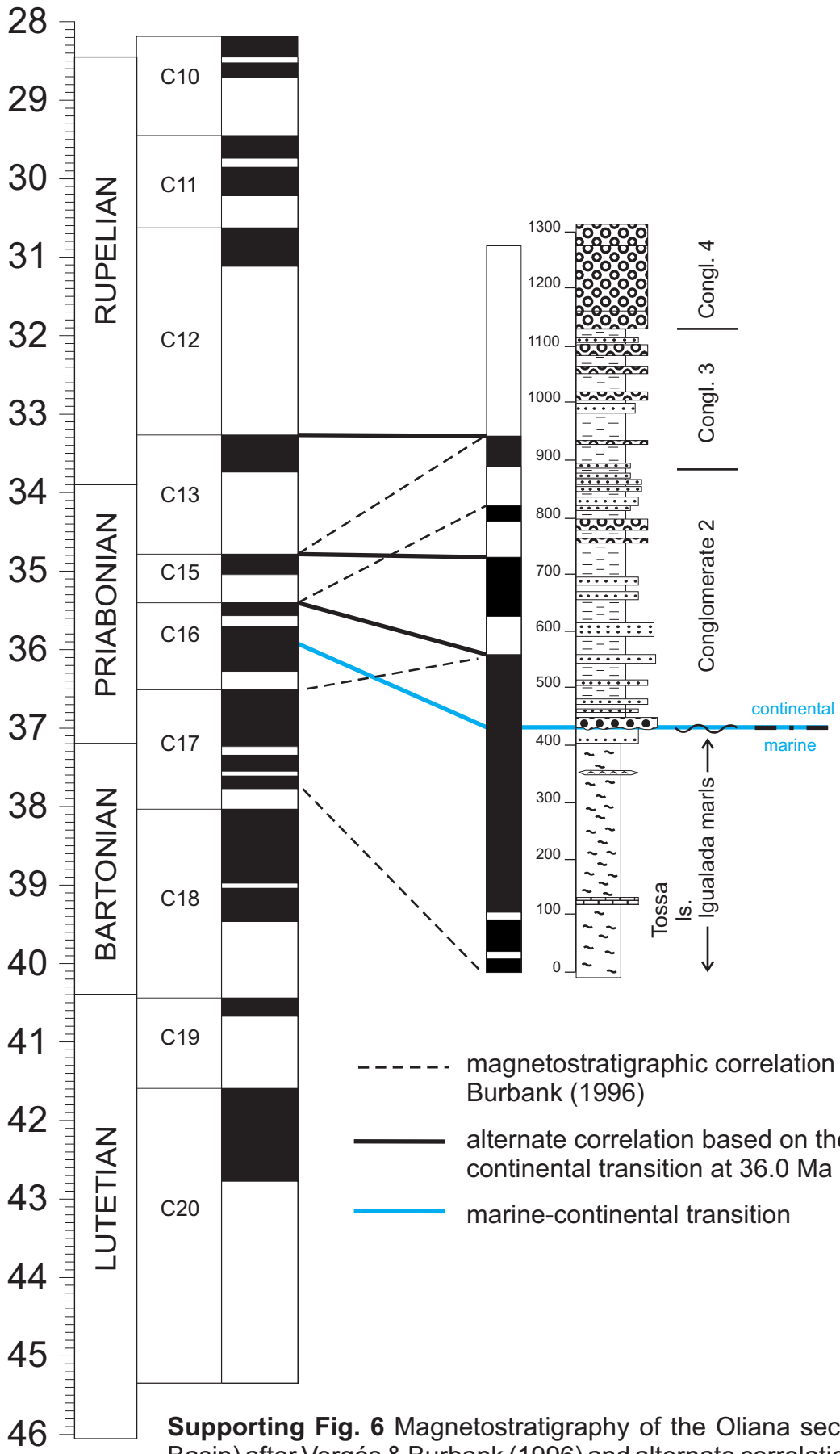

Supporting Fig. 6 Magnetostratigraphy of the Oliana section (eastern Ebro Basin) after Vergés & Burbank (1996) and alternate correlation assumed an age of the marine-continental transition in the eastern Ebro Basin at 36.0 Ma (this study).

Site No.	Stratigraphic level (m)	Geographic coordinates Dec. (º)	Geographic coordinates Inc. (º)	Stratigraphic coordinates Dec. (º)	Stratigraphic coordinates Inc. (º)	Dip az. (º)	Dip. (º)	VGP Lat. (º)
Maians Section								
MN001-2A	0.4	27.7	41.0	23.8	36.0	341	7	60.5
MN002-1A	3.1	0.8	22.2	360.0	15.6	341	7	56.6
MN003-1A	5.4	22.0	16.6	20.9	11.3	341	7	49.6
MN004-2B	7.6	86.5	-7.1	87.2	-5.2	341	7	0.4
MN005-1B	10.0	258.8	61.0	270.7	59.3	341	7	25.7
MN006-1B	13.2	359.9	52.4	355.0	48.0	314	6	76.9
MN007-1B	14.8	44.7	22.5	42.2	22.4	314	6	42.6
MN008-2B	16.9	334.8	26.4	333.9	20.8	314	6	51.7
MN009-1B	20.1	30.6	30.8	27.3	29.2	314	6	55.0
MN010-1A	23.5	49.7	40.8	44.5	41.1	314	6	49.0
MN011-1A	26.0	357.9	22.9	356.4	18.5	314	6	57.9
MN012-1A	34.0	319.2	36.6	318.9	30.6	314	6	46.8
MN013-1A	39.2	113.9	49.7	111.1	55.2	314	6	9.7
MN014-1B	41.3	107.5	85.1	7.8	87.3	314	6	46.9
MN015-1B	44.3	20.3	68.6	7.9	65.6	314	6	81.6
MN016-1A	46.8	61.7	74.9	39.0	75.5	314	6	58.8
MN017-1B	48.5	22.4	33.8	18.9	31.4	314	6	60.6
MN018-1A	51.8	8.9	59.5	1.5	55.7	314	6	84.6
MN019-1B	58.7	346.9	53.4	343.1	48.3	314	6	71.7
MN019-1A	58.7	355.9	61.3	349.7	56.6	314	6	80.9
MN020-2B	62.8	20.3	60.7	11.4	57.9	314	6	80.8
MN021-2B	66.0	218.9	66.9	232.9	66.7	314	6	12.0
MN022-1B	68.0	21.8	-29.8	25.2	-31.9	314	6	26.8
MN023-1B	68.7	229.3	20.5	231.5	19.8	314	6	-20.0
MN025-1A	70.0	5.8	55.1	359.8	51.1	314	6	80.4
MN026-1B	71.2	288.3	62.9	292.5	57.4	314	6	39.3
MN027-1B	71.9	330.0	24.1	329.4	18.3	314	6	48.1
MN028-1A	73.0	19.3	35.3	15.7	32.6	314	6	62.7
MN030-1B	73.4	64.1	4.0	63.6	6.0	314	6	21.5
MN031-1A	73.5	30.2	69.4	16.1	67.2	314	6	76.0
MN033-1B	74.8	11.8	50.0	6.3	46.6	314	6	75.4
MN034-2A	75.8	297.5	48.2	299.1	42.4	314	6	37.4
MN034-2B	75.8	348.1	41.5	345.5	36.4	314	6	65.5
MN036-2A	80.1	6.1	60.3	358.8	56.3	314	6	85.4
MN036-1A	80.1	4.7	19.4	3.3	15.6	314	6	56.3
MN037-1A	83.0	1.6	-33.9	4.9	-37.8	314	6	27.1
MN038-1B	84.0	345.1	43.5	342.5	38.3	314	6	65.2
MN039-1A	85.7	107.8	49.7	104.2	55.0	314	6	13.6
MN041-1A	88.8	299.1	-31.8	298.0	-37.6	314	6	5.2
MN042-1B	91.3	55.7	72.4	36.6	72.6	314	6	61.7
MN043-1A	92.2	236.3	45.4	242.0	43.9	314	6	-1.7
MN044-1A	95.3	350.8	47.7	347.3	42.8	314	6	70.3
MN045-1A	97.2	349.4	22.9	348.1	18.0	314	6	56.1
MN046-1A	98.3	17.6	-1.4	17.9	-4.1	314	6	43.5
MN048-1A	100.5	110.0	31.6	108.3	37.1	314	6	0.8
MN047-1A	101.0	23.5	37.0	19.5	34.7	314	6	62.1
MN049-2A	108.2	25.3	39.6	20.9	37.4	314	6	62.9
MN050-1A	112.8	351.8	33.8	349.6	29.0	314	6	62.5
MN051-1B	115.3	328.4	72.8	324.9	66.9	314	6	64.4
MN052-1A	116.5	65.5	43.7	59.9	45.6	314	6	39.5
MN054-1A	117.9	165.0	-56.7	161.0	-51.4	314	6	-72.1
MN056-2A	128.1	353.2	45.0	349.8	40.2	314	6	69.6
MN057-1A	129.2	25.4	30.5	22.2	28.5	314	6	57.4
MN058-1B	130.9	330.5	57.8	328.2	52.0	314	6	63.3
MN062-2B	134.5	283.5	22.1	284.5	16.9	314	6	16.6
MN059-1B	139.0	187.3	62.0	197.6	65.2	314	6	0.1
MN060-1A	142.7	25.9	35.3	22.0	33.2	314	6	60.0
MN061-1A	145.8	358.2	16.6	357.1	12.2	314	6	54.6
MN063-1B	153.2	355.1	22.3	353.7	17.8	314	6	57.1
MN064-1A	158.0	25.3	70.9	17.0	65.8	348	6	76.3
MN065-1B	163.5	161.1	5.0	161.4	10.3	314	6	-40.3
MN066-1A	170.0	229.9	-23.1	227.8	-20.1	348	6	-37.9
MN067-1A	172.5	133.3	-73.7	133.5	-67.7	314	6	-57.1
MN068-1A	181.0	266.3	-38.8	261.5	-39.4	348	6	-20.7
MN069-1B	187.0	185.0	-32.1	184.0	-26.3	348	6	-62.2

Site No.	Stratigraphic level (m)	Geographic coordinates Dec. (º)	Geographic coordinates Inc. (º)	Stratigraphic coordinates Dec. (º)	Stratigraphic coordinates Inc. (º)	Dip az. (º)	Dip. (º)	VGP Lat. (º)
MN070-2A	192.9	153.9	-19.4	154.3	-13.6	348	6	-48.6
MN071-1A	198.3	286.1	-74.7	270.6	-79.7	314	6	-38.3
MN072-1B	249.5	228.7	-25.8	226.4	-22.7	348	6	-39.9
MN073-2A	251.9	145.4	-42.1	147.2	-36.5	348	6	-55.1
MN074-1B	255.4	179.4	-41.0	178.5	-35.1	348	6	-67.8
MN075-1B	280.0	325.6	59.8	323.9	53.9	314	6	60.9
MN076-2C	289.5	190.5	-47.5	188.3	-42.0	348	6	-71.4
MN077-1B	292.8	344.8	-1.4	344.8	-7.4	348	6	42.7
MN078-1A	296.9	356.3	15.2	355.4	10.8	314	6	53.7
MN079-1A	307.6	7.0	39.6	5.6	33.9	348	6	66.6
MN080-1C	312.1	18.9	32.0	17.2	26.8	348	6	58.9
MN081-1B	314.7	279.7	30.2	281.4	25.2	314	6	17.2
MN082-2A	317.1	336.1	8.0	336.2	2.1	348	6	44.2
MN083-1B	319.8	250.5	4.5	251.0	5.3	348	6	-12.3
MN084-1B	323.1	319.5	57.6	318.7	51.6	314	6	56.1
MN085-1A	327.7	9.0	-0.5	9.1	-6.1	348	6	44.7
MN086-1A	331.5	342.9	34.2	343.4	24.3	348	10	57.8
MN087-2A	336.8	339.3	33.8	337.8	28.3	314	6	57.3
MN091-1A	348.1	16.6	25.6	14.3	22.7	314	6	57.8
MN092-2B	363.6	97.3	-29.2	102.1	-25.5	348	10	-17.8
MN093-1B	367.2	222.0	-13.1	220.6	-12.8	314	6	-39.8
MN094-2B	371.1	174.2	-60.1	172.8	-50.1	348	10	-77.9
MN095-1A	374.7	191.2	-52.3	187.2	-43.0	348	10	-72.4
MN096-1B	381.1	201.4	-60.2	192.5	-57.4	314	6	-79.8
MN097-1A	385.8	179.4	-24.8	178.7	-15.0	348	10	-56.1
MN098-1A	394.8	200.1	-53.0	194.5	-44.3	348	10	-70.4
MN099-2A	399.3	136.6	-70.4	149.7	-62.2	358	10	-67.6
MN099-1A	399.3	205.4	-67.2	194.9	-58.7	348	10	-78.5
MN100-2A	407.3	175.9	-48.8	174.7	-38.8	348	10	-69.9
MN100-1A	407.3	153.0	-40.9	151.5	-35.2	314	6	-57.3
MN101-1A	413.7	204.3	-40.6	200.1	-32.3	348	10	-60.5
MN101-1A	413.7	203.7	-41.5	199.5	-33.2	348	10	-61.3
MN102-1B	419.8	235.4	-15.7	233.2	-11.7	348	10	-31.0
MN103-1B	426.1	36.0	-5.0	36.6	-5.8	314	6	34.6
MN104-2B	429.3	190.3	-52.4	186.4	-43.0	348	10	-72.6
MN105-1A	432.5	158.6	57.8	163.4	63.2	314	6	-2.5
MN106-1A	441.6	213.1	-23.0	210.7	-21.8	314	6	-49.6
MN107-1B	444.3	92.8	-14.7	93.7	-10.2	314	6	-6.1
MN108-2A	452.3	192.2	-22.5	190.9	-13.3	348	10	-53.9
MN109-2A	455.5	200.4	-10.2	199.6	-7.8	314	6	-48.5
MN110-1B	461.8	215.7	-29.5	212.5	-28.4	314	6	-51.5
MN111-2B	465.1	190.5	-44.1	187.5	-34.7	348	10	-66.7
MN112-3A	474.1	199.3	-38.7	195.9	-30.0	348	10	-61.1
MN113-1B	482.3	182.0	-11.1	181.7	-1.4	348	10	-49.2
MN114-1B	483.9	201.6	-47.1	196.8	-38.6	348	10	-65.7
MN115-1A	488.3	173.1	-20.5	172.8	-10.6	348	10	-53.3
MN116-1B	492.7	205.8	-49.1	200.0	-40.9	348	10	-65.4
MN117-1A	499.3	200.3	0.1	200.7	8.5	348	10	-40.5
MN119-1B	506.3	216.7	-24.5	213.9	-17.7	348	10	-45.9
MN120-2A	517.4	199.8	-0.4	200.2	8.0	348	10	-40.9
MN121-2B	521.3	219.4	4.6	220.5	10.8	348	10	-30.3
MN122-1C	528.8	151.1	-18.7	151.8	-9.1	348	10	-45.3
MN123-2A	534.0	215.1	-50.1	207.8	-42.8	348	10	-61.6
MN124-1A	542.0	53.2	15.1	51.1	10.7	348	10	32.0
MN125-1D	551.8	95.4	26.9	90.2	29.4	348	10	10.2
MN126-1B	557.4	11.9	51.1	7.9	41.8	348	10	71.4
MN127-1B	562.3	1.2	48.5	359.2	38.7	348	10	70.3
MN128-2B	572.8	277.9	20.3	281.0	16.6	348	10	13.8
MN128-1B	572.8	341.3	67.2	343.2	57.3	348	10	76.6
MN150-2B	572.8	28.1	43.7	23.0	35.8	348	10	60.7
MN151-1B	574.4	204.7	-54.3	198.1	-46.0	348	10	-69.4
MN129-2B	576.2	326.7	56.9	330.9	47.4	348	10	63.0
MN130-1C	577.5	342.8	47.0	343.6	37.1	348	10	64.9
MN152-1B	580.0	357.5	-25.7	358.6	-35.6	348	10	28.7
MN153-2B	580.5	136.0	-71.4	146.6	-62.4	348	10	-65.5
MN131-2A	583.3	34.0	29.3	30.7	22.1	348	10	49.6

Site No.	Stratigraphic level (m)	Geographic coordinates Dec. (º)	Geographic coordinates Inc. (º)	Stratigraphic coordinates Dec. (º)	Stratigraphic coordinates Inc. (º)	Dip az. (º)	Dip. (º)	VGP Lat. (º)
MN131-1B	583.3	222.7	-54.8	213.0	-48.3	348	10	-60.7
MN154-2B	584.9	31.3	21.4	29.1	14.0	348	10	46.9
MN155-1A	587.8	6.0	51.6	3.0	42.0	348	10	72.4
MN156-1C	590.5	14.4	56.8	9.2	47.7	348	10	75.1
MN132-2B	590.9	27.5	22.2	25.4	14.4	348	10	48.9
MN132-1B	590.9	35.6	18.5	33.7	11.7	348	10	43.5
MN157-1A	592.0	4.9	30.8	3.5	21.2	348	10	59.2
MN158-1B	592.9	26.2	38.7	22.1	30.6	348	10	58.4
MN159-2B	593.8	10.8	45.8	7.7	36.5	348	10	67.7
MN160-1A	599.0	47.1	47.7	38.9	41.9	348	10	53.4
MN133-1B	600.9	204.6	-41.1	200.3	-32.9	348	10	-60.7
MN161-1B	605.4	34.8	39.2	29.8	32.0	348	10	54.8
MN162-1B	606.4	202.4	-60.2	194.9	-51.6	348	10	-74.9
MN163-1B	607.5	14.6	14.6	13.8	5.6	348	10	49.2
MN134-1A	609.3	291.7	38.8	297.5	32.8	348	10	32.2
MN134-1B	609.3	50.5	32.5	45.5	27.5	348	10	42.4
MN164-1A	611.3	59.0	53.0	47.7	48.8	348	10	50.0
MN135-2B	613.5	90.5	46.9	79.6	48.2	348	10	26.2
Rubió Section								
RB210-1A	580.0	355.1	20.4	354.4	14.8	334	6	55.5
RB209-1A	581.8	317.3	67.5	320.6	61.7	334	6	61.1
RB208-1B	585.0	34.9	18.0	33.4	15.0	334	6	45.0
RB206-1B	590.3	286.5	67.7	295.5	63.3	334	6	44.1
RB204-2A	597.6	21.3	39.2	18.0	35.0	334	6	62.9
RB203-1A	600.8	40.6	10.4	39.7	8.0	334	6	38.3
RB201-1A	613.6	324.0	55.2	325.2	49.3	334	6	59.8
RB001-1A	619.8	209.8	-45.0	204.7	-45.2	295	5	-64.9
RB004-1A	624.8	340.2	26.0	338.6	22.4	295	5	54.7
RB005-1B	630.6	209.8	-61.3	200.9	-60.6	303	5	-74.4
RB006-2A	635.3	202.4	-57.8	194.9	-56.6	303	5	-77.7
RB007-1A	637.8	45.3	60.2	36.5	60.9	303	5	63.0
RB009-2A	650.2	212.0	-50.0	206.1	-49.7	303	5	-66.2
RB010-1A	654.5	187.3	-39.5	185.8	-36.0	337	4	-67.8
RB011-1A	663.2	201.2	-46.2	198.5	-43.2	337	4	-67.5
RB012-1A	667.8	175.0	-49.1	173.7	-45.2	337	4	-74.3
RB013-2B	674.5	216.8	-12.6	216.1	-10.6	337	4	-41.5
RB015-2A	681.7	212.1	-47.6	208.8	-45.3	337	4	-62.2
RB017-1A	685.1	136.1	-71.4	139.6	-67.6	337	4	-61.0
RB019-1A	687.3	139.8	-33.6	140.5	-29.7	337	4	-47.5
RB021-1A	695.3	164.6	-36.5	164.3	-32.6	337	4	-62.5
RB022-2A	700.5	171.2	-51.3	170.1	-47.4	337	4	-74.6
RB023-2A	704.5	147.1	-27.0	147.4	-23.1	337	4	-49.0
RB024-1A	714.8	144.2	-80.9	144.5	-75.9	325	5	-60.1
RB025-1A	717.3	225.0	-73.5	209.7	-71.9	325	5	-65.7
RB026-2A	721.3	194.3	-58.8	188.7	-55.3	325	5	-81.1
RB027-1A	730.1	200.2	-33.7	197.7	-30.7	325	5	-60.7
RB029-1A	739.1	233.4	-57.5	225.7	-57.0	325	5	-55.0
RB030-1A	747.5	206.3	-41.1	202.7	-38.6	325	5	-62.4
RB031-1A	762.7	187.5	-40.8	184.9	-37.0	325	5	-68.6
RB032-1A	771.8	249.9	-51.5	243.6	-52.5	325	5	-39.9
RB033-2A	777.0	223.2	-21.7	221.3	-20.6	325	5	-42.4
RB035-2A	790.1	188.6	-29.6	186.8	-25.9	325	5	-61.4
RB036-2A	797.3	173.1	-57.8	169.9	-53.3	325	5	-78.9
RB037-1A	802.1	200.4	-53.2	195.4	-50.2	325	5	-73.7
RB038-2A	806.3	209.9	-36.6	206.7	-34.4	325	5	-57.8
RB039-2A	812.3	193.9	-59.6	188.2	-56.1	325	5	-81.9
RB042-1B	834.3	311.7	51.8	313.0	46.9	325	5	49.7
RB044-1A	847.1	251.2	-59.2	242.8	-60.2	325	5	-44.0
RB047-1A	860.3	193.7	-56.0	188.7	-52.6	325	5	-79.0
RB048-1A	863.7	235.5	-24.0	233.3	-24.0	325	5	-35.5
RB049-1A	869.6	218.7	-36.2	215.3	-34.7	325	5	-52.5
RB050-1C	873.6	187.1	-12.3	186.5	-8.6	325	5	-52.2
RB051-1A	877.8	200.6	-33.7	198.1	-30.7	325	5	-60.5
RB052-1A	880.3	198.5	-18.3	197.3	-15.3	325	5	-52.8
RB053-2A	883.6	178.8	-18.5	178.0	-14.3	325	5	-55.6

Site No.	Stratigraphic level (m)	Geographic coordinates Dec. (º)	Geographic coordinates Inc. (º)	Stratigraphic coordinates Dec. (º)	Stratigraphic coordinates Inc. (º)	Dip az. (º)	Dip. (º)	VGP Lat. (º)
RB054-1A	886.5	226.6	-55.0	219.7	-53.9	325	5	-58.2
RB055-1A	893.1	143.9	-41.1	144.0	-36.1	325	5	-52.8
RB057-1A	906.3	173.3	-44.0	171.2	-39.6	325	5	-69.4
RB059-1A	918.1	165.8	-11.3	165.3	-5.9	319	6	-49.1
RB060-1A	920.9	226.8	-29.4	223.5	-29.0	319	6	-44.4
RB061-1A	928.2	197.5	-63.2	189.8	-60.3	319	5	-82.6
RB063-1A	940.6	197.3	-26.0	195.0	-22.8	319	6	-57.4
RB064-1A	943.9	198.2	-64.7	188.6	-61.2	319	6	-83.5
RB065-1A	952.1	240.0	-50.6	232.7	-51.3	319	6	-47.4
RB066-2A	955.9	222.9	-56.4	214.1	-55.3	319	6	-62.9
RB067-2A	959.3	175.0	-60.0	169.8	-55.0	319	6	-80.0
RB068-1A	962.3	231.1	-35.3	226.9	-35.3	319	6	-44.7
RB070-1B	987.2	207.4	-45.2	202.1	-42.8	319	6	-65.2
RB071-1A	992.3	174.7	-37.6	172.3	-32.6	319	6	-65.2
RB072-1A	1000.1	227.6	-57.6	218.3	-56.9	319	6	-60.4
RB074-1A	1012.8	197.6	-13.2	196.5	-10.0	319	6	-50.5
RB075-1B	1027.2	161.4	-40.3	159.7	-34.7	319	6	-61.6
RB076-1A	1030.4	198.7	-37.5	195.0	-34.3	319	6	-63.8
RB080-1A	1050.8	258.8	-46.5	252.9	-49.2	319	6	-31.5
RB083-1A	1064.8	282.9	-57.4	276.4	-62.1	319	6	-23.2
RB084-2A	1077.6	240.5	-71.9	221.9	-72.2	319	6	-59.3
RB087-1A	1085.6	191.2	-47.1	186.6	-43.2	319	6	-72.6
RB089-1A	1101.6	155.3	-49.2	153.6	-43.4	319	6	-62.8
RB092-2A	1119.8	212.1	-71.0	197.3	-68.5	319	6	-74.5
RB094-1A	1132.5	218.7	-59.5	209.2	-58.0	319	6	-67.6
RB207-1D	588.2	262.9	9.6	263.6	6.2	319	6	-2.7
RB202-1A	611.5	7.9	11.9	7.1	7.9	319	6	51.8
RB008-1A	645.6	74.0	-18.0	75.7	-15.4	319	6	5.3
RB014-1A	678.1	353.3	42.7	350.5	37.7	319	6	68.1
RB043-1A	842.1	325.0	0.9	325.1	-5.1	319	6	35.6
RB079-1A	1045.3	194.2	-33.2	191.3	-29.7	319	6	-62.5
RB205-1B	592.8	36.9	-76.7	62.5	-76.7	319	6	-26.9
RB002-1A	620.2	234.3	33.3	238.1	32.5	319	6	-10.0
RB003-1A	624.2	118.9	22.5	117.9	28.2	319	6	-9.5
RB016-3A	684.5	210.3	-61.0	200.8	-58.6	319	6	-74.0
RB018-1A	685.8	257.2	-3.8	256.7	-6.6	319	6	-12.1
RB020-1A	690.7	165.0	23.2	166.3	28.6	319	6	-31.9
RB028-1A	734.9	200.9	-30.9	197.9	-28.0	319	6	-59.1
RB034-1B	786.8	182.0	-51.1	177.5	-46.5	319	6	-76.0
RB040-3A	822.5	104.9	-43.5	107.7	-38.5	319	6	-27.2
RB041-2A	830.3	107.7	53.1	102.9	58.1	319	6	16.7
RB045-1B	850.9	300.9	-24.4	300.0	-30.1	319	6	10.0
RB046-1A	854.8	203.4	4.3	203.9	6.8	319	6	-40.0
RB056-1A	897.3	233.9	-36.3	229.5	-36.6	319	6	-43.3
RB058-1B	913.7	161.7	-19.1	161.0	-13.6	319	6	-51.4
RB062-1A	931.5	266.8	-38.8	262.6	-42.3	319	6	-21.3
RB069-1A	981.4	240.1	37.5	244.5	36.1	319	6	-4.3
RB073-2A	1011.0	153.5	-6.0	153.4	-0.2	319	6	-42.0
RB077-1A	1036.1	117.5	-66.0	121.5	-60.3	319	6	-47.0
RB078-1A	1041.6	307.1	-41.6	305.9	-47.5	319	6	3.8
RB081-1A	1055.8	16.1	4.2	15.9	0.9	319	6	46.4
RB082-1A	1058.6	235.7	-13.9	234.2	-14.5	319	6	-31.2
RB085-2A	1081.1	67.1	-86.3	112.6	-82.0	319	6	-45.7
RB086-1A	1082.8	111.1	-18.1	111.9	-12.8	319	6	-20.6
RB090-1A	1108.5	169.7	-10.6	169.3	-5.5	319	6	-49.9
RB091-1A	1114.4	187.3	-74.8	174.5	-70.3	319	6	-76.8
RB093-1A	1129.1	192.2	-37.7	188.8	-34.0	319	6	-65.7
RB095-1A	1134.1	155.4	11.1	155.9	16.9	319	6	-35.0

Supporting Table 1: ChRM directions of the Maians and Rubió magnetostratigraphic sections. Site No., name and number of paleomagnetic site; Strat. level, stratigraphic position of the paleomagnetic site in the Mains-Rubió composite section; Dec. and Inc., declination and inclination in geographic (in situ) and stratigraphic coordinates (after bedding correction); Dip. Az. and Dip., azimuth of down dip direction of local bedding and angle of dip of local bedding; VGP Lat., latitude of the Virtual Geomagnetic Pole used to build the local magnetostratigraphy of Mains and Rubió sections (see Fig. 5).

CHAPTER 3.3:

CHRONOLOGY OF THE CONTINENTAL AND TRANSITIONAL UNITS IN THE MONTSERRAT AREA: *"TECTONIC AND CLIMATIC CONTROLS ON THE SEQUENTIAL ARRANGEMENT OF AN ALLUVIAL FAN / FAN-DELTS COMPLEX (MONTSERRAT, EOCENE, EBRO BASIN, NE SPAIN)"*

The PhD candidate is coauthor of Chapter 3.3: *Gómez-Paccard, M., López-Blanco, M., Costa, E., Garcés, M., Beamud, E., Larrasoaña, J.C., (submitted). Tectonic and climatic controls on the sequential arrangement of an alluvial fan/fan-delta complex (Montserrat, Eocene, Ebro basin, NE Spain). Basin Research.*

Tectonic and climatic controls on the sequential arrangement of an alluvial fan/fan delta complex (Montserrat, Eocene, Ebro Basin, NE Spain).

Gómez-Paccard, M. [1,2], López-Blanco, M. [1], Costa, E. [1], Garcés, M.[1], Beamud, E.[3], and Larrasoaña, J.C.[4]

[1] Grup de Geodinàmica i Anàlisi de Conques (GGAC), Department d'Estratigrafia, Paleontologia i Geociències Marines, Facultat de Geologia, Universitat de Barcelona
[2] Institut de Cienciès de la Terra Jaume Almera, CSIC
[3] Laboratori de Paleomagnetisme (CCiTUB-CSIC), Institut de Cienciès de la Terra Jaume Almera, CSIC
[4] Instituto Geológico y Minero de España, Unidad de Zaragoza

ABSTRACT

A magnetostratigraphy based chronological framework has been constructed in the Eocene sediments of the Montserrat alluvial fan/fan-delta complex (southeast Ebro Basin), in order to unravel forcing controls on their sequential arrangement and to revise the tectonosedimentary history of the region. The paleomagnetic study is based on 403 sites distributed along a 1880-m-thick composite section, and provides improved temporal constraints based on an independent correlation to the geomagnetic polarity time scale. The new chronological frame together with sequence stratigraphy and geohistory analysis allow to investigate the interplay between factors controlling the sequential arrangement of the Montserrat complex at the different temporal scales and to test for orbitally-driven climate forcing. The results suggest that the internal stacking pattern in transgressive and regressive sequences sets within the more than 1000-m-thick Milany Composite Megasequence can be explained as the result of subsidence-driven accommodation changes under a general increase of sediment supply. Composite sequences (tens to hundreds of meters thick) likely reflect orbitally-forced cyclicity related to the 400-kyr eccentricity cycle, possibly controlled by climatically induced sea-level fluctuations. This study also provides new insights on the deformational history of the area, and shows a correlation between (tectonic) subsidence and forelimb rotation measured on basin-margin deformed strata. Integration of subsidence curves from different sectors of the eastern Ebro Basin allows us to estimate the variable contribution of tectonic loads from the two active basin margins: the Catalan Coastal Ranges and the Pyrenees. The results support the presence of a double flexure from Late Lutetian to Late Bartonian, associated to the two tectonically active margins. From Late Bartonian to Early Priabonian the homogenization of subsidence values is interpreted as the result of the coupling of the two sources of tectonic load.

Keywords: Magnetostratigraphy, orbital forcing, tectonosedimentary evolution, fan-delta, Ebro Basin, Eocene.

INTRODUCTION

Montserrat is a conglomeratic massif located along the southeastern margin of the Ebro Foreland Basin adjacent to the Catalan Coastal Ranges (CCR), a NE-SW oriented and NW-verging intraplate chain resulting from Paleogene convergence between the Iberian and European plates (Anadón *et al.*, 1985b; Guimerà, 1988; López-Blanco, 2002).

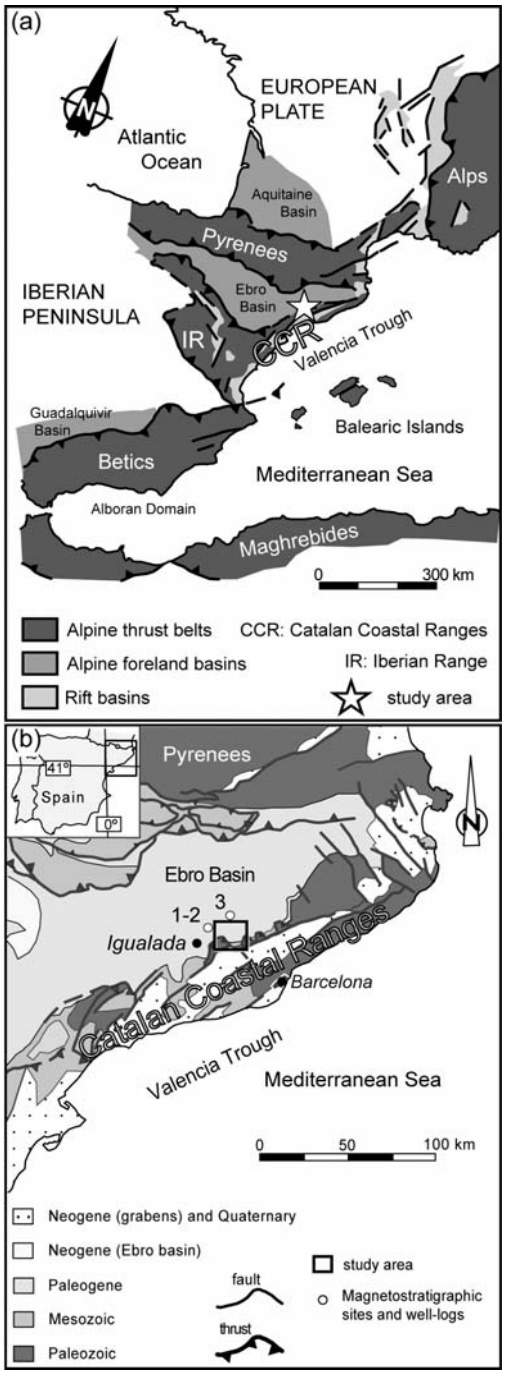

Fig. 1. (a) Location of the study area and main geological units of the western Mediterranean area and (b) location of the study area in the eastern margin of the Ebro Basin (northeast Spain). Numbers indicate locations of the magnetostratigraphic sections or well-logs cited in the text: 1, Maians-Rubió; 2, Castelfollit; 3, Santpedor.

Tectonic activity of the CCR during the Lutetian led to the development of this alluvial fan system which evolved to a fan-delta complex after the so-called "Bartonian transgression" (Serra-Kiel & Travé, 1995). Erosive processes during the Neogene and Quaternary have resulted in a series of long and deeply incised valleys where a 2000-m-thick Eocene stratigraphic succession crops out. The excellent and continuous outcrops make this area particularly suitable for the study of the architectural arrangement of these sediments and the interplay between tectonics, climate, relative sea-level changes and sediment supply in an active basin margin context. To achieve these goals a robust chronology of the sedimentary record is essential. In an earlier work magnetostratigraphy was applied to establish the age of the Montserrat stratigraphic succession (López-Blanco *et al.*, 2000a). However, the correlation proposed between the local magnetostratigraphy and the geomagnetic polarity time scale (GPTS) was based on chronological tie points which have been recently challenged (Cascella & Dinarès-Turell, 2009; Costa *et al.*, 2010). In addition, limited sampling resolution in López-Blanco *et al.* (2000a) yielded uncertain results regarding completeness of the magnetostratigraphic record. This study provides a new magnetostratigraphy of the Montserrat succession that involves a five-fold increase in sampling resolution and an independent correlation to the GPTS. The new chronology has been used to test for orbital forcing in the sequential arrangement of the studied fan delta and to revise the tectonosedimentary evolution of the Montserrat system and the adjacent CCR.

GEOLOGICAL SETTING

The Ebro Foreland Basin represents the last evolutionary stage of the South Pyrenean Foreland Basin (Fig. 1). It is limited to the north by the Pyrenees, to the southwest by the Iberian Range and to the southeast by

the CCR. Enhanced tectonic loading on the Pyrenean side of the basin led to an asymmetrical basin where subsidence rates and sedimentary thickness increased northward (Séguret, 1972; Choukroune & Séguret, 1973; Puigdefàbregas & Souquet, 1986; Muñoz, 1992; Vergés, 1993; Vergés *et al.,* 1998). The Paleogene development of the CCR and the Iberian Range occurred soon after the onset of Pyrenean deformation in the Late Cretaceous (Puigdefàbregas & Souquet, 1986).

In the study area, the Paleogene sedimentary fill is divided into four lithostratigraphic units: the Mediona, El Cairat Breccia, and La Salut Sandstone formations and Montserrat Conglomerates (Figs. 2a and b). The Mediona Formation overlies a regional unconformity on Triassic rocks, and its age is constrained to the Upper Thanetian-Lower Ypresian (Anadón, 1978). The El Cairat Breccia Formation mainly consists of Triassic-derived breccias with a Ypresian estimated age (Anadón, 1978). The La Salut Formation is predominantly composed of red sandstones with intercalated mudstones, siltstones and conglomerates. This formation, dated as Upper Ypresian-Lutetian (Anadón, 1978), includes distal alluvial and fluvial deposits with minor palustrine and lacustrine intervals. On top of the La Salut Formation rests the informal stratigraphic unit of the Montserrat Conglomerates (Riba, 1975; Anadón, 1978), which has been divided into nine units by Anadón *et al.* (1985b) (Fig. 2c). The lowermost Montserrat Conglomerates include syntectonic unconformities associated with folding in the basin margin (Anadón, 1978; Anadón *et al.*, 1985a; Anadón *et al.*, 1986; López-Blanco, 2002). These conglomerates grade basinward into distal alluvial sandstones and mudstones, which in turn grade into the marine deposits of the Santa Maria Group (Ferrer, 1971; Pallí, 1972). This group represents the submarine part of the Montserrat fan-delta system and comprises three main Formations: the Collbàs, Igualada and Tossa formations (Figs. 2a and b).

The structure of the CCR in the Montserrat area is characterized by contractional deformation associated with the NW-verging Prelitoral Fault, a shortcut developed in the footwall of the Mesozoic Vallès-Penedès Fault during its Paleogene reactivation under transpressive conditions (Gaspar-Escribano *et al.*, 2004). A tectonosedimentary evolution of the SE Ebro Basin margin has been proposed by López-Blanco (2002) based on the study of the different tectonic structures and stratigraphic units from this area. Three main stages linked to the evolution of the Prelitoral Fault (López-Blanco, 2002) have been identified (see Tectono-sedimentary evolution section)**.**

The sequential arrangement of the Paleogene succession of the SE Pyrenean Foreland Basin has led to a subdivision into a hierarchy of stratigraphic sequences (Puigdefàbregas *et al.*, 1986), and 3rd-order depositional cycles or megasequences (Vergés *et al.*, 1998). All these sequences have an internal transgressive (T) to regressive (R) architecture regardless of their thickness. The upper part of the Montserrat section (fan-delta) constitutes a >1000-m-thick megasequence (López-Blanco *et al.*, 2000b) which is equivalent to the Milany sequence of Puigdefàbregas *et al.* (1986) and the cycle IV of Vergés *et al.* (1998).

A detailed sequential analysis of the Montserrat fan delta and its lateral equivalent units at Sant Llorenç del Munt has been previously performed (López-Blanco, 1993 and 1996; López-Blanco *et al.*, 2000b; López-Blanco *et al.*, 2006). In that study, the cyclic arrangement of the fan-delta facies was studied by determining the migration of the shoreline in response to changes in accommodation and sediment supply. Sequence division and hierarchy have been based on key stratigraphic horizons such as maximum flooding surfaces (MFS, corresponding to the change in the shoreline from T to R) and sequence boundaries (SB,

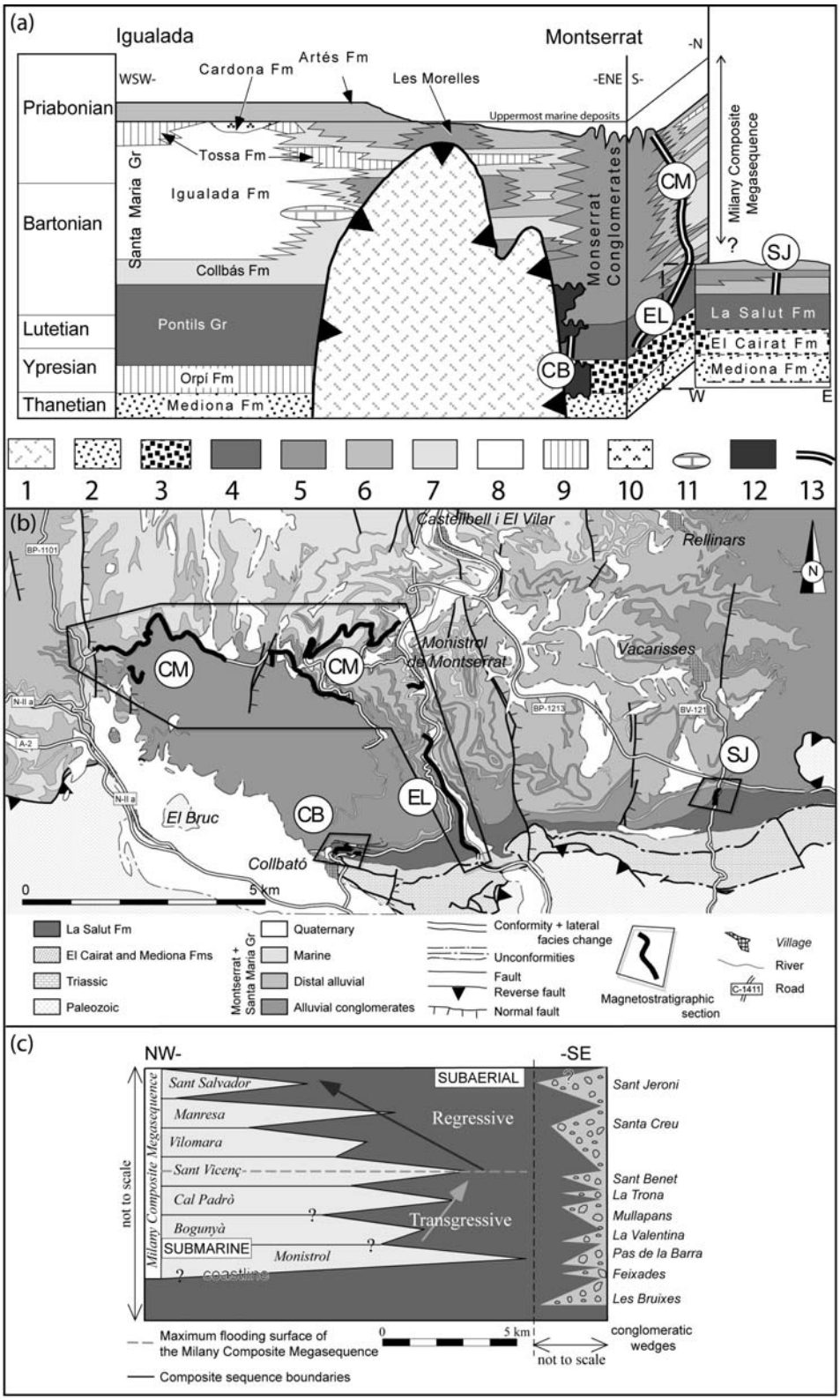
(a)
Igualada
Montserrat
WSW-
-ENE S-
-N
Cardona Fm
Artés Fm
Les Morelles
Priabonian
Bartonian
Lutetian
Ypresian
Thanetian
Uppermost marine deposits
Tossa Fm
Santa Maria Gr
Igualada Fm
Collbás Fm
Pontils Gr
Orpi Fm
Mediona Fm
Monserrat Conglomerates
Milany Composite Megasequence
CM
SJ
EL
CB
La Salut Fm
El Cairat Fm
Mediona Fm
W
E
1 2 3 4 5 6 7 8 9 10 11 12 13
(b)
Castellbell i El Vilar
Rellinars
Monistrol de Montserrat
Vacarisses
BP-1101
N-II a
A-2
BP-1213
BV-121
El Bruc
Collbató
0
5 km
La Salut Fm
El Cairat and Mediona Fms
Triassic
Paleozoic
Montserrat + Santa Maria Gr
Quaternary
Marine
Distal alluvial
Alluvial conglomerates
Conformity + lateral facies change
Unconformities
Fault
Reverse fault
Normal fault
Magnetostratigraphic section
Village
River
C-1411
Road
(c)
NW-
-SE
SUBAERIAL
SUBMARINE
Sant Salvador
Manresa
Vilomara
Sant Vicenç
Cal Padrò
Bogunyà
Monistrol
coastline
Regressive
Transgressive
Milany Composite Megasequence
not to scale
Sant Jeroni
Santa Creu
Sant Benet
La Trona
Mullapans
La Valentina
Pas de la Barra
Feixades
Les Bruixes
Maximum flooding surface of the Milany Composite Megasequence
Composite sequence boundaries
0
5 km
not to scale
conglomeratic wedges

corresponding to the shoreline trajectory shift from R to T). According to these key surfaces, the large-scale Milany Composite Megasequence (Figs. 2a and c) has been subdivided into seven medium-scale composite sequences (Monistrol, Bogunyà, Cal Padró, Sant Vicenç, Vilomara, Manresa, and Sant Salvador; Fig. 2c) that range from 100 to 250 meters in thickness. Each composite sequence has also been subdivided into seven to eleven minor-scale fundamental sequences, from 3 to 80 meters thick.

MAGNETOSTRATIGRAPHY

Four sections, Collbató (CB), Eix Llobregat (EL), Carretera Montserrat (CM) and Sant Jaume (SJ), spanning the La Salut Formation, the Montserrat Conglomerates and their lateral equivalents were sampled for magnetostratigraphy (Figs. 2a and b, Supplementary Fig.S1 and Table S1). The 274-m-thick CB section covers the basal strata of the La Salut Formation. Sections EL and CM constitute the Montserrat composite section, with a total thickness of 1770 meters, that includes the La Salut Formation, Montserrat Conglomerates and the laterally equivalent marine facies of the Santa Maria Group. Finally, the 200-m-thick SJ section represents the fine-grained marginal equivalents of the lowermost Montserrat Conglomerates. Paleomagnetic sampling was focused on mudstones and fine-grained sandstones. Although unsuitable coarse sandstones and conglomerates are common in the upper part of the Montserrat section, a mean sampling resolution of about 5 meters has been achieved, which represents a resolution five times higher than in López-Blanco *et al.* (2000a). Two oriented cores per site were drilled in situ from 403 different paleomagnetic sites. Samples were oriented using a magnetic compass coupled to a core orienting fixture.

Paleomagnetic measurements were made using a 2G superconducting rock magnetometer at the Paleomagnetism Laboratory of Barcelona (CCiTUB-CSIC). This magnetometer has a noise level of less than 10^{-7} A/m for a 10 cm^3 volume rock, which is much lower than the magnetization of the measured samples (Fig. 3). The paleomagnetic analysis was based on progressive thermal demagnetization and subsequent measurement of the remanent magnetization at intervals ranging between 10ºC and 50ºC. This was carried out on at least one sample per site up to a maximum temperature of 680ºC using TSD1 (Schönstedt) and MMTD-80 (Magnetic Measurements) furnaces. Characteristic remanent magnetization (ChRM) directions were calculated by fitting linear trends in the demagnetization plots (Kirschvink, 1980).

Fig. 2. (a) Litho and chronostratigraphic panel of the central SE margin of the Ebro Basin (Modified from Anadón *et al.* (1985b). 1: Paleozoic basement (hangingwall of the Prelitoral thrust), 2: Mediona Formation, 3: El Cairat Breccia Formation, 4: Distal alluvial, fluvial and lacustrine (Pontils Group and La Salut Formation), 5: Alluvial fan conglomerates, 6: Distal alluvial and fluvial (Vacarisses unit, Artés Formation and others), 7: Shallow water and coastal siliciclastic deposits (Collbàs Formation and others); 8: Off-shore and prodelta calcareous mudstones (Igualada Formation); 9: Carbonate platform (Orpí Formation, Tossa Formation and others), 10: Evaporites (Òdena and Cardona Formations), 11: Olistolith (Triassic limestones), 12: Erosional gaps related to syntectonic unconformities, 13: Magnetostratigraphic logs. (b) Geological map and location of the paleomagnetic sampling logs at Montserrat. The studied sections: CB, Collbató; CM, Carretera Montserrat; EL, Eix Llobregat; and SJ, Sant Jaume are indicated. (c) Stacking pattern of the successive T-R composite sequences (from Monistrol to Sant Salvador) showing a general transgressive top regressive trend (T-R Milany Composite Megasequence), after López-Blanco *et al.* (2000b). The lateral relation between the T-R composite sequences and the Montserrat conglomeratic wedges (Anadón *et al.*, 1985b) is also shown.

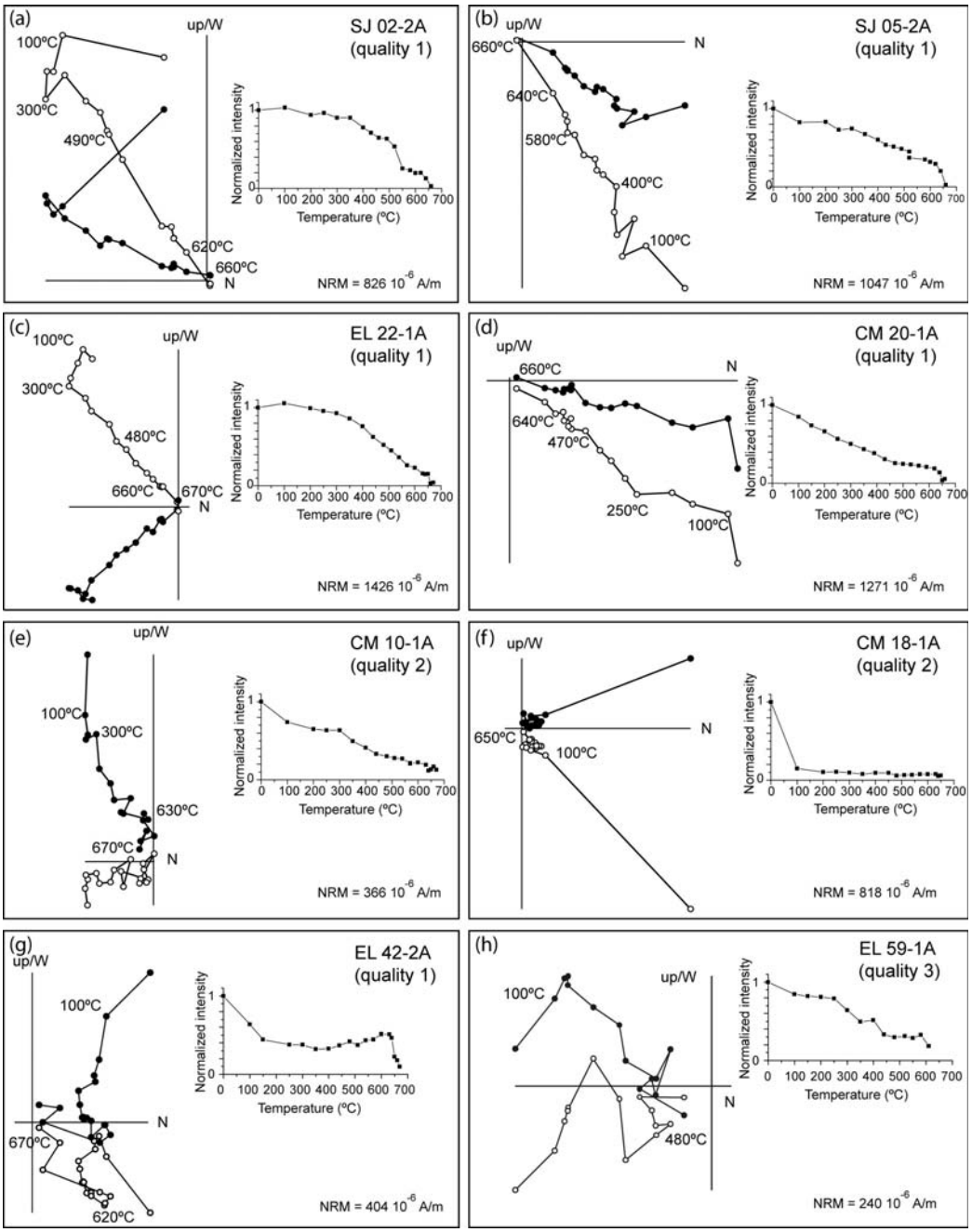

Fig. 3. Orthogonal vector end-point diagrams of stepwise thermal demagnetization data and normalized intensity decay plots of representative samples: quality 1 (a-d and g), quality 2 (e and f) and quality 3 (h). Solid (open) symbols denote projections in the horizontal (vertical) plane. All plots after bedding correction.

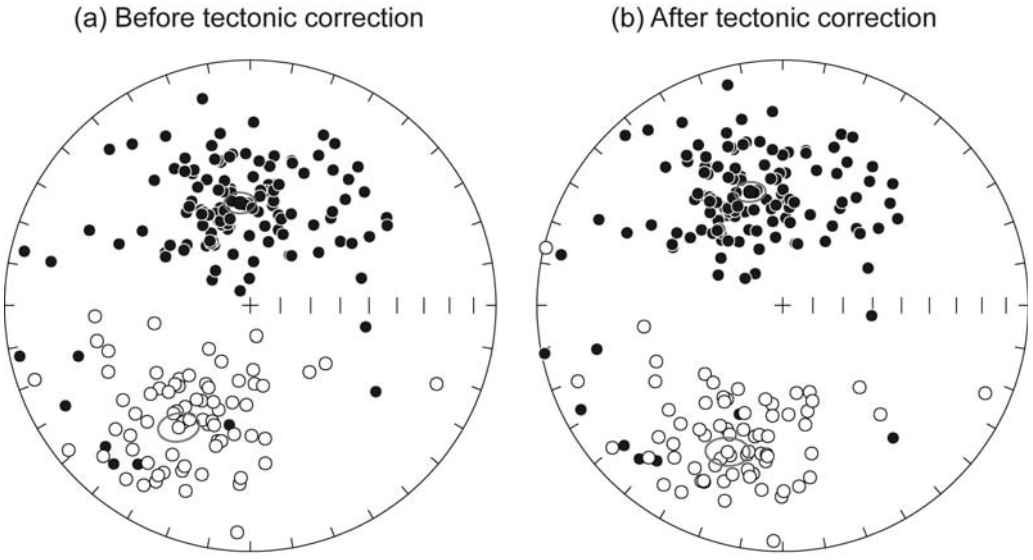

Polarity	n	Dec	Inc	k	α_{95}
Normal	123	354.3	55.4	9.2	4.4
Reversed	75	210.5	-42.1	7.9	6.2

Polarity	n	Dec	Inc	k	α_{95}
Normal	124	344.0	50.2	9.7	4.3
Reversed	74	200.7	-36.6	7.9	6.4

Fig. 4. Equal-area stereographic projection of quality 1 and 2 ChRM directions from the Montserrat composite section: (a) in geographic and (b) stratigraphic coordinates. Number of sites (n) taken into account in order to calculate the mean directions; declination (Dec), inclination (Inc), precision parameter (k) and α_{95} confidence limit from Fisher statistics (Fisher, 1953) also are shown.

Magnetic susceptibility was also measured after each demagnetization step using a magnetic susceptibility bridge KLY-2 (Geofizika Brno). Stepwise demagnetization reveals, in most of the studied samples, a viscous magnetization parallel to the present-day geomagnetic field that is removed after heating to 250-300ºC (Fig. 3). However, in other samples this parallelism is not observed and this component probably corresponds to a drilling induced magnetization acquired during sampling. This low temperature magnetization component will not be considered further. Above 300ºC, a ChRM of either normal or reversed polarity can be identified in about 68% of the samples. Thermal decay of the ChRM shows steep intensity decays below 580ºC although higher temperatures (up to 680ºC) are required for completely demagnetize most of the samples (Fig. 3a-g). This suggests that the natural remanent magnetization (NRM) is primarily carried by magnetite and hematite. In some cases an intermediate component with unblocking temperatures around 570-620ºC has been identified (Fig. 3g) and the high temperature component (620-680ºC) has been considered as the ChRM. Three different qualities of ChRM directions have been considered based on visual inspection of the orthogonal vector end-point diagrams of stepwise thermal demagnetization (Fig. 3). Quality 1 directions show well-defined linear trends that yield accurate paleomagnetic directions. Quality 2 directions show either non-linear decay trends or incomplete demagnetization diagrams during thermal treatment of the samples. As a result, quality 2 directions are considered to provide inaccurate directional data but, still, reliable polarity determinations by fitting clustered directions to the origin of the

demagnetization diagrams. Quality 3 directions correspond to unstable demagnetization behaviour and were excluded for subsequent analysis (Fig. 3h). Figure 4 shows the mean of normal and reverse ChRM directions derived from quality 1 (corresponding to 41% of the studied samples) and quality 2 (corresponding to 28%) samples from the Montserrat composite section. These means are not perfectly antipodal, with the reverse direction being approximately 12° shallower than the normal one. Important differences in declination are also observed (Fig. 4). This suggests an incomplete cleaning of the secondary components.

However, stratigraphic consistency of the magnetostratigraphic results provides confidence that the calculated ChRM directions correspond to a primary magnetization. The magnetic polarity was determined at sample level by calculation of the virtual geomagnetic pole (VGP) latitude for each ChRM direction (Supplementary Table S1). The obtained VGP latitudes provide a detailed sequence of magnetozones represented by two or more consecutive sites of same polarity (Fig. 5). Short magnetozones recorded by a single site are represented as half bars in the magnetic polarity log, but have not been taken into account for correlation purposes because it is uncertain whether they represent true geomagnetic reversals or secondary/delayed magnetizations. It is worth noting that only quality 1 and 2 directions have been considered in order to construct the magnetostratigraphic sections. Nevertheless, the general agreement between quality 1-2 and quality 3 directions attest to the confidence in the reliability of the proposed magnetostratigraphy. The resulting polarity reversal pattern of the Collbató and Montserrat composite section indicates the occurrence of six normal and six reversed magnetozones spanning a stratigraphic thickness of about 1880 meters. The presence of the short normal magnetozone N2 at the base of the Montserrat Conglomerates has been confirmed by studying the time-equivalent section of Sant Jaume. This supporting section was sampled in the same lithostratigraphic interval (transition from La Salut Formation to Montserrat Conglomerates), 5 kilometres east to the Montserrat section (Figs. 2a and b), where fine-grained lithologies allowed a higher-resolution sampling of the targeted stratigraphic interval.

Correlation between Collbató, Montserrat and Sant Jaume sections (Fig. 6) was first constrained by the lithostratigraphic correlation of the base of the Montserrat Conglomerates and finally guided by the local magnetostratigraphy of all sections. Detailed regional mapping, supported by 3D geometric reconstructions, indicates that strata time-equivalent to the evaporitic Cardona Formation (Fig. 2a), which correspond to the uppermost marine deposits in the eastern part of the Ebro Basin, stratigraphically overlie the Montserrat section. These topmost marine strata lie approximately 133 meters above the top of the Montserrat section (Fig. 6) and have been dated to ~36.0 Ma (chron C16n.2n) by Costa *et al.* (2010).

Considering these constraints, the best fit of our magnetostratigraphic section with the GPTS (Gradstein *et al.*, 2004) leads to the correlation shown in Fig. 6. The lower part of the La Salut Formation correlates with chrons C20n (N1) and C19r (R2), and its top with C19r. Therefore, a Lutetian age can be ascribed to the whole La Salut Formation. The age of the Montserrat Conglomerates spans from C19r to C16n (Upper Lutetian to Lower Priabonian). An age of ca. 40.7 Ma has been obtained for the basal Montserrat Conglomerates. The age of the uppermost conglomerates is uncertain. Geometric correlation with the evaporitic Cardona Formation indicates that they must be younger than ~36.0 Ma, whereas calculations

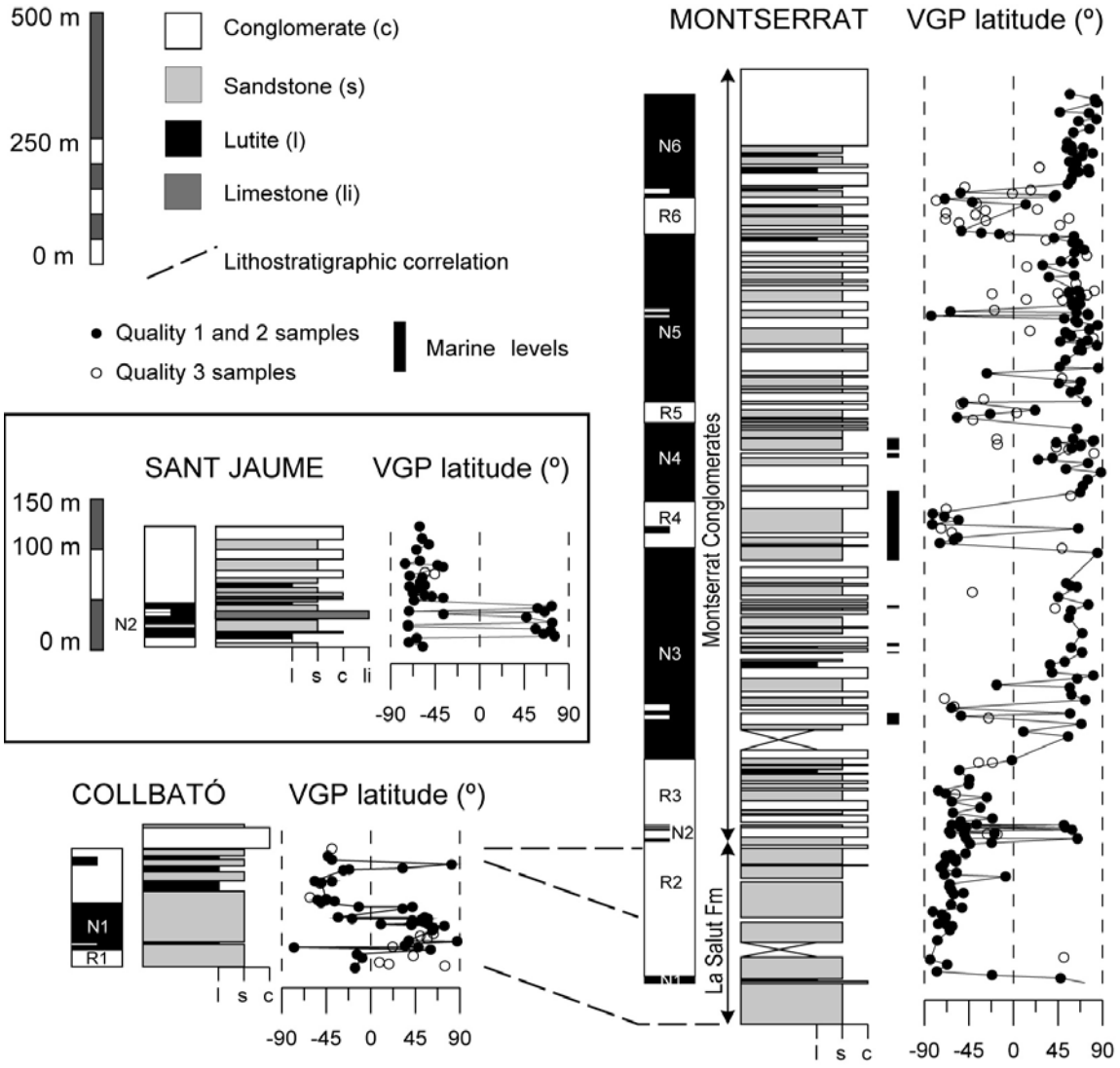

Fig. 5. Magnetostratigraphy of the Sant Jaume, Collbató and Montserrat composite sections (see location in Figs. 2a and b, and Supplementary Figure S1). Closed circles indicate VGP latitudes obtained from quality 1 and 2 palaeomagnetic samples and open circles from quality 3 samples (see text for explanation). Only quality 1 and 2 results have been taken into account for the establishment of the magnetostratigraphic sections. Single-site magnetozones are represented as half bars in the local magnetostratigraphy.

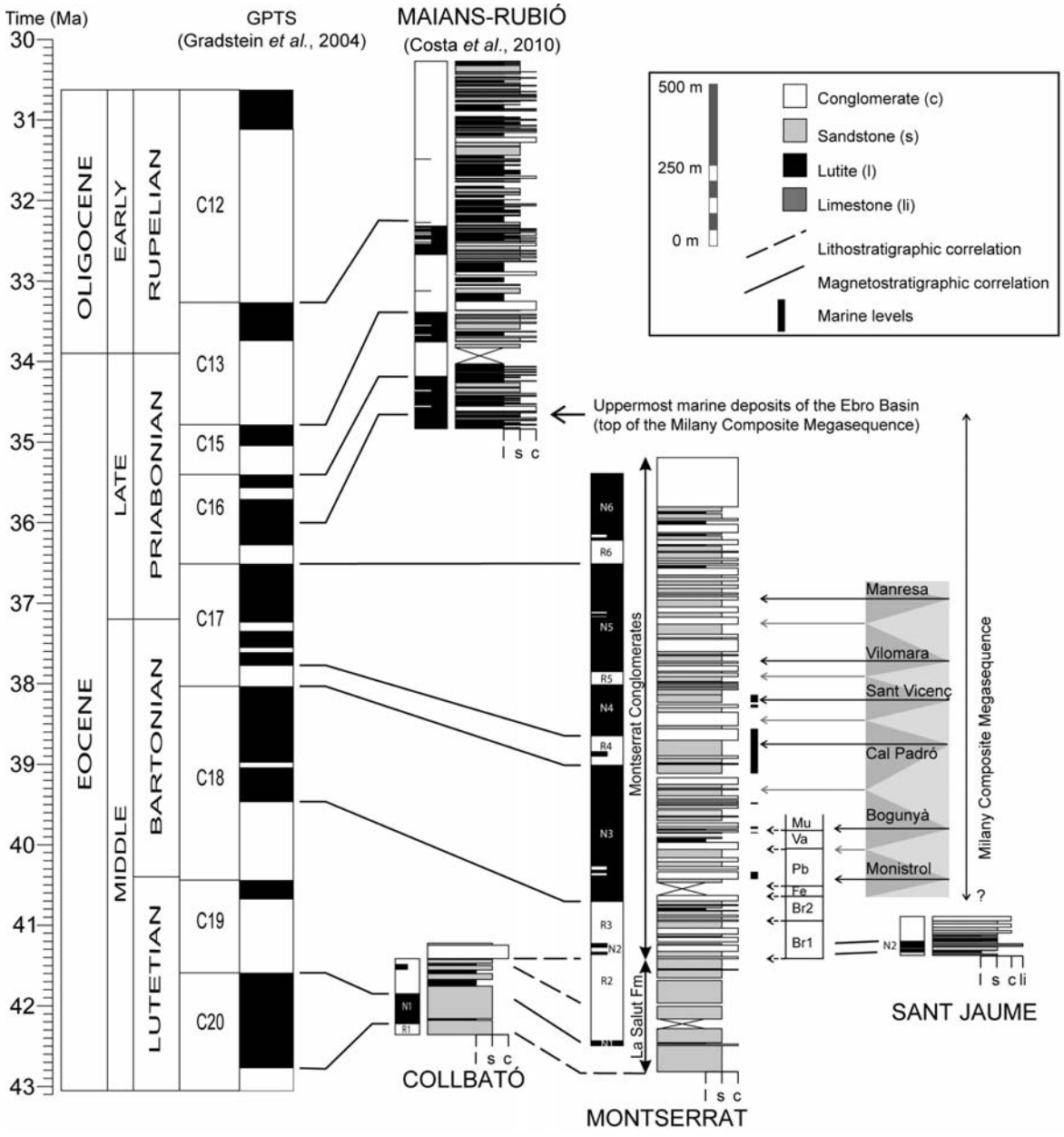

Fig. 6. Magnetostratigraphic correlation between the studied sections and the GPTS (Gradstein *et al.*, 2004). The Maians-Rubió section (Costa *et al.*, 2010) is also shown. Maximum flooding surfaces (black arrows) and basal sequence boundaries (grey arrows) of the different composite sequences are indicated. The lowermost Montserrat conglomeratic units are noted as Br1 (Les Bruixes 1), Br2 (Les Bruixes 2), Fe (Feixades), Pb (Pas de la Barra), Va (La Valentina), and Mu (Mullapans). The position of the top and base of each conglomeratic unit are denoted by dashed black arrows.

obtained considering constant accumulation rates through C16r+C16n.2n and C17n+C16r+C16n.2n give results of 35.6 Ma and 35.4 Ma, respectively. Therefore, the age of the top of the Montserrat Conglomerates is within C16n.2n, but the

magnetostratigraphic and geological information available is not enough to obtain a more precise date. The sedimentary record of this study represents approximately 7.2 Myr (from 43 to ~35.8 Ma).This new chronology challenges earlier results of López-Blanco *et al.* (2000a) since it indicates that the upper 330 meters of the Montserrat Conglomerates are Priabonian in age instead of Bartonian. Lithostratigraphic correlation with neighbouring areas (López-Blanco *et al.*, 2000b) shows that the top of the Vilomara composite sequence (Fig. 2c) corresponds to the boundary between the 1st and 2nd Bartonian cycles from Serra-Kiel & Travé (1995). Our results place this boundary within magnetozone N5 (C17n) (Fig. 6) and, therefore, indicate that the 2nd Bartonian cycle of Serra-Kiel & Travé (1995) is in fact of Priabonian age. These results are corroborated by new independent magnetobiostratigraphic dating of the uppermost marine sediments in the Ebro Basin (Costa *et al.*, 2010).

SUBSIDENCE ANALYSIS

Geohistory analysis is a quantitative approach used for studying the geological evolution of sedimentary basins (Van Hinte, 1978). The relative vertical movement of a stratigraphic horizon in a sedimentary basin, that is, the subsidence and uplift history of the basin since the horizon was deposited, can be determined. By subtracting the loading effect of the sediment and water, the tectonic component of the subsidence can also be obtained.

In the present work geohistory curves, based on local isostatic compensation, were calculated for stratigraphic intervals corresponding to magnetozones, so that absolute ages were directly derived from correlation with the GPTS (Gradstein *et al.*, 2004). Marine equations have been used, considering 3.3 and 1.0 g cm^{-3} for mantle and water densities. For subsidence analysis, a 1472.6-m-thick layer was added on top of the R6 magnetozone of the Montserrat section to account for the erosion since the end of deposition. The estimated thickness of this layer corresponds to the stratigraphic thickness between the top of the R6 magnetozone and the top of the Maians-Rubió section as estimated by Costa *et al.* (2010) and it is called Maians-Rubió in Table S2 (Supplementary Material). In addition to the age, present-day thickness and lithology, geohistory analysis requires a paleobathymetry estimate for each stratigraphic unit. Paleobathymetries of marine facies were estimated from their interpreted depositional environment. Where possible, paleoaltitude of continental deposits was estimated from their horizontal distance to their corresponding coastal sediments and the approximate paleoslope following estimates of alluvial and fluvial gradients presented by Blair & McPherson (1994). For subaerial deposits, as the position of their marine equivalents is unknown, a constant average paleoaltitude of 51 meters was considered according to Vergés *et al.* (1998). The uncompacted thicknesses of the stratigraphic units were calculated using an exponential relationship for changes in porosity with depth (Van Hinte, 1978) and the initial porosity and constant ***c*** values proposed by Sclater & Christie (1980). Table S2 (Supplementary Material) lists the input parameters for each interval considered and the resulting outputs, that is total and tectonic subsidences and decompacted thickness at successive stages in burial.

The resulting subsidence curves (Fig. 7) show the typical trend in foreland basins (Vergés *et al*., 1998), with a general increase of subsidence rate through time. However, closer inspection of the curves reveals three different stages in subsidence history. The first one corresponds to the lowermost La Salut Formation and is characterized by low mean tectonic and total subsidence rates (values below 10 cm/kyr), before 41.6 Ma. A second stage (from 41.6 to 39.5 Ma) initiates with a pulse of rapid subsidence followed by

steadily decreasing subsidence rates (from 42 ± 11 to 22 ± 6 cm/kyr for total subsidence). The third stage (from 39.5 to 36.3 Ma) is characterized by progressively increasing subsidence rates (up to 35 ± 3 cm/kyr for total subsidence). During this late stage, an increasing divergence between tectonic and total subsidence curves through time is depicted. This divergence indicates a progressive rise of the sedimentary load contribution to the total subsidence. In order to decipher real subsidence variations rather than changes in accommodation space, eustatic variations must be considered. The eustatic-corrected curves have been calculated by considering the mean sea-level variations established by Miller *et al.* (2005). The corrected and uncorrected curves yield nearly coincident subsidence trends, this indicating that the effect of absolute sea-level variations in the long-term accommodation changes was negligible. Then, total subsidence can be considered equivalent to accommodation during deposition of the Montserrat fan delta system.

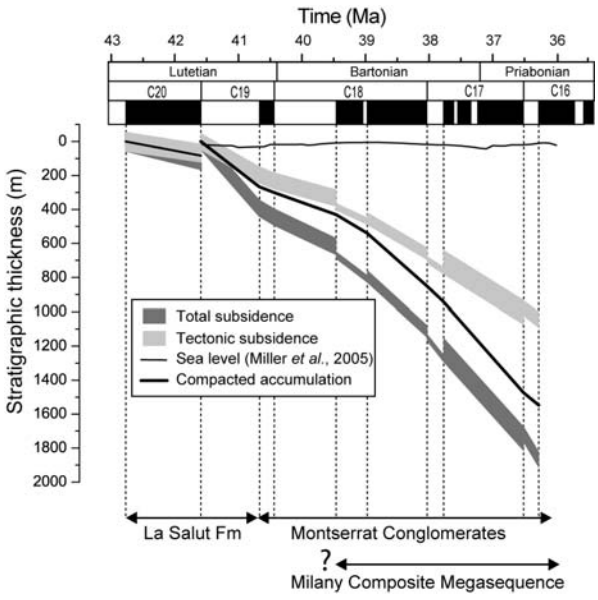

CONTROLS ON THE SEQUENTIAL ARRANGEMENT OF THE MONTSERRAT COMPLEX

One of the main goals of sequence stratigraphy is to investigate the interplay between factors controlling the arrangement of coastal sediments: accommodation space (governed mainly by eustatic and subsidence-driven sea level changes) and sediment supply (driven by climate and the tectonic evolution of the catchment basin). In this respect, assessing the periodic character of sedimentary sequences may reveal the presence of orbitally-driven climate forcing. Geohistory analysis can be used to decipher the total and tectonic subsidence changes in Montserrat. Altogether, these analyses can be used to investigate the tectonic and/or climatic controls on the sequential arrangement of the Montserrat complex.

Sequential arrangement in the time domain

Our new magnetostratigraphic study provides a chronological frame of the Montserrat sedimentary succession. Based on this the age and duration of the low, medium and high-frequency sedimentary sequences of the Montserrat complex (see section 2) can be obtained and the occurrence of relevant cyclicity in the Milankovitch frequency band can be tested. For dating purposes of the different stratigraphic levels constant accumulation rates within each magnetozone were considered.

Fig. 7. Subsidence history for the Montserrat area. Shaded areas around total and tectonic subsidence curves have been obtained from paleobathymetric estimates and indicate the error band associated to subsidence. The eustatic sea-level curve from Miller *et al.* (2005) and the compacted accumulation are also shown. Time scale after Gradstein *et al.* (2004).

The studied sediments constitute most of the Milany Composite Megasequence, its base being older than 39.2 Ma (age of the MFS of the Monistrol composite sequence, Figs. 2a and 6) and its top being dated to 36.0 Ma (Costa *et al.*, 2010). Then, a minimum duration for the Milany Composite Megasequence of 3.2 Myr can be deduced. Dating of composite sequences can be achieved by correlating their key surfaces with the Montserrat magnetostratigraphy (Fig. 6). Sequence boundaries are surfaces well constrained in the offshore region, but difficult to trace with precision into the conglomerate-dominated proximal areas of the Montserrat massif. On the other hand, MFS on top of the transgressive sequence sets are surfaces that can be best tied to the Montserrat magnetostratigraphic section. Stratigraphic position and magnetostratigraphy-derived age of six MFS associated to some of the composite sequences recognized in Montserrat (Fig. 2c) are presented in Table 1. Also are indicated the MFS-bounded sequence thickness, the duration of the different sequences (Δt), and the derived accumulation rates (m/Myr). An average duration of 481 ± 166 kyr is deduced. One of these, sequence nº 3, has a thickness and duration which exceeds significantly the values from the others. We noted the presence in this composite sequence of an out-of-sequence regressive event, which could be interpreted as sequence boundary, giving rise to an additional composite sequence between Bogunyà and Cal Padró. If sequence nº3 is taken as a double sequence, an average duration of composite sequences of 401 ± 67 kyr is found.

Finally, mean duration of the fundamental sequences can be estimated from the number of fundamental sequences present in a composite sequence and the duration of the corresponding composite sequence. The results obtained are not regular. The duration (and thickness) of fundamental sequences decreases from bottom to top of the Milany Composite Megasequence, being 96 kyr in chron C18n (N3), 44 kyr in chron C17r (R4) and 36 kyr in C17n (N4+R5+N5).

Origin of the T-R sequences

Milany Composite Megasequence

The lower and upper boundaries of the Milany Composite Megasequence have been interpreted as the response to the geodynamic evolution of the Pyrenees. The regional transgression (the so-called "Bartonian transgression") observed at its base has been related to the stacking of the Pyrenean antiformal stack, which led to the development of a basement-involving out-of-sequence thrust system that produced increased subsidence in the basin and a southwards displacement of the depocentres (Puigdefàbregas *et al.*, 1986). On the other hand, the end of marine conditions (Priabonian regression) at the top of the Milany Composite Megasequence has been related to the emplacement of allochthonous units in the western Pyrenees that favoured the isolation of the South Pyrenean Foreland Basin from the Atlantic Ocean (Coney *et al.*, 1996; Costa *et al.*, 2010).

The new chronological frame of the Montserrat succession allows assessing the relationships between the internal arrangement of the Milany Composite Megasequence, global sea-level changes and subsidence. In Figure 8 the global eustatic curve (Miller *et al.*, 2005) has been plotted together with subsidence rates of the Milany Composite Megasequence. It is shown that the rising sea-level stage is partly coincident with the transgressive composite sequence set and the falling stage with the regressive one (there is a 0.5 Myr mismatch between the Milany Composite Megasequence MFS and the maximum eustatic level). As above discussed, eustacy did not significantly contribute to long-term accommodation in

nº	MFS	stratigraphic level (m)	age (Ma)	sequence thickness (m)	Δt (My)	accumulation (m/Myr)
6	Manresa	1380	36.8	193	0.420	459
5	Vilomara	1187	37.2	121	0.307	394
4	Sant Vicenç	1066	37.5	135	0.368	366
3	Cal Padró	931	37.9	261	0.781	334
2	Bogunyà	670	38.6	154	0.528	292
1	Monistrol	516	39.2			

	duration (My)	standard deviation (My)
mean duration	0.481	0.166
mean duration (taking nº 3 as a double sequence)	0.401	0.067
mean duration (nº 3 excluded)	0.406	0.081

Table 1. Stratigraphic position of maximum flooding surfaces (MFS) associated to some of the composite sequences recognized in Montserrat (from Monistrol to Manresa). Also are indicated the magnetostratigraphy-derived age of the MFS, the MFS-bounded sequence thickness, the duration of the different sequences (Δt), and the derived accumulation rates (m/Myr).

in this sector of the basin, which was mainly controlled by subsidence. Under this scenario, a possible linkage between the eustatic curve and the sequential arrangement could be explained through climatically-induced changes in sediment supply.

Regarding the subsidence history of the Montserrat region (Figs. 7 and 8), the overall picture is that of relatively steady tectonic and total subsidence rates during the deposition of the Milany Composite Megasequence. In detail, however, a smooth shift in subsidence is recorded, first steadily increasing during transgressive conditions (C18n + C17r) and then slightly decreasing during the regressive episode (C17n). This suggests that tectonic-related subsidence variations exerted the prime control on T-R arrangement at this scale. Since eustatic variations are negligible at this scale, subsidence can be considered equivalent to accommodation. The transgressive sequence set of the Milany Composite Megasequence displays an aggradational stacking pattern which results from the balance between accommodation and sediment supply. During the regressive sequence set, the marked progradational trend indicates the effect of sediment supply rates exceeding accommodation (Fig. 8). Therefore, we envisage an scenario where the internal stacking pattern in transgressive and regressive sequence sets within the Milany Composite Megasequence can be explained as the result of subsidence-driven accommodation changes (first increasing and then almost constant) under a general increase of sediment supply. During the transgressive composite sequence set, sediment supply steadily increased in balance with accommodation. During the regressive composite sequence set accommodation rates stayed at constant to slightly decreasing values, which resulted in an overall shallowing-upwards evolution.

To produce the final progradational stacking pattern in the Montserrat and neighbouring systems, sediment supply must exceed accommodation, but a significant change in sediment supply trend is not required. This means that the alternate

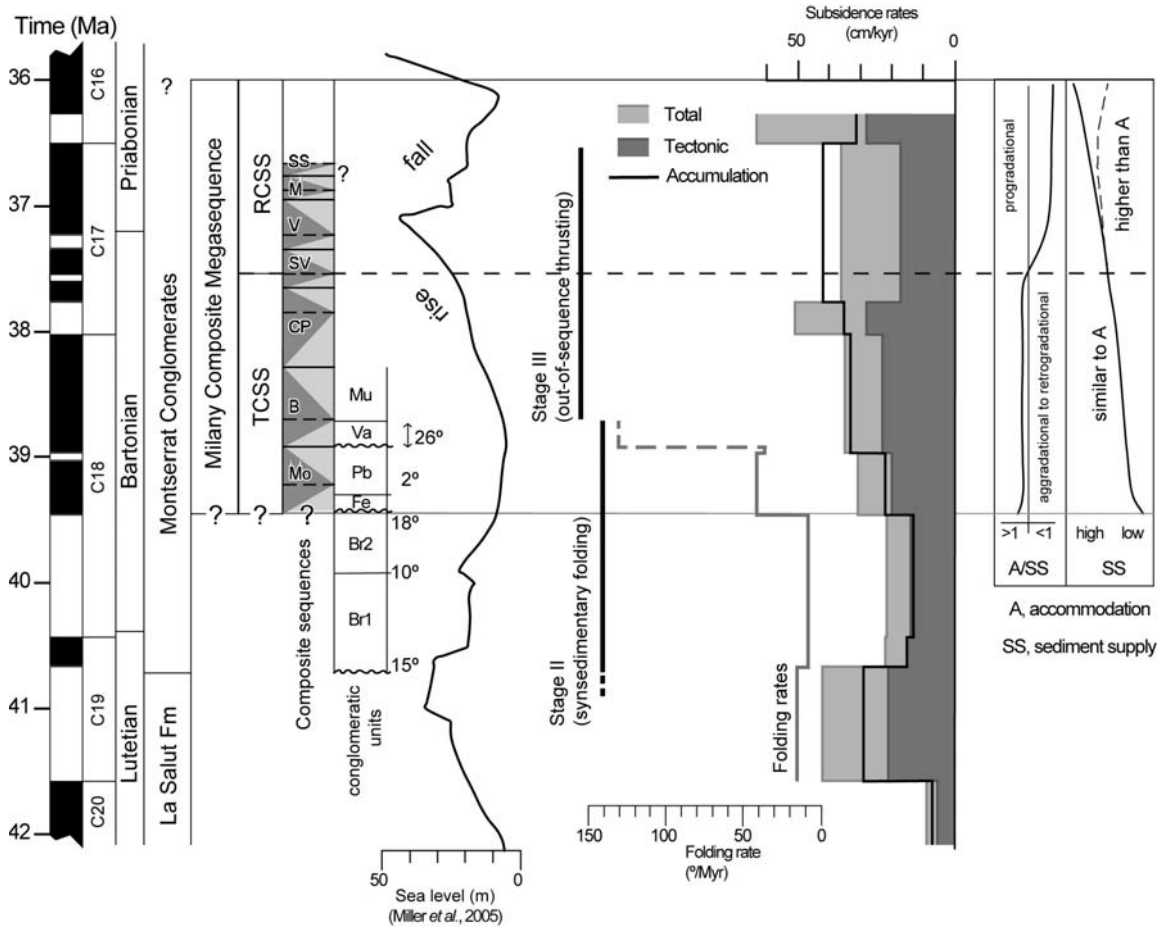

Fig. 8. Origin of the different scale T-R sequences. Different parameters related to the tectonic activity or to climate changes in the area are shown. TCSS (RCSS) indicates the transgressive (regressive) composite sequence set of the Milany Composite Megasequence. The composite sequences are noted as: Mo (Monistrol), B (Bogunyà), CP (Cal Padró), SV (Sant Vicenç), V (Vilomara), M (Manresa), and SS (Sant Salvador). The lowermost Montserrat conglomeratic units are noted as: Br1 (Les Bruixes 1), Br2 (Les Bruixes 2), Fe (Feixades), Pb (Pas de la Barra), Va (La Valentina), and Mu (Mullapans). Undulated lines represent unconformities. Rotation (°) associated with the unconformities, the conglomeratic unit boundaries and the rotation found within La Valentina conglomeratic unit are given. Time scale after Gradstein *et al.* (2004).

hypothesis of climatically-induced changes in sediment supply may not be relevant in this context. The unambiguous regressive nature of the upper part of the section resulting in 15 km of horizontal displacement of the coastline in approx. 1.5 Myr (López-Blanco, 1996; López Blanco *et al*., 2000b), its overall synchrony with an eustatic sea-level fall (Miller *et al.*, 2005), and the basinal character of the regression leading to the disconnection from oceanic basins (Costa *et al.*, 2010) point to a combination of local accommodation with other basinal or even global controls of the regression. Our results

differ from the earlier study of López-Blanco *et al.* (2000b) in which the Milany Composite Megasequence architectural arrangement was originally interpreted as being "supply-dominated".

Composite and Fundamental sequences

Composite sequences have been recognized, mapped and correlated in two different neighbouring complexes as Montserrat and Sant Llorenç del Munt (López-Blanco, 2006; López-Blanco *et al*.; 2000b). Therefore, composite sequences are not restricted to a single fan-delta system. The regional character of these units is not consistent with autogenic processes linked to single deltaic systems. Moreover, the physical field correlation of coastal sediments and alluvial deposits in these complexes (López-Blanco, 2006; López-Blanco *et al*., 2000b) shows that there is not a direct equivalence between composite sequences and alluvial fan retraction-progradation cycles in both Montserrat (Fig. 2c) and Sant Llorenç del Munt complexes. This indicates that composite sequences are not reflecting sediment supply changes affecting the proximal parts of the system. Then, an allocyclic and not supply-related origin for composite sequences must be considered.

The average duration of composite sequences (from 481 ± 166 kyr to 401 ± 67 kyr, see discussion above and Table 1) is consistent with an underlying control of deposition driven by the 400-kyr eccentricity cycle of the Earth orbit. Noteworthy, a magnetostratigraphy-mediated correlation of the Montserrat section with the eccentricity target curve (Laskar *et al.*, 2004) reveals a good match between MFS and times of eccentricity maxima, while SB correlate with eccentricity minima (Fig. 9). The only discordance comes from a missing eccentricity cycle at the level of the Cal Padró composite sequence (Fig. 9), which may explained by the presence of less pronounced regressive event, not taken originally as a sequence boundary. It is worth noting that the difficulties in establishing the sequential hierarchy at this particular interval may be linked to the occurrence of a 2.4-Myr eccentricity minima and its modulating effect in the amplitude of the 400-kyr eccentricity cycle (Laskar *et al.*, 2004).

The correlation of MFS and SB key horizons with the eccentricity curve (Fig. 9) suggests that composite sequences in Montserrat may well reflect orbitally-forced (Milankovitch) cyclicity. This implies that climatically induced sea-level fluctuations control the formation of these intermediate-scale sequences, a conclusion which is in agreement with a detailed stratigraphic study of the Vilomara composite sequence (Cabello *et al.*, 2010), where the vertical stacking pattern is interpreted as accommodation-driven. These conclusions challenge earlier studies in the area (López-Blanco, 1996; López-Blanco *et al.*, 2000b; López-Blanco *et al.*, 2006), where composite sequences were considered as non periodic. Other studies have already pointed to the role of 400-kyr eccentricity cycle as the pacemaker of 3rd order depositional sequences (Strasser *et al.*, 2000), with SB being developed at times of eccentricity minima, the same phase relationship as interpreted in this study. Furthermore, orbitally-driven cycles are also reported in Bartonian-Priabonian deltaic deposits from the South Pyrenean Foreland Basin (Kodama *et al.*, 2010), but there, sequences are interpreted as" supply-driven" and their correlation with eccentricity yielded an opposite phase relationship.

The lack of periodicity at a high order sequential arrangement in the sediments of Montserrat suggests that orbital forcing did not play a significant role in the formation of fundamental sequences. Our results indicate that fundamental sequences of longer duration developed under transgressive conditions while shorter duration sequences

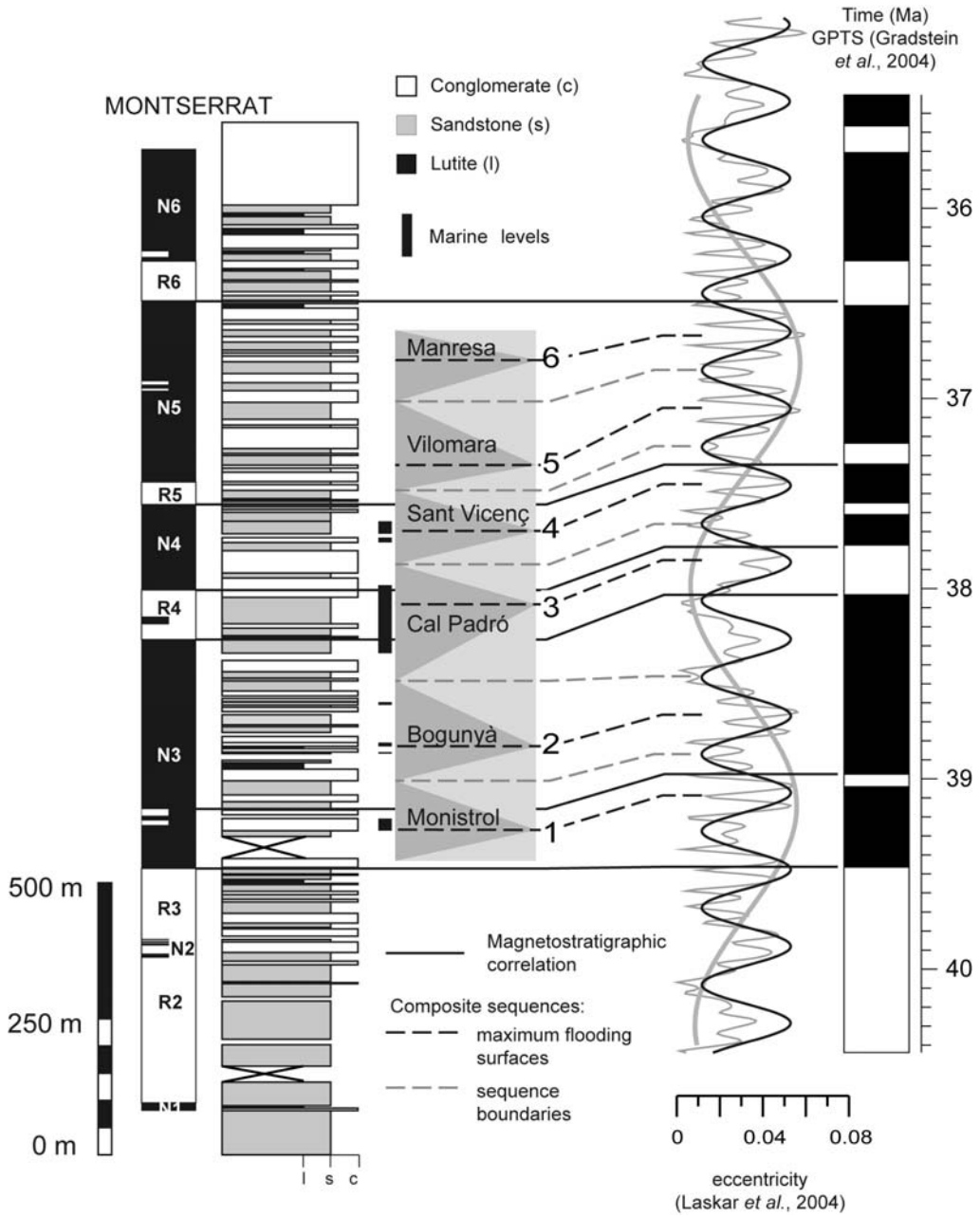

Fig. 9. Correlation of the composite sequences (López-Blanco *et al.*, 2000b) with eccentricity curve (Laskar *et al*., 2004). Numbers from 1 to 6 correspond to maximum flooding surfaces (MFS) labelled in Table 1.

developed under regressive conditions. This suggests that the long term T-R stacking pattern of the Milany Composite Megasequence controls the duration of fundamental sequences. It is plausible that under long term transgressive conditions, when accommodation is greater than sediment supply, autocyclic processes such as avulsion or lobe shifting occur at an average lower frequency than under

regressive conditions, when sediment supply rates are greater than accommodation.

TECTONOSEDIMENTARY EVOLUTION

Timing of the tectonosedimentary stages and deformation rates

The coupled evolution of the Montserrat complex and the CCR can be synthesized into three main stages linked to the evolution of the Prelitoral Fault (López-Blanco, 2002). The first stage, associated to the emplacement of shallow thrust wedges, is represented by El Cairat Breccia Formation which underlies the studied section (Figs. 2a and b). This early deformation event was followed by a period of relative quiescence before the re-activation of the structures that controlled the second and third stages. The second stage is characterized by synsedimentary fold growth, leading to the development of several unconformities in the lower Montserrat Conglomerates (up to the top of La Valentina conglomeratic unit, Fig. 10) in the area of Collbató. Two main folding episodes are revealed from the unconformity at the base of the Montserrat Conglomerates and the complex progressive unconformity developed between the top of Les Bruixes 2 and top of La Valentina units (Figs. 8 and 10). The third stage corresponds to major out-of-sequence thrusting (Prelitoral Thrust) and development of the large alluvial fans and fan-deltas of Montserrat and Sant Llorenç del Munt.

The timing of deformation and folding rates linked to the second and third stages of deformation can be derived from the magnetostratigraphic study. The lower part of the La Salut Formation reveals a clear constant thickness along the studied sections (Fig. 6), thus representing the pre-growth stage. As the upper La Salut Formation is unconformably truncated by the basal Montserrat Conglomerates, the oldest syn-growth sediments are post-lower La Salut Formation and pre-Montserrat Conglomerates. Our results yield an age of 40.9 Ma and 38.7 Ma for the oldest and youngest syn-fold deposits, respectively, which results in ~2.2 Myr duration for the growth strata**.** Field measurements estimate 71° of accumulated forelimb rotation between La Salut Formation and the Mullapans conglomeratic unit. This gives a minimum average forelimb rotation rate of 32.1 ± 3.4 °/Myr. However, forelimb rotation rates were not constant during this stage and show a general increasing trend reaching a maximum value of 130°/Myr during deposition of La Valentina conglomeratic unit (Fig. 8). These results give a similar kinematics of folding compared to other cases studied in the South Pyrenean front (Can Juncas fold in Vergés *et al.,* 1996). In contrast, average and maximum rotation rates are much higher in the Can Juncas fold (102°/Myr and 200°/Myr, respectively) compared to Montserrat.

The start of the third deformational stage is now magnetostratigraphically dated at 38.7 Ma. This stage is characterized by out-of-sequence thrusting related to the breakthrough of the Prelitoral thrust across the anticline-syncline pair generated during the second stage (López-Blanco, 2002). Probably the folding stopped as a consequence of the breaking through of the thrust. The end of this stage cannot be identified as there are no physical relations (cross-cutting unconformities) between the thrust and younger sediments of the Ebro Basin. However, a minimum duration of 2.2 Myr can be deduced dating the last syntectonic sediments cut by the fault (Les Morelles unit in Fig. 2a). Finally, it is worth noting that the horizontal displacement rates of thrust sheets obtained in the present study for the Prelitoral thrust (2.6 m/kyr) are similar to those found for the Himalayas, West Canada, Central Alps, Sierras Marginales (South-Central Pyrenees), and Eastern Pyrenees (Kukal, 1990; Vergés *et al.*, 1995; Meigs *et al.*, 1996).

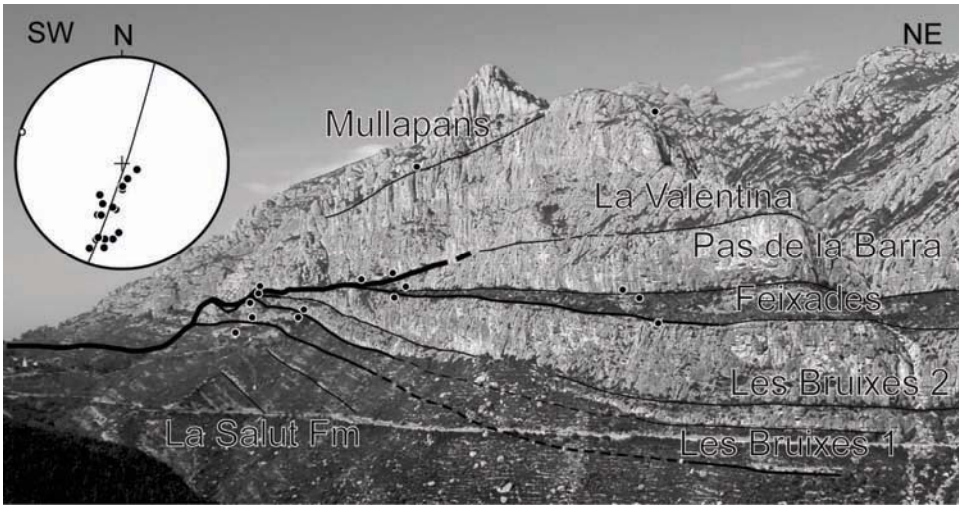

Fig. 10. Panoramic view of La Salut Formation, the lowermost Montserrat conglomeratic units, and the resulting progressive unconformity in Collbató area (labelled CB in Figs. 2a and b). Black dots in the outcrop image indicate the location of dip measurement sites. In the stereoplot, black dots represent S_0 values and white dot the fold axis (2/282).

Basin subsidence and tectonics

Subsidence changes in Montserrat section (Fig. 7) can be linked to the tectonic activity along the adjacent CCR. Subsidence curves display a convex-up shape with two inflection points reflecting episodes of subsidence acceleration. These inflection points are coeval with the development of syntectonic unconformities near the basin margin, and are thus interpreted as tectonic pulses during the growth of the anticline-syncline pair. The correlation between fold-growth (forelimb rotation) and subsidence (Fig. 8) indicates that times of fold growth and generation of unconformities near the basin margin represent tectonic load pulses, driving accelerated subsidence in more basinal areas.

Besides, it should be noted that growth of the CCR is the nearest but not the only contributor to the tectonic load in this region of the Ebro Basin. Influence of the Pyrenean foredeep flexure must be also considered in the subsidence analysis. To assess the variable contribution of tectonic loads from the CCR and the Pyrenees, a comparison of the results obtained for Montserrat with subsidence curves from other more basinal areas has been carried out (Fig. 11). The Castellfollit and Santpedor well-logs, located 10 and 23 km north from the basin margin, respectively (Vergés *et al.*, 1998), have been used. Tectonic subsidence curves were recalculated using our new age model and taking into account the age uncertainty of the Collbàs Formation. The results show similar trends for both sections with a first segment of low tectonic subsidence, with rates below 5 cm/kyr, followed by high subsidence rates (up to 26-31 cm/kyr), during the Late Bartonian-Priabonian (Fig. 11). The onset of high subsidence rates recorded in Montserrat at about 41.5 Ma is not recognized in Santpedor and Castellfollit, where low subsidence persisted until 40.4 and 37.7 Ma, respectively. These differences between marginal and more basinal sections point to a local source of load, linked to the tectonic deformation and growth of the CCR (Fig. 12). The onset of high subsidence rates in Castelfollit and Santpedor does not occur until deposition of the top of the Collbàs Formation, with an age ranging from 39.0 to

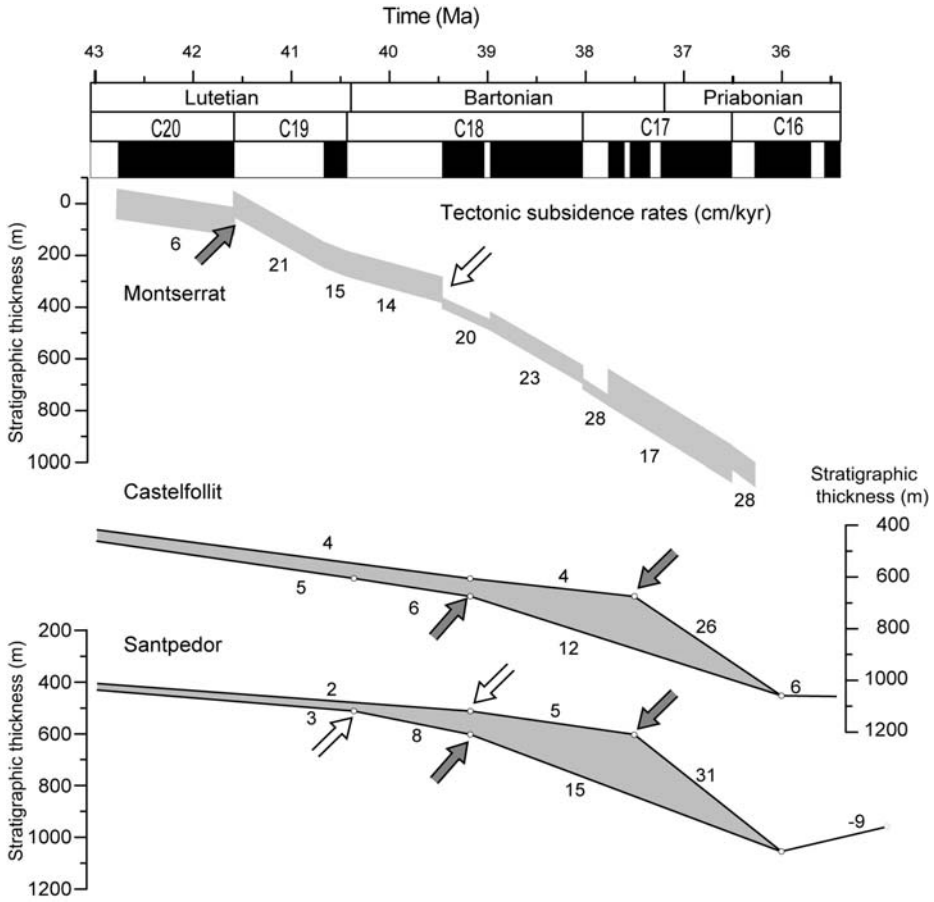

Fig. 11. Tectonic subsidence curves for the Montserrat section and the Castelfollit and Santpedor well-logs. Castellfollit and Santpedor curves include age uncertainties. The base of the Collbàs Formation has been considered to be located between the lower Bartonian (40.4 Ma) and the first transgression for the Montserrat area (39.2 Ma). Its top is located between the first transgression and the maximum flooding surface of the Milany Composite Megasequence (37.5 Ma). Subsidence rates (cm/kyr) are also indicated. Grey (white) arrows indicate strong (weak) breakpoints from low to high tectonic subsidence rates. Notice the 1 to 4 Myr delay for the onset of high subsidence rates in the "basinal" sections (Castellfollit and Santpedor) compared to Montserrat.

37.5 Ma. In other Ebro Basin sections located further north the initiation of high subsidence rates is recorded at progressively older ages, indicating the southwards migration of the South Pyrenean flexure (Vergés *et al.*, 1998). These facts support the presence of a double flexure in the Ebro Basin, associated to loading of both the Pyrenees and the CCR (Vergés *et al.*, 1998) during latest Lutetian and Bartonian times (Fig. 12). The double flexure favoured the presence of two subsiding depocentres, a fully marine sub-basin to the north and a southern continental depocentre that evolved to shallow marine conditions due to the increasing subsidence induced by the CCR tectonic activity. The above scenario changed during the Latest Bartonian and Early Priabonian, when subsidence rates in Castellfollit and Santpedor increased to

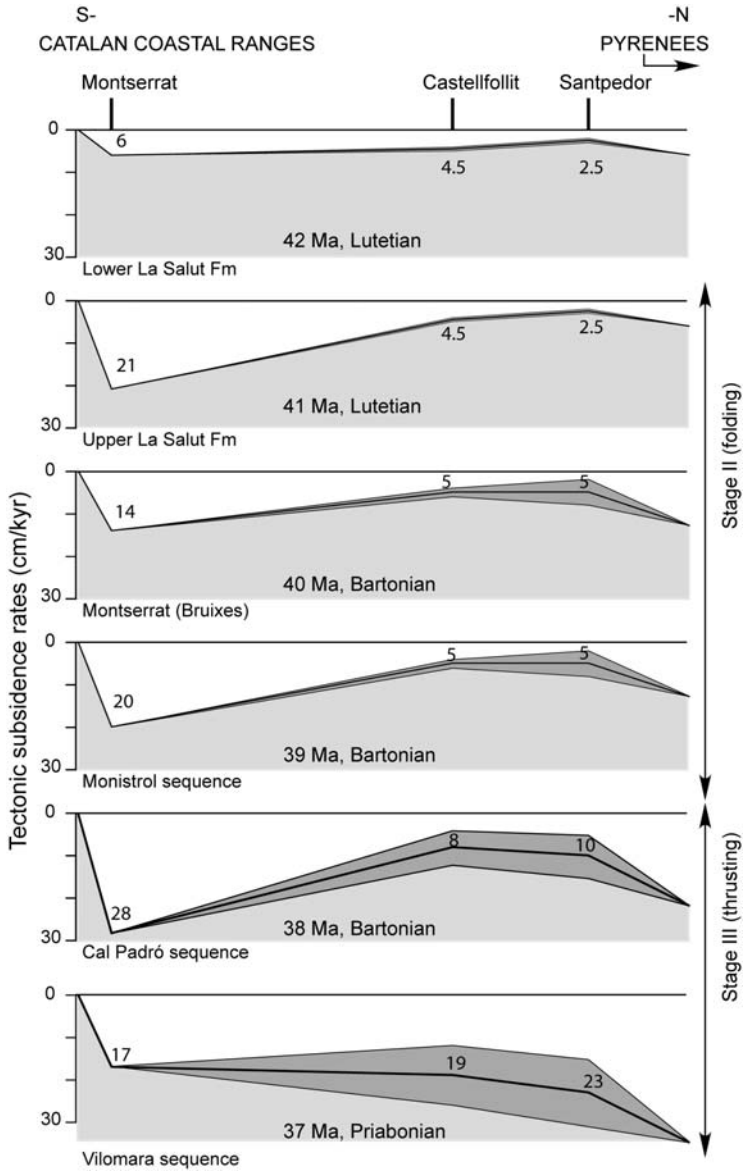

Fig. 12. Tectonic subsidence rates (cm/kyr) along a profile from the Catalan Coastal Ranges to central areas of the Ebro Basin. Subsidence values for the Montserrat section, and the Castellfollit and Santpedor well-logs have been plotted at intervals of 1 Myr, from 42 Ma to 37 Ma. Mean values are indicated and grey-shaded areas represent the corresponding errors.

values comparable to Montserrat (Figs. 11 and 12). This is interpreted as the result of the southwards displacement of the Pyrenean flexural wave related to the southwards transport of allochthonous thrust sheets (Vergés *et al.*, 1998). By that time, thrusting on the CCR was still active (López-Blanco, 2002), so that subsidence in Montserrat was dominantly controlled by local tectonics. The homogenization of subsidence values and change in sedimentary polarity of the basin is seen as the result of the coupling of the two sources of tectonic load: the CCR and the Pyrenees.

It is worth noting that the compacted accumulation rates obtained for Montserrat (up to 42 cm/kyr) are strikingly higher than average accumulation rates estimated (15 cm/kyr) in Priabonian to Oligocene synorogenic alluvial successions in other marginal areas of the SE Ebro Basin (Jones *et al.*, 2004; López-Blanco *et al.*, 2006;

Swanson-Hysell and Barbeau, 2007, as re-interpreted in Garcés *et al*., 2008; Costa *et al.*, 2010). These contrasting patterns of accumulation along the CCR-Ebro Basin foreland system may be related to differences in subsidence and, therefore, in the structural style. In Montserrat, characterized by a thick-skinned tectonic style, deformation was accommodated in a narrow belt with deep seated steep faults that created vertical stacking of basement units in a narrow zone. As a result subsidence was focused close to the mountain front. In other regions of the CCR, tectonic style was thin-skinned, with basinwards migration of the deformation front. In these cases, subsidence was distributed along a wider region ahead of the mountain front.

CONCLUSIONS

The magnetostratigraphic study of the Montserrat alluvial fan/fan-delta complex allows us to establish a new independent chronology of the Middle-Late Eocene Eastern Ebro Basin infill. The age of the La Salut Formation is established as Lutetian (C20r to C19r) and the Montserrat Conglomerates span from Upper Lutetian to Lower Priabonian (C19r to C16n). The new chronology, together with subsidence analysis, sequence stratigraphy, and cyclostratigraphic studies allows us to investigate the interplay between factors controlling the deposition of the studied sediments (accommodation space and sediment supply). The results suggest that the stacking pattern of the large-scale Milany Composite Megasequence can be explained as the result of subsidence-driven accommodation changes under a general increase of sediment supply. However, the megasequence boundaries themselves are responses to the geodynamic evolution of the Pyrenean chain, which in its turn had an influence in the basin configuration. The composite sequences in Montserrat are found to correlate with the 400-kyr eccentricity rhythm of the Earth's orbit, thus reflecting Milankovitch cyclicity, possibly driven by climatically-induced sea-level fluctuations. Nevertheless, the lack of periodicity at a high-order sequential arrangement suggests that orbital forcing did not play a prime role in the formation of high-frequency fundamental sequences, which are probably related with allocyclical processes (lobe-switching/lobe abandonment) whose frequency could be altered by large-scale variations in the accommodation vs. sediment supply rates.

In tectonically active basin margins, sediment supply and subsidence are usually considered as the main controls on sedimentary arrangement. In our study this assumption has been confirmed for large-scale (10^3 metres and 10^6 yr scale) sequences. However, at intermediate-scale sequences (10^2 meters and 10^5 yr scale) tectonic activity results in high subsidence and sediment supply rates favouring thick sedimentary successions where astronomical-related cycles are well developed and preserved. The location of subsiding depocentres close to the basin margin allowed the development of coastal facies (the ones that more easily reflect sea-level variations) depicting with their stacking pattern the orbital (eccentricity) cyclicity.

The geohistory analysis performed in Montserrat yields new insights on thrusting and folding histories of this area and shows a direct correlation between (tectonic) subsidence and forelimb rotation rates measured on the basin-margin deformed strata. These results suggest a tectonic load-driven subsidence for the lower half of the succession, corresponding to the synsedimentary folding stage (from 40.9 to 38.7 Ma). The two increasing (convex-up) cycles depicted by subsidence curves can be tied to two deformational episodes during the folding stage on the basin margin. Since both tectonic and total subsidence show a similar evolution through time, subsidence

on the upper part of the succession, corresponding to the out-of-sequence thrusting stage (from 38.7 Ma), is probably controlled by a relatively steady tectonic evolution. However, sedimentary load had a greater contribution to total subsidence during the last sedimentation stage.

Integration of subsidence curves from different sectors in the eastern Ebro Basin has unravelled the variable contribution of tectonic loads from the CCR and the Pyrenees. We suggest that the Middle to Late Eocene history of this region can be divided into three evolutionary stages:

1) Lutetian (~ 42 Ma): Relative passive margin experiencing low subsidence rates compared to the ones in the northern areas, where subsidence is related to the Pyrenean loading.

2) Late Lutetian-Late Bartonian (40.9 to 38.7 Ma): Highly subsiding active margin, leading to the development of a doubly verging flexure associated to the two tectonically active basin margins, the Pyrenees and the CCR.

3) Late Bartonian-Early Priabonian (38.7 to 36.5 Ma): High subsidence active margin grading into higher subsidence areas towards the basin. This configuration resulted from the coupling of two sources of tectonic load after the southwards migration of the Pyrenean flexural wave.

ACKNOWLEDGEMENTS

This manuscript is a contribution of the Institut de Recerca Geomodels and the Research Group of Geodynamics and Basin Analysis SGR 2009SGR1198, of the Agència de Gestió d'Ajuts Universitaris i de Recerca (AGAUR) de la Generalitat de Catalunya. It has been developed in the framework of the MCI projects REMOSS 3D/4D and CGL2007-66431-C02-02. Additional funding has also been provided by the Spanish Ministerio de Ciencia y Tecnologia and the ''Juan de la Cierva'' Fellowship Programme and by a CSIC JAE-Doc post-doctoral research contract (M. G-P). E.C. was funded by a FPI Grant of the Spanish MCyT. Thanks to the Laboratori de Paleomagnetisme (CCiTUB-CSIC). Sincere thanks are given to FGC and the Montserrat Natural Park for allowing and supporting the paleomagnetic sampling necessary for this work. We are also grateful to B. Horton, T. Lawton, D.L. Barbeau and an Anonymous reviewer, whose constructive criticism greatly improved this paper.

REFERENCES

Anadón, P. (1978) El Paleógeno continental anterior a la transgresión Biarritziense (Eoceno Medio) entre los ríos Gaià y Ripoll (Prov. de Tarragona y Barcelona). PhD Thesis, University of Barcelona, Barcelona, Spain. Abridged version in: *Est. Geol*, 34-5:341-440.

Anadón, P., Cabrera, L., Guimerà, J. & Santanach, P. (1985a) Paleogene strike-slip deformation and sedimentation along the southeastern margin of the Ebro basin. In: *Strike-Slip Deformation, Basin Formation and Sedimentation* (Ed. by K.T. Biddle and N. Christie-Blink), *Special Publication of the Society of Economic Paleontologists and Mineralogists*, 37, 303-318.

Anadón, P., Marzo, M. & Puigdefàbregas, C. (1985b) The Eocene Fan-delta of Montserrat (Southeastern Ebro Basin, Spain). In: *6th European Meeting Excursion Guidebook* (Ed. by M.D. Milà & J. Rosell), pp. 109-146. IAS/Institut d´estudis Ilerdencs.

Anadón, P., Cabrera, L., Colombo, F., Marzo, M. & Riba, O. (1986) Syntectonic intraformational unconformities in alluvial fan deposits, eastern Ebro basin margins (NE Spain). In: *Foreland Basins* (Ed. by P. Allen and P. Homewood), *Special Publication of the International Association of Sedimentologists*, 8, 259-271.

Anadón, P., Cabrera, L., Colombo, F., Marzo, M. & Riba, O. (1986) Syntectonic

intraformational unconformities in alluvial fan deposits, eastern Ebro basin margins (NE Spain). In: *Foreland Basins* (Ed. by P. Allen and P. Homewood), *Special Publication of the International Association of Sedimentologists*, 8, 259-271.

Blair, T.C. & McPherson, J.G. (1994) Alluvial Fans and their natural distinction from rivers based on morphology, hydraulic processes, sedimentary processes, and facies assemblages. *Journal of Sedimentary Research*, 64, 450-489.

Cabello, P., Falivene, O., López-Blanco, M., Howell, J., Arbues, P. & Ramos, E. (2010) Modelling facies belt distribution in fan deltas coupling sequence stratigraphy and geostatistics: The Eocene Sant Llorenç del Munt example (Ebro foreland basin, NE Spain). *Marine and Petroleum Geology*, 27, 254-272.

Cascella, A. & Dinarès-Turell, J. (2009) Integrated calcareous nannofossil biostratigraphy and magnetostratigraphy from the uppermost marine Eocene deposits of the southeastern pyrenean foreland basin: evidences for marine Priabonian deposition. *Geologica Acta*, 7, 281-296.

Choukroune, P.Y. & Séguret, M. (1973) Carte structurale des Pyrénées. Laboratoire de géologie structurale de l´Université des Sciences et techniques du Languedoc-Montpellier. *ELF-RAP*.

Coney, P.J., Muñoz, J.A., McClay, K.R. & Evenchick, C.A. (1996) Syntectonic burial and post-tectonic exhumation of the southern Pyrenees foreland fold-thrust belt. *Journal of the Geological Society*, 153, 9-16.

Costa, E., Garcés, M., López-Blanco, M., Beamud, E., Gómez-Paccard, M. & Larrasoaña, J.C. (2010) Closing and continentalization of the South Pyrenean foreland basin (NE Spain): magnetochronological constraints. *Basin Research*, 22, 904-917.

Ferrer, J. (1971) El Paleoceno y Eoceno del borde suroriental de la Depresión del Ebro (Cataluña). *Memoires Suisses de Paleontologie*, 90, 1-70.

Fisher, R.A. (1953) Dispersion on a sphere. *Proceedings of the Royal Society of London Series a-Mathematical and Physical Sciences*, 217, 295-305.

Garcés, M., Cabrera, L., Roca, E. & Gratacós, O. (2008) Comment on "The diachroneity of alluvial-fan lithostratigraphy? A test case from southeastern Ebro basin magnetostratigraphy" by N. Swanson-Hysell and D. L. Barbeau, Jr. *Earth and Planetary Science Letters*, 275, 181-186.

Gaspar-Escribano, J.M., García-Castellanos, D., Roca, E. & Cloetingh, S. (2004) Cenozoic vertical motions of the Catalan Coastal Ranges (NE Spain): The role of tectonics, isostasy, and surface transport. *Tectonics,* 23, TC1004.

Gradstein, F.M., Ogg, J.G. & Smith, A.G. (2004) *A Geologic Time Scale 2004*. Cambridge University Press, Cambridge.

Guimerà, J. (1988) Estudi estructural de l'enllaç entre la Serralada Ibérica i la Serralada Costanera Catalana. PhD Thesis, University of Barcelona, Barcelona, Spain.

Jones, M.A., Heller, P.L., Roca, E., Garces, M. & Cabrera, L. (2004) Time lag of syntectonic sedimentation across an alluvial basin: theory and example from the EbroBasin, Spain. *Basin Research*, 16, 467-488.

Kirschvink, J.L. (1980) The least-squares line and plane and the analysis of paleomagnetic data. *Geophysical Journal of the Royal Astronomical Society*, 62, 699-718.

Kodama, K.P., Anastasio, D.J., Newton, M.L., Parés, J.M. & Hinnov, L.A. (2010) High-resolution rock magnetic cyclostratigraphy in an Eocene flysch, Spanish Pyrenees. *Geochemistry Geophysics Geosystems*, 11, 1-22.

Kukal, Z. (1990) The rate of geological processes (Special Issue), *Earth-Science Reviews*, 28, 1-284.

Laskar, J., Robutel, P., Joutel, F., Gastineau, M., Correia, A.C.M. & Levrard, B. (2004) A long-term numerical solution for the insolation quantities of the Earth. *Astronomy & Astrophysics*, 428, 261-285.

López-Blanco, M. (1993) Stratigraphy and sedimentary development of the Sant Llorenç del Munt fan-delta complex (Eocene, southern pyrenean foreland basin, northeast Spain). In: *Tectonic Controls and Signatures in Sedimentary Successions* (Ed. by L. Frostick and R. J. Steel), *Special Publication of the International Association of Sedimentologists,* 20, 67-88.

López-Blanco, M. (1996) Estratigrafía secuencial de sistemas deltaicos en cuencas de antepaís: ejemplos de Sant Llorenç del Munt, Montserrat y Roda (Paleógeno, cuenca de antepaís Surpirenaica). *Acta Geologica Hispanica*, 31, 91-95.

López-Blanco, M. (2002) Sedimentary response to thrusting and fold growing on the SE margin of the Ebro basin (Paleogene, NE Spain). *Sedimentary Geology*, 146, 133-154.

López-Blanco, M., Marzo, M., Burbank, D.W., Vergés, J., Roca, E., Anadon, P. & Piña, J. (2000a) Tectonic and climatic controls on the development of foreland fan Deltas: Montserrat and Sant Llorenç del Munt Systems (Middle Eocene, Ebro Basin, NE Spain). *Sedimentary Geology*, 138, 17-39.

López-Blanco, M., Marzo, M. & Pina, J. (2000b) Transgressive-Regressive sequence hierarchy of foreland, fan-delta elastic wedges (Montserrat and Sant Llorenç del Munt, Middle Eocene, Ebro Basin, NE Spain). *Sedimentary Geology*, 138, 41-69.

López-Blanco, M., Garcés, M., Barberà, X. & Cabrera, L. (2006) Magnetostratigrafía de la sección de Vilanova de Prades y su implicación en la datación de estructuras de las Cadenas Costeras Catalanas (Paleógeno, margen SE de la Cuenca del Ebro). *Geotemas*, 9, 110-144.

Meigs, A.J., Vergés, J. & Burbank, D.W. (1996) Ten-million-year history of a thrust sheet. *Geological Society of America Bulletin*, 108, 1608-1625.

Miller, K.G., Kominz, M.A., Browning, J.V., Wright, J.D., Mountain, G.S., Katz, M.E., Sugarman, P.J., Cramer, B.S., Christie-Blick, N. & Pekar, S.F. (2005) The Phanerozoic record of global sea-level change. *Science*, 310, 1293-1298.

Muñoz, J.A. (1992) Evolution of a continental collision belt; Ecors-Pyrenees crustal balanced cross-section. In: *Thrust Tectonics* (Ed. by K.R. McClay), 235-246. Chapman & Hall, London.

Pallí, L. (1972) Estratigrafía del paleógeno del Empordà y zonas limítrofes. PhD Thesis. Universitat Autònoma de Barcelona, Barcelona, Spain.

Puigdefàbregas, C., Muñoz, J.A. & Marzo, M. (1986) Thrust belt development in the Eastern Pyrenees and related depositional sequences in the Southern foreland basin. In: *Foreland Basins* (Ed. by P. A. Allen & P. Homewood)*, Special Publication of the International Association of Sedimentologists*, 8, 229-246.

Puigdefàbregas, C. & Souquet, P. (1986) Tecto-sedimentary cycles and depositional sequences of the Mesozoic and Tertiary from the Pyrenees. *Tectonophysics*, 129, 173-203.

Riba, O. (1975) Le Bassin Tertiaire Catalan Espagnol et les gissements de Potasse. *IX Congr. Int. Sedimentologie (Nice). Livret-guide de l´excursion nº 20. Introduction.*, 9-13.

Sclater, J.G. & Christie, P.A.F. (1980) Continental stretching: an explanation of the post Mid-Cretaceous subsidence of the central North Sea basin. *Journal of Geophysical Research*, 85, 3711-3739.

Séguret, M. (1972) Étude tectonique des nappes et series décollées de la partie centrale du versant Sud des Pyrénées, caractère sedymentaire, ròle de la compression et de la gravité. PhD Thesis. University of Montpellier, Montepellier.

Serra-Kiel, J. & Travé, A. (1995) Lithostratigraphic and chronostratigraphic framework of the Bartonian sediments in the Vic and Igualada areas. In: *Field Trip C: Bioconstructions of the Eocene South Pyrenean Foreland Basin (Vic and Igualada Areas) and the Upper Cretaceous South Central Pyrenees (Tremp Area).Vii International Symposium on Fossil Cnidaria and Porifera* (Ed. by A. Perejón and P. Busquets), 11-14, Madrid.

Strasser, A., Hillgartner, H., Hug, W. & Pittet, B. (2000) Third-order depositional sequences reflecting Milankovitch cyclicity. *Terra Nova*, 12, 303-311.

Swanson-Hysell, N. & Barbeau, D.L. (2007) The diachroneity of alluvial-fan lithostratigraphy? A test case from southern Ebro basin magnetostratigraphy. *Earth and Planetary Science Letters*, 262, 343-362.

Van Hinte, J.E. (1978) Geohistory analysis. Application of Micro paleontology in exploration geology. *American Association of Petroleum Geologists Bulletin*, 62, 201-222.

Vergés, J. (1993) Estudi geològic del vessant Sud del Pirineu Oriental i Central. Evolució cinemàtica en 3D, PhD Thesis. University of Barcelona, Barcelona, Spain.

Vergés, J., Burbank, D.W. & Meigs, A.J. (1996) Unfolding: an inverse approach to fold kinematics. *Geology*, 24, 175-178.

Vergés, J., Marzo, M., Santaeulària, T., Serra-Kiel, J., Burbank, D.W., Muñoz, J.A. & Giménez-Montsant, J. (1998) Quantified vertical motions and tectonic evolution of the SE Pyrenean foreland basin. In: *Cenozoic Foreland Basins of Western Europe* (Ed. by A. Mascle, C. Puigdefàbregas, H.P. Luterbacher and M. Fernàndez), *Geological Society Special Publications*, 134, 107-134.

Vergés, J., Millán, H., Roca, E., Muñoz, J.A., Marzo, M., Cirés, J., Denbezemer, T., Zoetemeijer, R. & Cloetingh, S. (1995) Eastern Pyrenees and related foreland basins: precollisional, syncollisional and postcollisional crustal-scale cross-sections. *Marine and Petroleum Geology*, 12, 903-915.

APPENDIX OF CHAPTER 3.3:

SUPPORTING ELECTRONIC INFORMATION

Table S1 ChRM directions obtained for the Collbató, Montserrat and Sant Jaume magnetostratigraphic sections. Site No., name of paleomagnetic site and specimen code; X, Y and Z, UTM coordinates of paleomagnetic site (ED50 / zone 31N); Strat. level, stratigraphic position of the paleomagnetic sites in Collbató, Montserrat, and Sant Jaume sections; Dec. and Inc., declination and inclination in geographic (in situ) and stratigraphic coordinates (after bedding correction); MAD, value of the maximum angular deviation of the obtained ChRM directions; Quality, assigned quality of the ChRM directions after visual inspection of the Zijderveld plots (see Section 3 for further details); Dip Az. and Dip, azimuth of down dip direction of local bedding and angle of dip of local bedding; VGP Lat., latitude of the virtual geomagnetic pole used to build the local magnetostratigraphic sections (see Fig. 5).

Site No.	UTM coordinates (ED50 / zone 31N) X (m)	Y (m)	Z (m)	Strat. level (m)	Geographic coordinates Dec. (º)	Inc. (º)	Stratigraphic coordinates Dec. (º)	Inc. (º)	MAD (º)	Quality	Dip az. (º)	Dip (º)	VGP Lat. (º)
Collbató Section													
CB01-1A	402449.698	4603103.509	383	6.7	230.3	-9.8	232.4	28.4	18.5	2	34	40	-15.9
CB06-1A	402455.582	4603127.488	384	26.5	322.0	-46.5	277.7	-38.8	9.4	2	39	45	-8.7
CB08-1A	402463.894	4603125.525	388	33.9	295.1	-25.8	264.0	-27.5	8.8	2	22	43	-14.0
CB09-1A	402465.434	4603136.609	386	42.9	115.0	82.4	392.6	46.9	20.6	1	22	43	60.5
CB13-1A	402631.976	4603119.547	354	47.4	133.1	-64.5	174.4	-48.5	26.4	2	35	30	-77.6
CB10-1A	402462.756	4603144.047	392	48.1	69.2	68.4	399.9	30.7	8.1	1	22	43	47.9
CB15-1A	402629.247	4603123.286	356	51.2	56.7	44.4	410.8	16.0	14.9	2	35	30	34.4
CB11-1B	402461.466	4603151.468	391	54.5	316.8	19.8	323.1	-1.6	17.6	2	22	43	36.5
CB12-1B	402462.956	4603158.851	399	59.5	231.0	72.2	363.0	61.4	23.4	1	22	43	87.3
CB16-1A	402648.6	4603115.621	354	60.8	49.2	45.9	405.1	16.5	9.4	1	35	30	38.5
CB21-1A	402680.91	4603141.094	363	81.7	13.0	69.5	382.3	37.1	16.6	1	30	33	62.3
CB22-1A	402673.988	4603143.038	367	85.9	258.8	58.7	324.2	64.3	27.9	1	30	33	63.8
CB23-2A	402463.659	4603210.662	385	89.9	273.7	73.0	357.5	43.7	18.1	1	21	49	74.4
CB24-1A	402466.489	4603214.326	390	92	284.7	33.3	313.9	25.0	7.0	1	21	49	41.2
CB58-1A	402863.627	4603086.804	341	93.6	287.2	-12.6	282.6	2.1	7.4	2	32	49	10.2
CB25-1A	402468.176	4603205.88	395	94.3	335.7	59.5	358.4	17.0	9.9	1	21	49	57.7
CB26-1A	402484.477	4603208.53	396	95.9	332.3	28.1	338.9	-7.8	16.4	2	21	49	41.1
CB27-1A	402485.917	4603212.212	396	98.3	36.6	71.9	385.8	23.5	12.0	2	21	49	53.5
CB28-1A	402485.942	4603214.062	398	101	286.5	34.1	315.4	24.2	9.1	1	21	49	41.9
CB29-2A	402485.967	4603215.912	399	103	34.1	67.9	385.8	19.4	15.7	1	21	49	51.5
CB59-2A	402869.385	4603101.532	341	104.4	265.8	42.2	321.8	50.0	8.5	1	32	49	57.7
CB60-1A	402868.07	4603107.102	339	107.2	353.1	57.9	371.5	13.9	21.7	1	32	49	54.5
CB64-1A	402889.138	4603123.475	336	124.3	52.3	52.3	406.9	3.1	6.4	1	39	50	32.2
CB30-1A	402541.748	4603229.963	401	128	298.1	37.6	320.5	16.2	15.5	1	14	46	42.1
CB65-1A	402897.5	4603125.213	335	128.3	282.6	-44.9	259.3	-12.5	18.3	2	39	50	-12.2
CB66-1A	402910.031	4603126.894	335	136.3	249.9	-86.8	220.5	-37.3	9.6	1	39	50	-50.3
CB31-1A	402575.171	4603235.063	404	139	231.9	-43.3	220.4	-3.8	8.8	1	14	46	-36.6
CB32-1A	402578	4603238.725	401	141	220.7	-53.5	209.5	-10.2	6.8	1	14	46	-45.5
CB67-1A	402929.459	4603124.782	336	141.6	237.8	-79.8	222.3	-30.3	7.0	1	39	50	-46.0
CB33-1A	402579.289	4603231.305	409	142	202.9	-62.5	198.0	-16.7	5.1	1	14	46	-53.8
CB68-2A	402936.432	4603126.538	336	143.6	336.4	-79.2	231.8	-44.3	7.2	1	39	50	-45.0
CB37-2A	402701.691	4603238.903	411	176.2	258.4	-67.3	217.6	-31.6	22.6	2	14	46	-49.9
CB38-1A	402703.105	4603240.734	411	178.9	173.4	-25.1	174.3	18.5	21.5	2	14	46	-39.2
CB39-1A	402707.249	4603238.828	418	179.5	185.7	-63.2	189.8	-17.3	9.3	2	14	46	-56.7
CB40-1A	402776.724	4603237.889	417	200.5	124.0	-12.3	128.7	1.0	5.4	2	21	46	-27.8
CB41-1A	402778.113	4603237.87	418	202.2	228.5	-20.8	228.4	20.3	6.3	2	21	46	-21.9
CB43-1A	402784.986	4603232.225	421	204.9	289.6	22.2	306.2	15.7	11.2	2	21	46	32.2
CB46-1A	402801.685	4603233.849	422	212.5	222.1	53.7	365.8	65.9	32.3	1	28	58	81.7
CB47-1B	402776.849	4603247.14	422	221.7	271.9	-69.8	227.0	-21.8	19.1	2	28	58	-39.3
CB48-1A	402797.641	4603243.158	422	229	66.8	-27.0	119.4	-55.5	6.3	2	28	58	-43.3

Site No.	UTM coordinates (ED50 / zone 31N) X (m)	Y (m)	Z (m)	Strat. level (m)	Geographic coordinates Dec. (º)	Inc. (º)	Stratigraphic coordinates Dec. (º)	Inc. (º)	MAD (º)	Quality	Dip az. (º)	Dip (º)	VGP Lat. (º)
Montserrat Section													
EL001-1A	405294.179	4603180.253	121	1.3	182.2	-56.9	336.1	62.4	18.0	1	322	22	72.2
EL002-2B	405284.647	4603195.184	117	10.7	57.2	34.3	402.1	33.6	14.9	2	322	22	47.6
EL003-1B	405272.264	4603204.601	118	16.6	124.3	38.1	140.1	30.6	19.9	2	205	24	-21.7
EL004-1A	405252.957	4603215.96	120	23.8	176.8	-64.1	166.7	-53.7	4.2	1	322	22	-77.5
EL005-1A	405207.421	4603240.618	123	37.7	187.1	-46.3	193.5	-37.8	10.5	1	51	11	-67.1
EL007-1A	405167.174	4603244.851	116	47.3	223.9	-70.3	186.1	-57.0	6.3	1	330	22	-84.2
EL009-1A	405047.12	4603309.358	112	85.8	168.4	-79.8	162.6	-59.9	6.3	1	340	20	-76.9
EL011-1B	405018.967	4603387.461	120	105.8	199.6	-47.6	190.0	-31.2	5.7	1	340	20	-64.4
EL012-1A	405016.677	4603424.506	122	113.8	193.5	-42.9	186.5	-25.6	3.5	1	340	20	-61.9
EL013-1A	405008.585	4603443.12	116	117.7	207.1	-54.3	193.1	-39.0	4.4	1	340	20	-68.1
EL014-1A	405007.196	4603443.138	120	118.4	177.3	-68.8	169.2	-49.3	6.8	1	340	20	-76.1
EL015-2A	405008.149	4603515.304	122	132.0	196.9	-53.6	186.2	-36.5	5.5	1	340	20	-68.6
EL016-3A	404985.967	4603519.299	130	137.2	209.5	-60.1	192.0	-44.8	5.8	1	340	20	-72.4
EL017-1A	405008.785	4603563.415	131	142.7	207.4	-69.3	185.3	-53.0	8.9	1	340	20	-81.5
EL018-2A	405015.076	4603618.854	130	150.6	259.4	-57.4	228.8	-55.4	5.6	1	340	20	-52.0
EL019-3A	405011.813	4603687.374	123	157.0	212.8	-49.6	199.3	-35.7	8.5	1	340	20	-63.1
EL021-1A	405010.15	4603793.637	126	177.4	214.9	-46.6	202.1	-33.4	9.7	1	340	20	-60.4
EL022-1A	405013.818	4603839.108	125	179.5	127.4	-58.3	138.0	-40.3	3.5	1	340	20	-50.6
EL023-1A	405008.994	4603894.693	120	186.0	179.4	-46.1	174.8	-27.1	13.4	1	340	20	-63.0
EL024-1A	405006.704	4603931.738	121	192.7	224.2	-55.9	204.4	-44.2	7.7	1	340	20	-64.8
EL025-2A	405005.829	4603970.615	120	197.3	202.6	-48.4	192.0	-32.4	3.8	1	340	20	-64.4
EL026-1A	404981.774	4604043.111	119	212.4	257.7	4.5	258.7	1.4	11.8	2	340	20	-8.0
EL027-1A	404971.076	4604074.716	121	216.4	201.0	-55.6	188.3	-39.1	7.2	1	340	20	-69.9
EL028-3A	404956.185	4604104.523	116	220.3	227.7	-48.7	211.0	-38.5	12.0	1	340	20	-57.5
EL029-3A	404935.932	4604149.209	126	230.8	198.2	-49.1	190.3	-45.7	4.5	1	310	8	-73.7
EL030-1A	404920.919	4604169.766	115	233.4	209.8	-53.8	199.6	-51.8	3.5	1	310	8	-72.2
EL031-2A	404893.475	4604196.039	117	237.0	192.1	-43.1	186.1	-39.0	5.2	1	310	8	-70.4
EL032-2B	404863.45	4604237.152	114	242.0	207.6	-32.2	202.9	-30.2	5.9	1	310	8	-58.3
EL033-1A	404818.967	4604235.89	53	246.9	202.4	-28.2	198.5	-25.6	7.7	1	310	8	-58.1
EL034-2A	404815.559	4604293.308	128	250.8	221.7	-54.0	210.8	-53.6	4.6	1	310	8	-64.8
EL035-2A	404808.564	4604289.698	123	253.3	221.4	-59.1	208.2	-58.5	8.2	1	310	8	-68.5
EL036-1A	404764.572	4604325.445	115	255.3	223.9	-53.6	213.0	-53.5	9.2	1	310	8	-63.1
EL037-3A	404749.634	4604351.553	121	258.0	219.3	-25.4	215.5	-25.1	11.4	1	310	8	-48.4
EL040-2A	404635.66	4604558.495	111	277.4	227.5	-26.6	223.4	-27.4	21.6	2	310	8	-44.1
EL041-1A	404637.098	4604562.178	123	279.5	266.0	-36.8	261.3	-42.4	18.9	2	310	8	-22.1
EL042-2A	404636.446	4604617.709	158	287.8	257.0	-36.2	382.3	41.5	16.7	1	310	8	64.7
EL101-1A	404620.338	4604624.724	125	288.8	222.8	-28.9	218.4	-29.1	16.0	2	310	8	-48.0
EL043-1A	404617.66	4604667.928	138	298.0	226.8	-36.1	220.9	-36.7	15.6	1	310	8	-49.8
EL104-1A	404617.66	4604667.928	138	298.0	174.5	-35.8	170.9	-30.0	4.6	2	310	8	-63.3

Site No.	UTM coordinates (ED50 / zone 31N) X (m)	Y (m)	Z (m)	Strat. level (m)	Geographic coordinates Dec. (º)	Inc. (º)	Stratigraphic coordinates Dec. (º)	Inc. (º)	MAD (º)	Quality	Dip az. (º)	Dip (º)	VGP Lat. (º)
EL044-1A	404599.87	4604688.521	135	298.7	251.1	-8.1	249.8	-12.2	9.8	2	310	8	-19.2
EL106-1A	404578.189	4604724.353	120	302.5	209.8	-44.7	202.4	-42.8	5.9	2	310	8	-65.0
EL045-1A	404569.024	4604772.214	131	305.3	350.1	29.6	347.6	23.4	23.3	1	310	8	59.2
EL046-2A	404562.545	4604807.464	130	310.0	210.7	-16.2	208.5	-14.8	25.5	2	310	8	-48.0
EL109-1A	404562.545	4604807.464	130	310.0	313.9	60.8	313.0	52.8	10.5	2	310	8	52.3
EL110-1A	404547.166	4604819.547	123	313.7	199.2	-21.3	196.6	-18.3	5.2	2	310	8	-54.7
EL047-1A	404529.991	4604867.12	115	315.2	347.0	14.6	346.0	8.2	11.0	1	310	8	51.0
EL112-1A	404522.517	4604872.67	120	315.9	215.5	-45.3	207.6	-44.2	5.6	2	310	8	-62.4
EL113-2A	404509.343	4604870.12	122	316.6	245.1	-36.5	239.3	-39.6	5.6	2	310	8	-37.3
EL114-1A	404500.844	4604904.54	125	322.5	207.4	-24.5	204.0	-22.6	5.2	2	310	8	-53.5
EL049-1A	404472.851	4604958.565	122	328.0	112.7	-18.9	113.3	-11.2	6.6	2	310	8	-21.2
EL050-2A	404433.082	4604997.959	129	338.9	183.4	-28.2	180.3	-23.3	4.5	2	310	8	-61.2
EL051-2A	404397.604	4605046.549	140	349.8	252.4	-39.3	246.3	-43.2	13.5	2	310	8	-33.6
EL052-1B	404344.265	4605110.184	124	361.6	183.1	-30.5	179.7	-25.5	19.7	1	310	8	-62.4
EL053-2B	404300.109	4605132.981	130	369.8	220.8	16.1	223.1	15.8	18.9	2	310	8	-27.0
EL055-1A	404312.972	4605264.212	123	377.9	173.6	-44.8	168.9	-38.7	8.7	1	310	8	-68.7
EL056-1B	404332.582	4605380.548	128	383.3	170.9	-63.1	162.6	-56.7	18.9	2	310	8	-76.0
EL061-1A	404589.241	4605771.345	137	396.0	233.5	-35.8	227.6	-37.3	5.4	2	310	8	-45.2
EL062-1A	404523.528	4605844.397	131	405.8	215.6	-14.3	213.6	-13.6	12.5	1	310	8	-44.7
EL057-1A	404503.59	4605807.647	146	424.0	138.1	-60.4	136.6	-52.4	10.8	1	310	8	-54.8
EL060-1A	404478.44	4605796.877	179	444.1	253.7	28.0	256.9	23.4	9.9	2	310	8	-1.6
EL064-2A	404288.502	4606659.999	170	491.1	54.6	52.9	403.8	54.2	9.2	2	310	8	55.2
EL065-1A	404263.01	4606623.323	173	500.3	283.5	6.1	283.7	-1.0	15.9	2	310	8	10.0
EL066-1A	404005.007	4606650.824	208	515.6	342.9	55.8	337.6	48.8	24.1	1	310	8	68.6
CM002-1B	403834.198	4608002.302	161	531.7	208.2	-19.9	204.8	-22.5	12.2	2	280	9	-53.0
CM003-2A	403797.947	4607991.683	162	536.6	337.1	40.7	331.3	35.4	5.1	1	280	9	57.2
CM004-1B	403723.781	4607950.11	220	547.6	196.0	-29.3	190.9	-29.9	11.6	2	280	9	-62.8
EL068-2A	404018.026	4606689.516	210	563.2	345.3	63.0	338.1	56.2	6.2	2	310	8	72.5
CM008-1A	403595.381	4607800.07	187	574.1	41.9	41.5	394.3	45.8	5.4	1	280	9	58.6
CM009-1A	403979.825	4607987.399	781	588.6	336.4	41.0	330.7	35.6	10.7	1	280	9	56.9
CM010-1A	403521.138	4607752.947	198	593.4	241.6	15.6	242.8	8.5	7.1	2	280	9	-17.0
CM012-1A	403476.254	4607720.237	221	606.1	339.5	59.8	328.2	54.4	8.6	1	280	9	64.4
CM013-2A	403453.762	4607700.18	218	611.8	16.0	68.0	354.1	67.2	17.9	1	280	9	80.7
CM014-1A	403431.17	4607672.723	220	618.0	301.9	56.6	297.9	48.1	9.9	1	280	9	39.0
CM015-1A	403388.315	4607584.463	213	633.8	304.7	45.7	301.5	37.4	18.4	1	280	9	37.0
CM016-1A	403375.419	4607555.025	260	639.6	331.1	36.4	326.6	30.4	24.2	1	280	9	51.8
CM017-1A	403325.327	4607548.296	259	657.9	9.1	38.2	362.1	37.6	23.1	1	280	9	69.3
CM018-1A	403288.207	4607576.556	255	667.8	23.2	25.4	378.9	27.2	39.7	2	280	9	58.3
CM020-1A	403254.089	4607621.433	210	696.1	22.1	41.4	374.0	42.7	7.4	1	280	9	69.5
CM024-1A	403235.431	4607782.699	294	726.7	330.7	49.7	323.7	43.6	5.7	2	280	9	56.0
CM025-3A	403218.277	4607849.557	304	741.0	329.5	66.8	317.0	60.2	12.2	1	280	9	58.1

Site No.	UTM coordinates (ED50 / zone 31N) X (m)	Y (m)	Z (m)	Strat. level (m)	Geographic coordinates Dec. (º)	Inc. (º)	Stratigraphic coordinates Dec. (º)	Inc. (º)	MAD (º)	Quality	Dip az. (º)	Dip (º)	VGP Lat. (º)
CM027-1A	403269.024	4608008.038	321	753.0	359.3	66.8	340.8	63.7	9.3	1	280	9	75.6
CM028-1A	403201.873	4607971.927	319	768.3	303.8	74.8	295.3	66.3	10.2	2	280	9	45.2
CM030-2A	403108.763	4607967.63	324	788.0	339.7	57.0	329.4	51.8	12.8	2	280	9	64.1
CM031-1A	403102.02	4607982.527	337	789.9	358.2	81.1	319.2	76.1	6.3	1	280	9	57.8
CM032-1A	403057.785	4607997.93	329	795.7	37.8	29.2	392.9	33.1	10.2	1	280	9	53.4
CM036-3A	402785.343	4607775.819	348	855.6	10.5	63.1	353.3	61.8	11.5	1	280	9	84.9
CM038-1A	402726.66	4607852.495	366	875.3	196.8	-48.0	186.4	-45.6	3.0	2	295	10	-74.5
CM039-2A	402723.398	4607919.166	363	882.0	202.3	-30.2	196.6	-29.2	13.7	2	295	10	-60.3
CM040-1A	402723.724	4607943.221	362	886.1	228.5	-45.0	218.5	-48.2	11.3	2	295	10	-56.6
CM042-2A	402670.071	4607980.963	372	904.3	358.3	38.1	352.1	33.1	9.9	1	295	10	65.5
CM043-2A	402621.729	4607898.334	378	912.8	190.5	-57.2	176.9	-53.5	20.3	2	295	10	-82.1
CM044-2A	402563.666	4607815.837	381	921.0	221.6	-37.0	214.0	-39.2	8.3	2	295	10	-55.6
CM045-2B	402515.925	4607777.619	391	928.5	208.1	-46.5	197.6	-46.1	7.2	2	295	10	-69.9
CM046-1A	402483.232	4607722.54	389	933.5	207.0	-59.4	190.5	-58.3	6.6	2	295	10	-81.6
CM050-4B	402226.188	4607511.345	420	976.5	16.0	38.6	368.5	36.4	5.6	1	295	10	67.4
CM051-2A	402134.536	4607410.802	418	989.3	8.0	42.2	360.0	38.6	4.0	1	295	10	70.2
CM052-1A	402064.496	4607367.338	430	1001.5	11.3	48.3	361.2	45.1	14.5	1	295	10	75.0
CM053-1A	402005.11	4607392.207	427	1015.6	20.5	63.2	362.1	60.8	19.6	1	295	10	88.4
CM054-1A	402022.431	4607440.091	432	1022.8	58.5	49.9	407.1	54.6	6.9	1	295	10	53.0
CM055-1A	402026.597	4607541.825	450	1034.1	358.7	55.7	347.4	50.4	2.9	1	295	10	75.4
CM056-1A	402060.759	4607602.434	455	1041.4	295.1	28.6	295.1	18.6	3.4	1	295	10	25.0
CM057-1B	402076.59	4607642.935	457	1044.5	300.0	57.4	299.0	47.4	9.0	1	295	10	39.4
CM061-1A	402036.748	4607674.941	467	1063.4	332.9	54.0	326.0	45.8	10.6	2	295	10	58.8
CM064-1A	402011.702	4607671.581	471	1067.8	343.7	63.5	331.8	56.2	6.1	1	295	10	67.7
CM065-2A	402010.212	4607664.198	473	1070.1	350.5	50.2	342.0	44.0	3.6	1	295	10	68.3
CM067-2A	402012.611	4607636.404	481	1075.2	306.9	56.5	304.5	46.7	9.7	1	295	10	43.2
CM068-1A	401927.897	4607332.185	517	1077.8	4.8	58.5	351.3	54.1	3.0	1	295	10	80.2
CM069-2A	401913.859	4607321.272	503	1079.0	12.6	55.6	359.5	52.4	8.0	1	295	10	81.4
CM070-2A	401894.24	4607308.585	523	1082.8	331.7	62.6	322.9	54.2	12.8	2	295	10	60.3
CM073-2A	402730.052	4606462.531	657	1102.6	42.6	49.9	390.5	52.1	5.6	1	295	10	64.3
CM076-2B	402561.211	4606509.235	645	1125.1	234.5	-51.3	222.2	-55.4	8.6	2	295	10	-57.0
CM078-1A	402488.154	4606550.943	648	1131.9	225.8	19.0	228.6	15.1	6.2	2	295	10	-23.6
CM080-2A	402350.582	4606547.259	648	1139.6	100.6	50.5	96.6	60.1	4.2	2	295	10	21.8
CM082-1A	402187.628	4606617.952	638	1154.9	183.3	-8.4	182.2	-4.7	9.9	2	295	10	-50.7
CM083-1B	402163.892	4606609.021	621	1156.8	355.9	56.2	344.7	50.6	7.1	1	295	10	74.0
CM085-1A	402053.869	4606791.894	622	1175.4	329.4	58.9	322.1	50.3	4.1	1	295	10	58.0
CM086-1A	402049.98	4606812.306	637	1180.4	340.7	61.5	330.3	53.9	4.0	1	295	10	65.7
CM087-2A	402040.51	4606932.735	647	1192.5	322.6	36.0	319.8	27.1	4.3	1	295	10	45.9
CM088-1A	402026.749	4606942.176	655	1196.0	344.6	61.7	333.3	54.5	9.3	1	295	10	68.1
CM090-1A	401926.529	4606926.886	657	1212.7	215.3	22.1	219.1	19.9	11.5	2	295	10	-27.0
CM091-1A	401774.221	4607064.072	674	1223.1	24.8	63.9	365.2	62.3	3.8	1	295	10	85.7

Site No.	UTM coordinates (ED50 / zone 31N) X (m)	Y (m)	Z (m)	Strat. level (m)	Geographic coordinates Dec. (º)	Inc. (º)	Stratigraphic coordinates Dec. (º)	Inc. (º)	MAD (º)	Quality	Dip az. (º)	Dip (º)	VGP Lat. (º)
CM092-1A	401761.292	4607032.786	668	1225.4	309.9	61.2	306.3	51.5	6.0	1	295	10	46.7
CM093-1A	401692.288	4607166.985	660	1239.2	315.2	73.7	307.6	64.1	8.3	2	295	10	52.6
CM094-1A	401674.215	4607267.173	671	1257.8	350.5	51.5	341.6	45.3	10.1	2	295	10	68.9
CM095-1A	401670.378	4607291.285	673	1258.9	340.6	60.1	330.7	52.6	4.9	1	295	10	65.4
CM096-1A	401650.307	4607347.083	693	1268.1	17.5	58.3	362.4	55.8	3.1	1	295	10	84.4
CM097-1A	401639.629	4607378.693	684	1271.8	3.5	40.7	356.2	36.5	5.0	1	295	10	68.5
CM098-1A	401616.071	4607382.716	683	1275.9	60.0	43.3	411.1	48.5	7.8	2	295	10	47.3
CM099-1A	401595.697	4607416.309	684	1278.3	357.3	56.3	345.8	50.8	13.7	2	295	10	74.9
CM101-1A	401503.213	4607458.294	689	1287.3	346.5	33.4	342.0	27.0	7.1	1	295	10	58.5
CM102-1B	401548.964	4607452.114	692	1289.4	323.7	65.4	316.0	56.3	9.4	2	295	10	56.0
CM103-1A	401547.525	4607448.432	694	1290.8	325.6	52.1	320.3	43.3	13.6	1	295	10	53.5
CM104-1A	401540.556	4607446.677	698	1294.6	325.5	84.1	305.9	74.7	6.9	1	295	10	52.5
CM106-1A	401541.665	4607426.303	702	1299.8	38.0	68.9	371.8	68.9	4.7	2	295	10	76.6
CM107-1A	401223.505	4607016.097	527	1308.2	19.8	59.3	363.9	57.1	5.5	1	295	10	85.1
CM108-1B	401270.461	4607400.412	684	1313.9	341.5	72.2	325.6	64.3	8.1	2	295	10	65.0
CM109-1A	401221.307	4607462.163	684	1317.9	348.5	40.1	342.6	33.8	16.3	1	295	10	62.5
CM110-1B	401206.235	4607477.176	684	1321.3	331.1	36.4	327.4	28.2	9.8	1	295	10	51.3
CM111-1A	401304.848	4607375.88	707	1327.2	188.7	-64.8	170.9	-60.6	3.4	1	295	10	-83.2
CM112-1A	401306.262	4607377.711	717	1328.6	39.7	68.6	373.7	69.0	1.5	1	295	10	75.7
CM114-1A	401313.104	4607370.214	716	1331.1	8.6	48.8	358.6	45.2	3.0	1	295	10	75.1
CM115-1A	401318.43	4607353.484	672	1333.7	41.2	47.9	389.9	49.9	6.2	1	295	10	63.7
CM116-1A	401321.08	4607344.194	670	1335.5	223.5	-50.1	211.3	-52.4	18.0	2	295	10	-63.8
CM121-1B	401434.312	4607194.577	361	1347.2	341.0	44.9	335.0	37.6	10.2	2	295	10	60.6
CM122-1A	401432.695	4607177.943	361	1349.0	329.4	66.7	319.8	58.0	16.8	2	295	10	59.4
CM123-1A	401428.274	4607159.496	361	1350.5	344.9	57.1	335.2	50.0	22.7	2	295	10	67.4
CM124-1A	401431.026	4607157.607	361	1356.3	333.7	55.2	326.4	47.0	24.5	2	295	10	59.7
CM130-1A	401468.023	4607221.877	361	1365.2	16.5	39.3	368.7	37.3	12.2	1	295	10	68.0
CM135-1A	401520.977	4606930.581	365	1372.7	27.6	26.5	382.6	26.6	5.2	2	295	10	56.2
CM137-1A	401520.977	4606930.581	365	1375.9	346.6	50.6	338.5	43.9	6.3	1	295	10	66.2
CM141-1A	400014.297	4607562.142	685	1404.0	318.0	15.5	317.3	6.3	4.1	1	295	10	35.8
CM142-1B	399972.714	4607568.273	683	1407.0	347.5	39.1	341.9	32.7	7.1	2	295	10	61.6
CM144-1B	399316.347	4607908.729	640	1428.0	295.2	40.7	295.1	30.7	4.5	1	295	10	29.5
CM145-1A	399194.705	4607851.21	640	1432.7	346.4	38.6	341.0	32.1	7.9	1	295	10	60.8
CM146-1A	399107.346	4607957.333	635	1435.0	333.5	23.9	331.2	16.0	9.7	1	295	10	48.0
CM148-1B	399028.598	4608088.591	636	1453.0	24.5	33.3	378.0	32.7	15.4	2	295	10	61.7
CM149-1B	398997.39	4608140.852	630	1458.5	1.3	46.4	352.7	41.8	9.0	2	295	10	71.5
CM150-1B	398929.446	4608247.302	609	1470.5	52.2	61.1	393.7	64.4	9.7	2	295	10	65.5
CM151-1B	398914.902	4608299.329	623	1473.2	1.0	26.2	357.0	21.9	9.6	1	295	10	59.7
CM153-1B	398862.267	4608309.323	622	1481.5	323.9	19.7	322.6	10.9	13.8	2	295	10	40.9
CM155-1A	398836.856	4608280.068	631	1485.2	335.3	56.7	327.4	48.7	9.1	1	295	10	61.1
CM156-1A	398823.968	4608252.488	642	1489.8	190.0	49.3	201.8	50.8	6.6	2	295	10	-14.2

Site No.	UTM coordinates (ED50 / zone 31N) X (m)	Y (m)	Z (m)	Strat. level (m)	Geographic coordinates Dec. (º)	Inc. (º)	Stratigraphic coordinates Dec. (º)	Inc. (º)	MAD (º)	Quality	Dip az. (º)	Dip (º)	VGP Lat. (º)
CM157-1A	398813.804	4608221.168	636	1492.2	231.5	-6.3	230.2	-10.7	6.9	2	295	10	-32.6
CM158-1A	398802.2	4608186.166	637	1496.0	213.1	-24.7	208.4	-25.8	24.3	2	295	10	-52.7
CM168-1B	398526.304	4607729.213	661	1548.5	282.4	18.1	282.9	8.3	17.3	2	295	10	12.4
CM170-1A	398495.596	4607718.542	668	1553.5	224.3	-15.6	221.4	-18.8	7.9	2	295	10	-41.6
CM172-1A	398413.587	4607616.058	672	1559.7	193.8	-40.9	185.7	-38.4	6.8	2	295	10	-69.4
CM173-1A	398398.076	4607599.62	676	1563.2	76.2	51.5	426.4	58.9	10.9	2	295	10	40.9
CM174-1A	398347.297	4607544.815	686	1567.0	59.7	35.7	413.0	41.0	13.8	2	295	10	42.7
CM176-1A	398287.216	4607519.754	680	1572.0	208.5	-22.5	204.3	-22.9	11.6	2	295	10	-53.5
CM179-1B	398159.719	4607540.067	681	1589.0	328.4	50.9	322.9	42.3	3.9	1	295	10	54.9
CM181-1A	398094.896	4607572.45	672	1596.7	336.1	46.2	330.4	38.4	4.5	1	295	10	58.1
CM182-1A	398061.752	4607585.875	673	1601.5	332.1	55.3	325.0	47.1	4.2	1	295	10	58.7
CM183-1B	397960.351	4607585.464	695	1611.5	7.8	51.1	357.0	47.3	6.7	1	295	10	76.6
CM184-2B	397954.612	4607572.59	707	1612.9	348.4	47.0	341.0	40.6	5.8	1	295	10	65.7
CM185-1B	397925.766	4607595.209	690	1617.1	31.4	35.6	384.2	36.2	7.9	1	295	10	60.3
CM186-2A	397916.018	4607593.497	691	1619.2	5.2	51.1	354.6	46.9	10.2	2	295	10	75.8
CM188-2A	397840.74	4607574.208	706	1630.0	353.3	38.0	347.4	32.4	8.9	1	295	10	63.7
CM189-2B	397832.223	4607561.373	705	1633.7	337.5	40.0	332.7	32.4	4.3	1	295	10	56.5
CM190-1B	397815.348	4607546.807	714	1637.0	352.1	38.8	346.2	33.0	2.8	1	295	10	63.6
CM191-1A	397779.4	4607558.423	721	1640.4	344.6	49.6	337.0	42.7	4.7	1	295	10	64.6
CM192-1A	397766.955	4607562.302	701	1644.2	346.9	60.3	335.6	53.4	5.3	1	295	10	69.4
CM193-1A	397742.723	4607616.32	700	1650.5	12.6	54.1	360.2	51.0	19.1	2	295	10	80.0
CM194-2A	397701.194	4607626.165	701	1655.0	329.7	65.5	320.4	56.9	5.3	1	295	10	59.4
CM195-1B	397669.149	4607619.218	699	1659.9	336.2	34.7	332.3	27.0	3.2	1	295	10	53.7
CM196-2A	397615.613	4607566.308	714	1661.5	4.3	75.5	337.3	69.8	2.3	1	295	10	70.7
CM197-1B	397601.172	4607527.647	706	1664.7	327.8	65.5	319.0	56.7	3.6	1	295	10	58.3
CM221-2A	398299.242	4607290.086	779	1672.0	37.9	35.2	395.0	38.2	10.6	2	269	5	54.4
CM220-1A	398338.965	4607348.749	807	1691.3	328.1	64.7	319.9	61.8	6.7	1	269	5	60.6
CM222-1A	398401.775	4607173.887	818	1698.9	24.1	56.4	376.9	58.3	8.3	1	269	5	76.9
CM223-1A	398417.028	4606975.636	840	1714.1	38.2	55.7	392.0	58.7	7.3	1	269	5	65.7
CM224-1B	398485.683	4606919.143	846	1718.3	1.2	57.5	353.4	57.4	8.2	1	269	5	83.8
CM225-1A	398498.026	4606907.864	863	1730.0	349.9	54.4	343.3	56.6	20.0	2	232	5	76.4
CM226-1A	398513.329	4606909.499	866	1732.1	45.1	34.7	406.4	39.5	7.5	2	207	5	46.9
CM227-1B	398506.516	4606918.848	894	1751.4	5.1	53.2	356.2	56.3	9.0	1	245	7	84.4
CM228-1B	398512.359	4606939.125	896	1752.8	11.5	50.5	363.9	54.3	6.6	1	245	7	82.6
CM229-1A	398504.679	4606985.503	903	1757.6	13.4	48.0	366.4	55.2	10.4	2	228	9	82.3
CM230-1B	398522.103	4607038.93	915	1768.0	334.0	39.1	329.5	37.2	5.3	2	260	6	57.0
Sant Jaume Section													
SJ001-2A	410159.979	4604098.722	307	0.8	219.3	-48.8	207.0	-34.2	2.1	1	350	20	-57.6
SJ002-2A	410167.064	4604109.738	310	4.8	228.2	-68.7	201.6	-54.2	2.4	1	350	20	-71.7
SJ003-1A	410172.714	4604117.07	311	9.0	216.2	-55.6	202.0	-40.0	3.7	1	350	20	-63.7

Site No.	UTM coordinates (ED50 / zone 31N) X (m)	Y (m)	Z (m)	Strat. level (m)	Geographic coordinates Dec. (º)	Inc. (º)	Stratigraphic coordinates Dec. (º)	Inc. (º)	MAD (º)	Quality	Dip az. (º)	Dip (º)	VGP Lat. (º)
SJ004-1A	410176.974	4604124.42	312	11.0	332.2	76.4	342.2	56.8	9.5	2	350	20	75.7
SJ005-2A	410179.799	4604128.086	316	13.3	62.7	66.2	392.0	55.0	2.4	1	350	20	64.4
SJ006-1A	410181.327	4604139.171	311	16.5	43.7	67.4	380.2	52.2	4.6	1	350	20	71.7
SJ007-1A	410184.106	4604139.136	316	18.3	60.7	57.4	398.0	47.1	3.2	1	350	20	56.4
SJ008-1A	410179.961	4604141.039	315	20.5	195.5	-61.3	186.1	-42.5	1.2	1	350	20	-72.3
SJ009-2A	410184.268	4604152.09	312	22.0	184.1	-61.4	178.8	-41.8	1.0	1	350	20	-72.5
SJ010-1A	410181.512	4604153.974	314	24.5	55.6	72.3	381.8	58.5	3.1	2	350	20	73.3
SJ012-2A	410157.871	4604152.419	322	29.8	327.4	33.7	330.6	14.9	4.3	2	350	20	47.2
SJ013-2A	410163.59	4604165.302	319	33.0	234.3	-26.2	227.4	-16.5	4.6	2	350	20	-36.7
SJ014-1A	410160.858	4604169.038	321	35.3	349.9	54.3	349.8	34.3	4.8	2	350	20	65.6
SJ015-1A	410159.492	4604170.905	320	35.8	202.2	-61.3	190.4	-43.3	2.0	1	350	20	-71.5
SJ017-1A	410159.63	4604182.008	319	38.8	345.2	43.9	346.1	23.9	9.6	2	350	20	58.5
SJ018-1A	410156.875	4604183.893	323	41.0	27.2	64.0	372.5	46.5	9.2	2	350	20	72.8
SJ020-2A	410165.511	4604207.845	321	46.5	217.9	-59.5	201.3	-44.0	1.3	2	350	20	-66.4
SJ021-1A	410172.62	4604220.71	322	49.3	253.2	-40.7	237.7	-35.7	6.0	2	350	20	-36.9
SJ022-2A	410169.888	4604224.446	317	50.5	205.7	-26.2	202.0	-9.6	3.5	2	350	20	-48.4
SJ023-1A	410169.934	4604228.147	317	51.6	216.8	-44.8	206.4	-29.8	10.8	2	350	20	-55.8
SJ024-1A	410167.178	4604230.032	318	53.8	216.4	-60.3	200.0	-44.4	8.7	2	350	20	-67.4
SJ026-1A	410165.951	4604243.002	319	57.5	200.8	-55.6	191.3	-37.6	2.9	2	350	20	-67.4
SJ027-1A	410165.997	4604246.703	320	59.0	214.0	-51.5	202.0	-35.7	6.8	2	350	20	-61.3
SJ028-2A	410167.432	4604250.386	320	60.2	213.4	-63.6	196.4	-47.0	2.3	1	350	20	-71.1
SJ029-2A	410168.868	4604254.069	321	61.5	204.3	-38.5	198.2	-21.4	4.1	2	350	20	-55.6
SJ030-2A	410170.35	4604261.454	320	64.5	187.9	-42.6	184.2	-23.4	1.8	2	350	20	-60.4
SJ032-2A	410174.657	4604272.504	321	69.3	163.1	-44.0	164.5	-24.1	5.2	2	350	20	-58.0
SJ033-1A	410176.092	4604276.188	321	71.0	188.5	-58.8	182.2	-39.5	2.3	2	350	20	-70.8
SJ037-1A	410188.942	4604303.788	317	80.0	252.7	-40.7	237.3	-35.5	5.6	1	350	20	-37.1
SJ038-1A	410191.768	4604307.454	317	81.8	241.7	-41.0	227.9	-32.5	2.4	1	350	20	-42.7
SJ039-2A	410194.592	4604311.12	317	83.2	163.7	-70.9	166.6	-50.9	5.1	1	350	20	-75.4
SJ040-1A	410193.203	4604311.137	319	85.8	197.4	-44.4	191.4	-26.1	2.6	1	350	20	-60.5
SJ041-1A	410199.43	4604364.729	319	97.3	205.9	-52.3	195.8	-35.0	2.4	1	350	20	-64.0
SJ042-1A	410186.904	4604363.036	316	102.3	214.1	-36.6	206.8	-21.3	5.5	1	350	20	-51.5
SJ043-1A	410208.367	4604412.737	312	108.1	204.3	-43.1	197.1	-25.9	3.0	1	350	20	-58.3
SJ044-1A	410211.816	4604466.363	306	120.2	185.2	-43.2	181.9	-23.8	7.1	1	350	20	-60.8

Table S1: ChRM directions obtained for the Collbató, Montserrat and Sant Jaume magnetostratigraphic sections. Site No., name of paleomagnetic site and specimen code; X, Y and Z, UTM coordinates of paleomagnetic site (ED50 / zone 31N) ; Strat. level, stratigraphic position of the paleomagnetic sites in Collbató, Montserrat, and Sant Jaume sections; Dec. and Inc., declination and inclination in geographic (in situ) and stratigraphic coordinates (after bedding correction); MAD, value of the maximum angular deviation of the obtained ChRM directions; Quality, assigned quality of the ChRM directions after visual inspection of the Zijderveld plots (see Section 3 for further details); Dip Az. and Dip, azimuth of down dip direction of local bedding and angle of dip of local bedding; VGP Lat., latitude of the virtual geomagnetic pole used to build the local magnetostratigraphic sections (see Fig. 5).

Interval	Age	Present thickness	Density	Bathymetry		Total subsidence	Tectonic Subsidence	Decompacted thickness								
	(Ma)	(m)	(g/cm^3)	min (m)	max (m)	(m)	(m)	(m)								
								Ma:	40.67	40.44	39.46	39.98	38.03	37.77	36.51	36.28	31.10
Maians-Rubió(*)	*31.10*	*1472.6*	*2.58*	*-100*	*-10*	*3020.0*	*1573.0*										*1472.6*
C16r	36.28	72.9	2.60	-100	-10	**1879.4**	**939.7**									97.2	72.9
C17n	36.51	531.8	2.60	-100	40	**1805.2**	**902.6**								699.0	686.5	531.8
C17r	37.77	91.0	2.60	0	40	**1246.2**	**623.1**							130.3	110.7	108.9	91.0
C18n.1n	38.03	311.4	2.60	-50	20	**1136.2**	**568.1**						440.7	432.5	370.7	370.7	311.4
C18n.2n+1r	38.98	109.5	2.60	-20	20	**759.0**	**379.5**					163.2	146.0	143.5	128.0	126.1	109.5
C18r	39.46	129.7	2.60	-100	-2	**617.9**	**308.9**				195.8	188.4	169.3	166.4	151.3	149.1	129.7
C19n	40.44	34.1	2.60	-100	-2	**445.1**	**222.5**			52.2	50.2	48.4	44.3	42.9	39.1	39.1	34.1
C19r	40.67	267.0	2.60	-100	-2	**392.9**	**196.5**		392.9	392.9	371.9	359.1	335.9	330.6	306.3	301.8	267.0
				-100	-2	**0**	**0**		**392.9**	**445.1**	**617.9**	**759.0**	**1136.2**	**1246.2**	**1805.2**	**1879.4**	*3020.0*

Interval	Age	Present thickness	Density	Bathymetry		Total subsidence	Tectonic Subsidence	Decompacted thickness		
	(Ma)	(m)	(g/cm^3)	min (m)	max (m)	(m)	(m)	(m)		
								Ma:	41.59	36.1
Montserrat(*)	*36.10*	*1220.0*	*2.60*			*1303.00*	*776.0*			*1120.0*
Collbató (C20-N)	41.59	83.0	2.60	-100	-2	**104.00**	**66.0**		104.0	83.0
									104.0	*1203.0*

Table S2: Interval, intervals considered for subsidence analysis; Age, age (Ma); Present thickness, present thickness (m); Density, mean density (g/cm^3); Bathymetry, minimum and maximum bathymetries considered (m). Total subsidence, tectonic subsidence and decompacted thickness for each step calculation are given. *(*)*Data for Maians-Rubió and Montserrat are noted in italic because these layers was considered only for computation analysis (see text for explanation).

CHAPTER 3.4:

CHRONOLOGY OF THE CONTINENTAL UNITS OF THE VIC-MANRESA AREA:

"THE AGE OF THE "GRANDE COUPURE" MAMMAL TURNOVER: NEW CONSTRAINTS FROM THE EOCENE-OLIGOCENE RECORD OF THE EASTERN EBRO BASIN (NE SPAIN)"

Chapter 3.4 constitutes the third scientific paper of this PhD-Thesis: *Costa, E., Garcés, M., Sáez, A., Cabrera, L., López-Blanco, M., (2011). The age of the "Grande Coupure" mammal turnover: New constraints from the Eocene-Oligocene record of the Eastern Ebro Basin (NE Spain). Palaeogeography, Palaeoclimatology, Palaeoecology, 301, 97-107.* doi: 10.1016/j.palaeo.2011.01.005

Palaeogeography, Palaeoclimatology, Palaeoecology 301 (2011) 97–107

Contents lists available at ScienceDirect

Palaeogeography, Palaeoclimatology, Palaeoecology

journal homepage: www.elsevier.com/locate/palaeo

The age of the "Grande Coupure" mammal turnover: New constraints from the Eocene–Oligocene record of the Eastern Ebro Basin (NE Spain)

Elisenda Costa *, Miguel Garcés, Alberto Sáez, Lluís Cabrera, Miguel López-Blanco

Grup de Geodinàmica i Anàlisi de Conques (GGAC), Institut de Recerca GEOMODELS, Universitat de Barcelona, Spain
Departament d'Estratigrafia, Paleontologia i Geociències Marines, Facultat de Geologia, Universitat de Barcelona, Martí i Franquès s/n, 08028-Barcelona, Spain

ARTICLE INFO

Article history:
Received 4 February 2010
Received in revised form 11 January 2011
Accepted 12 January 2011
Available online 16 January 2011

Keywords:
Grande coupure
Fossil mammals
Eocene–Oligocene
Magnetostratigraphy
Ebro Basin
SW Europe

ABSTRACT

The Grande Coupure represents a major terrestrial faunal turnover recorded in Eurasia associated with the overall climate shift at the Eocene–Oligocene transition. During this event, a large number of European Eocene endemic mammals became extinct and new Asian immigrants appeared. The absolute age of the Grande Coupure, however, has remained controversial for decades. The Late Eocene–Oligocene continental record of the Eastern Ebro Basin (NE Spain) constitutes a unique opportunity to build a robust magnetostratigraphy-based chronostratigraphy which can contribute with independent age constraints for this important turnover. This study presents new magnetostratigraphic data of a 495-m-thick section (Moià-Santpedor) that ranges from 36.1 Ma to 33.3 Ma. The integration of the new results with previous litho- bio- and magnetostratigraphic records of the Ebro Basin yields accurate ages for the immediately pre- and post-Grand Coupure mammal fossil assemblages found in the study area, bracketing the Grande Coupure to an age embracing the Eocene–Oligocene transition, with a maximum allowable lag of 0.5 Myr with respect to this boundary. The shift to drier conditions that accompanied the global cooling at the Eocene–Oligocene transition probably determined the sedimentary trends in the Eastern Ebro Basin. The occurrence and expansion of an amalgamated-channel sandstone unit is interpreted as the forced response of the fluvial fan system to the transient retraction of the central-basin lake systems. The new results from the Ebro Basin allow us to revisit correlations for the controversial Eocene–Oligocene record of the Hampshire Basin (Isle of Wight, UK), and their implications for the calibration of the Mammal Palaeogene reference levels MP18 to MP21.

1. Introduction

The Grande Coupure was defined by Stehlin (1910) as a major faunal turnover affecting continental vertebrate faunas across Europe occurring close to the Eocene–Oligocene boundary. During this event, a large number of the European Eocene endemic mammals became extinct and new Asian immigrants appeared (Hooker, 1987, 1992; Berggren and Prothero, 1992; Prothero, 1994; Hooker et al., 2004). Only a few families (among them the rodents Theridomyidae and Gliridae) crossed the faunal divide undiminished. Several causes have been proposed as the triggering mechanism for the Grande Coupure; 1) climate deterioration at the Eocene–Oligocene transition (Hartenberger, 1973; Legendre and Hartenberger, 1992); 2) dispersal from outside the main European landmasses (as for instance, through the closing of the Turgai strait which connected continental Europe and Asia during the Eocene; Legendre, 1987; Berggren and Prothero, 1992; Janis, 1993; Prothero, 1994; Akhmetiev and Beniamovski, 2009); and 3) a combination of climate change (cooling) and competition following dispersal into Europe (Hooker et al., 2004). Most recent studies support the idea that climate exercised the prime control on faunal turnover (Joomun et al., 2008), as important crises are recorded in North America (Berggren and Prothero, 1992; Prothero and Swisher, 1992) and Asia (Meng and McKenna, 1998) at apparently the same age. However, despite the consensus among vertebrate palaeontologists on the correlation between the Grande Coupure and the Eocene–Oligocene transition, the precise absolute chronology of this crucial record of the Earth history has remained controversial for decades (Legendre, 1987; Tobien, 1987; Berggren and Prothero, 1992; Hooker, 1992; Legendre and Hartenberger, 1992; Köhler and Moyà-Solà, 1999; and references therein).

In this context, a relevant stratigraphic record is found in the Hampshire Basin of the Isle of Wight (UK), where stratigraphic superposition of marine and continental strata provide direct calibration points with the standard marine chronostratigraphy (Hooker et al., 2004). However, in spite of its ideal stratigraphic setting, the age of the Grande Coupure as recorded in the Solent Group

* Corresponding author. Departament d'Estratigrafia, Paleontologia i Geociències Marines, Facultat de Geologia, Martí i Franquès s/n, 08028-Barcelona, Spain. Tel.: +34 93 4034888; fax: +34 93 4021340.
E-mail addresses: elicosta@ub.edu (E. Costa), mgarces@ub.edu (M. Garcés), a.saez@ub.edu (A. Sáez), lluis.cabrera@ub.edu (L. Cabrera), m.lopezblanco@ub.edu (M. López-Blanco).

0031-0182/$ – see front matter © 2011 Elsevier B.V. All rights reserved.
doi:10.1016/j.palaeo.2011.01.005

has left contrasting results (Hooker et al., 2004, 2007, 2009; Gale et al., 2006, 2007). There, the correspondence between the Grande Coupure and the Eocene–Oligocene transition as proposed by Hooker et al. (2004) was subsequently challenged after an integrated magnetostratigraphy and cyclostratigraphy analysis (Gale et al., 2006), yielding a substantially different age (>2 Ma younger) for the Grande Coupure. Results of Gale et al. (2006) were questioned (Hooker et al., 2007) and, more recently, its magnetostratigraphic correlation re-interpreted (Hooker et al, 2009).

The late Eocene–Oligocene sedimentary record of the central areas of the Eastern Ebro Basin (NE Spain) fully meets the basic requirements of stratigraphic continuity, steady sedimentation, and mammal sites occurrence to build a magnetostratigraphy-based high-resolution continental chronology, as a tool to reliably link marine and continental time scales. In this paper, a new precise chronology across the continuous Eocene–Oligocene continental record in the Ebro Basin is provided. The new chronology further supports the close correlation between the dramatic terrestrial faunal turnover known as the Grande Coupure and the global climate changes that occurred at the Eocene–Oligocene transition.

2. Geological and stratigraphical setting

2.1. The Ebro Basin

The Ebro Basin (Fig. 1 A) represents the latest evolutionary stage of the South Pyrenean foreland system, formed as a result of the collision between the Iberian and the European plates (Muñoz, 1992; Vergés et al., 2002). The basin infill is dominated by continental sediments, interfingered by two widespread marine units of Ilerdian and Lutetian–Bartonian age (Ferrer, 1971; Riba et al., 1983; Puigdefàbregas and Souquet, 1986; Puigdefàbregas et al., 1986; Serra-Kiel et al., 2003; Pujalte et al., 2009). Marine connection of the Ebro Basin was maintained until the Priabonian (Costa et al., 2010), when the tectonic uplift of the western Pyrenees led to the closing of the basin drainage. Since then, uninterrupted late Eocene to middle Miocene continental sedimentation progressively filled the basin and eventually, backfilled onto the thrust-belt margins (Riba et al., 1983; Coney et al., 1996). In the central areas of the basin, this sedimentation was continuous and consisted of lacustrine deposits interfingering red clastic intervals that correspond to the medial-distal parts of fluvial fans draining from the basin margins (Anadón et al., 1989; Arenas et al., 2001; Luzón et al., 2002; Ortí et al., 2007; Sáez et al., 2007; Cuevas et al., 2010).

In the Eastern Ebro Basin, the late Eocene–Oligocene continental succession overlies marine sediments of the Santa Maria Group (Ferrer, 1971; Pallí, 1972; Serra-Kiel et al., 2003) and the halite-dominated Cardona Formation (including its lateral equivalents La Noguera, Artés, and Òdena evaporitic units) (Fig. 1B and C). Integrated calcareous nannofossil and magnetostratigraphic data from the youngest marine units have yielded a Priabonian age (Cascella and Dinarès-Turell, 2009), and the marine-continental transition has been precisely dated at ~36.0 Ma based on magnetostratigraphy (Costa et al., 2010). After the basin closure (Fig. 1B), the lower continental record in the study area corresponds to the Montserrat-Igualada

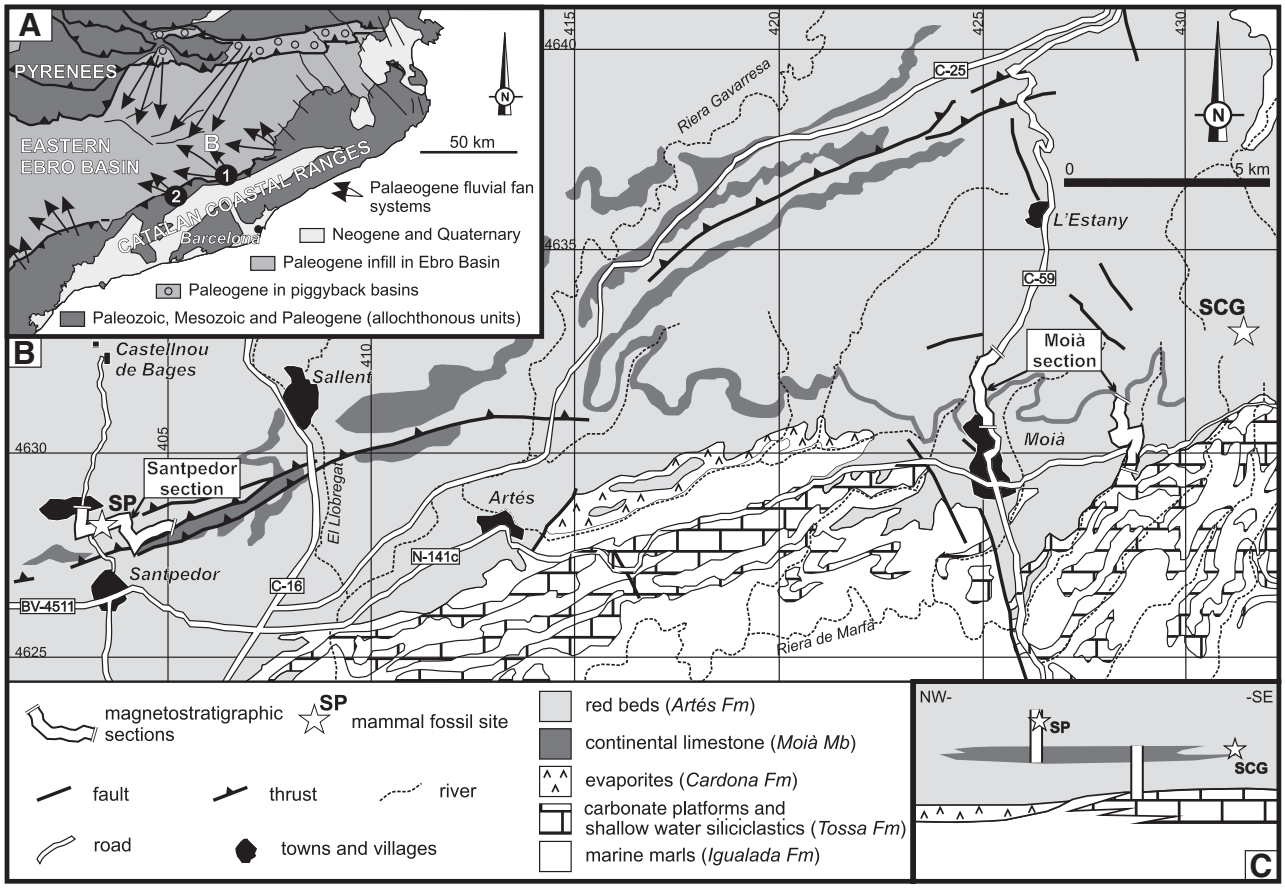

Fig. 1. Geological setting of the Moià-Santpedor composite section. (A) geological map of the Eastern Ebro Basin showing the main fluvial fan systems. 1: Montserrat-Igualada fluvial fan. 2: Montclar-Rocafort fluvial fan. B: location of the detailed geological map of the study area. (B) detailed geological map of the study area and (C) stratigraphy sketch of the SE margin of the Ebro Basin. The Moià and the Santpedor sampled sections are shown and the Sant Cugat de Gavadons (SCG) and Santpedor (SP) fossil assemblages are indicated with a white star symbol. A complete faunistic list for these localities is available at Agustí et al. (1987), Anadón et al. (1987, 1992), Sáez (1987), Arbiol and Sáez (1988). The lithostratigraphic correlation between the Moià and the Santpedor sections was established using the distinctive limestone beds of the Moià Limestone Member (Based in Sáez, 1987; Sáez et al., 2007). Map coordinates are in UTM projection, ED50 / zone 31.

fluvial fan (Sáez, 1987; Fig. 1A for location) that comprises the alluvial sediments of the Artés Formation (Ferrer, 1971) and the lacustrine limestones of the Moià Member of the Castelltallat Formation (Sáez, 1987; Sáez et al., 2007). Late Eocene (Sant Cugat de Gavadons) to Early Oligocene (Santpedor) vertebrate fossil assemblages have been reported in the basal sediments of the Artés Formation (Agustí et al., 1987; Anadón et al., 1987, 1992; Sáez, 1987; Arbiol and Sáez, 1988). Younger units south westwards have provided a complete Oligocene magnetostratigraphic record which contributed to the age calibration of the Western Europe MP mammal biochronology (Barberà, 1999; Barberà et al., 2001).

2.2. The Moià-Santpedor composite section

The medial-distal fluvial fan deposits of the Artés Formation consist of about 1000 m of red mudstones with some intervals of fluvial channel sandstones. One of these sandstone intervals is the Santpedor sandstone unit (Sáez, 1987). The Santpedor sandstone unit is composed of amalgamated incised channelled sandstone to gravelly sandstone beds, sourced from the Catalan Coastal Ranges (Sáez, 1987). This competent unique 20-m-thick coarse-grained unit is a continuous and extensive (traceable over most of the eastern margin of the Ebro Basin) key bed despite its variable thickness due to its erosive fluvial origin. Also intercalated into the Artés Formation, the 100-m-thick Moià Member consists of decimetre to metre-thick beds of lacustrine micritic limestone gently dipping <10° to the NW. In this sedimentary record, two sections (Moià and Santpedor) were sampled for magnetostratigraphy. A solid correlation between sections was established using the limestone key beds present in the Moià Member, yielding a 495-m-thick composite succession (see Fig. 1B and C).

Mammal biochronological constraints within the studied sections include the Late Eocene site of Sant Cugat de Gavadons and the Early Oligocene site of Santpedor (Fig. 1B and C). The Sant Cugat de Gavadons fossil site is located 4 km NE from Moià and can be correlated with the studied section according to Anadón et al. (1987). Its faunal assemblage is included in the *Theridomys golpeae* Biozone of the local biozonation of the Ebro Basin, and correlated to the pre-Grande Coupure MP19–20 European reference level (Agustí et al., 1987; Anadón et al., 1987, 1992; Sáez, 1987; Arbiol and Sáez, 1988). More recently, Hooker et al. (2009) suggested an alternative correlation of the Sant Cugat de Gavadons, as well as the Rocafort de Queralt (Anadón et al., 1987), with MP18, arguing that none of the taxa in these sites is diagnostic of the MP19–20, and most of them range at least from the MP18 to the MP20.

Of particular relevance for this study is the Early Oligocene (MP21) fauna of Santpedor. According to Agustí et al. (1987), Anadón et al. (1987, 1992), Sáez (1987), and Arbiol and Sáez (1988) the Santpedor fossil site contains *Theridomys* aff. *aquatilis*, *Gliravus* aff. *priscus*, *Pseudoltinomys gaillardi*, *Eucricetodon atavus*, *Plagiolophus annectens*, *Palaeotherium medium* and an undetermined Anoploteridae. This fossil site is directly located in the upper part of the Santpedor section only a few meters above the Santpedor sandstone unit (Figs. 1B and C).

3. Palaeomagnetic analysis

3.1. Sampling and methods

A total of 191 palaeomagnetic sites were sampled at a mean resolution of about 2.6 m, which is sufficient to allow a complete identification of the Upper Eocene–Lower Oligocene geomagnetic polarity reversals considering mean accumulation rates of about 10–15 cm/kyr reported in neighbouring areas of the Ebro Basin (Vergés et al., 1998; Barberà et al., 2001). Fine-grained sediments are abundant through the section, and sampling was focused on both red mudstones and white micritic limestones. At least, 2 oriented cores per site were obtained with an electrical portable drill and oriented in situ using a magnetic compass with inclinometer.

The palaeomagnetic analyses consisted in stepwise thermal demagnetization of the natural remanent magnetization (NRM) of at least one sample per site. In order to characterize the magnetic carriers, additional alternating field (AF) demagnetization of the NRM and progressive IRM acquisition and subsequent three-axial IRM demagnetization were conducted in a selected set of samples. Measurements of the magnetic remanence were performed using 2G superconducting rock magnetometers at the Palaeomagnetic Laboratories of the universities of Barcelona (Serveis Cientificotècnics UB-CSIC) and Utrecht. Stepwise thermal demagnetization was conducted in a Schönstedt TSD-1 thermal demagnetizer and a laboratory-built furnace (Utrecht) at intervals ranging between 10 °C and 50 °C and up to a maximum temperature of 680 °C. Magnetic susceptibility was also measured after each demagnetization step using a KLY-2 magnetic susceptibility bridge (Geofizika Brno). AF demagnetization, performed in an ASC D-Tech2000 alternating field demagnetizer, included a maximum of 12 steps with intervals of 5 mT, 10 mT, 20 mT and 50 mT up to 200 mT. Progressive IRM acquisition was carried out by means of an ASC IM10–30 pulse magnetizer up to a maximum pulse field of 1200 mT. Following Lowrie (1990), three fields of 1200 mT, 300 mT and 60 mT were respectively applied in the z, y and x sample axis for the subsequent thermal demagnetization of the samples.

3.2. Magnetic properties

The Zijderveld plots and the IRM experiments (Fig. 2) show that the behaviour of the NRM is related to lithology. In the white limestone samples (Fig. 2A–D) the NRM consist of two magnetic components: a viscous component and a high temperature stable component. The viscous component is unblocked at temperatures below 240 °C to 310 °C and parallels the present day field. The stable component, which yields maximum unblocking temperatures near 400 °C, shows both normal and reversed polarities and has been considered the characteristic remanent magnetization (ChRM). These two components are also observed in the AF demagnetization (Fig. 2B), being the samples completely demagnetized at peak fields of 60 mT. The saturation of the IRM of the white limestone samples is not achieved at the maximum fields of 1200 mT, but 80% of the remanence is achieved at relative low fields ~100 mT (Fig. 2C) and the soft component fraction (60 mT) demagnetizes completely below 480 °C (Fig. 2D). The NRM unblocking temperatures and coercivity spectra, together with the IRM acquisition and demagnetization data suggest the presence of magnetite as the principal magnetic carrier in the white limestone samples.

In the red bed samples (Fig. 2 E–L) a viscous component of the NRM is removed after heating to 250–300 °C. Further heating reveals a ChRM component with maximum unblocking temperatures ranging from 640 °C to 680 °C (Fig. 2 E and I). In addition, red bed samples having a normal polarity ChRM component, often reveal the presence of an intermediate component of reversed polarity (Figs. 2 I and 3 B). This intermediate component shows maximum unblocking temperatures ranging from 500 °C to 640 °C. The AF demagnetization of the red bed samples (Fig. 2 F and J) is only capable of removing a small fraction of the NRM at the maximum field of 200 mT, this corresponding to the soft viscous component. The IRM acquisition experiments (Fig. 2 G and K) yield unsaturated curves typical of high-coercivity minerals. Thermal demagnetization of both intermediate and hard-fraction coercivity fractions (300 mT and 1200 mT respectively) shows a maximum unblocking temperature of ~640 °C. It is concluded that, independently of the number of palaeomagnetic components contributing to the NRM, red bed samples depict a similar behaviour during the IRM experiments (Fig. 2 E–L), suggesting the same magnetic fraction composition. According to both the NRM and IRM unblocking

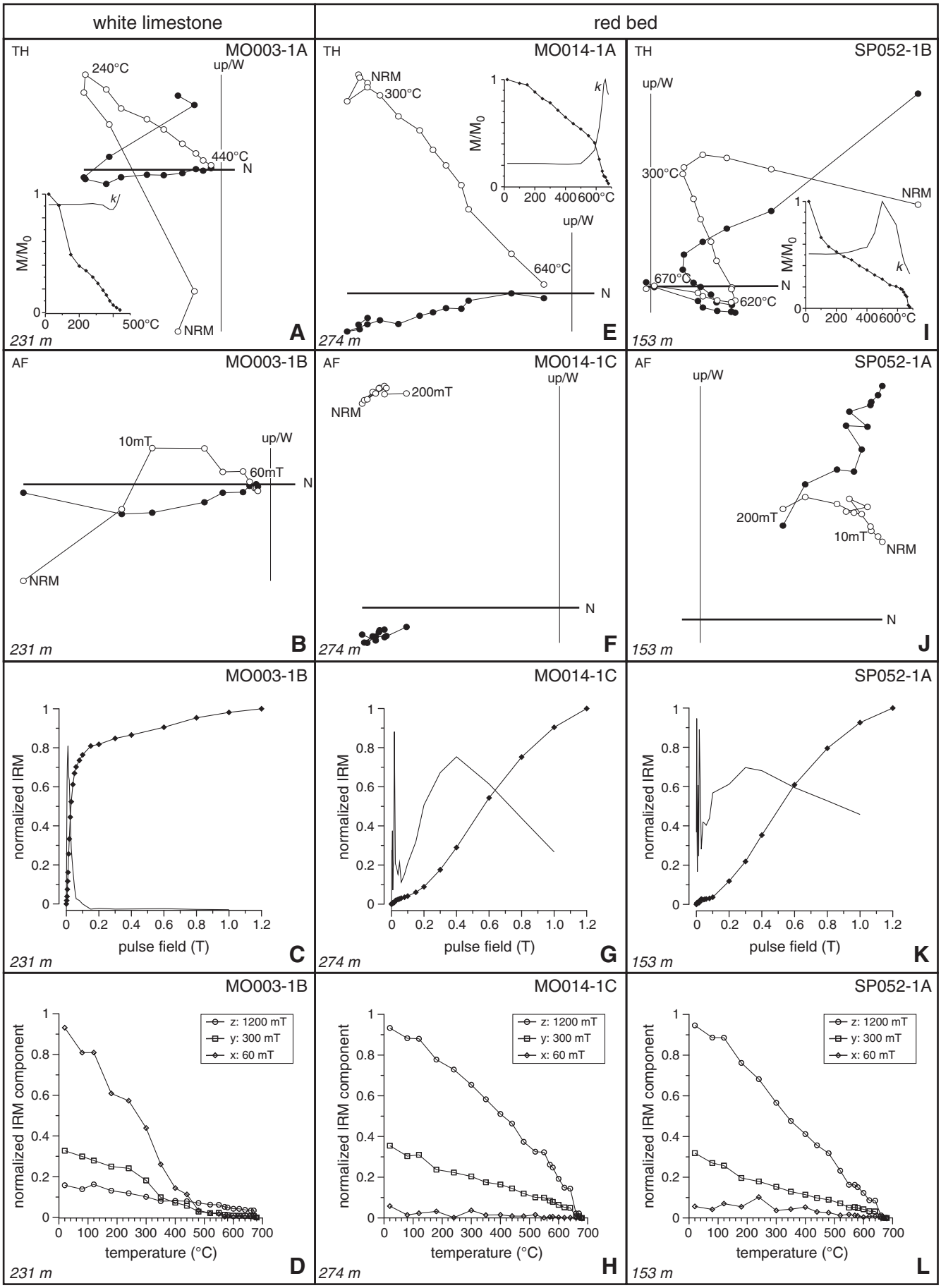
white limestone
red bed
TH
MO003-1A
240°C
up/W
440°C
N
NRM
M/M0
k
500°C
231 m
A
MO014-1A
NRM
300°C
640°C
274 m
E
SP052-1B
670°C
620°C
153 m
I
AF
MO003-1B
10mT
60mT
B
MO014-1C
200mT
F
SP052-1A
J
MO003-1B
normalized IRM
pulse field (T)
C
MO014-1C
G
SP052-1A
K
MO003-1B
normalized IRM component
z: 1200 mT
y: 300 mT
x: 60 mT
temperature (°C)
D
MO014-1C
H
SP052-1A
L

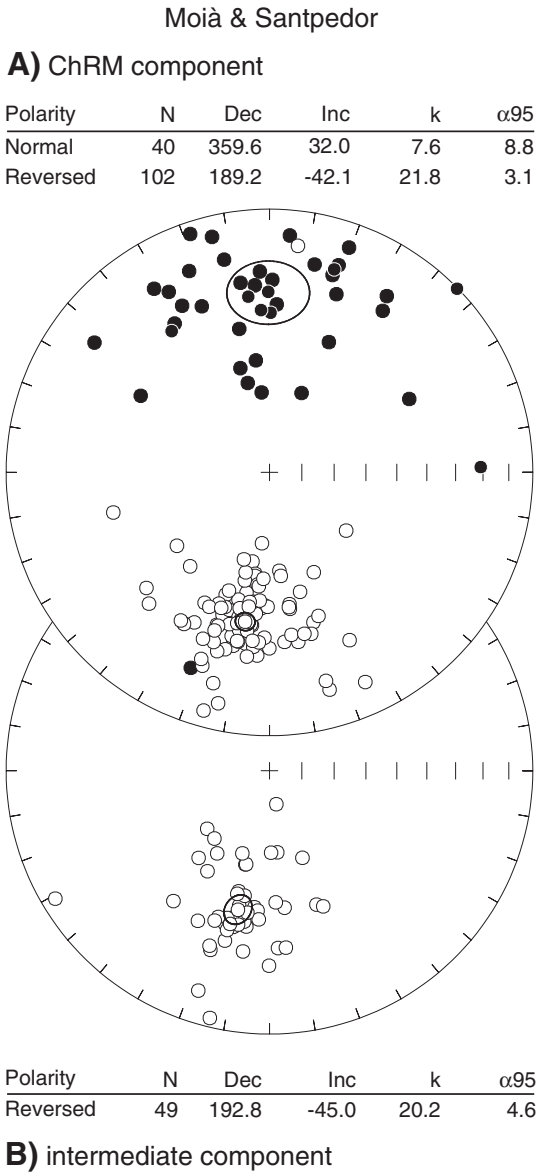

Fig. 3. Stereonet projection of the ChRM (A) and the intermediate component of the red beds (B) on the Moià-Santpedor composite section with calculated Fisherian means and statistics.

temperatures and the coercivity spectra, the magnetic fraction is dominated by haematite. Grain-size dependence of rock-magnetic properties in natural haematite as well as correspondence with remanence acquisition mechanisms in red beds has been reported in Dekkers and Linssen (1989). Therefore, the presence of two distinct magnetic components carried by haematite could be related to a bimodal grain-size distribution. Coarse-grained detrital haematite grains could be the carrier of the high-temperature ChRM, whereas fine-grained haematite cement would be responsible for the intermediate component acquired in a later burial stage. The nature and origin of this intermediate component will be discussed further (see Section 5.1.).

3.3. Magnetic stratigraphy of Moià-Santpedor

Palaeomagnetic components were calculated by means of least squares analysis (Kirschvink, 1980). The normal and reversed ChRM directions yield antipodal Fisherian means (Fig. 3 A) which conform to the palaeomagnetic references for the Late Eocene to Early Oligocene (Barberà, 1999; Costa et al., 2010). The reversed secondary component yielded a mean value which is also concordant with the ChRM mean direction (Fig. 3B).

ChRM directions were used to compute the latitude of the virtual geomagnetic pole (VGP) in order to obtain a local magnetic stratigraphy of the Moià-Santpedor composite section (see Supporting Table 1). Magnetozones were defined by at least two adjacent palaeomagnetic sites with the same polarity. Single-site reversals were denoted as half bar magnetozone in the local magnetostratigraphy, but were not used for magnetostratigraphic correlation purposes. Because of the existence of a widespread secondary magnetization of reversed polarity, we were cautious in the interpretation of stratigraphic intervals with alternating normal and reversed polarities. After the exclusion of these unreliable short events, a total of 7 magnetozones have been recognised along the 495-m-thick Moià-Santpedor local magnetostratigraphy (Fig. 4).

4. Correlation with the geomagnetic polarity time scale

A unique correlation of the local magnetostratigraphy of Moià-Santpedor with the Geomagnetic Polarity Time Scale (GPTS) 2004 (Gradstein et al., 2004) can be put forward on the basis of the available litho- and chronostratigaphic constraints (Fig. 5). First, the age of the marine-continental transition in the Ebro Basin, recorded at the bottom of the studied sections, has been recently correlated with chron C16n, at about 36 Ma, Priabonian (Costa et al., 2010). Second, a lithostratigraphic correlation between the Moià-Santpedor and the Maians-Rubió sections (Fig. 5 A and B) is feasible on the basis of the cartographic expression of the Santpedor sandstone unit.

The best fit of our composite magnetostratigraphy with the GPTS (Gradstein et al., 2004) is established by correlating with the range of chrons C16n.2n to chron C13n of the Late Eocene–Early Oligocene (Fig. 5). The short reversed magnetozone R1 correlates to C16n.2r, a subchron which was not confidently identified in the Maians-Rubió local magnetostratigraphy of Costa et al. (2010). Average sedimentation rates of about 20 cm/kyr are calculated for the Moià-Santpedor composite section, in close agreement with the observed trends in late Eocene–early Oligocene sections of the Eastern Ebro Basin (Barberà et al., 2001; Costa et al., 2010; Fig. 5 B, D and E).

5. Discussion

5.1. The sedimentary record of the Eocene–Oligocene transition in the Ebro Basin

According to the new magnetostratigraphic data and the derived average sedimentation of the Moià-Santpedor composite section (Fig. 5 E), the Eocene–Oligocene boundary can be placed by interpolation at ~80 m below the Santpedor fossil locality (see Figs. 4 and 5). 30 meters above the Eocene–Oligocene boundary and coinciding with the base of the chron C13n, the Santpedor sandstone unit occurs. This unit, which is interbedded within the red mudstone-dominated distal fluvial fan succession marks a progradation of the overall fluvial fan systems, as it is also recognised southwestwards in

Fig. 2. Representative palaeomagnetic results of the different studied rock types from the Moià and Santpedor sections. The stratigraphic position is shown in meters. (A), (E) and (I) shows the Zijderveld diagrams of the stepwise thermal demagnetization process. The NRM decay plots (squared curve) are obtained after the normalization of the vector subtraction module. The magnetic susceptibility (*K*) is also plotted. (B) AF demagnetization diagram of a white limestone sample kind. (F) and (J) show also AF demagnetization for the red beds samples, note how only the viscous component is demagnetized in these samples. All the thermal and AF demagnetization projections are in tectonic corrected coordinates. Progressive acquisition IRM curves for a white limestone sample (C) and for the one and two components of the red bed samples (G and K). (D), (H) and (L) three-axial IRM demagnetization curves following Lowrie (1990).

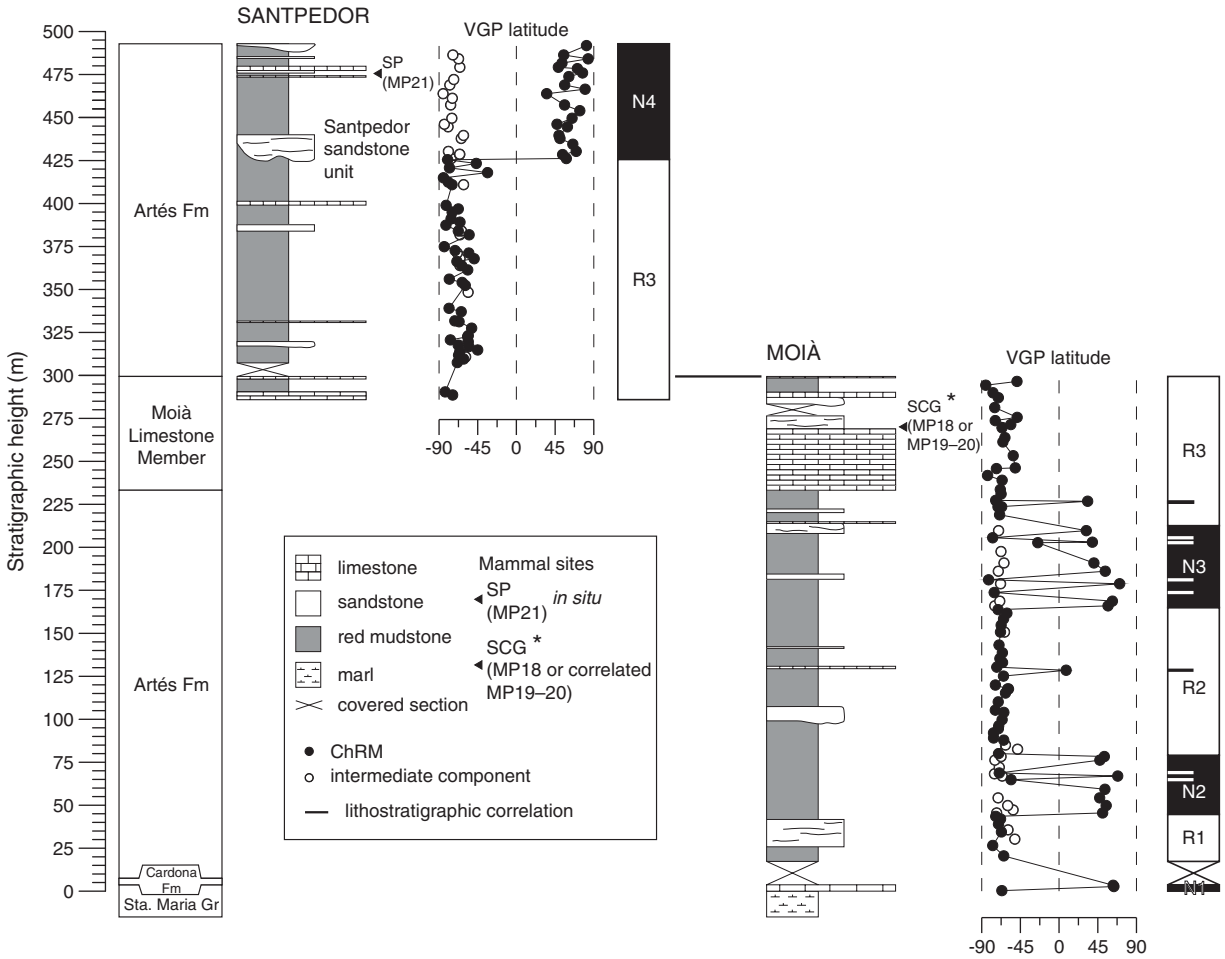

Fig. 4. Local litho- and magnetostratigraphic sections of Moià and Santpedor. The correlation between sections, which was established using the distinctive limestone beds of the Moià Limestone Member (see Figs. 1B and C), is also shown. The location of fossil mammal sites and their attribution to the MP reference levels are indicated. SCG, Sant Cugat de Gavadons. SP, Santpedor. Asterisk (*) indicates fossil mammal site correlated to the magnetostratigraphic section. Circles show the VGP latitude. Solid symbol is used for the ChRM component while open symbol indicates the presence of an intermediate component of exclusively reversed polarity. Stable magnetozones were defined by at least 2 adjacent palaeomagnetic sites showing the same polarity. Half bar zones denote one site reversals.

the Montclar-Rocafort fluvial fan succession as a sharp transition from lacustrine to alluvial deposits (Fig. 5; Fig. 1 A for Montclar-Rocafort fluvial fan location).

The age correspondence with the base of the chron C13n, and thus to the Oi-1 event (Katz et al., 2008) advocates a climate control on the expansion of the Santpedor sandstone unit (Figs. 5 and 7). Sedimentological data suggest that climate forcing was transmitted by a drop in the base level of the basin, similar to those described in the fluvial fan deposits of the Pyrenean margin (Sáez et al., 2007). The retraction of the central-basin lake systems and the basinwards expansion and incision of the fringing fluvial fans is interpreted as a response to the aridification process that accompanied the Late Eocene–Oligocene global cooling. Evidences of this palaeoenvironmental aridification are found in the Late Eocene Ebro Basin palaeofloral record (Cavagnetto and Anadón, 1996; Barberà et al., 2001) as well as in vast regions of Eurasia (Collinson and Hooker, 2003; Dupont-Nivet et al., 2007; Akhmetiev and Beniamovski, 2009).

Environmental changes occurring during the Eocene–Oligocene transition probably affected early burial diagenetic conditions in the alluvial sediments of the Ebro Basin. A consequence of shifting burial conditions could be the pervasive reversed-polarity secondary magnetization found in this study (Fig. 3 B and open symbol in Fig. 4; see Section 3.2.), as well as in the late Eocene sediments of the Maians-Rubió section (Costa et al., 2010). The fact that no equivalent signatures are reported in the younger Oligocene sediments in the Ebro Basin lead us to suggest that this single-polarity secondary magnetization is linked to a unique event. It is hypothesized that deepening of the phreatic levels could have enhanced the acquisition of a late magnetization via renewed oxidation of buried sediments, and precipitation of haematite cement in sediment porosity. Examples of a secondary magnetization linked with the drop of phreatic levels are found in the younger Messinian sediments of the Fortuna Basin (Garcés et al., 2001).

5.2. The age of the Grande Coupure

The magnetostratigraphy-based chronology of the Moià-Santpedor section allows the establishment of a reliable chronostratigraphy of the late Eocene to the early Oligocene continental record of the Eastern Ebro Basin. These results provide an age of 33.4 Ma (within the chron C13n) for the Santpedor fossil site, supporting an earliest Oligocene age, as envisaged from its biochronological ascription (Agustí et al., 1987; Anadón et al., 1987, 1992; Sáez, 1987; Arbiol and Sáez, 1988). Likewise, the age of the pre-Grande Coupure site of Sant Cugat de Gavadons can be estimated to about 34.5 Ma. These results bracket the Grande Coupure to an age interval embracing the Eocene–Oligocene boundary, dated at 33.9 Ma (Gradstein et al., 2004). Further, the Santpedor fossil assemblage is of special interest because of the rare coexistence of pre- and post-Grande Coupure fauna (Agustí et al., 1987; Hooker et al., 2009). Thus, if Santpedor is to be considered

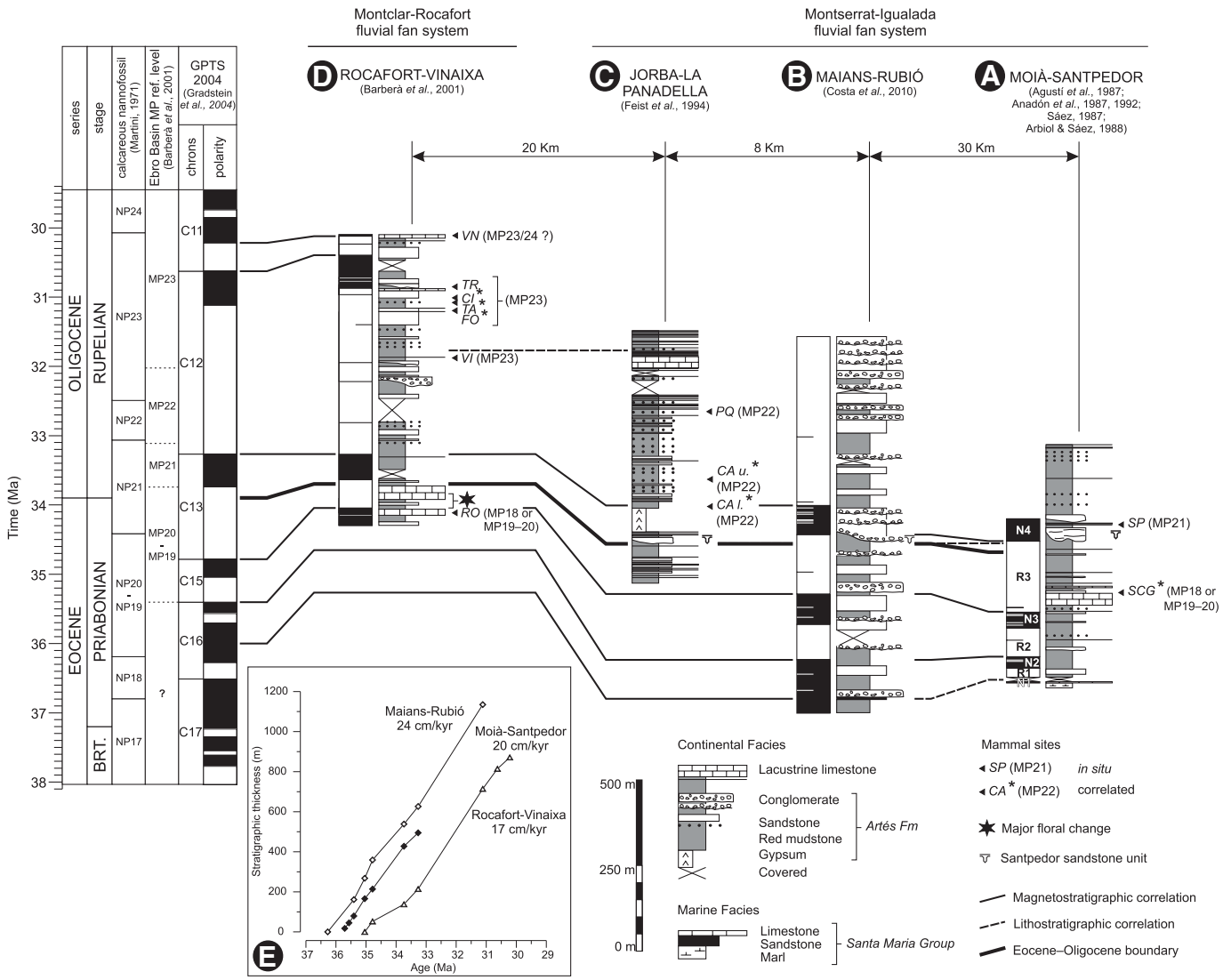

Fig. 5. Correlation of the local magnetostratigraphy of the Moià-Santpedor composite section (A) to the GPTS (Gradstein et al.;, 2004) with indication of the vertebrate localities and their corresponding MP reference levels (Agustí et al., 1987; Anadón et al., 1987, 1992; Sáez, 1987; Arbiol and Sáez, 1988; Barberà et al., 2001). SCG, Sant Cugat de Gavadons. RO, Rocafort de Queralt. SP, Santpedor. CA l., Lower Calaf. CA u., Upper Calaf. PQ, Porquerisses. VI, Vimbodí. FO, Forés. TA, Tàrrega. CI, Ciutadilla. TR, Tarrés. VN, Vinaixa. Asterisk (*) indicates fossil mammal site correlated to the sections. The Rocafort-Vinaixa log (D) is a composite section from the Rocafort, Sarral, Solivella, Tarrés and Vinaixa magnetostratigraphic sections of Barberà et al. (2001). The Jorba-La Panadella lithostratigraphic section (C) (Feist et al., 1994) correlates the Maians-Rubió composite section (B) of Costa et al. (2010) with the Rocafort-Vinaixa section of Barberà et al. (2001) The regional significant Santpedor sandstone unit has been used to correlate the Moià-Santpedor composite section with the magnetostratigraphic composite sections of Maians-Rubió (Costa et al., 2010) and Rocafort-Vinaixa (Barberà et al., 2001). (E) accumulation curves and the mean sedimentation rates derived from the proposed correlation of the Moià-Santpedor local magnetostratigraphy are also compared to the values for the Maians-Rubió (Costa et al., 2010) and Rocafort-Vinaixa (Barberà et al., 2001).

among the oldest post-Grande Coupure records, a (maximum) lag of 0.5 Myr relative to the Eocene–Oligocene boundary is determined.

5.3. Correlation between the Ebro and the Hampshire basins

The age of the Grande Coupure in the Hampshire Basin (Isle of Wight, UK) has become controversial since Gale et al. (2006) provided the Solent Group succession with a first magnetostratigraphy (Gale et al., 2006, 2007; Hooker et al., 2007, 2009). For the sake of clarity, we summarize in Fig. 6 all the alternative magnetostratigraphic correlations of the Solent Group succession with the GPTS (Gradstein et al., 2004). Gale et al. (2006) substantiated their correlation according solely to the presence of diagnostic nannofossils *Discoaster saipanensis* and *Ismolithus recurvus* of the Zone NP19–20 in the Brockenhurst Bed, located at the base of the sampled section (Fig. 6 A). Following this constraint, they correlated the lower thick normal magnetozone to the chron C15n and found a best match by correlating their Bembridge Normal Polarity Zone (BNPZ) to the chron C13n. This correlation yielded an age for the Grande Coupure (MP20–MP21 boundary) about 2 Myr younger than the Eocene–Oligocene boundary, being in apparent contradiction with previous chronostratigraphic interpretations of the Solent Group succession (Hooker, 1992; Hooker et al., 2004).

Alternative correlations for the Solent Group succession were put forward in order to reconcile magnetostratigraphy and mammal biochronology (Hooker et al., 2007, 2009) (Fig. 6 B and C). Hooker et al. (2009) favoured a correlation of the basal normal magnetozone in the Solent Group succession with chron C16n since this option was also in accordance with the range of the Zone NP19–20 (Gradstein et al., 2004). Hooker et al. (2009) also proposed the correlation of the BNPZ to C13r.1n, a short subchron not present in the GPTS 2004 (Gradstein et al., 2004), but recorded at Site 1090 of the South Atlantic Ocean (Channell et al., 2003). The existence of subchron C13r.1n, however, is controversial since it has not been recorded in other high-

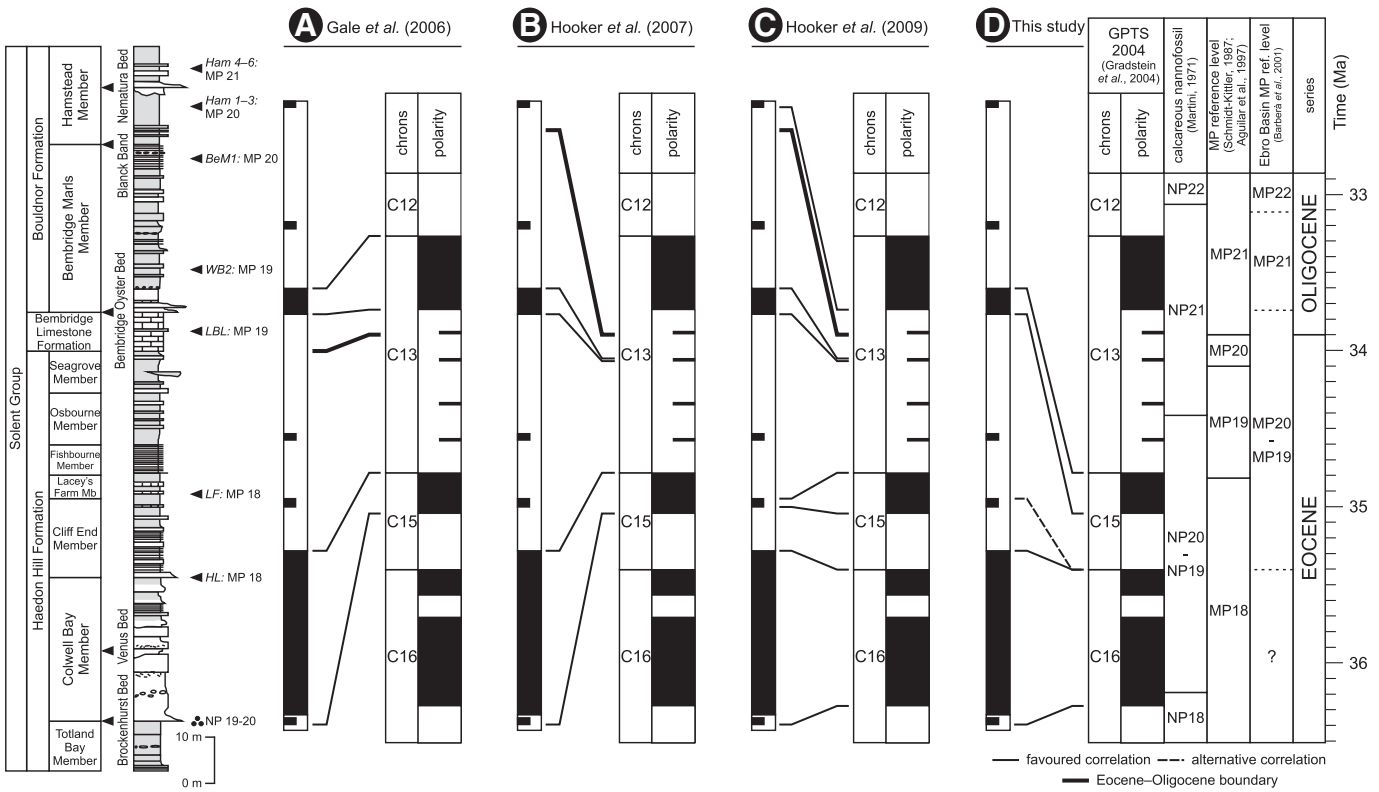

Fig. 6. Successive proposed correlations for the magnetostratigrapic record of the Solent group in the Hampshire Basin (Isle of Wight, UK). Litho- and magnetostratigraphic information come from Gale et al. (2006). Biochronological information has been compiled from Hooker (1992, 2010); Hooker et al. (2004, 2007, 2009), and Gale et al. (2006). HL, Hartherwood Lignite Bed. LF, Lacey's Farm Member. LBL, Limestone of the Bembridge Limestone Formation. WB2, Whitecliff Bay 2. BeM1, Bembridge Marls 1. Ham 1–3, Hampstead Member 1, 2 and 3. Ham 4–6, Hampstead Member 4, 5 and 6. The location of the Eocene–Oligocene boundary according to different options is marked with a thick black line. Subchrons in chron C13r come from Cande and Kent (1995).

resolution records elsewhere (Lowrie and Lanci, 1994; Lanci et al., 1996; Parés and Lanci, 2004). The correlation proposed by Hooker et al. (2009) yields a considerable mismatch with the pattern of chrons of the GPTS since a short, single-site magnetozone is correlated with chron C15n while the thicker BNPZ is correlated with C13r.1n, a short event of unknown nature (cryptochron or subchron), duration and age (Fig. 6 C).

Further arguments to constrain the correlation of the BNPZ with the GPTS rely on the biomagnetostratigraphic record of the Ebro Basin (Barberà et al, 2001) and the biochronological interpretation of the Sant Cugat de Gavadons mammal site. As discussed above (Section 2.2.), Hooker et al. (2009) assigned to this locality a MP18 age, while the magnetostratigraphy of the Moià-Santpedor composite section dictates a correlation of this site with chron C13r. Since the BNPZ in the Solent Group succession is found associated to fossil sites of MP19 age, Hooker et al. (2009) derived that BNPZ must correlate to a normal subchron within C13r (Fig. 6 C).

It must be noted, however, that consensus on the biochronological significance of Sant Cugat de Gavadons is not yet reached. The endemism affecting fossil assemblages of the Ebro Basins (Badiola et al., 2009) has possibly hampered the establishment of a robust biochronology linking both regions. Therefore, it is worth considering the alternate scenario where Sant Cugat de Gavadons is assigned to MP19–20, following Agustí et al. (1987), Anadón et al. (1987; 1992) and Badiola et al. (2009). Under this assumption, a correlation of the BNPZ with chron C15n is derived (Fig. 6 D), leaving uninterpreted (unreliable) all single-site normal magnetozones in the Solent Group succession (Fig. 6 D). Such alternative was already analysed by Gale et al. (2007) in their reply to Hooker et al. (2007), but rejected arguing that the magnetostratigraphic data from the Ebro Basin (Barberà et al., 2001) were not as reliable to be taken into account (Gale et al., 2007).

5.4. Implications for the European land mammal chronology

This paper contributes to further support to the magnetostratigraphy-based chronological framework of the Eocene–Oligocene sedimentary record of the Ebro Basin (Barberà et al., 2001). Its significance for the calibration of the European Land Mammal chronology should be discussed in the light of the endemism of Iberian faunas with respect to the central European MP reference levels (Badiola et al., 2009). Regarding the Late Eocene, the uncertain biochronological assignment of the fossil assemblage of Sant Cugat de Gavadons has led to two alternative correlations of the Solent Group succession in the Hampshire Basin (Fig. 7, see discussion above). Option A follows Hooker et al. (2009), and results in a calibration of the MP19, MP20 and MP21 units within a very short-ranged time span. In Option B the alternative correlation of the Solent Group succession with the GPTS 2004 (Gradstein et al., 2004) as discussed in Section 5.3. is considered. Option B assigns a longer duration for the MP zones with the MP18 and MP19 zones pinned down to an age older than the presently accepted (Schmidt-Kittler, 1987; Aguilar et al., 1997). Earlier calibrations constrained the age of the MP20 reference level to a short period of 200 kyr at precisely the latest Eocene (Schmidt-Kittler, 1987; Aguilar et al., 1997). Based on limits derived from Option B, MP20 is correlated within chron C13r, but its exact age and duration is not so tightly constrained (Fig. 7).

Finally, a minimum age of 33.4 Ma is determined for the MP21 reference level, based on the calibration of the locality of Santpedor in the Ebro Basin (Fig. 7). The MP21 locality high in the Hampshire Basin succession (Ham 4–6) does not provide further constraints since it lacks magnetostratigraphy (Fig. 6). This lead to the conclusion that, considering the magnetostratigraphy-based ages of the MP20 and MP21 reference levels, the Grande Coupure lags the Eocene–

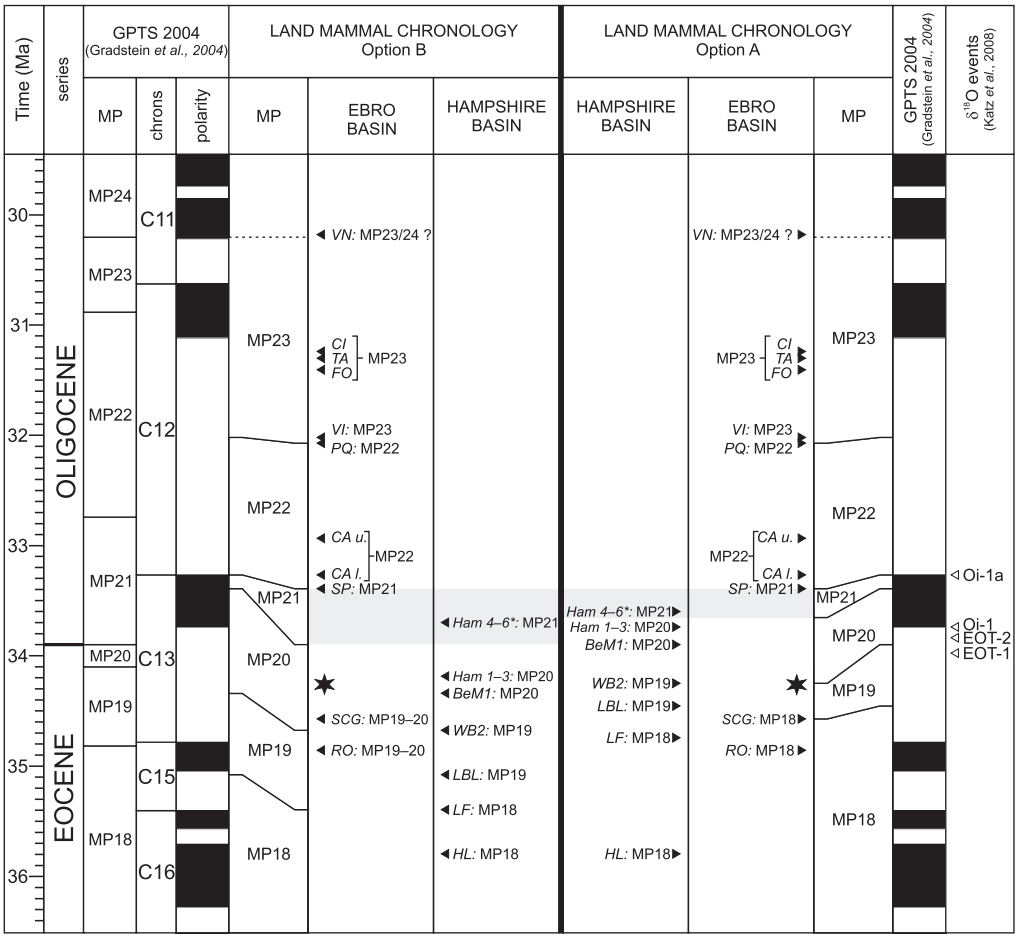

Fig. 7. Calibration of the MP reference levels to the GPTS (Gradstein et al., 2004) across the Eocene–Oligocene boundary. Biostratigraphic data of the Eastern Ebro Basin comes from Agustí et al. (1987), Anadón et al. (1987, 1992), Sáez (1987), Arbiol and Sáez (1988), Barberà et al. (2001), and this study. SCG, Sant Cugat de Gavadons. RO, Rocafort de Queralt. SP, Santpedor. CA l., Lower Calaf. CA u., Upper Calaf. PQ, Porquerisses. VI, Vimbodí. FO, Forés. TA, Tàrrega. CI, Ciutadilla. TR, Tarrés. VN, Vinaixa. The star symbol indicates major floral change in the Ebro Basin (Cavagnetto and Anadón, 1996; Barberà et al., 2001). Biostratigraphic data of the Hampshire Basin comes from Hooker (1992, 2010) and Hooker et al. (2004, 2007, 2009). HL, Hartherwood Lignite Bed. LF, Lacey's Farm Member. LBL, Limestone of the Bembridge Limestone Formation. WB2, Whitecliff Bay 2. BeM1, Bembridge Marls 1. Ham 1–3, Hampstead Member 1, 2 and 3. Ham 4–6, Hampstead Member 4, 5 and 6. Asterisk (*) in Ham 4–6 indicates no direct magnetostratigraphic data available (see Fig. 6). Option A: assumes an MP18 age for the SCG and RO fossil localities in the Eastern Ebro Basin (Hooker et al., 2009) and the correlation of the MP reference levels in the Hampshire Basin (Isle of Wright, UK) follows Hooker et al. (2009) correlation to the GPTS. Option B: assumes an MP19–20 age for the SCG and RO fossil localities in the Eastern Ebro Basin (Agustí et al., 1987; Anadón et al., 1987, 1992) and the calibration of the fossil sites in the Hampshire Basin (Isle of Wright, UK) is derived from the alternative correlation to the GPTS proposed in Fig. 6D (see text for discussion). Grey-shaded area indicates the possible range of the Grande Coupure for both options.

Oligocene boundary by a maximum of 0.5 Myr as shown with the grey-shaded areas in Fig. 7.

6. Conclusions

New magnetostratigraphic data of the 495-m-thick Moià-Santpedor composite section, together with previous bio- and magnetostratigraphic studies in the Ebro Basin; confirms an earliest Oligocene age (~33.4 Ma) for the post- Grande Coupure Santpedor fossil site. This, in turn supports the close correlation between the dramatic terrestrial faunal turnover known as the Grande Coupure and the Eocene–Oligocene transition, with a (maximum) lag of time of 0.5 Myr. As in other Eocene–Oligocene records of Eurasia, in the Eastern Ebro Basin, the Grande Coupure might coincide with a shift to drier climatic conditions, as it has been deduced from sedimentological evidences, which includes incision of fluvial fan channel deposits as a consequence of the drop of the base level at a regional scale.

The precise Eocene–Oligocene continental chronology of the Ebro Basin allows an alternative interpretation of the Hampshire Basin sedimentary record (Isle of Wight, UK) which reconciles all the available marine and continental biostratigraphy from the Solent Group succession. From the integration of the Ebro and Hampshire basin records, a magnetostratigraphy-based calibration of the Late Eocene–Oligocene European mammal biochronology (MP reference levels) has resulted.

Supplementary materials related to this article can be found online at doi:10.1016/j.palaeo.2011.01.005.

Acknowledgements

This paper has been developed in the framework of the Spanish MCI projects: CENOCRON CGL2004-00780 and REMOSS 3D-4D CGL2007-66431-C02-02/BTE. This research was supported by the Research Group of "Geodinàmica i Anàlisi de Conques" (2009 GGR 1198 — Comissionat d'Universitats i Recerca de la Generalitat de Catalunya) and the Research Institute GEOMODELS. The authors wish to thank Bet Beamud from the "Laboratori de Paleomagnetisme" (Serveis Cientificotècnics UB-CSIC) and Dr. Cor Langereis from the Paleomagnetic Laboratory "Fort Hoofddijk" (Utrecht Universiteit). We are grateful to Mireia Butillé and Rubén Calvo who assisted during field work and the laboratory analysis. The comments and suggestions of Jaume Dinarès-Turell and Jerry Hooker have significantly improved this paper. E.C. was funded by a PhD grant of the Spanish MCI.

References

Aguilar, J.P., Legendre, S., Michaux, J., 1997. Actes du Congrès BiochroM'97. Mémoires et Travaux de l'Institut de Montpellier, Montpellier.

Agustí, J., Anadón, P., Arbiol, S., Cabrera, L., Colombo, F., Sáez, A., 1987. Biostratigraphical characteristics of the Oligocene sequences of North–Eastern Spain (Ebro and Campins Basins). Münchner Geowissenschaftliche Abhandlungen 10, 35–42.

Akhmetiev, M.A., Beniamovski, V.N., 2009. Paleogene floral assemblages around epicontinental seas and straits in Northern Central Eurasia: proxies for climatic and paleogeographic evolution. Geologica Acta 7 (1–2), 297–309. doi:10.1344/105.000000278.

Anadón, P., Vianey-Liaud, M., Cabrera, L., Hartenberger, J.L., 1987. Gisements à vertébrés du paléogène de la zone orientale du bassin de l'Ebre et leur apport à la stratigraphie. Paleontologia i Evolució 21, 117–131.

Anadón, P., Cabrera, L., Colldeforns, B., Colombo, F., Cuevas, J.L., Marzo, M., 1989. Alluvial fan evolution in the SE Ebro Basin: Response to tectonics and lacustrine base level changes. Excursion Guidebook. 4th International Conference on Fluvial Sedimentology. Publicacions del Servei Geològic de Catalunya, Barcelona.

Anadón, P., Cabrera, L., Choi, S.J., Colombo, F., Feist, M., Sáez, A., 1992. Biozonación del Paleógeno continental de la zona oriental de la Cuenca del Ebro mediante carófitas; implicaciones en la biozonación general de carófitas de Europa occidental. Acta Geologica Hispánica 27 (1–2), 69–94.

Arbiol, S., Sáez, A., 1988. Sobre la edad oligocénica inferior del yacimiento de Santpedor (Cuenca del Ebro, provincia de Barcelona). Acta Geologica Hispánica 23 (1), 47–50.

Arenas, C., Millán, H., Pardo, G., Pocoví, A., 2001. Ebro Basin continental sedimentation associated with late compressional Pyrenean tectonics (north–eastern Iberia): controls on basin margin fans and fluvial systems. Basin Research 13, 65–89.

Badiola, A., Checa, L., Cuesta, M.A., Quer, R., Hooker, J.J., Astibia, H., 2009. The role of new Iberian finds in understanding European Eocene mammalian paleobiogeography. Geologica Acta 7 (1–2), 243–258. doi:10.1344/105.000000281.

Barberà, X., 1999. Magnetostratigrafia de l'Oligocè del sector sud-oriental de la Conca de l'Ebre: implicacions magnetobiocronològiques i seqüencials. PhD thesis, Universitat de Barcelona, 247 pp.

Barberà, X., Cabrera, L., Marzo, M., Parés, J.M., Agustí, J., 2001. A complete terrestrial Oligocene magnetostratigraphy from the Ebro Basin, Spain. Earth and Planetary Science Letters 187 (1–2), 1–16. doi:10.1016/S0012-821(01)00270-9.

Berggren, W.A., Prothero, D.R., 1992. Eocene–Oligocene climatic and biotic evolution: an overview. In: Prothero, D.R., Berggren, W.A. (Eds.), Eocene–Oligocene climatic and biotic evolution. Princeton University Press, Princeton, pp. 1–28.

Cande, S.C., Kent, D.V., 1995. Revised calibration of the geomagnetic polarity time scale for the Late Cretaceous and Cenozoic. Journal of Geophysical Research 100, 6093–6095.

Cascella, A., Dinarès-Turell, J., 2009. Integrated calcareous nannofossil biostratigraphy and magnetostratigraphy from the uppermost marine Eocene deposits of the southeastern Pyrenean foreland basin: evidences for marine Priabonian deposition. Geologica Acta 7 (1–2), 281–296. doi:10.1344/105.000000282.

Cavagnetto, C., Anadón, P., 1996. Preliminary palynological data on floristic and climatic changes during the Middle Eocene-Early Oligocene of the eastern Ebro Basin, northeast Spain. Review of Palaeobotany and Palynology 92 (3–4), 281–305. doi:10.1016/0034-6667(95)00096-8.

Channell, J.E.T., Galeotti, S., Martin, E.E., Billups, K., Scher, H.D., Stoner, J.S., 2003. Eocene to Miocene magnetostratigraphy, biostratigraphy, and chemostratigraphy at ODP Site 1090 (sub-Antarctic South Atlantic). Geological Society of America Bulletin 11 (5), 607–623. doi:10.1130/0016-7606(2003.

Collinson, M.E., Hooker, J.J., 2003. Paleogene vegetation of Eurasia: framework for mammalian faunas. Deinsa 10, 41–84.

Coney, P.J., Muñoz, J.A., McClay, K.R., Evenchick, C.A., 1996. Syntectonic burial and post-tectonic exhumation of southern Pyrenees foreland fold-thrust belt. Journal of the Geological Society of London 153, 9–16.

Costa, E., Garcés, M., López-Blanco, M., Beamud, E., Gómez-Paccard, M., Larrasoaña, J.C., 2010. Closing and continentalization of the South Pyrenean foreland Basin (NE Spain): magnetochronological constraints. Basin Research 22, 904–917. doi:10.1111/j.1365-2117.2009.00452.x.

Cuevas, J.L., Cabrera, L., Marcuello, A., Arbués, P., Marzo, M., Bellmunt, F., 2010. Exhumated channel sandstone networks within fluvial fan deposits from the Oligo–Miocene Caspe Formation, South–east Ebro Basin (North–east Spain). Sedimentology 57, 162–189. doi:10.1111/j.1365-3091.2009.01096.x.

Dekkers, M.J., Linssen, J.H., 1989. Rockmagnetic properties of fine-grained natural low-temperature haematite with reference to remanence acquisition mechanisms in red beds. Geophysical Journal International 99, 1–18.

Dupont-Nivet, G., Krijgsman, W., Langereis, C.G., Abels, H.A., Dai, S., Fang, X., 2007. Tibetan plateau aridification linked to global cooling at the Eocene–Oligocene transition. Nature 445, 635–638. doi:10.1038/nature/05516.

Feist, M., Anadón, P., Cabrera, L., Choi, S.J., Colombo, F., Sáez, A., 1994. Upper Eocene–Lowermost Miocene charophyte succession in the Ebro Basin (Spain). Contribution to the charophyte biozonation in Western Europe. Newsletters on Stratigraphy 30 (1), 1–32.

Ferrer, J., 1971. El Paleoceno y Eoceno del borde suroriental de la Depresión del Ebro (Cataluña). Memories Suisses de Paleontologie 90, 1–70.

Gale, A.S., Huggett, J.M., Pälike, H., Laurie, E., Hailwood, E.A., Hardenbol, J., 2006. Correlation of Eocene–Oligocene marine and continental records: orbital, cyclicity, magnetostratigraphy and sequence stratigraphy of the Solent Group, Isle of Wight, UK. Journal of the Geological Society 163, 401–415. doi:10.1144/0016-764903-175.

Gale, A.S., Huggett, J.M., Laurie, E., 2007. Discussion on the Eocene–Oligocene boundary in the UK. *Journal*, Vol. 163, pp. 401–415. Journal of the Geological Society 164, 685–688. doi:10.1144/0016-76492006-098.

Garcés, M., Krijgsman, W., Agustí, J., 2001. Chronostratigraphic framework and evolution of the Fortuna basin (Eastern Betics) since the Late Miocene. Basin Research 13, 199–216. doi:10.1046/j.1365-2117.2001.00144.x.

Gradstein, F.M., Ogg, J.G., Smith, A., 2004. A geologic time scale 2004. Cambridge University Press, Cambridge.

Hartenberger, J.L., 1973. Les rongeurs de l'Eocène d'Europe. Leur évolution dans leur cadre biogéographique. Mémoires du Muséum National d'Historie Naturelle, Sciences de la Terre 24 (3), 49–70.

Hooker, J.J., 1987. Mammalian faunal events in the English Hampshire Basin (late Eocene–early Oligocene) and their application to European biostratigraphy. Münchener Geowissenschaftliche Abhandlungen 10, 109–116.

Hooker, J.J., 1992. British mammalian paleocommunities across the Eocene–Oligocene transition and their environmental implications. In: Prothero, D.R., Berggren, W.A. (Eds.), Eocene–Oligocene Climatic and Biotic Evolution. Princeton University Press, Princeton, pp. 494–515.

Hooker, J.J., 2010. The "Grande Coupure" in the Hampshire Basin, UK: taxonomy and stratigraphy of the mammals on either side of this major Paleogene faunal turnover. In: Whittaker, J.E., Hart, M.B. (Eds.), Micropalaeontology, Sedimentary Environments and Stratigraphy: A Tribute to Dennis Curry (1912–2001): The Micropalaeontological Society, Special Publications, pp. 147–215. doi:10.1144/TMS004.8.

Hooker, J.J., Collinson, M.E., Sille, N.P., 2004. Eocene–Oligocene mammalian faunal turnover in the Hampshire Basin, UK: calibration to the global time scale and the major cooling event. Journal of the Geological Society 161, 161–172. doi:10.1144/0016-764903-091.

Hooker, J.J., Collinson, M.E., Grimes, S.T., Sille, N.P., Mattey, D.P., 2007. Discussion on the Eocene–Oligocene boundary in the UK. Journal, Vol. 163, pp. 401–415. Journal of the Geological Society 164, 685–688. doi:10.1144/0016-76492006-098.

Hooker, J.J., Grimes, S.T., Mattey, D.P., Collinson, M.E., Sheldon, N.D., 2009. Refined correlation of the UK Late Eocene–Early Oligocene Solent Group and timing of its climate history. In: Koeberl, C., Montanari, A. (Eds.), The Late Eocene Earth-Hothouse, Icehouse and Impacts: The Geological Society of America, Special Paper, 452, pp. 179–195. doi:10.1130/2009.2452(12.

Janis, C.M., 1993. Tertiary mammal evolution in the context of changing climates, vegetation, and tectonic events. Annual Reviews of Ecology and Systematics 24, 467–500.

Joomun, S.C., Hooker, J.J., Collinson, M.E., 2008. Dental wear variation and implications for diet: An example from Eocene perissodactyls (Mammalia). Palaeogeography, Palaeoclimatology, Palaeoecology 263 (3–4), 92–106. doi:10.1016/j.palaeo.2008.03.001.

Katz, M.E., Miller, K.G., Wright, J.D., Wade, B.S., Browning, J.V., Cramer, B.S., Rosenthal, Y., 2008. Stepwise transition from the Eocene greenhouse to the Oligocene icehouse. Nature Geoscience 1 (5), 329–334. doi:10.1038/ngeo179.

Kirschvink, J.L., 1980. The least-squares line and plane and the analysis of paleomagnetic data. Geophysical Journal of the Royal Astronomical Society 62, 699–718.

Köhler, M., Moyà-Solà, S., 1999. A finding of Oligocene primates on the European continent. Proceedings of the National Academy of Sciences 96 (25), 14664–14667.

Lanci, L., Lowrie, W., Montanari, A., 1996. Magnetostratigraphy of the Eocene/Oligocene boundary in a short drill-core. Earth and Planetary Science Letters 143, 37–48.

Legendre, S., 1987. Les immigrations de la "Grande Coupure" sont-elles contemporaines en Europe occidentale? Münchner Geowissenschaftliche Abhandlungen 10, 141–148.

Legendre, S., Hartenberger, J.L., 1992. Evolution of mammalian faunas in Europe during the Eocene and Oligocene. In: Prothero, D.R., Berggren, W.A. (Eds.), Eocene–Oligocene Climatic and Biotic Evolution. Princeton University Press, Princeton, pp. 516–528.

Lowrie, W., 1990. Identification of ferromagnetic minerals in a rock by coercivity and unblocking temperature properties. Geophysical Research Letters 17 (2), 159–162.

Lowrie, W., Lanci, L., 1994. Magnetostratigraphy of the Eocene–Oligocene boundary sections in Italy: No evidence for short subchrons within chrons 12R and 13R. Earth and Planetary Science Letters 126, 247–258.

Luzón, A., González, A., Muñoz, A., Sánchez-Valverde, B., 2002. Upper Oligocene–Lower Miocene shallowing-uppward lacustrine sequences controlled by periodic and non-periodic processes (Ebro Basin, northeastern Spain). Journal of Paleolimnology 28, 441–456. doi:10.1023/A:1021675227754.

Meng, J., McKenna, M.C., 1998. Faunal turnovers of Paleogene mammals from the Mongolian Plateau. Nature 394, 364–367. doi:10.1038/28603.

Muñoz, J.A., 1992. Evolution of a continental collision belt: ECORS-Pyrenees crust balanced cross-section. In: McClay, K.R. (Ed.), Thrust Tectonics. Chapman & Hall, London, pp. 235–246.

Ortí, F., Rosell, L., Inglès, M., Playa, E., 2007. Depositional models of lacustrine evaporites in the SE margin of the Ebro Basin (Paleogene, NE Spain). Geologica Acta 5 (1), 19–34.

Pallí, L., 1972. Estratigrafía del Paleógeno del Empordà y zonas limítrofes. PhD thesis, Universitat Autònoma de Barcelona, 338 pp.

Parés, J.M., Lanci, L., 2004. A Middle Eocene – Early Miocene Magnetic Polarity Stratigraphy in Equatorial Pacific Sediments (ODP Site 1220). In: Channell, J.E.T., Kent, D.V., Lowrie, W., Meert, J.G. (Eds.), Timescales of the Paleomagnetic Field: Geophysical Monograph Series, 145, pp. 131–140.

Prothero, D.R., 1994. The late Eocene–Oligocene extinctions. Annual Reviews of the Earth and Planetary Sciences 22, 145–165. doi:10.1146/annurev.ea.22.050194.001045.

Prothero, D.R., Swisher III, C.C., 1992. Magnetostratigraphy and geochronology of the terrestrial Eocene–Oligocene transition in North America. In: Prothero, D.R., Berggren, W.A. (Eds.), Eocene–Oligocene Climatic and Biotic Evolution. Princeton University Press, Princeton, pp. 46–73.

Puigdefàbregas, C., Souquet, P., 1986. Tecto-sedimentary cycles and depositional sequences of the Mesozoic and Tertiary from the Pyrenees. Tectonophysics 129, 173–203. doi:10.1016/0040-1951(86)90251-9.

Puigdefàbregas, C., Muñoz, J.A., Marzo, M., 1986. Thrust belt development in the eastern Pyrenees and related depositional sequences in the southern foreland basin. In: Allen, P.A., Homewood, P. (Eds.), Foreland Basins: Special Publication of the International Association of Sedimentologists, 8, pp. 229–246. Blackwell Scientific, Oxford.

Pujalte, V., Schmitz, B., Baceta, J.I., Orue-Etxebarria, X., Bernaola, G., Dinarès-Turell, J., Payros, A., Apellaniz, E., Caballero, F., 2009. Correlation of the Thanetian–Ilerdian turnover of larger foraminifera and the Paleocene–Eocene thermal maximum: confirming evidence from the Campo area (Pyrenees, Spain). Geologica Acta 7 (1–2), 161–175. doi:10.1344/105.000000276.

Riba, O., Reguant, S., Villena, J., 1983. Ensayo de síntesis estratigráfica y evolutiva de la cuenca terciaria del Ebro. In: Comba, J.A. (Ed.), Geología de España. Libro Jubilar J.M. Ríos, Tomo II. Publicaciones del Instituto Geológico y Minero de España (IGME), Madrid, pp. 131–159.

Sáez, A., 1987. Estratigrafía y sedimentología de las formaciones lacustres del tránsito Eoceno–Oligoceno del noreste de la cuenca del Ebro. PhD thesis, Universitat de Barcelona, 353 pp.

Sáez, A., Anadón, P., Herrero, M.J., Moscariello, A., 2007. Variable style of transition between Palaeogene fluvial fan and lacustrine systems, southern Pyrenean foreland, NE Spain. Sedimentology 54, 367–390. doi:10.1111/j.1365-3091.2006.00840.x.

Schmidt-Kittler, N., 1987. European reference levels and correlation tables. Münchener Geowissenschaftliche Abhandlungen 10, 13–32.

Serra-Kiel, J., Travé, A., Mató, E., Saula, E., Ferràndez-Cañadell, C., Busquets, P., Tosquella, J., Vergés, J., 2003. Marine and transitional Middle/Upper Eocene Units of the Southeastern Pyrenean Foreland Basin (NE Spain). Geologica Acta 1 (2), 177–200.

Stehlin, H.G., 1910. Remarques sur les faunules de Mammifères des couches Éocènes et Oligocènes du Bassin de Paris. Bulletin de la Societe Geologique de France 9 (4), 488–520.

Tobien, H., 1987. The Position of the "Grande Coupure" in the Paleogene of the Upper Rhine Graben and the Mainz Basin. Münchner Geowissenschaftliche Abhandlungen 10, 197–202.

Vergés, J., Marzo, M., Santaeulària, T., Serra-Kiel, J., Burbank, D.W., Muñoz, J.A., Giménez-Montserrat, J., 1998. Quantified vertical motions and tectonic evolution of the SE Pyrenean foreland basin. In: Mascle, A., Puigdefàbregas, C., Luterbacher, H.P., Fernàndez, M. (Eds.), Cenozoic Foreland Basins of Western Europe: Geological Society Special Publication, 134, pp. 107–134.

Vergés, J., Fernàndez, M., Martínez, A., 2002. The Pyrenean orogen: pre-, syn-, and post-collisional evolution. In: Rousenbaum, G., Lister, L.G. (Eds.), Reconstruction of the Evolution of the Alpine-Himalayan Orogen: Journal of the Virtual Explorer, 8, pp. 55–74. doi:10.3809/jvirtex.2002.00058.

APPENDIX OF CHAPTER 3.3:

SUPPORTING ELECTRONIC INFORMATION

Site No.	Stratigraphic level (m)	Geographic coordinates Dec. (º)	Geographic coordinates Inc. (º)	Stratigraphic coordinates Dec. (º)	Stratigraphic coordinates Inc. (º)	Dip Az. (º)	Dip. (º)	VGP Lat. (º)
Moià Section								
PR001-1B	0.3	181.1	-37.3	180.0	-33.6	340	4	-66.6
PR002-1B	2.7	356.3	33.3	355.6	29.5	340	4	63.7
PR003-1C	3.4	361.7	31.4	360.9	27.7	340	4	62.9
TC003-2A	20.5	201.2	-41.7	199.0	-38.7	340	4	-64.4
TC006-1B	26.6	193.7	-55.0	190.8	-51.6	340	4	-77.2
TC009-2B	34.5	200.8	-45.7	198.3	-42.6	340	4	-67.1
TC011-1A	39.0	191.4	-45.0	189.5	-41.6	340	4	-70.5
TC012-1B	42.0	194.6	-43.1	192.6	-39.8	340	4	-68.1
TC013-1A	43.5	196.5	-52.1	193.6	-48.8	340	4	-73.7
TC015-1A	45.5	346.4	12.7	346.3	8.7	340	4	50.6
TC017-2A	49.8	332.1	33.3	332.4	29.3	340	4	54.7
TC019-2B	54.3	394.9	22.9	393.6	20.6	340	4	47.2
TC021-2A	59.3	365.3	14.2	364.9	10.6	340	4	53.3
TC023-1C	64.9	212.0	-36.9	209.7	-34.5	340	4	-55.9
TC024-1B	67.0	363.8	39.9	362.5	36.3	340	4	68.2
TC026-1B	68.8	198.8	-47.9	196.2	-44.8	340	4	-69.6
TC028-1B	76.2	341.6	9.1	341.6	5.1	340	4	47.4
TC029-1B	78.3	338.2	22.8	338.3	18.8	340	4	52.6
TC030-2D	80.0	192.8	-45.6	190.7	-42.2	340	4	-70.4
TC033-2B	87.9	193.6	-36.9	192.0	-33.6	340	4	-64.4
TC034-1B	89.1	186.3	-50.9	184.2	-47.3	340	4	-76.2
TC035-2B	92.1	185.2	-50.8	183.3	-47.2	340	4	-76.3
TC036-2B	94.5	194.3	-46.6	192.0	-43.3	340	4	-70.6
TC037-2B	96.2	203.0	-52.1	199.7	-49.1	340	4	-70.2
TC038-1B	99.8	189.4	-38.2	188.0	-34.7	340	4	-66.3
TC039-1B	104.0	193.3	-36.6	191.8	-33.2	340	4	-64.3
TC040-2B	105.3	190.1	-49.5	188.0	-46.0	340	4	-74.2
TC041-1A	110.1	193.0	-46.2	190.9	-42.8	340	4	-70.8
TC043-2B	115.3	195.6	-34.6	194.1	-31.4	340	4	-62.4
TC045-2B	117.6	208.9	-39.1	206.6	-36.4	340	4	-58.9
TC046-1A	119.9	189.9	-49.3	187.8	-45.8	340	4	-74.1
TC047-2B	125.1	184.9	-34.6	183.8	-31.0	340	4	-64.7
TC049-2B	128.5	449.9	19.5	448.6	20.8	340	4	8.2
TC050-2B	130.3	194.8	-49.4	192.3	-46.1	340	4	-72.5
TC051-1B	133.0	194.8	-39.7	193.0	-36.4	340	4	-65.8
TC052-1A	135.3	183.0	-40.9	181.8	-37.2	340	4	-68.9
TC053-1B	138.7	170.9	-38.9	170.3	-35.0	340	4	-66.0
TC054-1D	143.2	192.1	-44.5	190.1	-41.1	340	4	-69.9
TC057-1B	150.7	192.7	-42.3	190.8	-38.9	340	4	-68.2
TC058-1B	154.7	196.9	-43.3	194.7	-40.1	340	4	-67.4
TC059-2C	158.4	200.7	-41.6	198.5	-38.5	340	4	-64.6
TC060-1B	161.7	197.8	-33.1	196.3	-30.0	340	4	-60.7
TC061-1A	163.8	188.3	-44.8	186.5	-41.2	340	4	-71.0
TC062-1B	166.0	373.1	23.6	372.3	20.3	340	4	56.9
TC063-2B	168.7	351.8	31.9	351.3	28.0	340	4	62.0
TC065-1A	173.7	172.4	-52.0	171.3	-48.1	340	4	-75.5
TC066-1B	178.8	361.7	42.9	360.4	39.2	340	4	70.4
TC067-1A	181.1	195.2	-65.1	190.7	-61.8	340	4	-82.0
TC068-1B	186.1	326.9	37.3	327.5	33.4	340	4	53.7
TC069-1B	190.9	366.7	-10.8	367.2	-14.3	340	4	40.5
TC072-1B	202.7	258.8	-38.1	255.6	-38.7	340	4	-24.8
TC073-1D	203.0	298.3	45.6	300.8	42.5	340	4	38.7
TC074-2B	205.6	184.5	-51.9	182.5	-48.3	340	4	-77.3
TC075-1B	209.7	405.7	1.9	405.6	0.3	340	4	31.6
TC077-1B	218.9	194.1	-44.4	192.1	-41.1	340	4	-69.2
MO001-1A	223.6	166.2	-48.0	163.7	-40.4	327	8	-66.8
MO001-2A	223.6	192.3	-47.3	187.0	-41.4	327	8	-71.1
TC078-1B	226.8	305.8	21.7	306.6	18.4	340	4	33.2
MO002-2A	227.3	192.4	-50.7	186.3	-44.9	327	8	-73.8
MO003-1A	231.0	178.2	-42.5	174.9	-35.6	327	8	-67.5
MO004-1B	233.6	175.6	-44.8	172.3	-37.8	327	8	-68.4
TC081-2B	239.0	186.6	-37.5	185.3	-33.9	340	4	-66.3
MO005-1B	241.8	198.4	-63.6	187.9	-58.1	327	8	-83.2
MO006-1B	245.8	194.1	-50.1	188.0	-44.4	327	8	-72.9
TC086-1A	246.2	123.0	-63.3	127.2	-60.0	340	4	-51.0

Site No.	Stratigraphic level (m)	Geographic coordinates Dec. (º)	Geographic coordinates Inc. (º)	Stratigraphic coordinates Dec. (º)	Stratigraphic coordinates Inc. (º)	Dip Az. (º)	Dip. (º)	VGP Lat. (º)
MO007-1B	253.3	165.4	-23.1	164.5	-15.5	327	8	-53.4
MO010-1B	261.3	167.8	-44.3	165.4	-36.8	327	8	-65.4
MO011-1A	263.8	213.8	-47.5	206.4	-44.0	327	8	-63.0
MO012-2A	269.6	163.4	-49.6	161.1	-41.9	327	8	-66.4
MO013-1B	271.4	155.3	-38.0	154.5	-30.1	327	8	-56.2
MO014-1A	273.7	175.9	-53.6	171.5	-46.5	327	8	-74.3
MO015-1A	275.6	155.8	-21.4	155.4	-13.5	327	8	-48.8
MO016-2B	281.3	176.4	-54.2	171.8	-47.1	327	8	-74.9
MO018-1B	287.1	158.7	-63.7	156.0	-55.9	327	8	-70.7
MO019-1A	289.9	186.8	-54.0	180.8	-47.7	327	8	-76.9
MO020-1B	294.3	182.5	-66.0	174.3	-59.2	327	8	-85.3
MO021-1B	296.5	242.2	-52.9	231.6	-53.0	327	8	-49.0
Santpedor Section								
MP001-1B	288.6	200.3	-59.4	185.5	-45.2	335	18	-74.2
MP010-1A	290.4	214.0	-65.2	187.9	-57.4	320	16	-82.9
SP001-1B	307.5	203.7	-51.7	198.3	-45.3	345	8	-68.8
SP002-1B	309.5	201.6	-39.2	198.2	-32.7	345	8	-61.4
SP003-1A	311.8	206.9	-51.8	201.0	-45.6	345	8	-67.3
MP003-1A	313.9	201.3	-48.5	190.5	-35.0	335	18	-65.8
SP004-1B	314.8	232.4	-39.4	226.8	-36.1	345	8	-45.1
SP005-1C	316.8	164.9	-27.1	164.8	-19.1	345	8	-55.3
MP004-1C	317.6	193.1	-50.5	183.6	-35.5	335	18	-67.7
SP006-1B	319.6	211.8	-38.0	209.4	-34.3	350	5	-56.1
MP005-2A	320.6	205.0	-62.6	187.0	-49.0	335	18	-76.8
SP007-1B	322.5	225.5	-54.4	220.2	-51.5	350	5	-56.8
MP006-1B	323.1	206.8	-35.3	199.1	-23.3	335	18	-56.0
MP008-2B	327.4	196.3	-20.3	192.5	-11.1	320	16	-52.1
MP009-1A	331.2	180.9	-57.2	167.8	-37.4	324	23	-66.7
SP009-1A	331.7	202.4	-55.1	198.9	-50.8	350	5	-71.7
SP012-1C	337.0	209.3	-49.8	204.1	-43.4	350	8	-64.2
SP013-1B	339.0	198.8	-62.5	192.8	-55.4	350	8	-78.4
SP016-1B	352.3	205.0	-39.1	201.8	-32.5	350	8	-59.5
SP017-1A	354.0	202.7	-43.4	199.2	-36.6	350	8	-63.1
SP018-1B	355.9	189.1	-60.1	184.3	-49.6	350	11	-78.1
SP020-1C	361.3	203.6	-34.8	200.1	-25.5	350	11	-56.7
SP021-1B	363.8	189.6	-40.6	187.0	-30.2	350	11	-63.7
SP022-1B	366.2	191.9	-49.4	188.0	-39.1	350	11	-69.2
SP023-1B	367.8	196.5	-16.7	195.5	-6.8	350	11	-49.2
SP024-1C	371.1	217.1	-42.6	210.9	-34.8	350	11	-55.4
SP025-2B	372.5	192.2	-52.5	187.9	-42.3	350	11	-71.4
SP026-1B	374.8	181.3	-68.9	173.7	-57.5	340	12	-84.0
SP029-2B	381.7	198.0	-27.8	194.9	-18.3	340	12	-55.0
SP030-1C	383.9	193.9	-42.7	185.8	-35.9	315	12	-67.6
SP031-1B	387.3	202.6	-60.8	186.0	-54.7	315	12	-82.0
SP032-1B	389.0	199.1	-41.0	190.8	-35.1	315	12	-65.7
SP033-1A	391.0	197.9	-58.7	188.6	-48.8	340	12	-76.0
SP034-1B	394.8	201.4	-53.1	188.8	-47.2	315	12	-74.8
SP035-1B	396.7	211.6	-48.4	199.6	-44.6	315	12	-67.6
SP036-1B	398.8	201.6	-60.4	185.4	-54.2	315	12	-81.8
SP038-1B	410.8	176.4	-61.0	165.6	-51.3	315	12	-74.9
SP039-1B	412.3	213.1	-62.3	193.4	-58.0	315	12	-79.3
SP040-1B	414.8	201.0	-63.2	183.3	-56.7	315	12	-84.9
SP041-1B	417.8	198.2	16.2	201.9	21.1	315	12	-33.6
SP042-1A	420.5	219.8	-65.3	196.4	-61.8	315	12	-77.9
SP043-1B	423.1	230.2	-32.4	222.5	-32.8	315	12	-46.7
SP047-1B	425.3	217.5	-72.7	186.0	-67.9	315	12	-80.0
SP044-1A	426.0	387.3	32.7	380.6	28.5	315	12	58.0
SP045-1B	428.3	382.6	23.0	378.5	18.1	315	12	53.7
SP046-1B	430.1	365.0	46.5	357.0	38.2	315	12	69.5
SP050-1B	434.3	359.4	42.2	353.1	33.2	315	12	65.6
SP051-1B	437.6	332.8	34.0	330.9	22.6	315	12	50.6
SP052-1B	439.4	382.0	15.1	379.5	10.3	315	12	49.5
SP053-1B	444.4	341.9	43.3	337.9	32.4	315	12	59.3
SP054-1B	445.9	329.2	30.4	327.9	18.7	315	12	47.2
SP055-1C	449.4	396.7	47.6	384.5	44.7	315	12	64.7

Site No.	Stratigraphic level (m)	Geographic coordinates Dec. (º)	Geographic coordinates Inc. (º)	Stratigraphic coordinates Dec. (º)	Stratigraphic coordinates Inc. (º)	Dip Az. (º)	Dip. (º)	VGP Lat. (º)
SP056-1C	453.7	47.1	65.6	382.0	63.4	315	12	73.7
SP057-1B	457.1	351.0	28.3	348.0	18.5	315	12	56.0
SP059-1B	463.6	430.8	35.2	422.3	39.8	315	12	35.2
SP060-1B	466.2	364.2	70.5	346.3	61.4	315	12	79.9
SP061-1B	468.7	382.8	27.3	377.7	22.4	315	12	56.1
SP064-1B	473.6	362.0	33.0	357.3	24.6	315	12	61.0
SP065-1B	475.7	357.2	66.0	344.4	56.2	315	12	76.9
SP066-1B	478.2	356.5	53.1	348.1	43.6	315	12	70.9
SP067-2C	479.0	401.0	27.3	395.0	26.0	315	12	48.7
SP068-1B	481.4	327.5	46.8	325.3	35.0	315	12	53.0
SP069-1B	483.9	379.3	72.5	354.4	65.1	315	12	83.4
SP070-1B	486.1	382.3	25.1	377.7	20.2	315	12	55.0
SP073-1B	491.6	367.6	63.1	353.1	54.7	315	12	81.5

Supporting Table 1: ChRM directions of the Moià and Santpedor magnetostratigraphic sections. Site No., name of paleomagnetic site and specimen code; Stratigraphic level, stratigraphic position of the paleomagnetic site in the Moià-Santpedor composite section; Dec. and Inc., declination and inclination in geographic (in situ) and stratigraphic coordinates (after bedding correction); Dip. Az. and Dip., azimuth of down dip direction of local bedding and angle of dip of local bedding; VGP Lat., latitude of the Virtual Geomagnetic Pole used to build the local magnetostratigraphy of Moià and Santpedor sections (see Fig. 4).

Site No.	Stratigraphic level (m)	Geographic coordinates Dec. (º)	Geographic coordinates Inc. (º)	Stratigraphic coordinates Dec. (º)	Stratigraphic coordinates Inc. (º)	Dip Az. (º)	Dip. (º)	VGP Lat. (º)
Moià Section								
TC008-1A	30.3	198.6	-16.4	197.9	-13.3	340	4	-51.5
TC010-1B	35.7	199.8	-32.2	198.2	-29.1	340	4	-59.4
TC015-1A	45.5	195.2	-49.8	192.6	-46.5	340	4	-72.6
TC016-1B	47.3	219.2	-40.6	216.4	-38.5	340	4	-53.5
TC017-2A	49.8	200.5	-33.5	198.9	-30.5	340	4	-59.8
TC019-2B	54.3	192.5	-46.2	190.4	-42.8	340	4	-71.0
TC024-1B	67.0	198.6	-42.6	196.5	-39.5	340	4	-66.2
TC025-1B	68.3	188.4	-50.3	186.3	-46.7	340	4	-75.2
TC027-2B	72.1	190.2	-43.4	188.4	-39.9	340	4	-69.6
TC028-1B	76.2	197.4	-54.2	194.3	-51.0	340	4	-74.7
TC029-1B	78.3	194.9	-42.3	193.0	-39.0	340	4	-67.5
TC031-1B	82.6	193.8	-7.1	193.6	-3.9	340	4	-48.3
TC032-1C	85.0	180.9	-30.6	180.1	-26.8	340	4	-62.4
TC045-2B	117.6	207.8	-39.7	205.5	-37.0	340	4	-59.8
TC057-1B	150.7	196.4	-37.0	194.7	-33.7	340	4	-63.5
TC062-1B	166.0	186.8	-49.3	184.8	-45.7	340	4	-74.8
TC063-2B	168.7	193.7	-44.0	191.7	-40.7	340	4	-69.0
TC066-1B	178.8	160.8	-49.2	160.7	-45.2	340	4	-68.1
TC068-1B	186.1	195.0	-47.1	192.7	-43.8	340	4	-70.7
TC069-1B	190.9	189.6	-34.7	188.3	-31.3	340	4	-64.1
TC070-2B	197.6	198.3	-44.6	196.0	-41.4	340	4	-67.6
TC075-1B	209.7	191.4	-44.9	189.5	-41.5	340	4	-70.4
TC078-1B	226.8	185.8	-46.4	184.1	-42.8	340	4	-72.7
Santpedor Section								
MP002-1B	310.8	246.5	-58.6	219.1	-54.9	335	18	-59.1
SP015-1A	348.3	242.9	-66.9	227.0	-63.6	350	8	-56.2
SP021-1B	363.8	229.4	-66.4	212.3	-59.5	350	11	-65.7
SP023-1B	367.8	205.4	-50.1	199.2	-40.9	350	11	-65.6
SP024-1C	371.1	196.1	-50.1	191.5	-40.1	350	11	-68.8
SP029-2B	381.7	201.8	-46.8	194.9	-37.5	340	12	-65.7
SP030-1C	383.9	228.0	-54.0	211.7	-53.0	315	12	-63.8
SP038-1B	410.8	253.1	-83.3	168.4	-79.5	315	12	-61.5
SP044-1A	426.0	205.5	-55.3	191.2	-50.0	315	12	-75.8
SP045-1B	428.3	183.9	-41.4	177.2	-33.1	315	12	-66.1
SP048-1B	428.5	164.8	-54.6	158.4	-43.9	315	12	-66.0
SP046-1B	430.1	215.9	-63.9	194.4	-59.9	315	12	-79.1
SP051-1B	437.6	210.1	-43.2	200.1	-39.3	315	12	-64.2
SP052-1B	439.4	241.9	-61.5	219.1	-62.9	315	12	-61.6
SP053-1B	444.4	215.5	-64.1	194.0	-60.0	315	12	-79.5
SP054-1B	445.9	198.7	-72.1	174.5	-64.6	315	12	-83.9
SP055-1C	449.4	184.1	-55.2	173.7	-46.6	315	12	-75.1
SP057-1B	457.1	222.8	-65.9	198.2	-63.0	315	12	-76.5
SP058-1C	461.0	173.8	-71.3	159.2	-61.0	315	12	-74.6
SP059-1B	463.6	204.0	-71.2	178.9	-64.6	315	12	-85.3
SP061-1B	468.7	189.1	-56.5	177.3	-48.5	315	12	-77.5
SP062-2B	471.9	200.3	-50.6	188.8	-44.6	315	12	-72.9
SP067-2C	479.0	181.0	-41.7	174.7	-33.0	315	12	-65.8
SP069-1B	483.9	204.4	-44.8	194.4	-39.7	315	12	-67.3
SP070-1B	486.1	209.1	-54.7	194.6	-50.1	315	12	-73.9
SP071-1D	488.4	240.0	-2.7	239.2	-5.9	315	12	-24.6

Supporting Table 2: Intermediate directions of the Moià and Santpedor magnetostratigraphic sections. Site No., name of paleomagnetic site and specimen code; Stratigraphic level, stratigraphic position of the paleomagnetic site in the Moià-Santpedor composite section; Dec. and Inc., declination and inclination in geographic (in situ) and stratigraphic coordinates (after bedding correction); Dip. Az. and Dip., azimuth of down dip direction of local bedding and angle of dip of local bedding; VGP Lat., latitude of the Virtual Geomagnetic Pole used to build the local magnetostratigraphy of Moià and Santpedor sections (see Fig. 4).

CHAPTER 4:

SUMMARY OF RESULTS AND DISCUSSION

Detailed results, discussions, and their derived conclusions have been presented in the appropriate sections of Chapter 3. In the following, a synthesis of the results derived from the study of the Paleogene record of the SE margin of the Ebro Basin will be put forward. An integrative discussion is presented which focuses on: *i*) the main objective of this PhD-Thesis, which is to provide an independent chronological framework of the sedimentary record of the SE margin of the Eastern Ebro Basin, and *ii*) the biochronological and tectonosedimentary implications for the overall Ebro Basin.

4.1. The Sampled Magnetostratigraphic Sections

According to geological and geographical criteria, three sectors along the SE margin of the Ebro Basin have been distinguished. From SW to NE these sectors are the Igualada, Montserrat, and Vic-Manresa areas. In each of these areas, a set of correlative and overlapped sections have been sampled with the main objective to obtain a continuous and long magnetostratigraphy. Achieving a very long magnetostratigraphic record was crucial in order get a characteristic, unique, pattern of polarity reversals. This uniqueness of the magnetostratigraphic record was the key to achieve an independent correlation to the Geomagnetic Polarity Time Scale (GPTS) of Gradstein *et al.* (2004), and to provide further constraints for the calibration of the marine and continental biostratigraphy.

In the Igualada area two magnetostratigraphic composite sections have been obtained: the Miralles-La Tossa section (Chapter 3.1) and the Maians-Rubió section (Chapter 3.2). Both sections record the uppermost marine units of the South Pyrenean Foreland Basin of Lutetian-Bartonian/Priabonian age (Ferrer, 1971; Puigdefàbregas & Souquet, 1986; Riba *et al.*, 1983; Serra-Kiel *et al.*, 2003). The Miralles-La Tossa section includes the continental Pontils Group, and the marine Santa Maria Group and "Terminal Complex", encompassing the so-called "Bartonian" transgression (Serra-Kiel & Travé, 1995). The Maians-Rubió section consists entirely of continental sediments of the Artés Formation of Priabonian-Rupelian age. However, detailed lithostratigraphic correlation indicates that the lower 50 meters of the Maians-Rubió section grade basinwards into the uppermost marine sediments of the Santa Maria Group, the "Terminal Complex", and the Òdena Gypsum Formation (sulphate belt of the halite-dominated Cardona Formation; Fig. 2 in Chapter 3.2).

In the Montserrat area, a thick conglomerate sequence represents the development of alluvial fan and fan-delta complexes that resulted from the tectonic growth during the Paleogene of the Catalan Coastal Ranges (Guimerà, 1984; Anadón *et al.*, 1985; López-Blanco *et al.*, 2000b; López-Blanco, 2002, 2006). In this proximal sector, continental sediments of the Montserrat and Sant Llorenç del Munt conglomerates alternate with marine sediments (Santa Maria Group) of the South Pyrenean Foreland Basin (Fig. 2 in Chapters 3.1 and 3.3). A new magnetostratigraphic section of Montserrat (Chapter 3.3), encompassing the La Salut Formation and the Montserrat Conglomerates (including also their lateral equivalent sediments of the Santa Maria Group), was constructed aimed to improve the age constraints for these units compared to results from earlier studies in the same area (López-Blanco *et al.*, 2000a).

In the Vic area, abundant magnetostratigraphic data for the Middle-Upper Eocene marine units were available (Burbank *et al.*, 1992; Taberner *et al.*, 1999). For this reason, focus was given to obtain magnetostratigraphic results from the continental units overlying the marine sediments of the Tossa Formation of the Santa Maria Group (Chapter 3.4). The Moià and the Santpedor sections encompass the Artés Formation and have been firmly correlated using the key bed of the Moià Member of the lacustrine Castelltallat Formation, which is interbedded within the distal alluvial and fluvial Artés Formation (Figs. 1 and 4 in Chapter 3.4).

4.2. Correlation of the Studied Magnetostratigraphic Sections to the Geomagnetic Polarity Time Scale

The integration of the local magnetostratigraphic sections with the available biostratigraphic data allows an approximation to the age interval represented in the studied stratigraphic record. However, existing calibrations of specific biostratigraphic datums have not been taken as constraints for further anchoring of the sections with the GPTS. Correlation with the time scale was guided by the characteristic pattern of reversals of the local magnetostratigraphy and its best-fit with the GPTS. This is possible because reversals of the geomagnetic field do not occur at periodic intervals. Having a sufficiently long record assures obtaining a polarity pattern which is characteristic enough to establish a correlation with the GPTS. In this PhD-Thesis, the shortest local magnetostratigraphy is ~500 meters (Moià-Santpedor composite section; Chapter 3.4), and it is integrated in a set of other magnetostratigraphic sections that are correlative and or overlapped to it (*e.g.*, Maians-Rubió composite section in Chapter 3.2, Rocafort-Vinaixa composite section from Barberà *et al.*,

2001). This has resulted in a long magnetostratigraphic record which allows an independent calibration with the GTS2004 (Gradstein *et al.*, 2004), in the sense that biostratigraphy is not used to anchor specific magnetozones with a particular chron of the time scale. The resulting correlation of these sections with the GPTS (Gradstein *et al.*, 2004) is shown in Fig. 4.1 and, in the following a general view on the procedure of correlation is given.

Two types of biostratigraphical constraints are available in the marine record of the Igualada area, the larger foraminifers and the calcareous nannofossil. From the biostratigraphic study performed in the Miralles-La Tossa composite section (Fig. 3 in Chapter 3.1) it is concluded that the marine units of Igualada area range from Bartonian to Priabonian in age. Form this first-order constraint, a good fit of the Miralles-La Tossa magnetostratigtraphy with the GPTS (Gradstein *et al.*, 2004) is achieved by correlating the three thickest normal magnetozones with chrons C18n to C16n, spanning the complete Bartonian stage and the lower Priabonian.

Although no direct available biostratigraphic constraints are found in the continental record of the Igualada area, the Maians-Rubió composite section has been lithostratigraphically correlated to other magnetostratigraphic sections yielding Late Eocene to Early Oligocene vertebrate fossil assemblages (Agustí *et al.*, 1987; Anadón *et al.*, 1987, 1992; Sáez, 1987; Arbiol & Sáez, 1988; Barberà *et al.*, 2001), as discussed in Chapters 3.2 and 3.4. The Maians-Rubió composite section has been correlated southwestwards to the Rocafort-Vinaixa magnetostratigraphic section of Barberà *et al.* (2001) as shown in Fig. 6 of Chapter 3.2, while northeastwards it has been correlated to the Moià-Santpedor section in the Vic-Manresa area (Fig. 5 in Chapter 3.4). Correlation of the Maians-Rubió composite section with the Rocafort-Vinaixa and the Moià-Santpedor magnetostratigraphic sections was feasible because the conglomerate strata at the top of the Maians section and at the base of the Rubió section

Figure 4.1. Correlation of the local magnetostratigraphies of the Miralles-La Tossa, Maians-Rubió, Montserrat, and Moià-Santpedor to the GPTS (Gradstein *et al.*, 2004) with indication of all the available biostratigraphical constraints calcareous nannofossil and larger foraminifers biozonations, and the vertebrate localities with their corresponding MP reference levels (Agustí *et al.*, 1987; Anadón *et al.*, 1987, 1992; Sáez, 1987; Arbiol & Sáez, 1988; Barberà *et al.*, 2001). Asterisk (*) indicates fossil mammal site correlated to the sections. The Rocafort-Vinaixa log is a composite section from the Rocafort, Sarral, Solivella, Tarrés and Vinaixa magnetostratigraphic sections of Barberà *et al.* (2001). The regional significant Santpedor sandstone unit has been used to correlate the Moià-Santpedor section with the magnetostratigraphic section of Maians-Rubió, the Jorba-La Panadella lithostratigraphic section (Feist *et al.*, 1994), and the Rocafort-Vinaixa magnetostratigraphy.

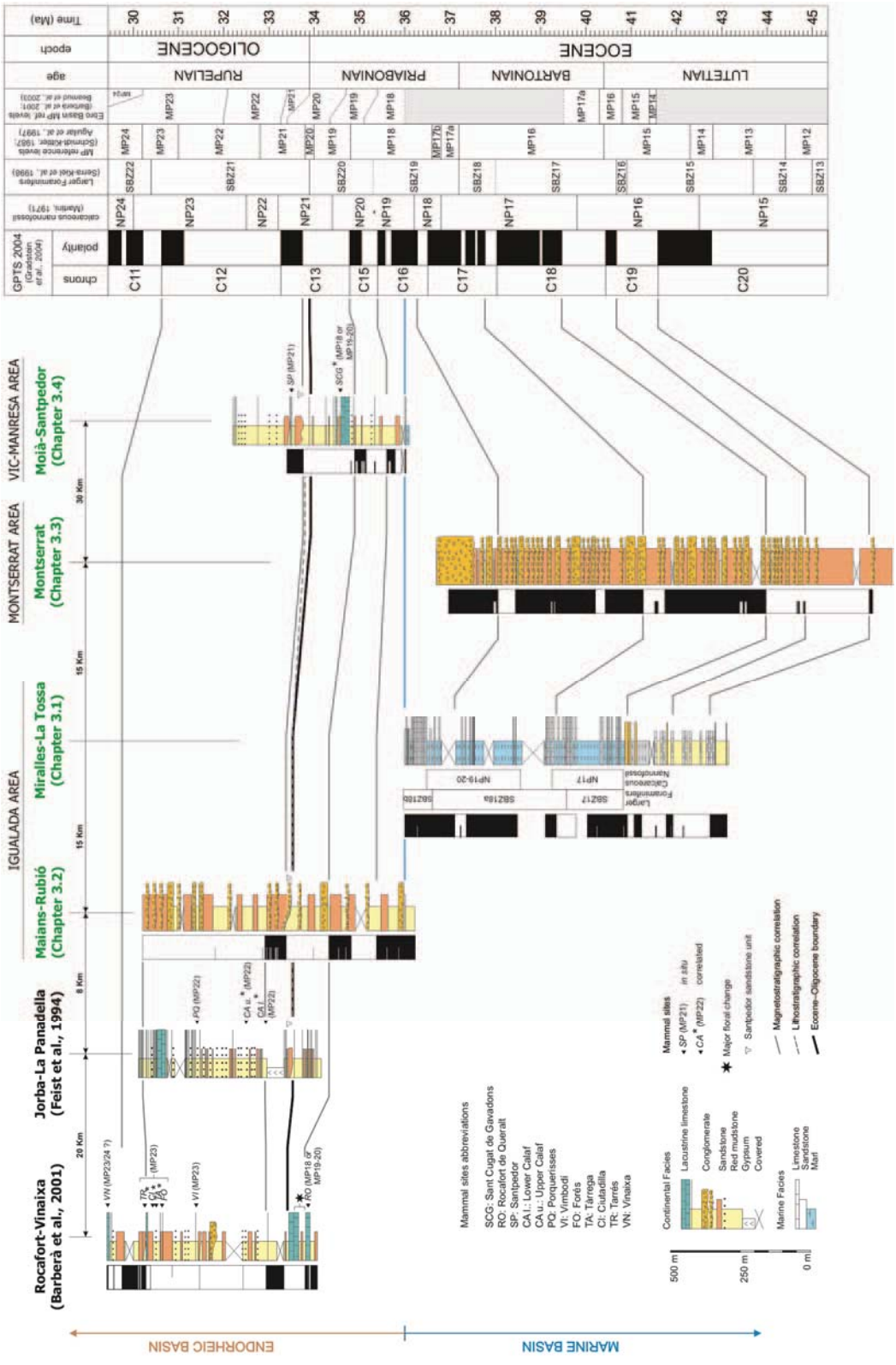
IGUALADA AREA
MONTSERRAT AREA
VIC-MANRESA AREA
Rocafort-Vinaixa (Barberà et al., 2001)
Jorba-La Panadella (Feist et al., 1994)
Maians-Rubió (Chapter 3.2)
Miralles-La Tossa (Chapter 3.1)
Montserrat (Chapter 3.3)
Moià-Santpedor (Chapter 3.4)
20 Km
8 Km
15 Km
15 Km
30 Km
Time (Ma)
epoch
age
chrons
polarity
GPTS 2004 (Gradstein et al., 2004)
OLIGOCENE
EOCENE
RUPELIAN
PRIABONIAN
BARTONIAN
LUTETIAN
Mammal sites abbreviations
SCG: Sant Cugat de Gavadons
RO: Rocafort de Queralt
SP: Santpedor
CA l.: Lower Calaf
CA u.: Upper Calaf
PQ: Porquerisses
VI: Vimbodí
FO: Fordó
TA: Tàrrega
CI: Ciutadilla
TR: Tàrrés
VN: Vinaixa
Mammal sites
SP (MP21) in situ
CA (MP22) correlated
Major floral change
Santpedor sandstone unit
Magnetostratigraphic correlation
Lithostratigraphic correlation
Eocene–Oligocene boundary
Continental Facies
Lacustrine limestone
Conglomerate
Sandstone
Red mudstone
Gypsum
Covered
Marine Facies
Limestone
Sandstone
Marl
500 m
250 m
0 m
ENDORHEIC BASIN
MARINE BASIN

constitute a competent continuous horizon of regional significance (Santpedor sandstone unit) that can be traced for tens of kilometers along the SE margin of the Eastern Ebro Basin (Figs. S4, 5, and 6 in Chapter 3.2; Fig. 5 in Chapter 3.4). Thus, in this sector of the Eastern Ebro Basin, the best correlation of the sampled continental Artés Formation to GPTS (Gradstein *et al.*, 2004) is then established to chrons C16n to C12r, based on the characteristic predominantly-reverse coupled magnetozones recorded in the Maians-Rubió and Moià-Santpedor magnetostratigraphies containing Late Eocene to Lower Oligocene vertebrate fossil assemblages. Finally, no biostratigraphic data are found in the Montserrat section (Chapter 3.3) however, this section can be lithostratigraphically correlated to the Maians-Rubió composite section as discussed in Chapter 3.3 and shown in its Fig.6.

4.3. Paleogene Chronostratigraphy of the SE Margin of the Eastern Ebro Basin

The biomagnetostratigraphy-based chronology derived from this PhD-Thesis (Fig. 4.1) together with the integration of previous biomagnetostratigraphic data available in this sector of the basin (Burbank *et al.*, 1992; Taberner *et al.*, 1999; Barberà *et al.*, 2001), have allowed establishing a reliable chronostratigraphy of the Paleogene units of the SE margin of the Ebro Basin. Figure 4.2 shows this new chronostratigraphic framework, which ranges from chron C20n to chron C12r (*ca.* 43-31 Ma), that is, from the Lutetian to Rupelian stages. In the following, a synthesis of how the new chronology challenges earlier results will be considered.

4.3.1. Chronology of the Middle-Late Eocene Marine Units and the Final Marine-Continental Transition of the South Pyrenean Foreland Basin in the Eastern Ebro Basin

Relevant changes in the chronological attribution of the marine units in the Igualada area occur as derived from the biomagnetostratigraphy of the Miralles-La Tossa composite section and the Maians-Rubió magnetostratigraphy. While earlier studies attributed to the Santa Maria Group a Bartonian age according to its fossil contents (Serra-Kiel *et al.*, 2003; Fig. 2 in Chapter 3.1), the new magnetostratigraphy of Miralles-La Tossa sections demonstrates that the Igualada Formation embraces a large part of the Priabonian stage, in accordance with the pioneering study of planktonic foraminifers of Ferrer (1971a,b). Moreover, uppermost marine units such as Tossa Formation, the "Terminal Complex", and the Òdena Gypsum Formation are correlated to chron C16n (*i.e.*, Priabonian). This correlation, supported by results from both the Miralles-Tossa and the Maians-Rubió composite sections (Figs. 4.1; Fig. 6 in Chapter 3.1; Figs. 2 and 6 in Chapter 3.2), indicates that the final marine-continental transition in the Igualada area correlates with the Priabonian, yielding an interpolated age of *ca.* 36.0 Ma (Chapter 3.2).

The results obtained in the Igualada area call for a reinterpretation of earlier magnetostratigraphic studies spanning the Middle to Late Eocene marine units of the Eastern Ebro Basin in the Vic area (Burbank *et al.*, 1992; Taberner *et al.*, 1999), since correlations to the GPTS in these studies were mainly forced on the presumed "Bartonian" age of the uppermost marine units according to its fossil contents. In Chapter 3.2, a convincing alternate correlation of the Vic magnetostratigraphic section of Burbank *et al.* (1992) has been put forward (Fig. S5 in Chapter 3.2) assuming the obtained age of the marine-continental transition in the Igualada area and integrating recent biomagnetostratigraphic data from the same region (Cascella & Dinarès-Turell, 2009). The new calibration of the Vic magnetostratigraphy yields a better fit with the GPTS (Gradstein *et al.*, 2004), smooth sediment accumulation rates which better match with the long term trends observed in other records of Eastern Ebro Basin (Fig. 8 in Chapter 3.2). In the chronostratigraphic panel shown in Fig 4.2, the set of magnetostratigraphic sections of Taberner *et al.* (1999) have been correlated to the GPTS (Gradstein *et al.*, 2004) according to the new constraints. Therefore, the uppermost marine units in the Vic area such as the La Guixa and Vespella Marls, the uppermost Centelles Sandstone, the Sant Martí Xic deltaic complex, and the evaporitic Cardona Formation are Priabonian in age according to its revised correlation spanning from chrons C17n to C16n. Noteworthy, the obtained age of the marine-continental transition is significantly older than the assigned to the Cardona Formation on the basis of $^{87}Sr/^{86}Sr$ ratios in anhydrite samples (Taberner *et al.*, 1999). As discussed in Chapter 3.2, the environment during the deposition of the Cardona Formation likely corresponded to a highly restricted water mass, with isotopic ratios largely influenced by incoming continental waters (Ayora *et al.*, 1994; Cendón *et al.*, 2003). Under this scenario, the chronostratigraphic significance of $^{87}Sr/^{86}Sr$ ratios is highly precarious, and easily explains the observed discrepancy with the magnetostratigraphy-based chronology.

Finally, the integrated results from the Igualada and Vic areas (Fig 4.2) has led to the conclusion that the former 2nd Bartonian cycle of Serra-Kiel & Travé (1995) and Serra-Kiel *et al.* (2003) is in fact Priabonian in age.

Figure 4.2. Chronostratigraphy of the Paleogene units of the SE margin of the Ebro Basin.

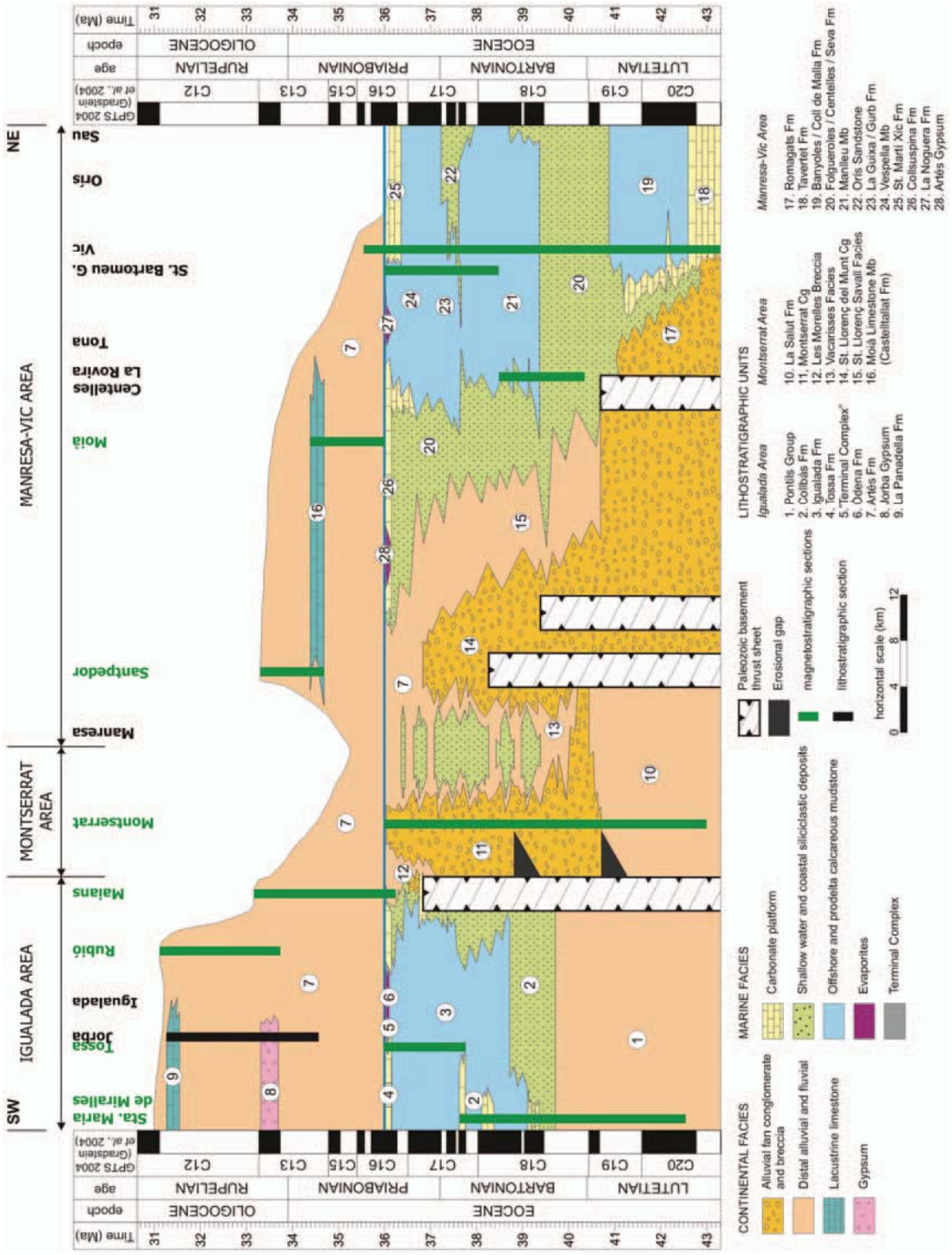
SW
NE
IGUALADA AREA
MONTSERRAT AREA
MANRESA-VIC AREA
Sta. Maria de Miralles
Tossa
Jorba
Igualada
Rubió
Malans
Montserrat
Manresa
Sanpedor
Moià
Centelles
La Rovira
Tona
St. Bartomeu G.
Vic
Orís
Sau
Time (Ma)
epoch
age
GPTS 2004 (Gradstein et al., 2004)
EOCENE
OLIGOCENE
LUTETIAN
BARTONIAN
PRIABONIAN
RUPELIAN
C20
C19
C18
C17
C16
C15
C13
C12
CONTINENTAL FACIES
Alluvial fan conglomerate and breccia
Distal alluvial and fluvial
Lacustrine limestone
Gypsum
MARINE FACIES
Carbonate platform
Shallow water and coastal siliciclastic deposits
Offshore and prodelta calcareous mudstone
Evaporites
Terminal Complex
Paleozoic basement thrust sheet
Erosional gap
magnetostratigraphic sections
lithostratigraphic section
horizontal scale (km)
LITHOSTRATIGRAPHIC UNITS
Igualada Area
1. Pontils Group
2. Collbàs Fm
3. Igualada Fm
4. Tossa Fm
5. "Terminal Complex"
6. Òdena Fm
7. Artés Fm
8. Jorba Gypsum
9. La Panadella Fm
Montserrat Area
10. La Salut Fm
11. Montserrat Cg
12. Les Moreles Breccia
13. Vacarisses Facies
14. St. Llorenç del Munt Cg
15. St. Llorenç Savall Facies
16. Moià Limestone Mb (Castellfollit Fm)
Manresa-Vic Area
17. Romagats Fm
18. Tavertet Fm
19. Banyoles / Coll de Malla Fm
20. Folgueroles / Centelles / Seva Fm
21. Manlleu Mb
22. Orís Sandstone
23. La Guixa / Gurb Fm
24. Vespella Mb
25. St. Martí Xic Fm
26. Collsuspina Fm
27. La Noguera Fm
28. Artés Gypsum

4.3.2. Chronology of the Middle Eocene-Oligocene Continental Units of the SE Margin of the Eastern Ebro Basin

The new magnetostratigraphic section of Montserrat (Chapter 3.3) challenges earlier magnetochronological attributions of the alluvial fan and fan-delta complex of Montserrat (López-Blanco *et al.,* 2000a). These authors based their correlation on the assumed "Bartonian" age of the marine units of the Santa Maria Group (Serra-Kiel *et al.*, 2003). According to Figs. 4.1, 4.2 and Fig. 6 in Chapter 3.3, a Lutetian age can be ascribed to the whole La Salut Formation and the age of the Montserrat Conglomerates spans from C19r to C16n (*i.e.*, Upper Lutetian to Lower Priabonian). Results of this PhD-Thesis have led to the conclusion that the upper 330 meters of the Montserrat section, corresponding to the upper Vilomara, Manresa, and San Salvador Composite Sequences of López-Blanco *et al.* (2000a), are Priabonian in age.

Lithostratigraphic correlation of the Montserrat alluvial fan and fan-delta complex with the neighboring Sant Llorenç del Munt system (López-Blanco *et al.*, 2000b) shows that the uppermost Sant Llorenç del Munt Conglomerates are also Lower Priabonian in age. Finally, and as derived from the composite sections of Maians-Rubió (Igualada area; Chapter 3.2) and Moià-Santpedor (Vic-Manresa area; Chapter 3.4), the Artés Formation spans from Priabonian to Rupelian stages (Fig. 4.2).

4.4. Biochronological Implications

The Geologic Time Scale (GTS) is inextricably linked with Earth science as it constitutes the measurement yardstick and the key to reconstruct Earth history. The construction of the GTS comes from the integration of relative chronostratigraphic disciplines such as biostratigraphy and magnetostratigraphy with absolute dating techniques including radiometric geochronometry and astrochronology (Fig. 1.1). For the Paleogene System, the integration of the several chronostratigraphic scales has not reached stability; instead it is in constant evolution since refined chronologies are available (Gradstein *et al.*, 2004; Hilgen, 2008). From the biomagnetostratigraphic-based chronology resulting from this PhD-Thesis, a step forward to refine the GTS can be done by calibrating the recorded biohorizons of the studied sections along the central SE margin of the Ebro Basin. In the marine realm, the biostratigraphic study of the Miralles-La Tossa composite section (Chapter 3.1) has contributed to the intercalibration of the Bartonian-Priabonian calcareous nannofossil and the larger foraminifers

Shallow Benthic Zones, as well as their calibration with the absolute time scale. Finally, the mammal fossil assemblages in the Artés Formation have contributed to the calibration of the European Late Eocene to earlymost Oligocene vertebrate Mammal Paleogene (MP) reference levels (Chapter 3.4) in the continental realm.

4.4.1.The Marine Realm: Calibration of the Bartonian-Priabonian Calcareous Nannofossil and Larger Foraminifers Biozonations

Calcareous nannofossil form a heterogeneous group of minute objects (1-30 μm) which constitutes an important portion of the deeper marine sediments. It is generally accepted that calcareous nannofossil are the fossil remains of unicellar algae Haptophyceae. Its recognition in the sedimentary record has been successfully used as a handy tool for biostratigraphic correlations since they have a wide biogeographic distribution and high evolutionary trends (Gradstein *et al.*, 2004; Fornaciari *et al.*, 2010). Two widely used Paleogene zonal schemes differing between low and high latitudes exist. The NP zonation of Martini (1971) relied of studies on land sequences from largely temperate areas, whereas the CP zonation (Bukry, 1973, 1975; Okada & Bukry, 1980) was developed in low-latitudes oceanic sections. Successive high-resolution studies have re-defined and subdivided theses zonations (Gradstein *et al.*, 2004; and references therein) and, more recently, Fornaciari *et al.* (2010) have proposed additional biohorizons in order to improve the accuracy of these zonations as a correlation tool because, the markers adopted in both zonal schemes, are based on index species that are latitudinally restricted, facies dependent, and/or poorly defined.

Larger foraminifers have for long been a decisive stratigraphic tool in shallow-marine tropical to temperate areas. Zones for larger foraminifers are ideally based on successions of biometric populations within phylogenetic linages, being the species considered as morphometric units (Gradstein *et al.*, 2004). Usefulness of these microfossils as a biostratigraphic tool was revealed during the 60's up to the 80's of the last century, when a number of monographs on larger foraminifers groups were published (*e.g.*, Hottinger, 1960, 1977; Schaub, 1981; Less, 1987). Later, Serra-Kiel *et al.* (1998) published a larger foraminifers zonation of the Paleocene and Eocene of the Tethyan area. Noteworthy, no correlation of the Paleogene larger foraminifers zonation with the GPTS is provided in the GTS2004 (Gradstein *et al.*, 2004), despite that Serra-Kiel *et al.* (2003) attempted a magnetostratigraphic calibration based on data from the Vic section (Burbank *et al.,* 1992). Moreover, intercalibration between calcareous nannofossil and larger foraminifers zonations is still somewhat fragmentary and

discontinuous leaving some leeway for subjective interpretations (Luciani *et al.*, 2002; Gradstein *et al.*, 2004).

From the chronostratigraphy of the Middle-Upper Eocene marine record of the Igualada area (Fig. 6 in Chapter 3.1 and Fig. 4.2), a revision of the calcareous nannofossil and the larger foraminifers calibration to the GPTS (Gradstein *et al.*, 2004) has resulted (Chapter 3.1). Magnetostratigraphic calibration of calcareous nannofossil in the Ebro Basin has revealed a mismatch with the current calibration of Zone NP19-20 (Fig. 7 in Chapter 3.1), suggesting that FO of *Isthmolithus recurvus* is a diachronic event, of low reliability for long-distance correlations. Particularly relevant are the results obtained for the larger foraminifers since the traditional division of the Bartonian stage into two complete larger foraminifers zones, SBZ17 and SBZ18, has been challenged (Fig. 7 in Chapter 3.1). Zone SBZ17 embraces most of the Bartonian, while Zone SBZ18 extends from late Bartonian to early Priabonian. In addition, a new Subzone (SBZ18b = *Nummulites variolarius/incrassatus* Biozone), recognized in both the Ebro Basin and the Priabonian type sections of Italy, has been proposed, while the Subzone SBZ18a is equivalent to the former Zone SBZ18 of Serra-Kiel *et al.* (1998). Finally, a correlation of the calcareous nannofossil Zone NP19-20 to the larger foraminifers Zone SBZ18 (uppermost Bartonian-early Priabonian) has been established (Fig. 7 in Chapter 3.1).

4.4.2.The Continental Realm: Calibration of the Late Eocene-Oligocene MP reference levels

During the Paleogene, the various continental masses had distinctive land mammal fauna. Since these fauna exhibit rapid evolution trends, they have been widely used for biostratigraphic correlation of non-marine strata (Gradstein *et al.*, 2004). However, fossil mammal correlations has often proved to be “more problematic” than other biozonations owing to: *i*) rare occurrence of mammals as fossils compared to other faunal groups; *ii*) endemism; and *iii*) the intrinsic discontinuous nature of the continental strata which may make mammal fossil occurrences to be in isolated exposures with unknown superposition relationships. Despite that, it has been proved that when solid stratigraphic frameworks (long and continuous sections including other biostratigraphic data and/or isotope radiometric constraints) are provided, fossil mammal assemblages can constitute a valuable biostratigraphic tool (Woodburne & Swisher, 1995).

The zonation scheme used to correlate fossil mammal assemblages across Europe is the Mammal Paleogene (MP) scale. It consists of a list of reference levels (localities) ordered in theoretical evolutionary grade, with no real boundaries defined between successive reference

levels (Schmidt-Kittler, 1987). That is, no appearance or disappearance of a single taxa defines these units. A first list of MP reference levels was elaborated in the *International Symposium on Mammal Stratigraphy of the European Tertiary* held in Munich in 1975 (Fahlbusch, 1976). Later revisions and updates were done in the *International Symposium on Mammalian Biostratigraphy and Paleoecology of the European Paleogene* held in Mainz in 1987 and in the congress *BiochroM'97* held in Montpellier in 1997 (Schmidt-Kittler, 1987; Aguilar *et al.*, 1997). In the *BiochroM'97* congress the agreements of the Mainz symposium were reaffirmed. Mammal fossil localities around Europe can be in principle assigned to a particular MP reference level on the basis of their affinities as expressed by evolutionary stages.

Calibration of mammal fossil assemblages to the GPTS has been successfully achieved through radioisotopic methods combined to magnetostratigraphy in the extraordinary continuous sedimentary record of North America (Emry, 1992; Woodburne & Swisher, 1995). In Europe however, calibration of MP reference levels has been limited to the Hampshire Basin (Isle of Wight, UK), through intercorrelation with other biozonations of the marine strata (Hooker, 1992, 2010; Hooker *et al.*, 2004, 2007, 2009; Gale *et al.*, 2006, 2007), or the fragmentary magnetostratigraphies focused in the mammal fossil localities of Western France and Spain (Lévêque, 1993). In the Ebro Basin, previous magnetostratigraphic studies have provided a robust chronological framework to correlate the MP mammal localities of Spain (Barberà *et al.*, 2001; Beamud *et al.*, 2003).

From the chronostratigraphy of the Upper Eocene-Lower Oligocene continental record of the SE margin of the Ebro Basin in the Vic-Manresa area (Fig. 7 in Chapter 3.4 and Fig. 4.2), a chronology for the Late Eocene to Early Oligocene mammal fossil assemblages in the Eastern Ebro Basin have resulted (Chapter 3.4). New magnetostratigraphic data of the Moià-Santpedor composite section, together with the Rocafort-Vinaixa composite section of Barberà *et al.* (2001) have confirmed an earliest Oligocene age (*ca.* 33.4 Ma) for the post-*Grande Coupure* Santpedor fossil site. This, in turn have supported the close correlation between the dramatic terrestrial faunal turnover known as the *Grande Coupure* (Sthelin, 1910) and the Eocene-Oligocene transition, with a (maximum) lag of time of *ca.* 0.5 Myr (Fig. 5 in Chapter 3.4). As in other Eocene-Oligocene records of Eurasia, in the Eastern Ebro Basin, the *Grande Coupure* might coincide with a shift to drier climatic conditions, as it has been deduced from sedimentological evidences (Santpedor sandstone units), which includes incision of fluvial fan channel deposits as a consequence of the drop of the base level at a regional scale. Moreover, the precise Eocene-Oligocene continental chronology of the Ebro Basin has allowed

an alternative interpretation of the Hampshire Basin sedimentary record (Isle of Wight, UK) which reconciles all the available marine and continental biostratigraphy from the Solent Group succession (Fig.6 in Chapter 3.4). From the integration of the Ebro and Hampshire basin records, a magnetostratigraphy-based calibration of the Late Eocene-Oligocene European mammal biochronology (MP reference levels) has resulted (Fig. 7 in Chapter3.4).

4.5. Tectonosedimentary Evolution Implications

From the chronology of the sedimentary marine and continental units of the SE margin of the Ebro Basin (Fig 4.2), the timing of tectonosedimentary events shaping the Ebro Basin and its surrounding thrust-belts can be constrained. In the Montserrat area, the Montserrat Conglomerates (Chapter 3.3) record the Paleogene tectonic evolution of the Catalan Coastal Ranges. The Maians-Rubió magnetostratigraphy in the Igualada area (Chapter 3.2) has provided new clues on the timing and character of the continentalization process of the South Pyrenean Foreland Basin. In the following, a short summary of the tectonosedimentary evolution implications derived from this PhD-Thesis is provided.

4.5.1. Tectonosedimentary Evolution of the Central Catalan Coastal Ranges

In the proximal area of Montserrat (Chapter 3.3), the new magnetostratigraphic section has been used to perform a geohistory analysis that has provided new insights on the thrusting and folding history of this area (López-Blanco *et al.*, 2002). Results of the geohistory analysis have shown direct correlation between (tectonic) subsidence and forelimb rotation rates measured on the basin-margin deformed strata of the Montserrat area (Figs. 7 and 8 in Chapter 3.3). Duration of the synsedimentary folding stage (López Blanco *et al.*, 2002) has been constrained to occur from Late Lutetian to Middle Bartonian (*ca.* 40.9 Ma to 38.7 Ma) and the beginning of the out-of-sequence thrusting stage has been dated at Middle Bartonian (*ca.* 38.7 Ma), being its minimum duration tightened to *ca.* 2.2 Myr (Fig. 8 in Chapter 3.3). Analysis of the subsidence and accumulation curves has suggested that during the synsedimentary folding and the out-of-sequence thrusting stages subsidence was driven by tectonic load, while sedimentary load had a greater contribution to total subsidence during the last stage.

Integration of subsidence curves of Montserrat together with re-calibrated subsidence curves of more basinal sectors in the Eastern Ebro Basin (Castellfollit and Santpedor well-logs from Vergés *et al.*, 1998), has unravelled the variable contribution of tectonic loads from the

Catalan Coastal Ranges and the Pyrenees in the Montserrat area (Figs. 11 and 12 in Chapter 3.3). From this integration, three evolutionary stages have been suggested to occur during the Middle to Late Eocene in the Montserrat area (Chapter 3.3). During the Lutetian (*ca.* 42 Ma) this area constituted a relative passive margin experiencing low subsidence rates compared to the northern areas, where subsidence has been related to the Pyrenean loading. From Late Lutetian to Late Bartonian (*ca.* 40.9 Ma to 38.7 Ma) the Montserrat area became a highly subsiding active margin, leading to the development of a doubly verging flexure associated to the two tectonically active basin margins, the Pyrenees to the north and the Catalan Coastal Ranges to the south. Finally, from Late Bartonian to Early Priabonian (*ca.* 38.7 Ma to 36.5 Ma) the homogenization of subsidence values of the Montserrat area and the more basinal positions has been interpreted as the result of the coupling of the two sources of tectonic load after the southwards migration of the Pyrenean flexural wave.

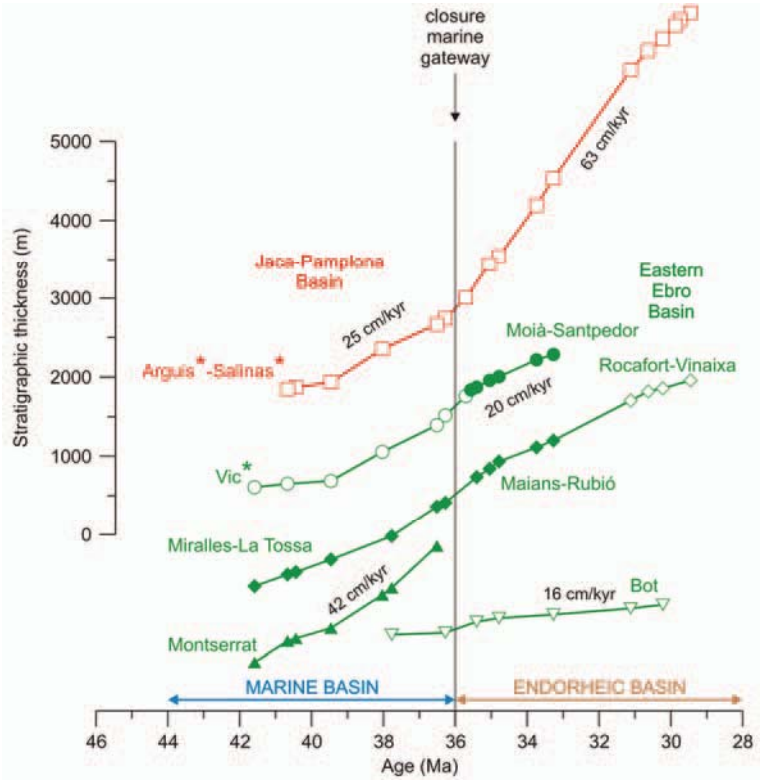

Figure 4.3. Undecompacted sedimentation trends in the Western (Jaca-Pamplona Basin) and the Eastern sectors of the Ebro Basin from Lutetian to Oligocene. Asterisks (*) indicates reinterpreted magnetostratigraphic sections in this PhD-Thesis (Arguis-Salinas from Hogan & Burbank [1996]; Vic from Burbank *et al.* [1992], and Taberner *et al.* [1999] and shown in Figs. S5 and S6 of Chapter 3.2). Rocafort-Vinaixa magnetostratigraphic section from Barberà *et al.* (2001), and Bot magnetostratigraphic section from Garcés *et al.*, (2008). A very important increase of sedimentation rates occurs in the Western sector at transition time from open to closed basin, while no changes are observed in the Eastern region. Contrasting patterns of accumulation rates in the Eastern Ebro Basin have been related to differences in subsidence linked to the structural style. Note the floating character of the stratigraphic thickness axis.

Finally, a comparison of the undecompacted sediment accumulation rates obtained for the Montserrat area and other Priabonian to Oligocene synorogenic alluvial successions in other marginal areas of the SE Ebro Basin is shown in Fig. 4.3. Noteworthy, Montserrat accumulation rates (up to 42 cm/kyr) are strikingly higher than the average accumulation rates obtained for the other sectors of the SE margin (20 cm/kyr). These contrasting patterns of accumulation along the Catalan Coastal Ranges-Ebro Basin foreland system have been related to differences in subsidence linked to the structural style. As discussed in Chapter 3.3, the Montserrat area, was characterized by a thick-skinned tectonic style, deformation was accommodated in a narrow belt with deep seated steep faults that created vertical stacking of basement units in a narrow zone. As a result subsidence was focused close to the mountain front. In other regions of the Catalan Coastal Ranges, tectonic style was thin-skinned, with basinwards migration of the deformation front. In these cases, subsidence was distributed along a wider region ahead of the mountain front.

4.5.2. Timing and Character of the Continentalization of the South Pyrenean Foreland Basin

As discussed above, the integrated magnetochronological framework of the Eastern Ebro Basin, allows constraining the timing of the continentalization process in this sector of the basin within chron C16n (Fig. 4.2). In Chapter 3.2, the timing of the marine-continental transition in the Western South Pyrenean Foreland Basin is discussed on the basis of the re-evaluated magnetostratigraphic records of Arguis and Salinas (Hogan & Burbank, 1996). As shown in Fig. 7 of Chapter 3.2 the marine-continental transition in the Jaca-Pamplona Basin can be best correlated with chron C16n. Therefore, all available chronostratigraphic information indicates that the transition from marine to continental sedimentation was a basinwide rapid, likely isochronous, event occurring at *ca.* 36.0 Ma (Late Priabonian). This result contrasts with the time-transgressive nature of lithostratigraphic units in foreland systems, but is coherent with a scenario of basin continentalization that resulted from seaway closure driven by the tectonic uplift of its margins. Coinciding with the marine to continental transition, the South Pyrenean Foreland Basin experienced a sudden increase in sedimentation rates, from 25 cm/kyr during marine deposition to 63 cm/kyr during continental deposition (Fig. 4.3). This change in the sedimentation rates trends has been interpreted as a consequence of the interruption of sediment bypass towards the oceanic domain after seaway closure, since acceleration of the Central Pyrenean Axial Zone clearly post-dates this change as demonstrated in recent combined magnetostratigraphy and fission track study of Beamud *et al.* (2011). During this process, the Jaca-Pamplona trough evolved from an efficient sediment

transfer zone to a sediment trap for all the erosion products of the Central Pyrenean Axial Zone. Moreover, as it has been pointed in Chapter 3.3, it results that the progressive filling of the Ebro Basin could have forced deformation to migrate hindward toward the interior of the orogen, a plausible picture coherent with the foreland chronostratigraphy and the exhumation history derived from the thermochronology (Fitzgerald, *et al.*, 1999; Sinclair *et al.*, 2005; Beamud *et al.*, 2011). As shown in Fig 4.3, in the Eastern Ebro basin, the change from open to closed basin drainage did not have significant effects on sedimentation rates due to the already restricted paleogeographic configuration and its limited connectivity with the open ocean.

4.6. References

AGUILAR, J.P., LEGENDRE, S., MICHAUX, J., (1997). Actes du Congrès BiochroM'97. Mémoires et Travaux de l'Institut de Montpellier de l'École Pratique des Hautes Études, Montpellier. 818pp.

AGUSTÍ, J., ANADÓN, P., ARBIOL, S., CABRERA, L., COLOMBO, F., SÁEZ, A., (1987). Biostratigraphical characteristics of the Oligocene sequences of North-Eastern Spain (Ebro and Campins Basins). *Münchner Geowissenschaftliche Abhandlungen*, **10**, 35-42.

ANADÓN, P., CABRERA, L., CHOI, S.J., COLOMBO, F., FEIST, M., SÁEZ, A., (1992). Biozonación del Paleógeno continental de la zona oriental de la Cuenca del Ebro mediante carófitas; implicaciones en la biozonación general de carófitas de Europa occidental. *Acta Geologica Hispanica*, **27**, 69-94.

ANADÓN, P., MARZO, M., PUIGDEFÀBREGAS, C., (1985). The Eocene fan-delta of Montserrat (Southeastern Ebro Basin, Spain). In: Milà, M.D., Rosell, J., (Eds.). *6th European Meeting Excursion Guidebook*, pp. 109-146. Institut d´Estudis Ilerdencs, Lleida.

ANADÓN, P., VIANEY-LIAUD, M., CABRERA, L., HARTENBERGER, J.L., (1987). Gisements à vertébrés du paléogène de la zone orientale du bassin de l'Ebre et leur apport à la stratigraphie. *Paleontologia i Evolució*, **21**, 117-131.

ARBIOL, S., SÁEZ, A., (1988). Sobre la edad oligocénica inferior del yacimiento de Santpedor (Cuenca del Ebro, provincia de Barcelona). *Acta Geologica Hispanica*, **23**, 47-50.

AYORA, C., GARCÍA-VEIGAS, J., PUEYO, J.J., (1994). The chemical and hydrological evolution of an ancient potash-forming evaporite basin as constrained by mineral sequence, fluid inclusion composition, and numerical simulation. *Geochemica et Cosmochimica Acta*, **58**, 3379-3394. doi:10.1016/0016-7037(94)90093-0

BARBERÀ, X., CABRERA, L., MARZO, M., PARÉS, J.M., AGUSTÍ, J., (2001). A complete terrestrial Oligocene magnetostratigraphy from the Ebro Basin, Spain. *Earth and Planetary Science Letters*, **187**, 1-16. doi: 10.1016/S0012-821(01)00270-9

BEAMUD, E., GARCÉS, M., CABRERA, L., MUÑOZ, J.A., ALMAR, Y., (2003). A new middle to late Eocene continental chronostratigraphy from NE Spain. *Earth and Planetary Science Letters*, **216**, 501-514. doi: 10.1016/S0012-821X(03)00539-9

BEAMUD, E., MUÑOZ, J.A., FITZGERALD, P.G., BALDWIN, S.L., GARCÉS, M., CABRERA, L., METCALF, J.R., (2011). Magnetostratigraphy and detrital apatite fission track thermochronology in syntectonic conglomerates: constraints on the exhumation of the South-Central Pyrenees. *Basin Research*, **23**, 309-331. doi: 10.1111/j.1365-2117.2010.00492.x

BUKRY, D., (1973). Low latitude coccolith biostratigraphic zonation. In: Edgar, N., Kaneps, A., Herring, J., (Eds.). *Initial Reports of the Deep Sea Drilling Project*, **15**, pp. 658-677. Washington DC. doi:10.2973/dsdp.proc.15.116.1973

BUKRY, D., (1975). Coccolith and silicoflagellate stratigraphy, northwestern Pacific Ocean. In: Gardner, J., (Ed.). *Initial Reports of the Deep Sea Drilling Project*, **32**, pp. 677-701. Washington DC. doi:10.2973/dsdp.proc.32.124.1975

BURBANK, D.W., PUIGDEFÀBREGAS, C., MUÑOZ, J.A., (1992). The chronology of the Eocene tectonic and stratigraphic development of the eastern Pyrenean foreland basin, northeast Spain. *Gelogical Society of America Bulletin*, **104**, 1101-1120. doi: 10.1130/0016-7606(1992)104<1101:TCOTET>2.3.CO;2

CASCELLA, A., DINARÈS-TURELL, J., (2009). Integrated calcareous nannofossil biostratigraphy and magnetostratigraphy from the uppermost marine Eocene deposits of the southeastern pyrenean foreland basin: evidences for marine Priabonian deposition. *Geological Acta*, **7**, 281-296. doi: 10.1344/105.000000282

CENDÓN, D.I., AYORA, C., PUEYO, J.J., TABERNER, C., (2003). The geochemical evolution of the Catalan potash subbasin, South Pyrenean foreland basin (Spain). *Chemical Geology*, **200**, 339-357. doi: 10.1016/S0009-2541(03)00195-5

EMRY, R.J., (1992). Mammalian range zones in the Chadronian White River Formation at Flagstaff Rim, Wyoming. In: Prothero, D.R., Berggren, W.A., (Eds.). *Eocene-Oligocene Climatic and Biotic Evolution*, pp. 106-115. Princeton University Press, Princeton.

FAHLBUSCH, V., (1976). Report on the International Symposium on Mammalian Stratigraphy of the European Tertiary. *Newsletters on Stratigraphy*, **5**, 160-167.

FEIST, M., ANADÓN, P., CABRERA, L., CHOI, S.J., COLOMBO, F., SÁEZ, A., (1994). Upper Eocene-Lowermost Miocene charophyte succession in the Ebro Basin (Spain). Contribution to the charophyte biozonation in Western Europe. *Newsletter on Stratigraphy*, **30**, 1-32.

FERRER, J., (1971a). El Paleoceno y Eoceno del borde suroriental de la Depresión del Ebro (Cataluña). *Mémoires suisses de Paléontologie*, **90**, 1-70.

FERRER, J., (1971b). Presencia de macroforaminíferos priabonienses en el Eoceno de Igualada. *Acta Geologica Hispanica*, **6**, 4-7.

FITZGERALD, P.G., MUÑOZ, J.A., CONEY, P.J., BALDWIN, S.L., (1999). Asymmetric exhumation across the Pyrenean orogen: implications for the tectonic evolution of a collisional orogen. *Earth and Planetary Science Letters*, **173**, 157-170. doi: 10.1016/S0012-821X(99)00225-3

FORNACIARI, E., AGNINI, C., CATANZARITI, R., RIO, D., BOLLA, E.M., VALVASONI, E., (2010). Mid-Latitude calcareous nannofossil biostratigraphy and biochronology across the middle to late Eocene transition. *Stratigraphy*, **7**, 229-264.

GALE, A.S., HUGGETT, J.M., LAURIE, E., (2007). Discussion on the Eocene-Oligocene boundary in the UK. *Journal*, Vol. 163, pp. 401-415. *Journal of the Geological Society*, **164**, 685-688. doi: 10.1144/0016-76492006-098

GALE, A.S., HUGGETT, J.M., PÄLIKE, H., LAURIE, E., HAILWOOD, E.A., HARDENBOL, J., (2006). Correlation of Eocene-Oligocene marine and continental records: orbital, cyclicity, magnetostratigraphy and sequence stratigraphy of the Solent Group, Isle of Wight, UK. *Journal of the Geological Society*, **163**, 401-415. doi: 10.1144/0016-764903-175

GARCÉS, M., CABRERA, L., ROCA, E., GRATACÓS, O., (2008). Comment on "The diachroneity of alluvial-fan lithostratigraphy? A test case from southeastern Ebro basin magnetostratigraphy" by N. Swanson-Hysell and D. L. Barbeau, Jr. *Earth and Planetary Science Letters*, **275**, 181-186. doi: 10.1016/j.epsl.2008.07.024

GRADSTEIN, F.M., OGG, J.G., SMITH, A.G., (2004). *A Geologic Time Scale 2004*. Cambridge University Press, Cambridge. 589pp.

GUIMERÀ, J., (1984). Paleogene evolution of deformation in the northeastern Iberian Peninsula. *Geological Magazine*, **121**, 413-420. doi: 10.1017/S0016756800029940

HILGEN, F.J., (2008). Recent progress in the standardization and calibration of Cenozoic Time Scale. *Newsletters on Stratigraphy*, **43**, 15-22. doi: 10.1127/0078-0421/2008/0043-0015

HOGAN, P.J., BURBANK, D.W., (1996). Evolution of the Jaca piggyback basin and emergence of the External Sierra, southern Pyrenees. In: Friend, P.F., Dabrio, C.J., (Eds.). *Tertiary basins of Spain. The stratigraphic record of crustal kinematics*, pp. 153-160. Cambridge University Press, Cambridge.

HOOKER, J.J., (1992). British mammalian paleocommunities across the Eocene–Oligocene transition and their environmental implications. In: Prothero, D.R., Berggren, W.A., (Eds.). *Eocene-Oligocene Climatic and Biotic Evolution*, pp. 494-515. Princeton University Press, Princeton.

HOOKER, J.J., (2010). The "Grande Coupure" in the Hampshire Basin, UK: taxonomy and stratigraphy of the mammals on either side of this major Paleogene faunal turnover. In: Whittaker, J.E., Hart, M.B., (Eds.). *Micropalaeontology, Sedimentary Environments and Stratigraphy: A Tribute to Dennis Curry (1912–2001)*, pp. 147–215. The Micropalaeontological Society, Special Publications. doi: 10.1144/TMS004.8

HOOKER, J.J., COLLINSON, M.E., GRIMES, S., SILLE, N., MATTEY, D., (2007). Discussion on the Eocene-Oligocene boundary in the UK. *Journal*, Vol. 163, 2006, pp.401-415. *Journal of the Geological Society*, **164**, 685-688. doi: 10.1144/0016-7692006-098.

HOOKER, J.J., COLLINSON, M.E., SILLE, N., (2004). Eocene-Oligocene mammalian faunal turnover in the Hampshire Basin, UK: calibration to the global time scale and the major cooling event. *Journal of the Geological Society*, **161**, 161-172. doi: 10.1144/0016-764903-091

HOOKER, J.J., GRIMES, S.T., MATTEY, D.P., COLLINSON, M.E., SHELDON, N.D., (2009). Refined correlation of the UK Late Eocene-Early Oligocene Solent Group and timing of its climate history. In: Koeberl, C., Montanari, A., (Eds.). *The Late Eocene Earth-Hothouse, Icehouse and Impacts*, pp. 179-195. The Geological Society of America, Special Paper 452. doi: 10.1130/2009.2452(12)

HOTTINGER, L., (1960). Recherches sur les Alvéolines du Paléocène et de l'Éocène. *Mémoires suisses de Paléontologie*, **75/76**, 1-243.

HOTTINGER, L., (1977). Foraminifères operculiniformes. *Mémoires du Museum National d'Histoire Naturelle de Paris*, **C40**, 1-159.

LESS, G., (1987). The zonation of the Mediterranean Upper Paleocene and Eocene by Orthophragminae. *Slovenska Akademija Znanosti in Umetnosti, Razred za Naravoslovne Vede Dela*, **34**, 21-43.

LÉVÊQUE, F., (1993). Correlating the Eocene-Oligocene mammalian biochronological scale from SW Europe with the marine magnetic anomaly sequence. *Journal of Geological Society of London*, **150**, 661-664. doi: 10.1144/gsjgs.150.4.0661

LÓPEZ-BLANCO, M., (2002). Sedimentary response to thrusting and fold growing on the SE margin of the Ebro basin (Paleogene, NE Spain). *Sedimentary Geology*, **146**, 133-154. doi: 10.1016/S0037-0738(01)00170-1

LÓPEZ-BLANCO, M., (2006). Stratigraphic and tectonosedimentary development of the Eocene Sant Llorenç del Munt and Montserrat fan-delta complexes (Southeast Ebro basin margin, Northeast Spain). *Contributions to Science*, **3,** 125-148. doi: 10.2436/20.7010.01.1

LÓPEZ-BLANCO, M., MARZO, M., BURBANK, D.W., VERGÉS, J., ROCA, E., ANADÓN, P., PIÑA, J., (2000a). Tectonic and climatic controls on the development of foreland fan deltas: Montserrat and Sant Llorenç del Munt systems (Middle Eocene, Ebro Basin, NE Spain). *Sedimentary Geology*, **138**, 17-39. doi: 10.1016/S0037-0738(00)00142-1

LÓPEZ BLANCO, M., MARZO, M., PIÑA, J., (2000b). Transgressive-regressive sequence hierachy of foreland, fan-delta clastic wedges (Montserrat and Sant Lloarenç del Munt, Middle Eocene, Ebro Basin, NE Spain). *Sedimentary Geology*, **138**, 41-69. doi: 10.1016/S0037-0738(00)00143-3

LUCIANI, V., NEGRI, A., BASSI, D., (2002). The Bartonian-Priabonian transition in the Mossano section (Colli Berici, north-eastern Italy): a tentative correlation between calcareous plankton and shallow-water benthic zonations. *Geobios*, **35**, Supplement 1, 140-149. doi: 10.1016/S0016-6995(02)00055-4

MARTINI, E., (1971). Standard Tertiary and Quaternary calcareous nannoplankton zonation. In: Farinaci, A., (Ed.). *Proceedings of the II Planktonic Conference, Roma 1970, vol. 2*, pp. 739-785. Edizioni Tecnoscienza, Roma.

OKADA, H., BUKRY, D., (1980). Supplementary modification and introduction of code numbers to the low-latitude coccolith biostratigraphic zonation (Bukry, 1973; 1975). *Marine Micropaleontology*, **5**, 321-325. doi: 10.1016/0377-8398(80)90016-X

PUIGDEFÀBREGAS, C., SOUQUET, P., (1986). Tecto-sedimentary cycles and depositional sequences of the Mesozoic and Tertiary from the Pyrenees. *Tectonophysics*, **129**, 173-203. doi: 10.1016/0040-1951(86)90251-9

RIBA, O., REGUANT, S., VILLENA, J., (1983). Ensayo de síntesis estratigráfica y evolutiva de la cuenca terciaria del Ebro. In: Comba, J.A., (Ed.). *Geología de España. Libro Jubilar J.M. Ríos, Tomo II*, pp. 131-159. Instituto Geológico y Minero de España, Madrid.

SÁEZ, A., (1987). Estratigrafía y sedimentología de las formaciones lacustres del tránsito Eoceno-Oligoceno del noreste de la cuenca del Ebro. PhD-Thesis, Universitat de Barcelona. 353pp.

SCHAUB, H., (1981). Nummulites et Assilines de la Tethys Paléogène. Taxonomie, phylogénèse et biostratigraphie. *Mémoires suisses de Paléontologie*, **104/105/106**, 1-236.

SCHMIDT-KITTLER, N., (1987). European reference levels and correlation tables. *Münchener Geowissenschaftliche Abhandlungen*, **10**, 13–32.

SERRA-KIEL, J., HOTTINGER, L., CAUS, E., DROBNE, K., FERRÀNDEZ-CAÑADELL, C., JAUHRI, A.K., LESS, G., PAVLOVEC, R., PIGNATTI, J., SAMSÓ, J.M., SCHAUB, H., SIREL, E., STROUGO, A., TAMBAREAU, Y., TOSQUELLA, J., ZAKREVSKAYA, E., (1998). Larger Foraminiferal Biostratigraphy of the Tethyan Paleocene and Eocene. *Bulletin de la Societé géologique de France*, **169**, 281-299.

SERRA-KIEL, J., TRAVÉ, A., (1995). Lithostratigraphic and chronostratigraphic framework of the Bartonian sediments in the Vic and Igualada areas. In: Perejón, A., Busquets, P., (Eds.). *Field Trip C: Bioconstructions of the Eocene South Pyrenean Foreland Basin (Vic and Igualada Areas) and the Upper Cretaceous South Central Pyrenees (Tremp Area). VII International Symposium on Fossil Cnidaria and Porifera*, pp. 11-14.

SERRA-KIEL, J., TRAVÉ, A., MATÓ, E., SAULA, E., FERRÀNDEZ-CAÑADELL, C., BUSQUETS, P., TOSQUELLA, J., VERGÉS, J., (2003). Marine and Transitional Middle/Upper Eocene Units of the Southeastern Pyrenean Foreland Basin (NE Spain). *Geologica Acta*, **1**, 177-200.

SINCLAIR, H.D., GIBSON, M., NAYLOR, M., MORRIS, R.G., (2005). Asymmetric growth of the Pyrenees revealed through measurement and modeling of orogenic fluxes. *American Journal of Science*, **305**, 369-406. doi: 10.2475/ajs.305.5.369

STEHLIN, H.G., (1910). Remarques sur les faunules de Mammifères des couches Éocènes et Oligocènes du Bassin de Paris. *Bulletin de la Société Géologique de France*, **9**, 488–520.

TABERNER, C., DINARÈS-TURELL, J., GIMÉNEZ, J., DOCHERTY, C., (1999). Basin infill architecture and evolution from magnetostratigraphic cross-basin correlations in the southeastern Pyrenean foreland basin. *Geological Society of America Bulletin*, **111**, 1155-1174. doi: 10.1130/0016-7606(1999)111<1155:BIAAEF>2.3.CO;2

VERGÉS, J., MARZO, M., SANTAEULÀRIA, T., SERRA-KIEL, J., BURBANK, D.W., MUÑOZ, J.A., GIMÉNEZ-MONTSANT, J., (1998). Quantified vertical motions and tectonic evolution of the SE Pyrenean foreland basin. In: Mascle, A., Puigdefàbregas, C., Luterbacher, M., (Eds.). *Cenozoic Foreland Basins of Western Europe*. Geological Society, Special Publication, **134**, 107-134.

WOODBURNE, M.O., SWISHER, C.C. III, (1995). Land mammal high-resolution geochronology, intercontinental overland dispersals, sea level, climate, and vicariance. In: Berggren, W.A., Kent, D.V., Aubry, M.P., Hardenbol, J., (Eds.). *Geochronology, Time Scales and Global Stratigraphic Correlation.* Society for Sedimentary Geology, SEPM Special Publication, **54**, 335-364.

CHAPTER 5:

CONCLUDING REMARKS

The results presented in this Thesis are derived from a new magnetostratigraphy-based calibration of key stratigraphic sections spanning the marine and continental Paleogene record of the Eastern Ebro Basin, and its integration with previous biostratigraphic and magnetostratigraphic studies. From the chronology obtained in this PhD-Thesis, the timing of tectonosedimentary events shaping the Ebro Basin and its surrounding thrust-belts can be constrained.

The new chronostratigraphic framework, summarized in Chapter 4, challenges the results of earlier biostratigraphic and magnetostratigraphic studies carried out in the Ebro Basin. These contrasting results are in part derived from the methodological approach followed here, which differs from earlier studies. The calibration exercise carried out in this PhD-Thesis, takes into account the fact that the construction of the Geologic Time Scale (GTS) comes from the integration of relative chronostratigraphic disciplines such as biostratigraphy and magnetostratigraphy with absolute dating techniques including radiometric geochronometry and astrochronology. All these disciplines have their sources of error or inconsistencies that need to be considered when attempting a calibration exercise. Absolute ages based in radioisotopic decay are in permanent progress, with increasing precision and accuracy, but, at the same time, systematic bias is now detected between the most widely used systems (U-Pb and Ar-Ar methods), claiming for an effort of synchronization of geochronometers. Astronomical dating, on the other hand, also needs intercalibration with the radioisotopic clocks. Marine biostratigraphy, which provides with the concepts for the division of the stratigraphic record into time units, needs to assess the provincialism in current biostratigraphic zonations. Thus, crucial for the use of this tool to long-distance correlations is the assessment of the isochronoy of bioevents and its geographic (latitudinal, paleoenvironmental) range.

Magnetostratigraphy is unique in that it allows the division of the rock record into fundamentally isochronous time slices (magnetic chrons), which are in principle independent geographically and global in nature. This global nature of reversals provides a sharp tool to correlate discontinuous and fragmentary archives over long distances, through the help of the other stratigraphic disciplines (biostratigraphy, chemostratigraphy). Usefulness of magnetostratigraphy for calibration purposes depend, however, on its ability to establish

independent correlations, that is, correlations which are not dictated by the correspondence of a biostratigraphic datum with a geomagnetic chron.

Because of the non-periodic character of the inversions of the Earth magnetic field, independent magnetostratigraphic correlations are feasible if the length of the magnetostratigraphic record is sufficient to provide with a characteristic pattern of reversals (bar-code) which is unique. Indeed, for this exercise to be successful, no gaps and steady sedimentation is required at the time resolution of magnetostratigraphy, say at the 10^5 year scale. Assumed this, the sequence of geomagnetic reversals (in time units) is faithfully recorded in the magnetostratigraphy (in stratigraphic thickness). Because these conditions are not always present, a good knowledge of the integrated stratigraphic context of the study region is fundamental to support a preferred correlation.

In practice, source data sets are always incomplete and fragmentary, and interpolation is always present in the process of construction of a time scale for global use. Despite stability of the GTS is demanded by the Earth science community, it becomes clear that the GTS is in permanent evolution as new higher-resolution data become available. Therefore, every magnetostratigraphic study may have a feedback on the GTS, and the correlation exercise has a two-way work flow.

The magnetostratigraphy-based chronology derived from this PhD-Thesis has contributed to the calibration of the marine (calcareous nannofossil and larger foraminifers) and continental biostratigraphy. This has been possible because an independent correlation of the magnetostratigraphic record to the Geomagnetic Polarity Time Scale (GPTS) was achieved through the study of long successions, providing a local composite magnetostratigraphy with a unique pattern of polarity reversals. Crucial points to obtain this uniqueness are two, *i)* the length and continuity of the magnetostratigraphic record, and *ii)* full integration of all chronostratigraphic tools (marine and continental biostratigraphy and magnetostratigraphy). Otherwise, correlations too dependent on assumed calibrated ages of a single bioevent can derive into circular reasoning.